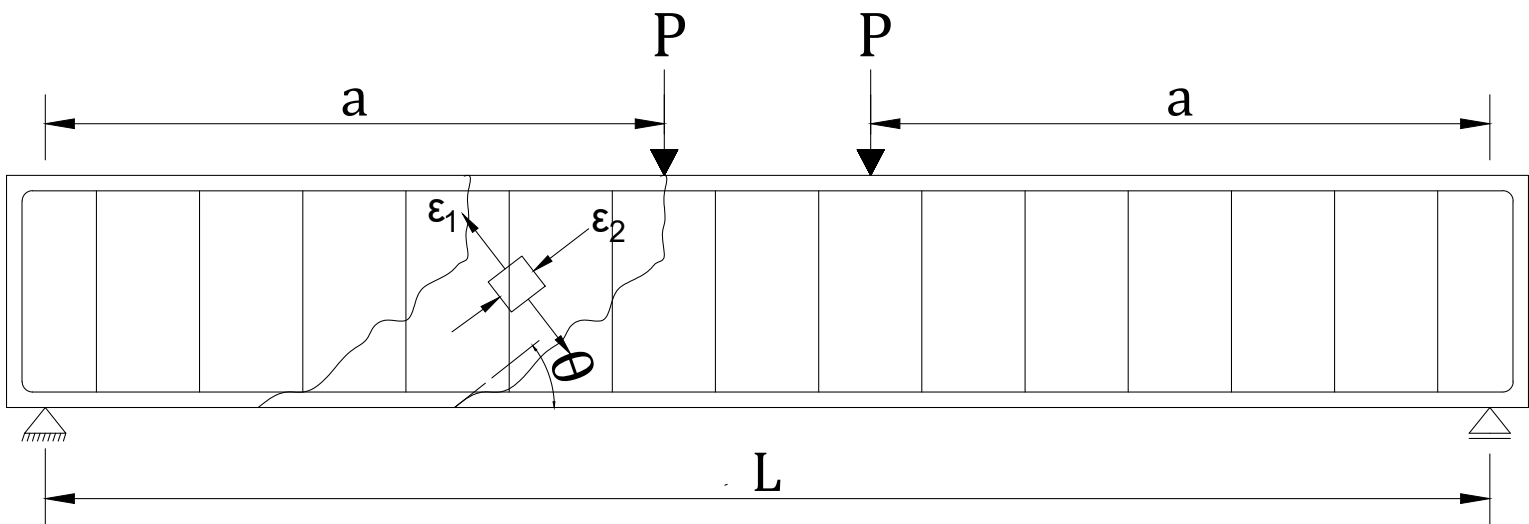


Engineering Models for Shear Crack Width and Shear Deflection in Slender Reinforced Concrete Beams

Anshuman Tiwari



Engineering Models for Shear Crack Width and Shear Deflection in Slender Reinforced Concrete Beams

by

Anshuman Tiwari

in partial fulfilment of the requirements to obtain the degree of Master of Science
at the Delft University of Technology,
to be defended publicly on Monday November 25, 2019 at 04:00 PM.

Student number: 4749529
Project duration: January 25, 2019 – November 25, 2019
Thesis Committee: Dr. ir. drs. C.R. Braam, TU Delft, Supervisor, Chairperson
Dr. Y. Yang, TU Delft
Dr. ir. P.C.J. Hoogenboom, TU Delft
Ir. L.J.M. Houben, TU Delft

An electronic version of this thesis is available at <http://repository.tudelft.nl/>.

I dedicate this work to my beloved parents Seema Tiwari and Pramod Tiwari, my brother Akshay, Baby Mausii, Gudii Didi and Gopi Bhaiya, my mentors and to all my friends whom I truly love and want to serve. You make my life beautiful and inspire me to become more and serve more.

Acknowledgements

The last two years of my life at the TU Delft completely transformed me in my professional and personal life. I am extremely grateful to this great University to give me a chance to become a part of the TU Delft family. I realized that being a part of this amazing Institution is an honor and a great responsibility. I came here with a fascination to pursue higher education but I am leaving even more hungry to learn more, become better and serve.

Last nine months in particular went by quickly thanks to the incredible field of cracking in concrete that Dr. Braam (my supervisor and chair) generously introduced me to. I just fell in love with the topic of my Master thesis. It is hard to believe that I am concluding my thesis work as I am writing this. Dr. Braam, your knowledge, humility and keen observation of details is truly awe inspiring for me. Sir, the lesson on simplicity as a foundation of sound technical contribution and clarity in technical communication using figures and sketches is simply precious and something I will carry forward to my professional career. You believed in my ability to steer my graduation thesis work and I can't thank you enough in words for instilling the confidence in me to do that. I shall forever be indebted to you.

Next, I would like to thank Dr. Yang for your critical remarks and thought provoking discussions during my thesis committee meetings. Your passion for concrete structures is extremely inspiring and something I look forward to develop in myself. I am really grateful to you for pushing me and asking me to go deep in the fundamentals to find answers. I would then like to acknowledge Mr. Houben and Dr. Pierre for your valuable inputs during the course of my Master thesis. You were always willing to support me throughout the course of my thesis.

Shantanu, Shozab and Abhijeet, I can't thank you enough for pushing me to report my research work in an elegant manner. For me, this thesis is a piece of my heart and you guys made sure that it is healthy and beautiful as I put forth this work in the service of my profession.

Next, I would like to thank my parents and my brother, my greatest wealth in the world for always being there for me for everything. You are the reason behind all my endeavours. I am also incredibly indebted to Baby Mausi, Gopi Bhaiya, Gudia Didi and other family members for your incredible love, support and believe in my goals and dreams. I love you so much.

Thanks to Narotam Sekhsaria Foundation also for providing me the Scholarship to pursue my dream Master at TU Delft in the first place. None of this would be possible without the incredible support of the Foundation. Being a cohort of this prestigious scholarship is a great honor and a great responsibility to set an example for others and inspire them.

Last, but not the least, I would like to extend my sincere gratitude to all my friends in Delft for the deep personal bond that we have developed which is something that gives me lot of strength and energy make my life more beautiful every single day.

Anshuman Tiwari
Delft, November 2019

Abstract

Shear cracking in slender reinforced concrete beams with thin webs can result in significant shear crack width and deflection which is usually ignored in practice due to lack of availability of the engineering models in design codes. This can lead to unconservative predictions of the crack width and total deflection in the SLS (Serviceability Limit State). The large crack widths can cause problems related to durability, aesthetic appeal, maintainability and fluid tightness of the structure. An inspection in 2001 reveals extensive shear cracks in Grondal and Alvik bridges in Sweden. The problem is so severe that the bridges are temporarily closed. Later, the investigations reveal that although the bridges are designed according to Swedish codes, the provided shear reinforcement is insufficient for crack width control under service loads on the bridge. Therefore, it becomes imperative to evaluate the available crack width models and develop robust models for shear crack width prediction.

A literature review of the available models for shear crack width is performed to identify the crucial parameters influencing shear crack width. Shear crack width is influenced by several parameters, but the most critical parameters are shear crack spacing, shear stirrup strain, principle strain in the cracked concrete and diagonal compression strut angle. Thereafter, various models available to evaluate these parameters are reviewed to understand their applicability and limitations.

This is followed by a study for the analysis of performance of the models with respect to the experimental observations. Based on the limited experimental dataset, it is found that the Zakaria et al. (2011) shear crack spacing model, and the fib MC 2010 (Model Code 2010) crack spacing model (for members with orthogonal reinforcement) provide a conservative estimate for the shear crack spacing in RC (reinforced concrete) beams. The predictions from the current EC2 crack spacing model are slightly unconservative. All the three crack spacing models take into account the influence of bond transfer length on the stress distribution in concrete and reinforcement.

It is also found that the SMCFT (Simplified Modified Compression Field Theory), CFT (Compression Field Theory) and CCC (Compression Chord Capacity) model provide estimates for the shear crack angle with small deviations from the experimentally observed values. However, all these three models predict flatter (smaller) mean shear crack angles as compared to the experimentally observed values. The SMCFT and CFT determine the diagonal compression strut angle with a consideration of deformations of reinforcement (transverse and longitudinal) and diagonally cracked concrete. On the other hand, the CCC model predicts the diagonal shear crack angle based on the assumption that the horizontal projection of the first branch of flexural-shear crack is equal to $0.85d$ where d is the effective depth to the longitudinal tensile reinforcement.

According to comparison with the experimental observations referred in this study, the CCC model provides a conservative estimate for the concrete contribution to shear resistance which is required to evaluate the shear stirrup strains. Using concrete contribution to shear resistance from this model, an engineering strategy to estimate the concrete contribution to shear resistance at service loads is proposed. Thereafter, five different models

for mean shear crack width (the first three models with two variants each) and four different models for shear deflection are proposed. The comparison of the predictions from the mean shear crack width models with the experimental data reveals that a conservative estimate for the shear crack width can be made by equating shear crack width as the product of mean principle tensile strain in the cracked concrete and the shear crack spacing (Model-IIIB, Model-IV and Model-V). It is observed that the assumption of zero concrete contribution to shear resistance (shear-force transfer) at service loads (in B variants of Models-I, II and III) result in relatively higher predicted mean shear crack widths (as compared to the corresponding A variants) and therefore, more conservative estimates. Moreover, the assumption of mean shear crack angle equal to 45 degrees also leads to relatively more conservative estimates of mean shear crack width. Model-IV and Model-V seem to outperform other mean shear crack width models considering mean and consistency of the models together as a metric. The mean and SD of the predictions from Model-IV are 0.85 and 0.30 for the original formulation of the model. However, with the assumption of mean shear crack angle equal to 45 degrees, the mean and SD values are observed to be 0.37 and 0.13 respectively.

It is found that a conservative estimate for shear deflection can be obtained by assuming a linear shear force versus deflection response for a slender reinforced concrete beam (Model-I). The ratio of the experimentally observed to predict shear deflection for Model-I is 0.85 with a SD (Standard Deviation) of 0.31.

The proposed Models-IIIB, IV and V (in their original formulation) and Models- IB, IIA, IIB, IIIA, IIIB and IV (with an assumption of mean shear crack angle equal to 45 degrees) for the shear crack width and Model-I for shear deflection provide a conservative estimate for the range of experimental beam specimen data covered in this MSc thesis. These models (especially Model-IV for mean shear crack width and Model-I for shear deflection) seem to be potentially useful engineering models for use in engineering practice to evaluate mean shear crack width and shear deflection for slender beams with thin webs (for example slender webs of bridge girders). However, the models require further validation with an experimental study to assess and establish suitability for wider application in design practice.

Contents

List of Figures	xix
List of Tables	xxv
1 Introduction	1
1.1 Background and Motivation	2
1.2 Research Objectives and Methodology	4
1.3 Research Questions	4
1.4 Scope	4
1.5 Outline	5
2 Literature Review	7
2.1 Shear Cracks in Concrete.	8
2.2 Shear Crack Width.	9
2.2.1 Shear Crack Spacing	13
2.2.2 Diagonal Compression Strut Angle	22
2.3 Concrete Contribution to Shear Resistance Models.	28
2.3.1 Force Transfer in a Shear Reinforced Beam.	28
2.3.2 Shear Transfer Action Types.	28
2.3.3 Concrete Contribution to Shear Resistance Models	31
2.4 Conclusion	41
3 Evaluation of the Available Models	45
3.1 Shear Crack Spacing	46
3.1.1 Experimental Details	46
3.1.2 Observations.	51
3.2 Diagonal Compression Strut Angle.	60
3.2.1 Experimental Details	60
3.2.2 Observations.	62
3.3 Concrete Contribution to the Shear Resistance	66
3.3.1 Experimental Details	66
3.3.2 Observations.	72
3.4 Conclusion	76
4 Proposed Models	77
4.1 Concrete and Steel Contribution to Shear Resistance.	78
4.2 Principle Strains and the Stirrups Strain.	79
4.3 Shear Crack Width.	81
4.3.1 Model-IA	81
4.3.2 Model-IB	92
4.3.3 Model-IIA.	93
4.3.4 Model-IIB.	96

4.3.5	Model-III A	96
4.3.6	Model-III B	98
4.3.7	Model-IV	98
4.3.8	Model-V.	101
4.3.9	Results	104
4.4	Shear Deflection	127
4.4.1	Experimental Details	130
4.4.2	Results	132
4.5	Overview of the Proposed Shear-Crack Width and Shear Deflection Models	138
4.6	Conclusion	142
5	Conclusions and Recommendations	145
5.1	Conclusions	146
5.2	Future Recommendations	148
	Appendices	149
A	Appendix A	151
A.1	Crack Width Models-Review.	152
B	Appendix B	155
B.1	Types of Shear Failure.	155
B.2	Zararis (2003) Model for Concrete Contribution to Shear Resistance	158
B.2.1	Shear-Unreinforced Beams	158
B.2.2	Beams Reinforced with Stirrups:	161
C	Appendix C	165
C.1	Nominal Shear Capacity from EC2 VSIM Model	165
D	Appendix D	171
D.1	Shear Crack Width Calculation	171
D.1.1	Model-IA	173
D.1.2	Model-IB	175
D.1.3	Model-IIA.	177
D.1.4	Model-IIB.	179
D.1.5	Model-III A	181
D.1.6	Model-III B	183
D.1.7	Model-IV	185
D.1.8	Model-V.	187
D.2	Shear Crack Deflection Calculation	188
D.2.1	Model-I	189
D.2.2	Model-II	190
D.2.3	Model-III	191
D.2.4	Model-IV	192
E	Appendix E- Integral Design Management Perspective	193
E.1	Introduction	193
E.2	Cantilever Balanced Bridge	193
E.3	Proposed Models and Quality Management	206
E.4	Proposed Models and Time to Maintenance	208

E.5	Proposed Models and Cost Range Estimates	210
E.6	Shear Cracking Risk Assessment	217
E.7	Conclusion	220
E.8	Reflection	220
F	Appendix F	223
E.1	Dowel Action	223
	Bibliography	229

List of Symbols

Symbol	Description
α_{cc}	factor to account for long term effects.(taken as =1.0 in this study).
α_e	modular ratio ($=E_s/E_c$).
β	factor accounting for influence of diagonal cracking in concrete on shear and tensile resistance.
β	factor to account for shear resistance of cracked concrete.
$\delta_{avg,exp}$	experimentally measured shear deflection at the section considered.
$\delta_{avg,pred}$	shear deflection at the section considered predicted by the considered shear deflection prediction model.
ΔM	additional moment induced due to flexural stress $\Delta\sigma$.
δ_s	shear deflection of the beam segment.
$\Delta\sigma$	flexural stress to counteract the couple due to shear force over the length Δx .
ΔV	shear deflection at the section under consideration.
ΔV_d	additional shear force in the longitudinal reinforcement due to opening of the second branch of the crack.
$\epsilon_{c'}$	strain in concrete corresponding to the maximum compressive stress.
ϵ_{cm}	mean strain in concrete in between the cracks.
ϵ_{sm}	additional mean strain in the steel reinforcement relative to concrete under the applied load (including the effect of imposed deformations).
ϵ_w	strain in the stirrup at the location of intersection with the crack.
ϵ_x	longitudinal strain at the mid-depth of the reinforced concrete beam.
ϵ_y	strain in the stirrup at the location of intersection with the crack.
ϵ_1	mean principle tensile strain in the cracked concrete.
ϵ_2	principle strain in the diagonal compression strut.
γ	shear strain.
γ_{cr}	shear strain of the section at which shear force = V_{cr} (load at which diagonal shear crack occurs).
γ_x	shear strain at cross section having a shear force $V(x)$.
γ_y	shear strain of the section at which shear force = V_y (yield shear force).
γ_c	material factor of safety for concrete.
λ	factor to take into account the low density concrete.
λ_v	shear force coefficient and is = $(V - V_{cr}) / (V_y - V_{cr})$.
ν_1	factor to account for the transverse tension in the strut.
ϕ	diameter of the reinforcement bar.
ϕ_c	resistance factor for concrete =0.65 (recommended value in CSA-2004).
$\phi_{eff,x}$	equivalent diameter of the longitudinal reinforcement .
$\phi_{eff,y}$	equivalent diameter of the transverse reinforcement .
ϕ_s	diameter of the tension reinforcement bar.

ϕ_w	diameter of the stirrup.
ρ	longitudinal reinforcement ratio.
ρ	the longitudinal reinforcement percentage.
ρ'	percentage compression reinforcement ratio.
$\rho_{eff,x}$	effective reinforcement ratio of the longitudinal reinforcement.
$\rho_{eff,y}$	effective reinforcement ratio of the shear reinforcement.
ρ_l	longitudinal reinforcement ratio.
$\rho_{p,eff}$	the effective reinforcement ratio of the tension reinforcement bar based on the effective height of the hidden tensile member given in EC2 (2004).
ρ_s	reinforcement percentage in the direction of slip length or bond transfer length.
ρ_t	shear reinforcement ratio.
ρ_v	shear reinforcement ratio.
ρ_w	longitudinal reinforcement percentage.
ρ_w	shear reinforcement ratio.
ρ_x	ratio of the amount of longitudinal reinforcement including including pre-stressing steel to the effective cross section area of the hidden tensile member
ρ_y	ratio of cross-sectional area of the shear-reinforcement bars to the effective cross-sectional area of the hidden tensile member.
ζ	factor to account for slenderness and size effect.
σ_{ai}	normal stress at the crack surface.
σ_b	bond stress between reinforcement and concrete.
σ_m	stress in the extreme fiber in the compression zone corresponding to the cracking moment.
σ_s	stress in the reinforcement bar assuming that the section is cracked.
σ_{se}	stress in the reinforcement outside the disturbed zone.
σ_{sr}	stress in the reinforcement at the location of intersection with the crack.
σ_{strut}	is the principle compressive stress in the diagonal concrete strut.
$\sum_{i=1}^{i=n} V_{si}$	shear resistance contribution from stirrups.
σ_x	normal stress in concrete in the longitudinal direction.
σ_y	normal stress in concrete in the transverse direction.
τ_{ai}	shear stress at the crack surface.
τ_{bm}	mean bond stress between the reinforcement bar and concrete.
τ_{xy}	shear stress in concrete.
θ	Angle of inclination of the principle compressive stress (or angle of diagonal compression strut). The definition is explicitly mentioned in the report where the definition differs.
$\theta_{avg,exp}$	Angle of inclination of the principle compressive stress (or angle of diagonal compression strut) measured experimentally as mean shear crack angle.
$\theta_{avg,pred}$	Angle of inclination of the principle compressive stress (or angle of diagonal compression strut) predicted by the considered diagonal compression strut angle prediction model.
θ_{exp}	diagonal shear crack angle observed experimentally.
θ_{pred}	predicted value of the diagonal shear crack angle from various models.

θ_s	Angle of inclination of the principle compressive stress (or angle of diagonal compression strut).
------------	--

Symbol	Description
$A_{cy,eff}$	effective concrete area around the shear stirrups.
A_w	area of shear reinforcement.
a	distance of line of action of the point load from the support.
A	Neutral Axis of the beam.
a/d	shear span ratio.
$A_{c,eff}$	cross sectional area of the effective hidden tensile member.
A_c	area of cross-section of concrete.
$A_{cx,eff}$	the cross sectional area of the hidden tensile member around the longitudinal reinforcement bars.
$A_{cy,eff}$	the cross sectional area of the hidden tensile member around the shear stirrups.
A_p	area of the prestressing tendons.
A_{ps}	cross sectional area of the prestressing steel.
A_s	area of tensile longitudinal reinforcement.
A_S	cross sectional area of the longitudinal reinforcement in tension (part of the tension chord of the equivalent truss).
A_{sl}	cross sectional area of the longitudinal reinforcement extended to a section
A_{strut}	total cross- section area of the diagonal compression strut.
A_{sw}	cross-sectional area of stirrups.
A_{sx}	cross-sectional area of longitudinal reinforcement.
A_{sy}	cross-sectional area of transverse reinforcement.
A_v	cross-sectional area of the shear stirrups.
A_w	total cross- section area of the stirrup (both legs).
B	concrete tension zone surface.
b	cross- section width.
b_v	cross sectional width of the beam adjusted for the presence of pre-stressing ducts (in the present study the effect of pre-stressing is not studied and therefore, no ducts are present).
b_v	minimum web width throughout the effective shear depth.
$b_{v,eff}$	effective shear width of the cross-section taking into account the influence of compression flange.
b_w	smallest width of the cross-section in the tensile region.
b_w	width of the beam cross-section.
b_w	width of the web of beam.
c	clear cover to the reinforcement bar.
c	depth of the neutral axis.
C	flexural compression force.
$\frac{c}{d}$	ratio of compression zone height to the effective depth to longitudinal reinforcement and can be obtained using eqn.
c_l	clear cover to the longitudinal reinforcement.
c_s	side concrete cover to stirrups.
C_u	axial compression force in the concrete compression zone.

c_x	the distance between the horizontal line at the mid-depth of the cross section and the nearest longitudinal reinforcement bars.
d	effective depth to the longitudinal reinforcement.
D	predictions of the crack width from eqn.
d'	effective depth to the compression reinforcement.
d_{bx}	diameter of the longitudinal reinforcement bars.
d_{by}	diameter of the stirrup.
d_e	effective depth of the longitudinal reinforcement bars including prestressing bars.
d_p	effective depth to the prestressing steel rebars.
d_s	effective depth to the longitudinal reinforcement.
d_v	effective shear depth = $\max(0.9d, 0.72h)$
E	Actual crack width on the beam surface.
E_c	Modulus of Elasticity of concrete.
E_p	Modulus of elasticity of the prestressing tendons.
E_s	Modulus of Elasticity of the longitudinal reinforcement.
$E_{s,l}$	Modulus of Elasticity of the longitudinal reinforcement.
$E_{s,w}$	Modulus of Elasticity of the transverse reinforcement.
F_c	normal force in the concrete compression zone.
f_c	compressive strength of concrete.
f'_c	compressive strength of concrete.
f'_{cd}	design concrete compressive strength.
f_{ck}	characteristic compressive strength of concrete.
f_{cm}	mean compressive strength of concrete.
f_{ct}	splitting tensile strength of concrete.
$f_{ct,eff}$	mean tensile strength of concrete at the time of first expected cracks occurring.
f_{ctm}	mean axial tensile strength of concrete.
f_{cx}	force resisted by the concrete in the x direction.
f_{cy}	force resisted by the concrete in the y direction.
F_d	dowel shear force acting on the reinforcement bar.
f_{po}	stress in the prestressed tendons such that the stress in the concrete in the vicinity is zero. This may be considered as 1.1 times the residual prestressing stress after all losses have occurred.
F_s	tensile force in the longitudinal reinforcement.
f_{sx}	force resisted by the reinforcement in x direction.
f_{sxcr}	force resisted by the reinforcement in x direction at the location of crack.
f_{sy}	force resisted by the reinforcement in y direction.
f_{syncr}	force resisted by the reinforcement in y direction at the location of crack.
f_t	concrete tensile strength
f_y	yield strength of stirrups.
f_{ym}	mean steel yield strength of the shear stirrups.
f_{yv}	yield strength of the shear stirrups.
f_{ywm}	mean steel yield strength.
f_z	clamping stress in the transverse direction.
f_1	mean principle tensile stress in and between the cracked concrete.

f_2	mean principle compressive stress in and between the cracked concrete.
G_c	shear modulus of concrete.
h	height of cross-section of the beam.
$h_{c,eff}$	effective height of the hidden tensile member around the reinforcement.
h_f	thickness of the compression flange.
jd	flexural lever arm of the reinforced concrete beam = $0.9d$.
K	constant to account for the stirrup type.
k_1	coefficient to account for the bond properties of the reinforcement
k_2	coefficient to account for the type of strain distribution
k_{max}	correlation factor = 1.4.
k_s	constant to account for the type of hook of shear stirrups.
k_t	constant to account for the type shear stirrup rebars.
k_t	factor to take into account the duration of the load.
$K_{v,e}$	elastic shear stiffness of the reinforced concrete beam.
$K_{v,y}$	yield shear stiffness of the reinforced concrete beam.
k_1	factor to account for the bond characteristics of the reinforcement.
k_2	factor to account for the shape of the stress distribution.
l_{bd}	design anchorage length.
$l_{s,max}$	bond transfer length. It can also be called bond-slip length.
$l_{sx,k}$	bond transfer length along the x-direction.
$l_{sy,k}$	bond transfer length along the y-direction.
M_E	Moment at the section at distance " d_v " away from the support.
M_f	moment due to factored loads (in the present study this is the moment corresponding to the service shear load).
M_o	flexural moment required to nullify the stress at extreme fiber (corresponding to design flexural moment) due to axial force.
M_u	factored moment at section.
M_{ud}	flexural capacity of the member assuming zero axial force.
M	Moment due to service load at a section at distance d_v from the face of the support.
N_c	shear resistance from concrete compression zone.
N_{Ed}	axial force in the cross section due to external loads or due to prestressing.
n	modular ratio.
N'_d	design axial compression force.
N_{Ed}	axial force in the cross section due to external loads or due to prestressing (this is equal to zero in this study).
N_f	factored axial force in the cross section occurring along with V_f and includes the influence of tensile forces due to shrinkage and creep (tension is taken as positive while compression is taken as negative).
N_u	axial force on the concrete member in ultimate limit state.
N_v	axial force in the longitudinal reinforcement bars to resist the shear force.
P	externally applied point load.
P_u	the reaction generated at the support.
s	spacing between the shear stirrups.
s_{avg}	mean spacing between the shear cracks.

$s_{avg,exp}$	mean spacing between the shear cracks measured experimentally.
$s_{avg,pred}$	mean spacing between the shear cracks predicted using the considered shear crack spacing model.
s_{exp}	shear crack spacing observed experimentally.
$s_{m\theta}$	mean crack spacing in the stabilized cracking phase.
$s_{m\theta-avg}$	mean crack spacing in the crack formation phase.
$s_{m,x}$	crack spacing in direction perpendicular to the stirrups.
$s_{m,y}$	crack spacing in direction perpendicular to the longitudinal reinforcement.
s_{pred}	predicted shear crack spacing from the various models.
$s_{r,max}$	maximum spacing between the cracks.
$s_{r,max,y}$	maximum spacing between the cracks along y direction.
$s_{r,max,z}$	maximum spacing between the cracks along z direction.
$Ssin\theta_{cr}$	shear resistance due to aggregate interlock effect.
s_v	spacing of the stirrups.
s_x	spacing between the longitudinal rebars.
s_y	the stirrup spacing.
S	concrete contribution from the aggregate interlock effect.
T_s	axial force in the longitudinal reinforcement.
T	flexural tension force.
T_u	axial force in the longitudinal reinforcement.
T_u	axial force in the longitudinal reinforcement.
V	Applied shear force.
V	shear force due to service load at a section at distance d_v from the face of the support.
\bar{V}	shear deflection at the section due to a unit force applied at the section under consideration (at which shear deflection is being measured).
V_{ai}	shear resistance contribution from the aggregate interlock effect.
V_c	nominal shear strength.
V_c	shear force resisted by concrete compression zone.
V_c	concrete contribution to shear resistance.
V_{cc}	concrete compression zone shear resistance.
$V_{c,CCC}$	predicted concrete contribution to the shear resistance of a shear reinforced beam at ULS.
V_{ccr}	concrete compression zone shear resistance.
V_{cd}	shear resisted by dowel action.
$V_{c,exp}$	concrete contribution to shear resistance observed experimentally.
$V_{c,pred}$	concrete contribution to shear resistance predicted by the considered concrete contribution to shear resistance model.
V_{cr}	first diagonal shear cracking load.
$V_{cr,CCC}$	predicted first diagonal shear cracking load from the compression chord capacity model. In this study it is $=V_{c,CCC}$.
$V_{cr,pred}$	experimentally measured first diagonal shear cracking load.
$V_{cr,pred}$	predicted first diagonal shear cracking load from the considered concrete contribution to shear resistance model.
ν_{ci}	aggregate interlocking shear stress at the crack surface.
$V_{c,pred}$	concrete contribution to shear resistance predicted by various models.

$V_{c,pred,ser}$	concrete contribution to shear resistance predicted at service loading conditions predicted by the proposed model.
V_d	shear resisted by dowel action.
V_{dcr}	shear resistance of the longitudinal reinforcement.
V_E	Shear force at a section at distance " d_v " away from the support.
V_{Ed}	design shear force on the beam.
V_f	factored shear force (in the present study this is the shear force corresponding to the service shear load).
V_l	shear resistance contribution from dowel action.
V_{nom}	nominal shear resistance of a shear reinforced beam from EC2 [19].
V_p	the vertical tensile force component of the inclined prestressed tendons.
$V_{Rd,c}$	shear strength of the shear unreinforced beam according to EC2.
V_s	shear resistance offered by the stirrups.
v_{ser}	shear stress at the service shear load ($=0.6V_{nom,EC2}/(bd)$).
V_{ser}	applied shear force at service load condition.
V_{strut}	axial compressive force in the diagonal compression strut.
V_u	factored shear force.
V_y	Yield shear force i.e. force at which the shear stirrups yield.
w	crack width.
w_{avg}	mean crack width.
$w_{avg,exp}$	mean crack width measured experimentally.
$w_{avg,pred}$	mean crack width predicted by the crack width models.
w_k	characteristic crack width.
w_{max}	average diagonal crack width.
x	height of the compression zone.
x_o	height of the compression zone.
z	internal lever arm of the beam.

Abbreviation	Full form
AASHTO	American Association of State Highway and Transportation Officials
ACI	American Concrete Institute
ASCE	American Society of Civil Engineers
CCC	Compression Chord Capacity
CFT	Compression Field Theory
COV	Coefficient of Variation
CSA	Canadian Standards Association
EC	Euro Code
fps	foot-pound-second
HYSD	High Yield Strength Deformed Bars
JSCE	Japanese Society of Civil Engineers
MC	Model Code
MCFT	Modified Compression Field Theory
Max	Maximum
Min	Minimum
N.A	Neutral Axis
RC	Reinforced Concrete
PC	Prestressed Concrete
PSC	Prestressed Concrete
NLFEA	Non Linear Finite Element Analysis
SD	Standard Deviation
SLS	Serviceability Limit State
SMCFT	Simplified Modified Compression Field Theory
ULS	Ultimate Limit State
VSIM	Variable Strut Inclination Method

List of Figures

1.1	The monitoring of web cracking in Grondal bridge [55]	3
1.2	Shear cracks and flexural cracks in a RC (Reinforced Concrete) beam	3
1.3	Shear and flexural deformations in a RC beam (Adapted from Chiu et al. [13])	3
1.4	Organization of thesis into various chapters	5
2.1	Various types of cracks in reinforced concrete beam	8
2.2	Overview of the topics discussed in Chapter 2	9
2.3	Development of bond stresses along the transfer length around a crack	11
2.4	Effective height of the hidden tensile member for different structural elements	11
2.5	The definition of theta in EC2 [19] crack spacing model	15
2.6	The orientation of axes in EC2 [19] crack spacing model	16
2.7	Variation of crack width with respect to distance from the reinforcement bars (Adapted from EC2 [19])	16
2.8	Assumed diagonal shear cracks at a constant crack spacing	17
2.9	Assumed horizontal cracks caused by transverse tension with crack spacing s_{my} in between the two adjacent cracks	17
2.10	Assumed vertical cracks caused by axial tension with crack spacing s_{mx} in between the two adjacent cracks	17
2.11	The definition of theta in fib MC [23] crack spacing model	18
2.12	The orientation of axes in fib MC 2010 [23] crack spacing model	19
2.13	Various geometrical parameters used in the shear crack spacing model [65]	20
2.14	The condition for strut inclination at failure [28]	22
2.15	Determination of longitudinal strain in a reinforced concrete non-prestressed beam [4]	23
2.16	Evolution of the critical shear crack (adapted from [15])	24
2.17	Compression Field Theory [4]	26
2.18	Truss analogy for a shear reinforced beam subjected to shear and flexure force	28
2.19	Different shear strength transfer mechanisms of a reinforced concrete beam without shear reinforcement Yang [62]	29
2.20	Different shear strength components of a reinforced concrete beam with shear reinforcement (Hu and Wu [32])	29
2.21	Different mechanisms of shear transfer by dowel action [50]	30
2.22	The longitudinal reinforcement in Equation 2.41 [19]	32
2.23	Notations for a T beam [15]	33
2.24	Determination of longitudinal strain in the web of a reinforced concrete non-prestressed beam [14]	36
2.25	Determination of shear strength from AASHTO model [7]	36
2.26	Determination of longitudinal strain in the longitudinal reinforcement of a reinforced concrete non-prestressed beam [4].	37

2.27	Free body diagram of the segment of the beam above the critical diagonal crack [67]	39
2.28	The FBD (Free Body Diagram) showing various stresses and forces at a cracked section as considered by Tureyen and Frosch [6]	40
3.1	The measurement of average shear crack spacing [66]	47
3.2	The mechanical scheme and cross section details for the reinforced concrete beams in series I [66]	48
3.3	The mechanical scheme and cross section details for the reinforced concrete beams in Series II and III [66]	49
3.4	The mechanical scheme and cross section details for the reinforced concrete beams [37]	49
3.5	The mechanical scheme and cross section details for the reinforced concrete beams [31]	50
3.6	The ratio of $s_{avg,exp}/s_{avg,pred}$ versus a/d for the EC2 model [19]	54
3.7	The ratio of $s_{avg,exp}/s_{avg,pred}$ versus a/d for the Zakaria et al. model [65]	54
3.8	The ratio of $s_{avg,exp}/s_{avg,pred}$ versus ρ_l/ρ_w for EC2 model [19]	55
3.9	The ratio of $s_{avg,exp}/s_{avg,pred}$ versus ρ_l/ρ_w for the Zakaria et al. model [65]	55
3.10	The ratio of $s_{avg,exp}/s_{avg,pred}$ versus c_s for the EC2 model [19]	56
3.11	The ratio of $s_{avg,exp}/s_{avg,pred}$ versus c_s for Zakaria et al. model [65]	56
3.12	The ratio of $s_{avg,exp}/s_{avg,pred}$ versus c_l for the EC2 model [19]	57
3.13	The ratio of $s_{avg,exp}/s_{avg,pred}$ versus c_l for Zakaria et al. model [65]	57
3.14	The ratio of $s_{avg,exp}/s_{avg,pred}$ versus $\phi_{eff,x}/\rho_{eff,x}$ for the EC2 model [19]	58
3.15	The ratio of $s_{avg,exp}/s_{avg,pred}$ versus $\phi_{eff,x}/\rho_{eff,x}$ for Zakaria et al. model [65]	58
3.16	The ratio of $s_{avg,exp}/s_{avg,pred}$ versus ϕ_w/ρ_w for the EC2 model [19]	59
3.17	The ratio of $s_{avg,exp}/s_{avg,pred}$ versus ϕ_w/ρ_w for fib MC 2010 model [23]	59
3.18	The ratio of $s_{avg,exp}/s_{avg,pred}$ versus d/b for fib MC 2010 model [23]	60
3.19	The application of service load to the different mechanical schemes considered in the calculation of shear crack angle from different models	61
3.20	The ratio of $\theta_{avg,exp}/\theta_{avg,pred}$ versus a/d for the Theorem of Plasticity [19]	63
3.21	The ratio of $\theta_{avg,exp}/\theta_{avg,pred}$ versus d/b for the Theorem of Plasticity [19]	63
3.22	The ratio of $\theta_{avg,exp}/\theta_{avg,pred}$ versus $\rho_w f_{ym}$ for the CFT [16]	64
3.23	The ratio of $\theta_{avg,exp}/\theta_{avg,pred}$ versus $\rho_w f_{ym}$ for the SMCFT [7]	64
3.24	The values of θ versus $\rho_w f_{ywm}$ as observed by Oladimeji [48]	66
3.25	The cross section details for the reinforced concrete beams [26]	69
3.26	The cross section and the mechanical schemes of the reinforced concrete beams [32]	69
3.27	The cross section and the mechanical schemes of the RC beams [44]	71
3.28	The cross section and the mechanical schemes of the RC beams [38]	72
3.29	The variation of concrete and stirrup contribution to shear resistance for the beam with a/d 2.5 (Left) and 3.1 (Right) respectively [32]	72
3.30	$V_{c,avg,exp}/V_{c,avg,pred}$ versus d/b for predictions by CCC model [15]	76
4.1	Variation of V_c and V_s for two beam specimens with shear span ratio of 2.5 and 3.1 respectively [32]	79
4.2	Proposed method to calculate V_c at service load condition	79
4.3	The local stress and strain at the crack surface of an RC beam	80

4.4	The components of the applied shear force along and perpendicular to the diagonal compression strut	81
4.5	The Mohr circle for strains for different values of θ [41]	81
4.6	Figure showing stress distribution in concrete and longitudinal reinforcement close to flexural cracks	82
4.7	Figure showing assumed stress distribution in concrete and longitudinal reinforcement close to shear cracks	83
4.8	Effective area of the hidden tensile member around longitudinal reinforcement as per EC2 [19]	83
4.9	Assumed effective area of the hidden tensile member around stirrups.	83
4.10	Effective area of the hidden tensile member around stirrups as given in fib MC 2010 [23]	84
4.11	Notations for a T beam [15]	86
4.12	The orientation of axes in EC2 [19] crack spacing model	88
4.13	The definition of θ in EC2 [19] crack spacing model	88
4.14	Variation of crack width with respect to distance from the reinforcement bars (Adapted from EC2 [19])	89
4.15	Assumed diagonal shear cracks at a constant crack spacing	89
4.16	Assumed horizontal cracks caused by transverse tension with crack spacing s_{my} in between the two adjacent cracks	90
4.17	Assumed vertical cracks caused by axial tension with crack spacing s_{mx} in between the two adjacent cracks	90
4.18	Evolution of the critical shear crack (adapted from [15])	91
4.19	Various geometrical parameters used in the shear crack spacing model [65]	95
4.20	Determination of longitudinal strain in the longitudinal reinforcement of a reinforced concrete non-prestressed beam [4].	99
4.21	Determination of longitudinal strain in the web of a reinforced concrete non-prestressed beam [14]	100
4.22	Stresses in the reinforcement and cracked concrete	103
4.23	Stresses in the reinforcement and concrete under varying compressive stress along the depth	103
4.24	Experimental setup for the shear crack width study [37]	105
4.25	The ratio of $w_{avg,exp}/w_{avg,pred}$ versus a/d for the proposed Model-IA.	112
4.26	The ratio of $w_{avg,exp}/w_{avg,pred}$ versus a/d for the proposed Model-IB.	112
4.27	The ratio of $w_{avg,exp}/w_{avg,pred}$ versus a/d for the proposed Model-IIA	113
4.28	The ratio of $w_{avg,exp}/w_{avg,pred}$ versus a/d for the proposed Model-IIB	113
4.29	The ratio of $w_{avg,exp}/w_{avg,pred}$ versus a/d for the proposed Model-IIIA	114
4.30	The ratio of $w_{avg,exp}/w_{avg,pred}$ versus a/d for the proposed Model-IIIB	114
4.31	The ratio of $w_{avg,exp}/w_{avg,pred}$ versus a/d for the proposed Model-IV	115
4.32	The ratio of $w_{avg,exp}/w_{avg,pred}$ versus $\rho_w f_{ym}$ (MPa) for the proposed Model-IIA	115
4.33	The ratio of $w_{avg,exp}/w_{avg,pred}$ versus $\rho_w f_{ym}$ (MPa) for the proposed Model-IIB	116
4.34	The ratio of $w_{avg,exp}/w_{avg,pred}$ versus $\rho_w f_{ym}$ (MPa) for the proposed Model-IIIA	116

4.35	The ratio of $w_{avg,exp}/w_{avg,pred}$ versus $\rho_w f_{ym}$ (MPa) for the proposed Model-III B	117
4.36	The ratio of $w_{avg,exp}/w_{avg,pred}$ versus $\rho_w f_{ym}$ (MPa) for the proposed Model-IV	117
4.37	The ratio of $w_{avg,exp}/w_{avg,pred}$ versus ρ_l/ρ_w for the proposed Model-IIB	118
4.38	The ratio of $w_{avg,exp}/w_{avg,pred}$ versus ρ_l/ρ_w for the proposed Model-III A	118
4.39	The ratio of $w_{avg,exp}/w_{avg,pred}$ versus ρ_l/ρ_w for the proposed Model-III B	119
4.40	The ratio of $w_{avg,exp}/w_{avg,pred}$ versus ρ_l/ρ_w for the proposed Model-IV	119
4.41	The ratio of $w_{avg,exp}/w_{avg,pred}$ versus f_c (MPa) for the proposed Model-IIB	120
4.42	The ratio of $w_{avg,exp}/w_{avg,pred}$ versus f_c (MPa) for the proposed Model-III A	120
4.43	The ratio of $w_{avg,exp}/w_{avg,pred}$ versus f_c (MPa) for the proposed Model-III B	121
4.44	The ratio of $w_{avg,exp}/w_{avg,pred}$ versus f_c (MPa) for the proposed Model-IV	121
4.45	The ratio of $w_{avg,exp}/w_{avg,pred}$ versus $\phi_{eff,x}/\rho_{eff,x}$ for the proposed Model-IIB	122
4.46	The ratio of $w_{avg,exp}/w_{avg,pred}$ versus $\phi_{eff,x}/\rho_{eff,x}$ for the proposed Model-III B	122
4.47	The ratio of $w_{avg,exp}/w_{avg,pred}$ versus $\phi_{eff,x}/\rho_{eff,x}$ for the proposed Model-III A	123
4.48	The ratio of $w_{avg,exp}/w_{avg,pred}$ versus $\phi_{eff,x}/\rho_{eff,x}$ for the proposed Model-IV	123
4.49	The ratio of $w_{avg,exp}/w_{avg,pred}$ versus $\phi_{eff,y}/\rho_{eff,y}$ for the proposed Model-IIB	124
4.50	The ratio of $w_{avg,exp}/w_{avg,pred}$ versus $\phi_{eff,y}/\rho_{eff,y}$ for the proposed Model-III A	125
4.51	The ratio of $w_{avg,exp}/w_{avg,pred}$ versus $\phi_{eff,y}/\rho_{eff,y}$ for the proposed Model-III B	125
4.52	The ratio of $w_{avg,exp}/w_{avg,pred}$ versus $\phi_{eff,y}/\rho_{eff,y}$ for the proposed Model-IV	126
4.53	The three idealized models for prediction of shear stiffness degradation [28]	128
4.54	Illustrations for calculation of shear deformation for typical load configurations [28]	130
4.55	Mechanical scheme and instrumentation for specimens [60]	131
4.56	Mechanical scheme and instrumentation for specimens [25]	132
4.57	The ratio of $\delta_{s,exp}/\delta_{s,pred}$ versus a/d for shear deflection Model-I	134
4.58	The ratio of $\delta_{s,exp}/\delta_{s,pred}$ versus d/b for shear deflection Model-I.	135
4.59	The ratio of $\delta_{s,exp}/\delta_{s,pred}$ versus ρ_l/ρ_w for shear deflection Model-I	135
4.60	The ratio of $\delta_{s,exp}/\delta_{s,pred}$ versus $\rho_w f_{ym}$ (MPa) for shear deflection Model-I.	136
4.61	The ratio of $\delta_{s,exp}/\delta_{s,pred}$ versus d/b for Model-IV	137
4.62	The ratio of $\delta_{s,exp}/\delta_{s,pred}$ versus $\rho_w f_{ym}$ (MPa) for Model-IV	137
4.63	Strains in the reinforced concrete element in between the cracks	140
4.64	Various shear transfer mechanisms (Adapted from Yang et al. [62])	140
4.65	Basic approach behind the proposed models for average shear crack width prediction	141
4.66	Flowchart showing general calculation methodology of the proposed models for shear deflection.	142
A.1	Overview of the available crack width models [65]	152
A.2	Overview of the available crack width models [65]	153
B.1	Flexural Shear Failure Mode	155

B.2	Shear Tension Failure Mode	156
B.3	Web Crushing Failure Mode	156
B.4	Shear Stirrup Yielding Failure Mode	157
B.5	Various relations of the MCFT [4]	158
B.6	(a); Free body diagram with the first branch of the diagonal crack (b) Free body diagram of the triangular concrete element below the first branch of the diagonal crack (c) Distribution of normal compressive stress along the beam depth (d) Distribution of the shear stress along the beam depth [68].	159
B.7	(a) Line of Action of the resultant compressive force (b) Portion of the beam containing the dashed line along which diagonal splitting occurs [68].	160
B.8	Normal stresses along the second branch of diagonal crack [68]	161
B.9	The free body diagram of the segment of the beam above the critical diagonal crack [67]	162
B.10	Forces in the longitudinal reinforcement cover region susceptible to horizontal splitting as the second branch of the diagonal crack opens (a) no stirrups (b) stirrup spacing = transfer length for stresses from longitudinal reinforcement to concrete (c) stirrup spacing less than " l_t " [67]	163
C.1	Prediction of total shear resistance from EC2-VSIM versus experimental observations.	167
D.1	Experimental setup for the shear crack width study [37]	172
D.2	Mechanical scheme and instrumentation for specimens [25]	188
E.1	Schematic diagram of the cantilever balanced bridge and approach bridge	194
E.2	Schematic representation of carriage-way of the designed cantilever balanced bridge	194
E.3	Schematic representation of RC beam as beam on elastic foundation [43]	195
E.4	Variable self-weight intensity along the span	198
E.5	Side and Top view layout of the prestressing cables	200
E.6	Stress-strain relationship for the prestressing strands	202
E.7	Cross-section forces at ULS	203
E.8	Cross-section forces at ULS	204
E.9	Modification factor for the transverse tension in the compression strut	205
E.10	Original and New position of the perceived risk of extensive shear cracking in a bridge girder under service loads [58]	208
E.11	Original and New position of the perceived risk of extensive shear cracking in a bridge girder under service loads	209
E.12	Original and New position of the perceived risk of extensive shear cracking in a bridge girder under service loads	209
E.13	Original and New position of the perceived risk of extensive shear cracking in a bridge girder under service loads	211
E.14	Original and New position of the perceived risk of extensive shear cracking in a bridge girder under service loads	212
E.15	Original and New position of the perceived risk of extensive shear cracking in a bridge girder under service loads	213

E.16	Original and New position of the perceived risk of extensive shear cracking in a bridge girder under service loads	218
E.17	Different Levels of risk depending on the likelihood and consequences as defined by Hastings [27]	218
F.1	Schematic representation of RC beam as beam on elastic foundation[43] . . .	223
F.2	Bond stress and local slip around a reinforcement bar [53].	226
F.3	Bond deterioration zone around the RC interface [53].	227
F.4	The two cases for beam cover splitting [Moradi et al]	228

List of Tables

2.1	Basic principles and limitations of the reviewed models	42
3.1	Key characteristics of specimens referred for shear crack spacing study	47
3.2	Geometrical parameters for the different specimens in the test series of Zakaria et al. [66] and Hu and Wu [31]	51
3.3	Range of parameters for the specimens studies for evaluation of available shear crack spacing models	51
3.4	$s_{avg,exp}/s_{avg,pred}$ values of the different shear crack spacing models	53
3.5	Statistical parameters for $s_{avg,exp}/s_{avg,pred}$ for the different shear crack spacing models	53
3.6	Key characteristics of specimens referred for diagonal crack angle study	61
3.7	$\theta_{avg,exp}/\theta_{avg,pred}$ values of the different diagonal compression strut angle prediction models	65
3.8	Mean, SD and COV of $\theta_{avg,exp}/\theta_{avg,pred}$ for the different compression strut angle prediction models	66
3.9	Key characteristics of specimens referred for concrete contribution to shear resistance study	67
3.10	Geometrical parameters for the different specimens in the test series of Hu and Wu [32], Hu and Wu [31] and Munikrishna et al. [44] respectively	68
3.11	Range of parameters for the specimens studies for evaluation of available concrete contribution to shear resistance models	68
3.12	Range of parameters for the specimens studies for comparison of concrete cracking shear resistance with predictions from various models	68
3.13	$V_{cr,exp}/V_{c,pred}$ ratio for the concrete contribution to the shear resistance at first diagonal crack by different models	73
3.14	$V_{c,avg,exp}/V_{c,avg,pred}$ ratio for the concrete contribution to the ultimate shear resistance by different models (a)	74
3.15	$V_{c,avg,exp}/V_{c,avg,pred}$ ratio for the concrete contribution to the ultimate shear resistance by different models (b)	74
3.16	Statistical parameters for $V_{c,avg,exp}/V_{c,avg,pred}$ ratio for the concrete contribution to the ultimate shear resistance by different models (a)	75
3.17	Statistical parameters for $V_{c,avg,exp}/V_{c,avg,pred}$ ratio for the concrete contribution to the ultimate shear resistance by different models (b)	75
4.1	Key characteristics of experiments and specimens referred for diagonal crack width study	105
4.2	Range of parameters for the specimens studies for comparison of shear crack widths with predictions from various models	106
4.3	Mean shear crack width prediction ratios of the models proposed	107

4.4	Statistical parameters for the predictions of proposed models to evaluate the average diagonal crack width	107
4.5	Average crack width prediction ratios of the models proposewith a shear crack angle equal to 45 degrees	109
4.6	Statistical parameters for the predictions of proposed models to evaluate the mean diagonal crack width with a shear crack angle equal to 45 degrees . . .	110
4.7	The ratio of the experimentally obtained maximum crack width to the average crack width for the reinforced concrete beam specimens [38]	111
4.8	Summary of specimens analyzed for shear deflection study	132
4.9	Range of parameters for the specimens studies for comparison of shear deflection with predictions from various models	132
4.10	Shear-Deflection Results from various models	133
4.11	Statistical parameters for the $\delta_{s,exp}/\delta_{s,pred}$ by different models	133
C.1	Nominal shear capacity as calculated from EC2 VSIM (Variable Strut Inclination Method) and experimental observations.	165
D.1	Input parameters for the specimen B334-120 selected for mean shear crack width calculation from various models.	173
D.2	Calculation of the shear crack width according to the proposed model-IA . . .	173
D.3	Calculation of the shear crack width according to the proposed model-IB . . .	175
D.4	Calculation of the shear crack width according to the proposed model-IIA . .	177
D.5	Calculation of the shear crack width according to the proposed model-IIB . .	179
D.6	Calculation of the shear crack width according to the proposed model-IIIA . .	181
D.7	Calculation of the shear crack width according to the proposed model-IIIB . .	183
D.8	Calculation of the shear crack width according to the proposed model-IV . . .	185
D.9	Calculation of the shear crack width according to the proposed model-V . . .	187
D.10	Input parameters for the specimen S1 selected for shear deflection calculation from various models.	188
D.11	Calculation of the shear deflection according to the proposed model-I	189
D.12	Calculation of the shear deflection according to the proposed model-II	190
D.13	Calculation of the shear deflection according to the proposed model-III	191
D.14	Calculation of the shear deflection according to the proposed model-I	192
E.1	Cost range estimate for the original design method using Delphi-Beta method	214
E.2	Cost range estimate for the proposed design method using Delphi-Beta method	216
E.3	Semi-quantitative Risk register for a shear deficient bridge design for mean shear crack width control under service loads	219

1

Introduction

“Learn from yesterday, live for today, hope for tomorrow. The important thing is not to stop questioning.”

Albert Einstein

This Chapter comprises the introduction to current design practice pertaining to diagonal shear cracks under service loads and motivation behind this MSc thesis project. Moreover, the research objectives, research questions, scope and outline of the thesis are also described.

1.1. Background and Motivation

One of the crucial characteristics of the reinforced concrete structures is the presence of cracks. Although, reinforcement in concrete can not be activated unless there is some cracking in the concrete, the presence of cracks in concrete can jeopardize its serviceability and durability. The guidelines available in the design codes are applicable to flexural and tensile cracks and are not suitable to be directly used for the analysis of shear cracks [65].

An inspection in 2001 reveals extensive cracks in the web of concrete hollow box girders of Grondal bridge in Stockholm, Sweden just after two years of putting the bridge in service (Figure 1.1). After some time, similar problem is reported in the Alvik bridge in Stockholm [29]. The concerned authorities decide to temporarily close the bridges fearing the risk of shear failure. The bridges are designed in accordance with the Swedish codes. However, later it is found that the designs have inadequate shear reinforcement in serviceability limit state. It is observed that the crack width kept on increasing along with an increase in the number of cracks [24]. In general, the average crack width is found to be in the range of 0.1-0.3 mm whereas the maximum crack width is found in the range of 0.4-0.5 mm which is considered to pose problems concerning durability and serviceability of the structure [29]. Thus, it becomes important to evaluate the available models for the prediction of shear crack width under service loads.

The EC2 [19] provides a well-described method for the analysis of flexural and tensile cracks. However, a well-defined method with clear instructions for the calculation of shear crack widths is missing. This may lead to the problem of either under reinforced or over reinforced design for shear load under service load conditions. Both of these scenarios cause an increase in the cost to provide a safe and serviceable structure for use. Figure 1.2 shows schematic diagram of flexural and shear cracks in a slender reinforced concrete beam.

Moreover, the total deflections of the RC beams after shear cracking involves a significant magnitude of shear deformation besides flexural deformation [49]. Figure 1.3 shows the flexural and shear deformations in a portion of the reinforced concrete beam. Although, in the elastic stage only a minor shear deflection is expected, shear cracking may occur even under service loading conditions. This may cause shear deflections as high as up to 25% of the total deflections ([21], [20], [45], [40]). This shear deflection is primarily caused by diagonal shear cracks in concrete. However, in practice the shear cracking (unlike flexural cracking) is not duly considered because of a lack of practical models [28].

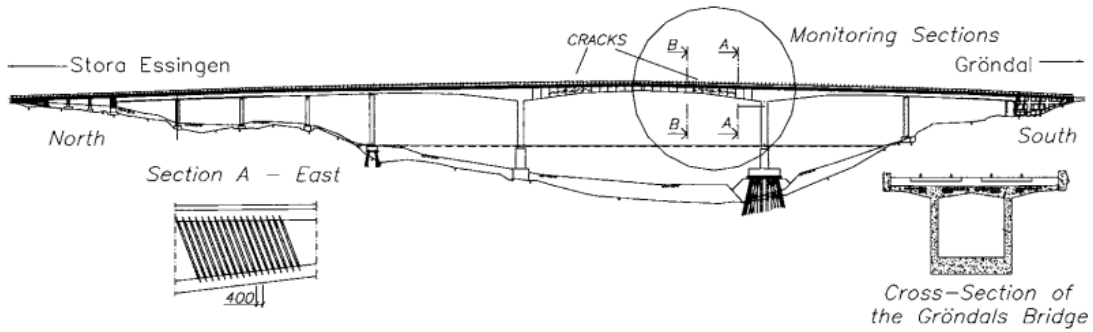


Figure 1.1: The monitoring of web cracking in Grondal bridge [55]

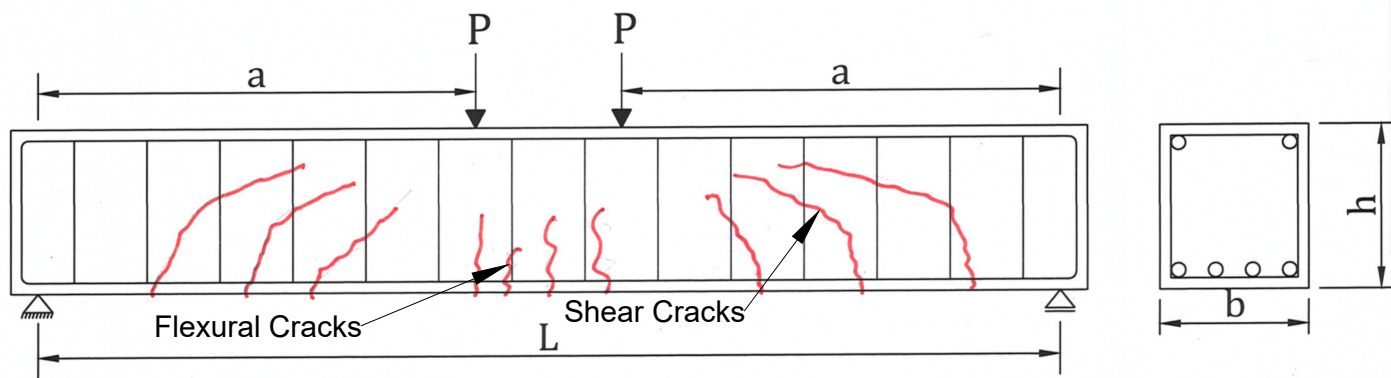


Figure 1.2: Shear cracks and flexural cracks in a RC (Reinforced Concrete) beam

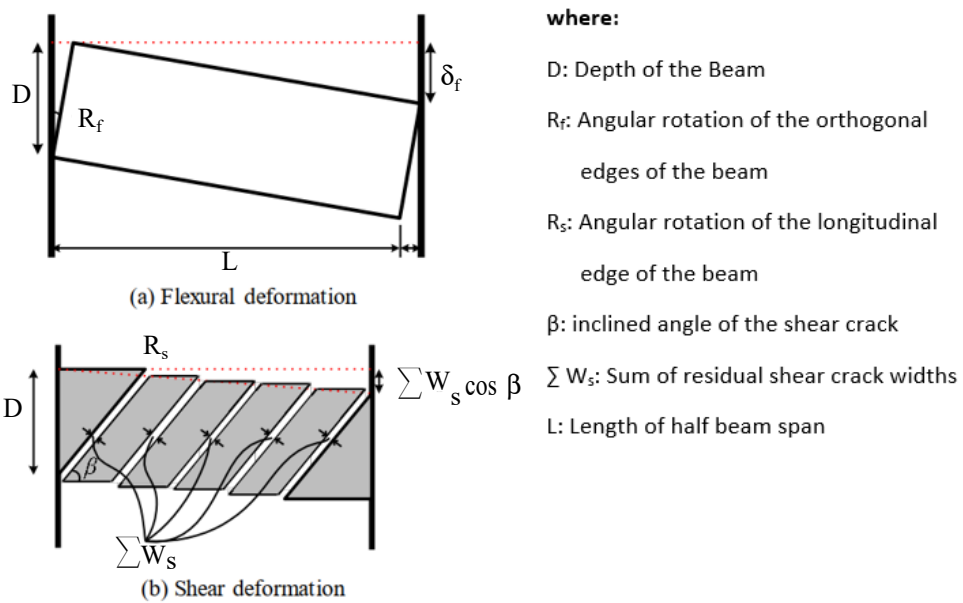


Figure 1.3: Shear and flexural deformations in a RC beam (Adapted from Chiu et al. [13])

1.2. Research Objectives and Methodology

There is a lack of simplified engineering models to predict shear crack width and shear deflection in slender reinforced concrete beams. Therefore, the following research objectives for this MSc thesis project are stated.

1. **To develop an engineering model for prediction of shear crack width in slender reinforced concrete beams.**
2. **To develop a simplified approach to predict shear deflections under service loads for the slender reinforced concrete beams.**

1.3. Research Questions

In order to successfully achieve the aforementioned research objectives, the following research questions are systematically answered in the thesis.

1. **How to develop a robust and effective prediction model for the shear crack width under service loading conditions?**

A comprehensive study of the available models for shear crack width and parameters affecting shear crack width is performed to understand the state of the art. The available models in the literature are compared and the common factors among the various models are identified to understand the most crucial parameters affecting shear crack width. After finding the most crucial factors impacting the shear crack width, the prediction accuracy of the available models in literature to evaluate these individual parameters is assessed by comparing with the experimental observations. The crucial factors in the models giving predictions close to the experimental values are then used to propose models for calculating shear crack width under service loads in slender reinforced concrete beams.

2. **How to develop a simplified approach to predict the shear deflections in the slender reinforced concrete beams under service loads?**

A simplified approach based on the assumption of variation of shear force-deflection response of a slender reinforced concrete beam in a predefined manner is used to develop the proposed models for predicting shear deflection in slender reinforced concrete beams under service loads.

3. **How to validate the proposed model for predicting the shear crack width and shear deflection of the reinforced concrete beams?**

The predictions of shear crack width and shear deflection from the proposed models are compared with and validated against the experimental observations. In this study, experimental data from the literature is referred and no new experiments are performed.

1.4. Scope

The goal of this MSc thesis is to develop an engineering approach for predicting shear crack width in slender reinforced concrete beams. In this study no distinction is made between

the predictions for average crack width of flexural-shear cracks and pure shear cracks in the shear span. The study is limited to the application of short term monotonic service loads. The behaviour under cyclic loading and creep behaviour are not a part of this MSc thesis. The experimental data in the literature is referred for validation in this study and therefore, no experiments are performed. The behavior under flexural cracking lies outside of the scope of this study.

1.5. Outline

Figure 1.4 shows the organization of thesis into various chapters.

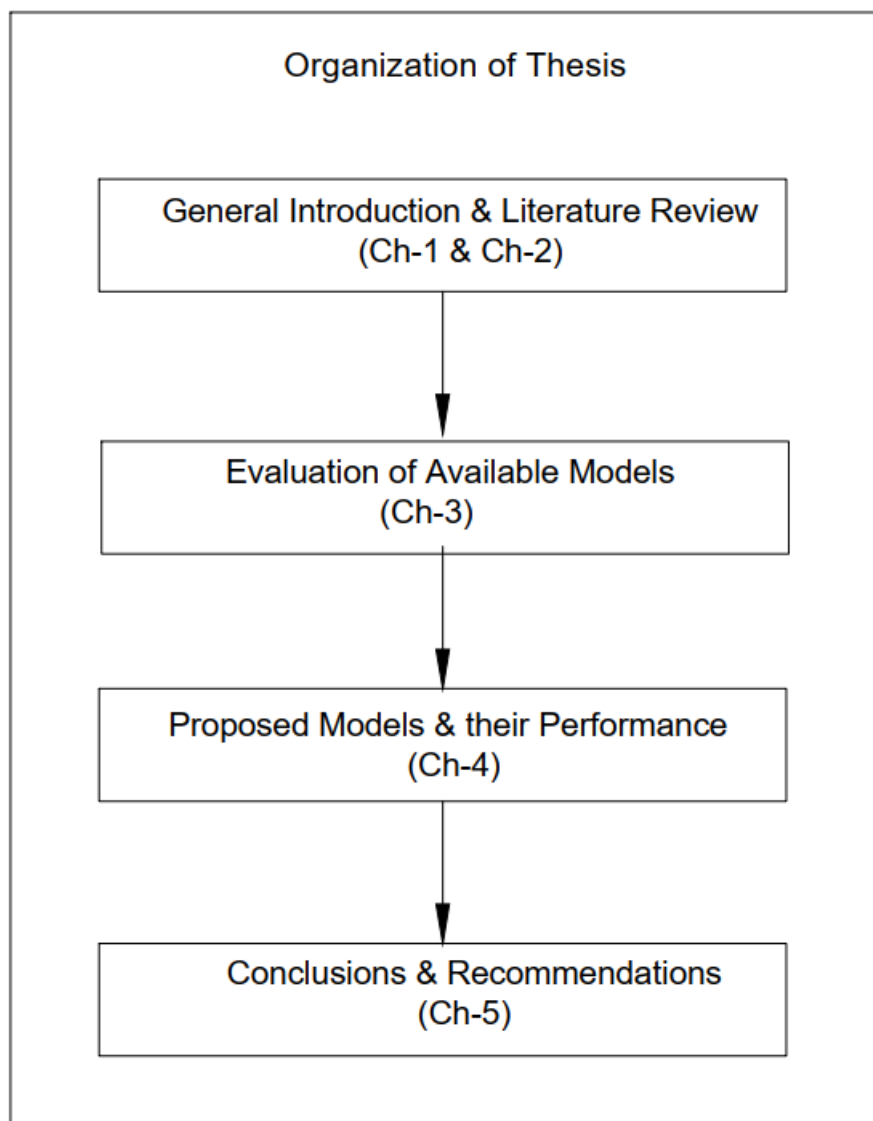


Figure 1.4: Organization of thesis into various chapters

Chapter 2 : This Chapter presents a literature review of the available models for the shear crack width. The crucial parameters affecting shear crack width are identified.

Chapter 3 : This Chapter presents the results of the prediction accuracy of the various models reviewed in Chapter 2) by comparing with experimental observations. The models with predictions closest to the experimental results are identified.

Chapter 4 : This Chapter presents the theoretical background and assessment of the proposed models for shear crack width and shear deflection under service load.

Chapter 5 : This Chapter presents the conclusions of this MSc thesis and a few recommendations for the future work.

2

Literature Review

“The only source of knowledge is experience.”

Albert Einstein

This Chapter begins with a description of two available shear crack width models. It may be noted that there are other available empirical models as well however, these models are presented in Appendix A for a clear and concise discussion. The most crucial parameters affecting shear crack width are then identified. This is followed by the study of available models in literature for the evaluation of these important parameters.

2.1. Shear Cracks in Concrete

Cracking in concrete is governed by the magnitude of principle tensile stresses which are the resultant of bending and shear stresses. Crack occurs at locations where principle tensile stress exceed the tensile strength of concrete. Generally, cracks are initiated in the extreme fiber of the beam where the bending stresses are maximum. However, in case of beams with extremely thin webs, cracks can also arise directly in the web [40]. As we go from the extreme fiber (with maximum bending stress) towards the neutral axis, the orientation of the principle stresses change which depends on the relative values of bending and shear stress. Therefore, the crack orientation changes and cracks are no more perpendicular to the longitudinal axis of the beam. The cracks which initially opened as pure bending (flexural) cracks at the extreme tension fiber of the beam rotate and form the so called flexure-shear cracks. The pure flexural cracks arise in the portion of the beam with zero shear force. Figure 2.1 shows the various types of cracks in concrete.

In the following sections, a review of the shear crack width models and the models for parameters affecting shear crack width is presented. It should be noted there are several empirical models available in the literature for shear crack width and its important parameters. However, the discussion in this Chapter is limited to the models identified as relevant and used later in the development of the proposed engineering models for shear crack width in this MSc thesis. Figure 2.2 shows the overview of the topics discussed in this Chapter.

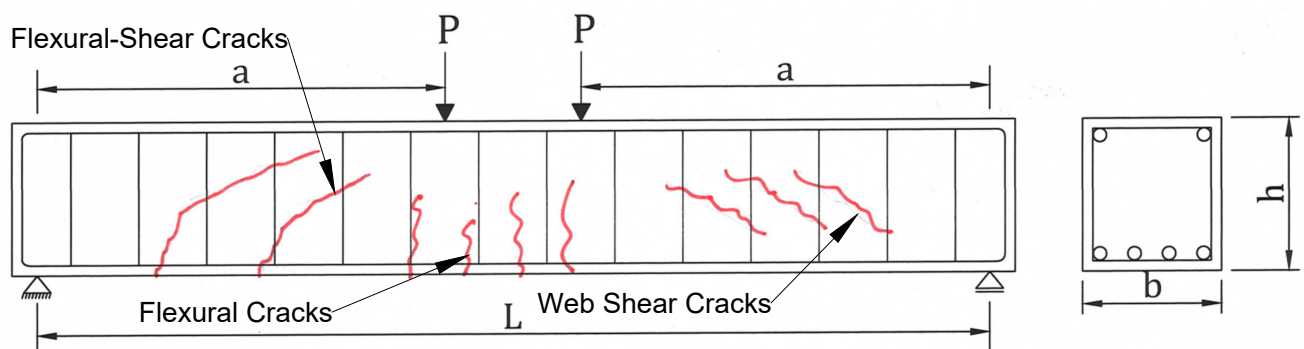


Figure 2.1: Various types of cracks in reinforced concrete beam

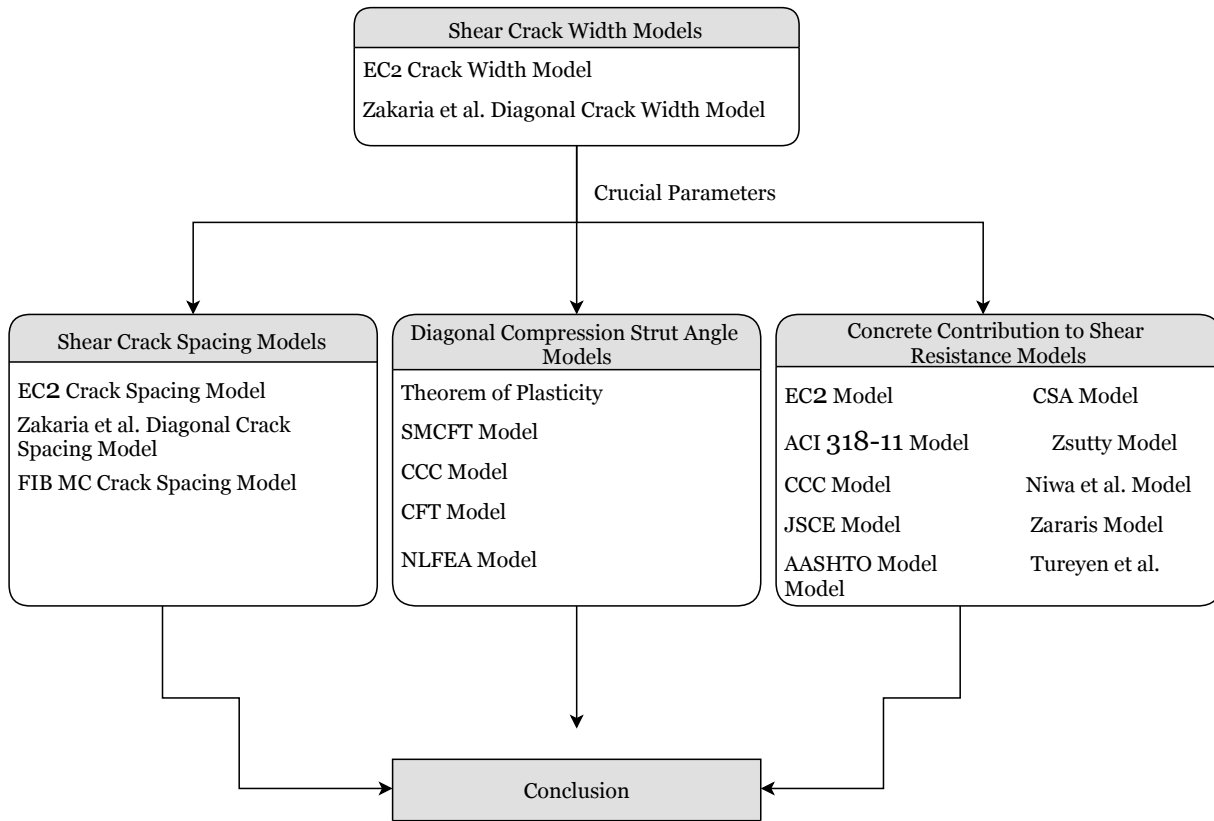


Figure 2.2: Overview of the topics discussed in Chapter 2

2.2. Shear Crack Width

In this section models namely EC2 crack width model and Zakaria et al. [65] crack width model are discussed. It may be noted that in all the equations in this Chapter the default units for the various parameters are in N and mm convention unless stated otherwise.

1. EC2 Crack Width Model [19]

This model is based on the expression of crack width in terms of the mean strain of the reinforcement bar considering the tension stiffening effect of concrete in between the cracks. It is assumed that the mean tensile strain in the reinforcement is absorbed in the crack width over the distance between two cracks. Equation 2.1 is given for the calculation of crack width. It may be noted that w_k seems to be the characteristic crack width (it is not clearly stated) going by the convention used in EC2 to indicate characteristic values with a sub-script k . It may also be maximum crack width. It is important to keep into consideration that this crack width needs to be converted to mean crack width for purpose of comparison with the experimental values.

$$w_k = s_{r,max}(\epsilon_{sm} - \epsilon_{cm}) \tag{2.1}$$

$$\epsilon_{sm} - \epsilon_{cm} = \frac{\sigma_s - k_t \frac{f_{ct,eff}}{\rho_{p,eff}} (1 + \alpha_e \rho_{p,eff})}{E_s} \geq 0.6 \frac{\sigma_s}{E_s} \tag{2.2}$$

where

k_t factor to take into account the duration of the load.
 =0.6 for short-term load.
 =0.4 for long-term load.

The mean strain in the reinforcement over the crack width depends on the stress distribution in the reinforcement as well as the concrete surrounding the reinforcement (Figure 2.3). Once a crack arises in the reinforced concrete, the entire tensile force is taken by the reinforcement at the crack location. However, gradually this force is transferred to the surrounding concrete over a certain distance through bond stresses. At a certain distance concrete carries the original magnitude of tensile force [12]. This minimum distance required by the reinforcement to transmit the forces to concrete is called transfer length. Among other factors, this length is influenced by the bond stress. It is experimentally observed that the bond stress between concrete and reinforcement can be assumed as constant for the purpose of calculation of crack width. Bond stress is expressed by Equation 2.3.

$$\tau_{bm} = 2f_{ctm} \quad (2.3)$$

where

τ_{bm} mean bond stress between the reinforcement bar and concrete.
 f_{ctm} mean axial tensile strength of concrete.

The assumption of constant bond stress leads to linear stress profiles for reinforcement and concrete within the transfer length. The maximum crack width can be expressed as the maximum crack spacing times mean difference in the steel and concrete strain over the transfer length. It may be noted that the predicted crack width is an estimation of the crack width only in the hidden tensile member region around the reinforcement (Figure 2.4).

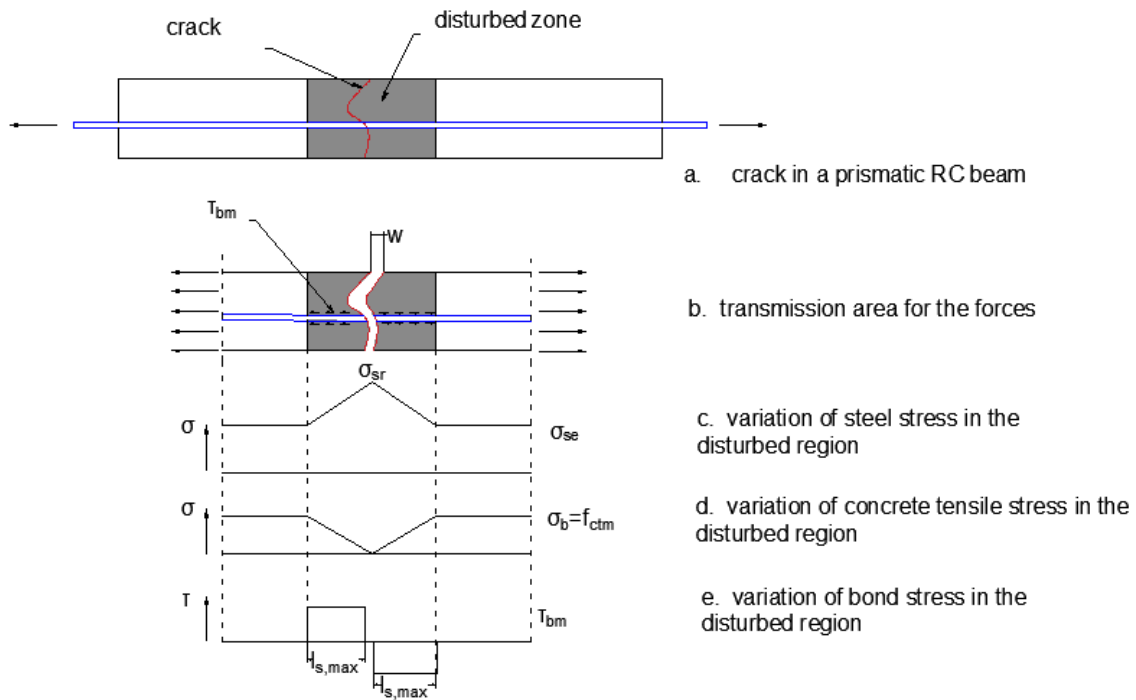


Figure 2.3: Development of bond stresses along the transfer length around a crack

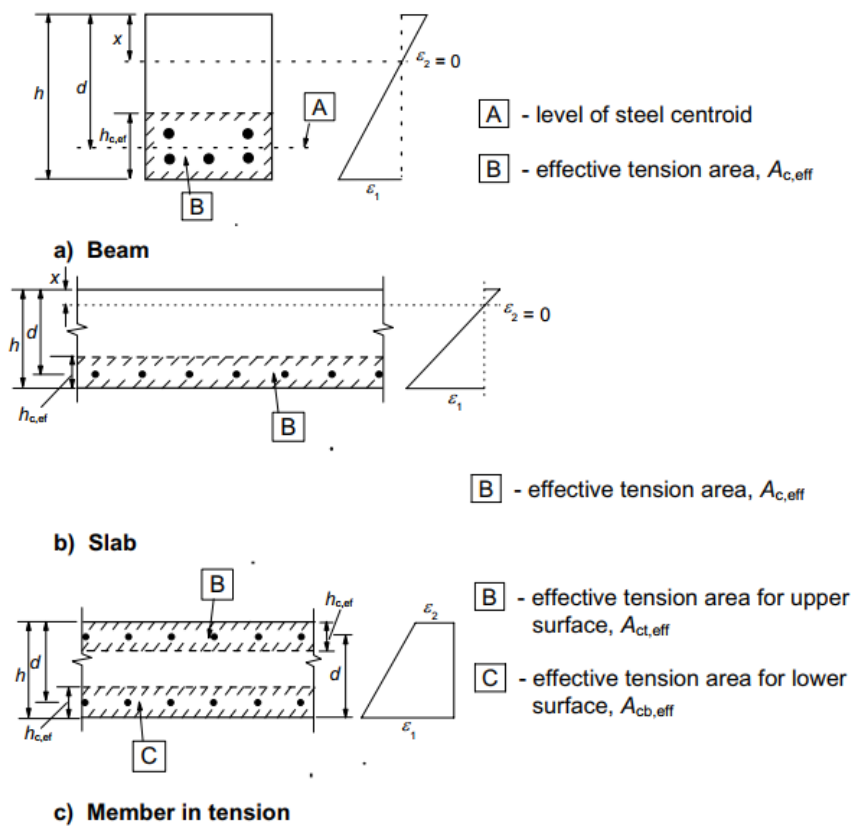


Figure 2.4: Effective height of the hidden tensile member for different structural elements

Assumptions/ Limitations of Model

- (a) The crack is assumed to open perpendicular to the reinforcement.
- (b) The crack width prediction is limited to the effective height of the hidden tensile member.

2. Zakaria et al. Shear Crack Width Model [65]

This model is based on the findings in the experimental study by Zakaria et al. [66]. The authors made the following observations regarding the diagonal crack width in reinforced concrete beams.

- (a) Shear crack width increases proportionately with the increase in the shear crack spacing and shear stirrup strain.
- (b) The shear crack width to shear crack spacing ratio decreases with increase in the transverse and longitudinal reinforcement. This ratio increases with increase in side concrete cover to shear stirrups.
- (c) The shear crack width to shear crack spacing ratio is also influenced by the type of reinforcement bar (deformed or plain reinforcement bar).

The empirical Equation 2.4 is proposed to evaluate the average diagonal shear crack width in reinforced concrete beams.

$$w_{avg} = K(c_s)^a \left(\frac{1}{\rho_w}\right)^b \left(\frac{1}{\rho_t}\right)^c (s_{m\theta-avg}) \epsilon_w \quad (2.4)$$

$$K = 0.112 k_s k_t \quad (2.5)$$

$$w_{max} = k_{max} w_{avg} \quad (2.6)$$

where

K	constant to account for the stirrup type.
k_s	= 1.0 for shear stirrups with conventional closed hook (135°).
k_s	= 1.2 for shear stirrups comprising of two U-shaped lap spliced parts.
k_t	constant to account for the type of shear stirrup rebar.
k_t	= 1.0 for HYSD (High Yield Strength Deformed) bars.
k_t	= 1.2 for plain reinforcement bars.
ρ_w	= $A_w / b_w s_y$.
a, b and c	empirical constants.
a	=0.05
b	=0.207
c	=0.252
k_{max}	correlation factor.
	=1.4

Zakaria et al. [65] perform an extensive review of the available shear crack width models. The equations for these models are included in the Appendix A. Since the proposed model by Zakaria et al. [65] is developed after an analysis of the performance and deficiencies of these models, the analysis of these models is omitted in this thesis for brevity and clarity of the content.

Assumptions/ Limitations of Model

- (a) This model comprises several empirical constants.
- (b) The formula to evaluate the stirrup strain is not given and therefore, in its current form the shear crack width can be calculated only when the stirrup strain is known experimentally.

3. Summary of the Crack Width Models

The most significant parameters for the prediction models for shear crack width are: shear crack spacing, side concrete cover to shear stirrups, shear reinforcement ratio, longitudinal reinforcement ratio, type of shear stirrup bars and shear reinforcement anchorage type. There are certain factors which affect both shear crack spacing and shear crack width such as: shear and longitudinal reinforcement type and ratios, side concrete cover to the shear stirrups etc [65]. Based on the above two models for shear crack width, it is clear that the shear crack spacing, diagonal compression strut angle and the strain in the reinforcement play a crucial role in the determination of shear crack width. Based on the truss analogy for the shear resistance of a beam, the shear stirrup force can be determined by subtracting the concrete contribution to shear resistance for a given applied load. The subsection 2.2.1, subsection 2.2.2 and section 2.3 comprise a discussion about the available models for calculation of shear crack spacing, diagonal compression strut angle and concrete contribution to shear resistance respectively.

2.2.1. Shear Crack Spacing

1. EC2 Crack Spacing Model [19]

(a) Reinforcement bars spaced $<5(c + \phi/2)$ c/c (centre to centre)

This model is derived using the cracking in a tension member model wherein the crack spacing between the two cracks is governed by the transfer length for the forces to get transferred from the steel reinforcement bar to concrete.

According to EC2 [19], if the reinforcement bars are located with respect to each other within a distance of $5(c + \phi/2)$, the maximum crack spacing may be calculated using the Equation 2.7.

$$s_{r,max} = k_3 c + k_1 k_2 k_4 \phi / \rho_{p,eff} \quad (2.7)$$

It is suggested to use ϕ_{eq} where more than one type of reinforcement bar diameters are present. If a section contains n_1 and n_2 reinforcement bars with diameters ϕ_1 and ϕ_2 respectively, then ϕ_{eq} is calculated using Equation 2.8.

$$\phi_{eq} = \frac{n_1 \phi_1^2 + n_2 \phi_2^2}{n_1 \phi_1 + n_2 \phi_2} \quad (2.8)$$

where

c the clear cover to the longitudinal reinforcement.

k_1 coefficient to account for the bond properties of the reinforcement.
= 0.8 for HYSD (High Yield Strength Deformed Bars).
= 1.6 for plain reinforcement bars.

k_2 coefficient to account for the type of strain distribution.
= 0.5 for flexure.
= 1.0 for pure tension.

It may be noted that the recommended values of k_3 and k_4 are 3.4 and 0.425 respectively. The second term on right hand side in the Equation 2.7 arises from the transfer length for the transfer of forces from the reinforcement bars to concrete. The first term on right hand side in the equation effectively provides a lower limit for the maximum crack spacing in case of beams with very high reinforcement ratios.

(b) **Reinforcement bars spaced $>5(c + \phi/2)$ c/c (centre to centre)**

In this case an maximum to the crack spacing is suggested as given in Equation 2.9.

$$s_{r,max} = 1.3(h - x) \quad (2.9)$$

It may be noted that for a shear stirrup this would mean that if the distance between the legs of the stirrups exceeds $5(c_s + \phi_s/2)$ (where c_s and ϕ_s are the side concrete cover to stirrups and shear stirrup diameter respectively) the crack spacing parameter $s_{r,max,y} = 1.3b$ (where b is the cross section width of the beam). The crack spacing in reinforced concrete members where the angle between the axes of principle stresses and the direction of reinforcement $> 15^\circ$ is given by Equation 2.10.

$$s_{r,max} = \frac{1}{\frac{\cos\theta}{s_{r,max,y}} + \frac{\sin\theta}{s_{r,max,z}}} \quad (2.10)$$

where

θ angle between the rebars in y direction and the direction of principle tensile stress as shown in Figure 2.5.

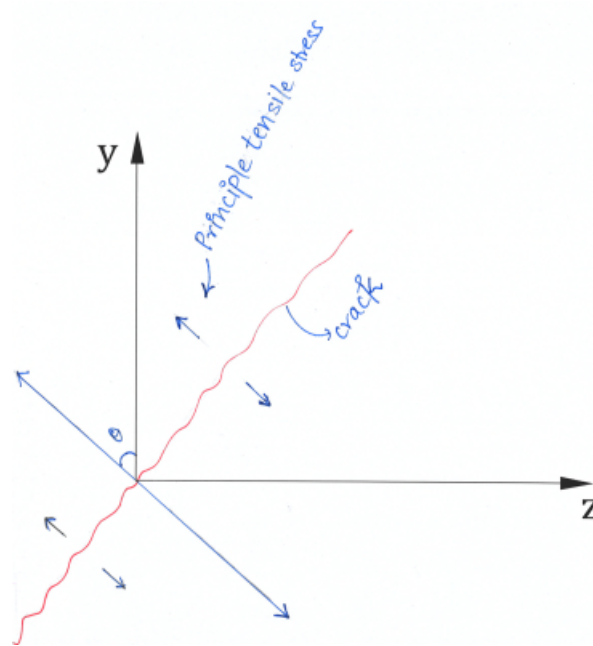


Figure 2.5: The definition of theta in EC2 [19] crack spacing model

It may be noted here that the different shear crack spacing models may look different in terms of taking sine or cosine of theta with respect to the crack spacing control characteristics of reinforcement in a particular direction. However, on close inspection it is clear that they are exactly the same because considering the angle between tensile stress and reinforcement in either longitudinal or transverse direction leads to the trigonometric ratio changing from cosine to sine.

Mean Shear Crack Spacing

In the derivation of the EC2 Crack Spacing Model, the maximum crack spacing corresponds to 2 times the transfer length (for the transfer of forces from reinforcement to concrete). The minimum crack spacing corresponds to the transfer length. Therefore, it can be assumed that the mean crack spacing corresponds to 1.5 times the transfer length. Therefore, the maximum crack spacing from EC2 Crack Spacing Model in Equation 2.10 is multiplied with $(1.5/2)$ to obtain the mean shear crack spacing.

$$s_{r,avg} = 0.75s_{r,max} \quad (2.11)$$

where

$s_{r,avg}$ average shear crack spacing.

Figure 2.6 shows the orientation of the axes as considered in EC2 crack spacing model.

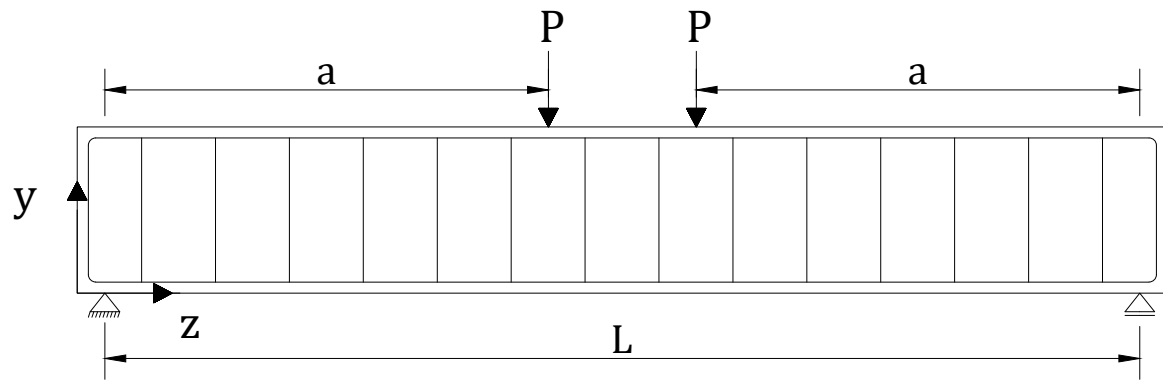


Figure 2.6: The orientation of axes in EC2 [19] crack spacing model

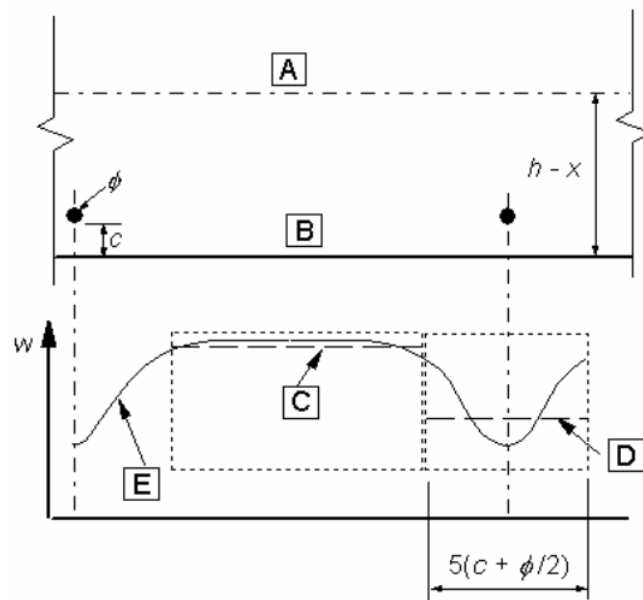


Figure 2.7: Variation of crack width with respect to distance from the reinforcement bars (Adapted from EC2 [19])

Figure 2.7 shows the variation in crack width with respect to the distance from the reinforcement bar.

where

c clear cover to the reinforcement bar.

A neutral axis of the beam.

B concrete tension zone surface.

C predictions of the crack spacing from Equation 2.9.

D predictions of the crack spacing from Equation 2.7.

E actual crack width on the beam surface.

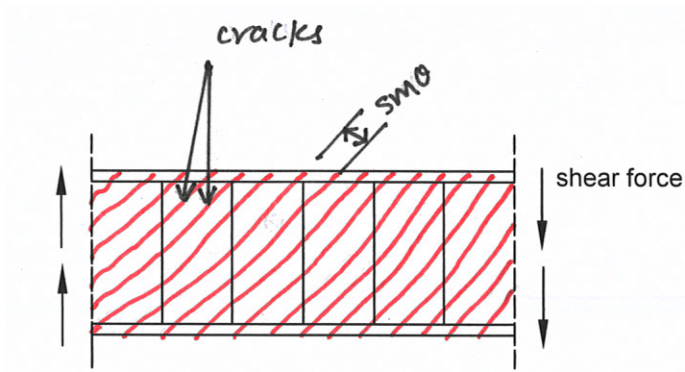


Figure 2.8: Assumed diagonal shear cracks at a constant crack spacing

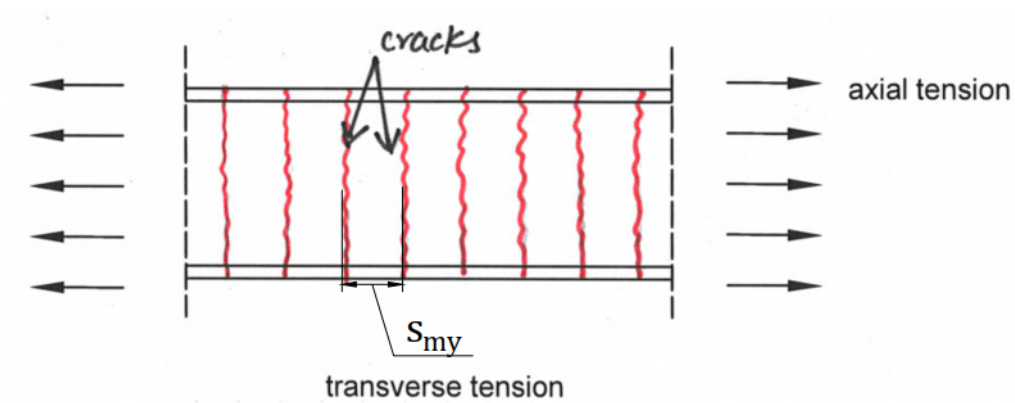


Figure 2.9: Assumed horizontal cracks caused by transverse tension with crack spacing s_{my} in between the two adjacent cracks

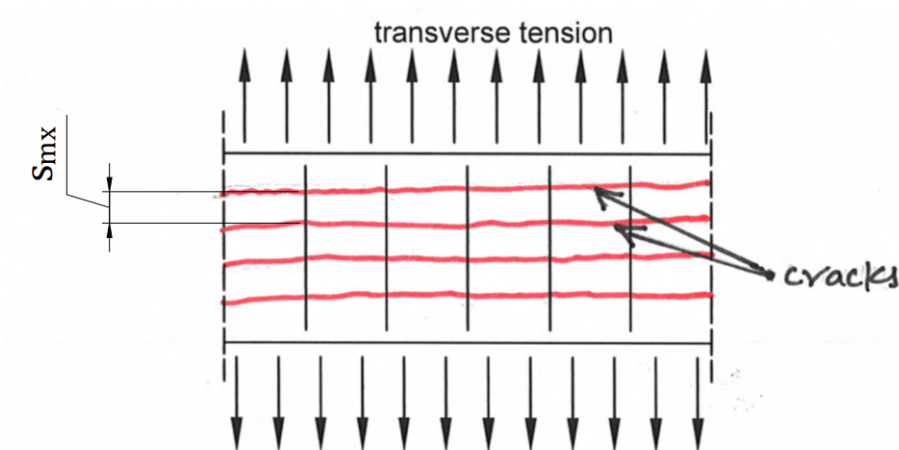


Figure 2.10: Assumed vertical cracks caused by axial tension with crack spacing s_{mx} in between the two adjacent cracks

Assumptions/ Limitations of Model

- (a) This model lacks a description about the crack control characteristics of reinforcement in transverse direction.
- (b) The shear cracks are assumed parallel to each other and at a constant spacing.

2. fib MC Crack Spacing Model [23]

The Equation 2.12 is proposed to obtain the maximum crack spacing for reinforced concrete members with reinforcements in orthogonal directions.

$$l_{s,max} = \left(\frac{\cos\theta}{l_{sx,k}} + \frac{\sin\theta}{l_{sy,k}} \right)^{-1} \quad (2.12)$$

where

θ is the angle between the reinforcement in x direction and direction of tensile stress (Figure 2.11).

$$l_{sx,k} = \frac{1}{4} \frac{f_{ctm}}{\tau_{bm}} \frac{\phi_s}{\rho_s} \quad (2.13)$$

It may be noted here that for a stabilized cracking stage and for short term loading τ_{bm} is equal to $1.8f_{ctm}$ [23]. Figure 2.12 shows the orientation of the axes in the fib MC [23] crack spacing model.

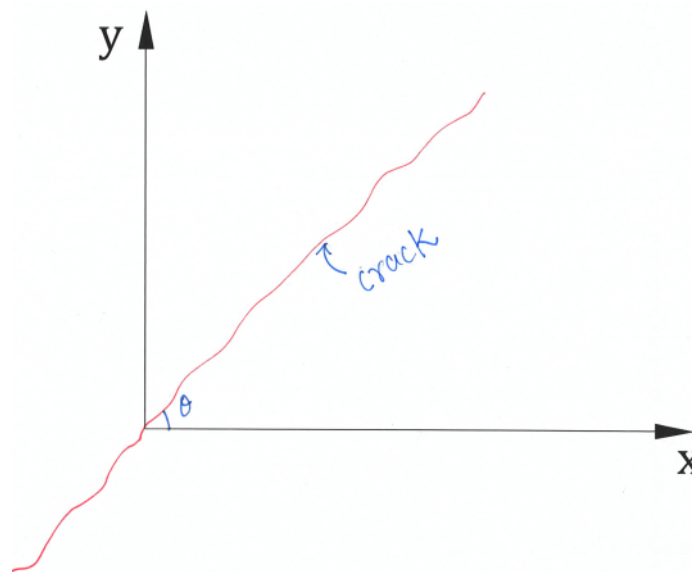


Figure 2.11: The definition of theta in fib MC [23] crack spacing model

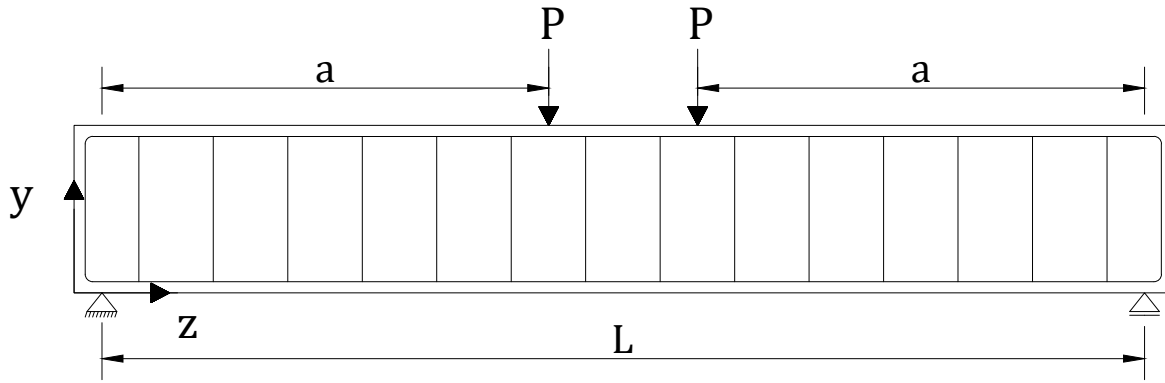


Figure 2.12: The orientation of axes in fib MC 2010 [23] crack spacing model

Assumptions/ Limitations of Model

The shear cracks are assumed parallel to each other and at a constant spacing.

3. Zakaria et al. Crack Spacing Model [65]

The Equation 2.14 is proposed based on the harmonization of the CEB-FIP MC 1978, CEB-FIP MC 1990 and Collins and Mitchell Model. The original CEB-FIP (1978) [18], the crack control characteristics of the longitudinal reinforcement $s_{m,x}$ is not included. This factor is introduced by Zakaria et al. Moreover, it may be noted here that SMCFT [7] suggests the simplification to use the crack control characteristic parameter of the longitudinal reinforcement $s_{m,x}$ equal to the vertical spacing (along the height of the beam) between the longitudinal reinforcement in the longitudinal cross section plane. However, this spacing is not considered either in the EC2 crack spacing model, or in the Zakaria et al. crack spacing model.

$$s_{\theta} = \frac{1}{\frac{\sin\theta}{s_{m,x}} + \frac{\cos\theta}{s_{m,y}}} \quad (2.14)$$

$$s_{m,x} = 2 \left(c_x + \frac{s_x}{10} \right) + k_1 k_2 \frac{d_{bx}}{\rho_x} \quad (2.15)$$

$$s_{m,y} = 2 \left(c_s + \frac{s_y}{10} \right) + k_1 k_2 \frac{d_{by}}{\rho_y} \quad (2.16)$$

$$\rho_x = \frac{A_s + A_{ps}}{A_{cx,ef}} \quad (2.17)$$

$$A_{cx,ef} = 2.5(h - d_e) b_w \quad (2.18)$$

$$d_e = \frac{A_s d + A_{ps} d_p}{A_s + A_{ps}} \quad (2.19)$$

$$\rho_y = \frac{0.5 A_w}{A_{cy,ef}} \quad (2.20)$$

$$A_{cy,ef} = \min(2.5(c_s + d_{by}/2) s_y, (b_w/2) s_y) \quad (2.21)$$

where

$$s_y \leq 15d_{by}.$$

k_1 factor to account for the bond characteristics of the reinforcement.

= 0.4 for HYSD bars.

= 0.8 for plain reinforcement bars.

k_2 factor to account for the shape of the stress distribution.

= 0.125 for in flexure.

= 0.25 for the pure tension.

Figure 2.13 shows the various crack spacing parameters used in this model. The authors also perform a review of the available diagonal crack spacing models [65]. The equations for these models are included in the Appendix A. Since the the proposed model by Zakaria et al. [65] is developed after an analysis of the performance and deficiencies of these models, the analysis of these models is omitted in this thesis for brevity and clarity of the content.

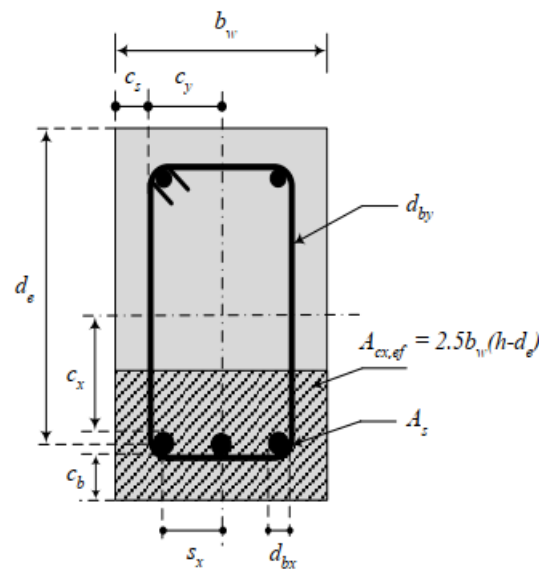


Figure 2.13: Various geometrical parameters used in the shear crack spacing model [65]

Assumptions/ Limitations of Model

The shear cracks are assumed parallel to each other and at a constant spacing.

4. Summary of the Shear Crack Spacing Models

The review of the available shear crack-spacing models leads to the following inferences.

- (a) The most significant parameters for shear crack -spacing based on the review of the available models are: shear crack orientation θ , location of the longitudinal and shear reinforcement in the cross section, shear reinforcement and longitudinal reinforcement ratios (ρ_l and ρ_w) and effective concrete areas around the stirrups and longitudinal rebars, bond properties of shear stirrups and longitudinal reinforcement [65].

- (b) It is recognized the shear crack spacing is governed by the crack control characteristics of both longitudinal and transverse reinforcements which is often represented by calculating the horizontal and vertical crack spacing components s_x and s_y . These vertical and horizontal cracks spacing are the spacings which would occur when cracking occurs perpendicular to the longitudinal and shear reinforcement respectively. The reinforcement diameters and reinforcement ratios appear to be the basic parameters which influence the shear crack spacing.
- (c) The position of the stirrups from the edge or the center of a cross section is also included as a parameter influencing shear crack spacing in the various models (mentioned in this Chapter as well as those in Appendix A). Similarly, effective depth of the beam and the cover to the longitudinal reinforcement are used to account for the position of the longitudinal reinforcement.
- (d) One of the primary parameters mentioned in most of the shear crack width models is the stirrup strain. The shear crack spacing is evaluated using the product of stirrup strain with shear crack spacing in majority of the models. The shear stirrup percentage is also a parameter that affected the shear crack width either directly or through shear crack spacing.
- (e) There are a limited number of models available to calculate the shear crack angle. The compression strut angle is close to the shear crack angle but not exactly the same [65]. If we compare the crack spacing models of EC2 [19] with fib MC [23] and model given by Zakaria et al. [65], the definition of the angle theta seems to be different. In EC2 [19], the angle theta is the angle between the reinforcement in y direction and tensile stresses while it the angle of compression strut (approximately equal to the shear crack angle) in the fib MC [23] and Zakaria et al. [65] model. This difference in definition is the reason for the reversed sine and cosine angles in the denominator of the $s_{m\theta-avg}$ expression in these models. Therefore, these apparently different forms of angle lead to similar expressions ultimately.
- (f) From the literature review, it is inferred that the value of the effective area around longitudinal and shear reinforcement is a crucial factor in determining the predicted values.
- (g) It can be seen that the different models assigned different significance to the parameters like shear and longitudinal reinforcement ratios, strains and shear and longitudinal reinforcement placement in the cross section etc. based on empirical fitting. However, these parameters may not be exhaustive when it comes to the shear cracking behavior under service loads. For instance, it is known that shear crack width varies along the crack trajectory [65]. Hence, it must be influenced by the distance of the location of measurement from the stirrups, longitudinal reinforcement and the crack tip etc.

2.2.2. Diagonal Compression Strut Angle

1. Theorem of Plasticity [19]

In the conventional truss analogy for a reinforced concrete beam, it is assumed that the shear force is carried by the compression struts once the shear reinforcement begins to yield [28]. The diagonal compression strut can be obtained using the Theorem of Plasticity by equating yield force in the shear stirrups to the diagonal compression strut capacity. In this theory, it is assumed that the strut would rotate to smaller values of angle as the force increases beyond the yield force of the steel reinforcement and the ultimate failure is characterized the crushing of the diagonal strut. The Equation 2.22 for θ can be obtained [48].

$$\theta = \sin^{-1} \sqrt{\frac{A_{sw} f_{yw} m}{b_w s_v v_1 \alpha_{cc} f_{cm}}} \quad (2.22)$$

$$v_1 = 0.6 \left(1 - \frac{f_{cm}}{250} \right) \quad (2.23)$$

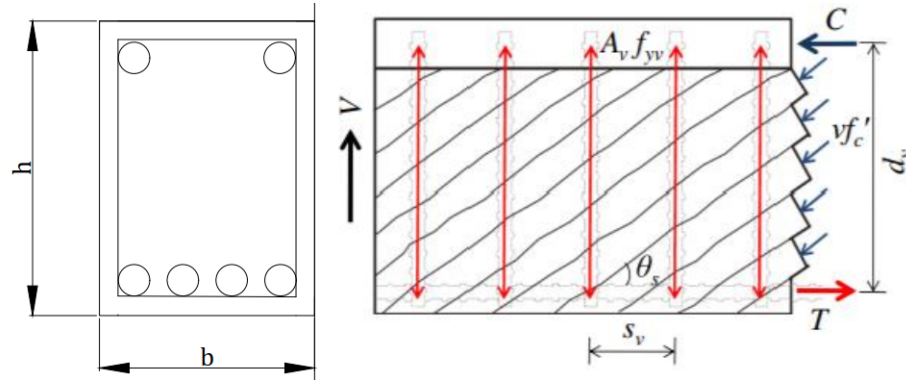


Figure 2.14: The condition for strut inclination at failure [28]

Assumptions/ Limitations of Model

The model assumes a constant value of the compression strut angle throughout the shear span.

2. SMCFT Model [7]

The determination of the diagonal compression strut angle is based on the compatibility of strains between the shear stirrup strains and the concrete strain and the equilibrium between the concrete and stirrup stresses. The theory assumes that the critical crack is aligned at a normal direction to the direction of principle tensile strain. According to the SMCFT [7], the angle of inclination can be obtained using Equation 2.24.

$$\theta = 29 + 7000 \varepsilon_x \quad (2.24)$$

It may be noted that the angle θ in Equation 2.24 is in degrees. SMCFT is obtained by making a few assumptions in the MCFT. It is assumed that the failure shear stress is $0.25 f_c$ (where f_c is the cylindrical compressive strength of concrete). The principle compressive stress-strain relationship is assumed as linear on account of the low

magnitude of compression stresses. The value of θ is obtained from curve fitting of the observations made for θ versus ϵ_x (longitudinal strain). An additional assumption of crack spacing equal to 300mm is made for the concrete members with reinforcements in orthogonal directions. The general shear provisions of the CSA-2004 code [5] are based on MCFT [57]. The longitudinal strain " ϵ_x " in the Equation 2.24 can be obtained using Equation 2.25 [5].

$$\epsilon_x = \frac{\frac{M_E}{d_v} + V_E}{2E_S A_S} \quad (2.25)$$

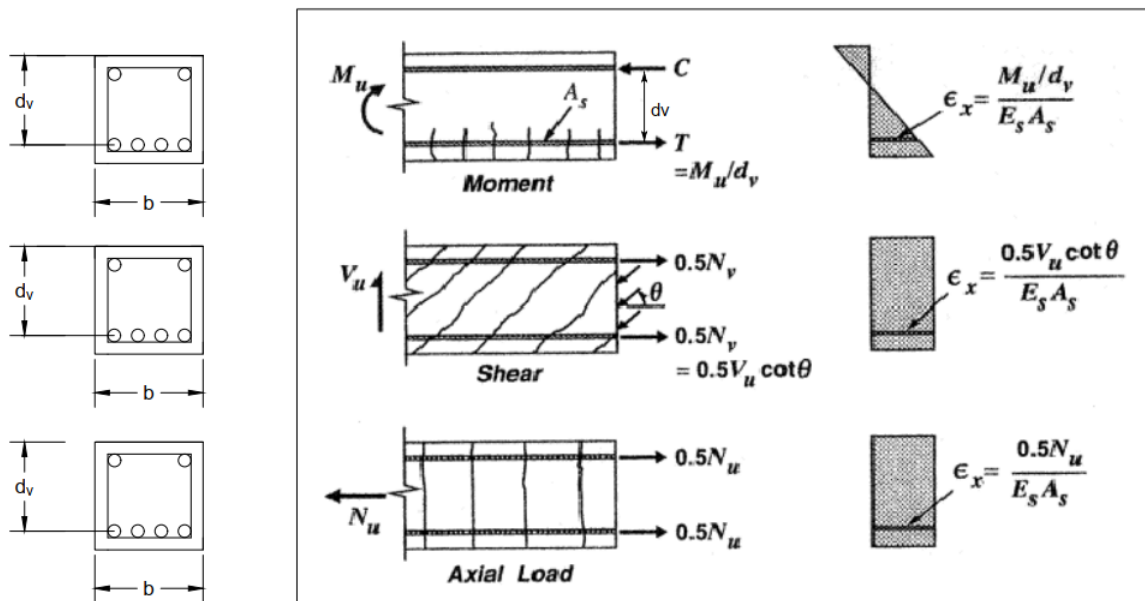


Figure 2.15: Determination of longitudinal strain in a reinforced concrete non-prestressed beam [4]

Figure 2.15 shows the contribution of the moment, shear force and axial force in the determination of the axial strain in the longitudinal reinforcement bars.

Assumptions/ Limitations of Model

- The model assumes a failure shear stress equal to $0.25f_c$.
- The clamping stress in the transverse direction is assumed equal to zero.
- The diagonal crack spacing is assumed equal to 300 mm in the model.

3. CCC Model [15]

This model give the inclination of the critical flexural shear crack in reinforced concrete beam. The critical crack is assumed as the crack closest to the section with zero bending moment. It is assumed that the critical flexural shear crack opens when the bending stress in the extreme fiber of the cross section reached the flexural tensile strength. It is observed through experiments that the horizontal projection of the first branch of the flexural shear crack could be approximated as almost equal to $0.85d$

(see Figure 2.16). The model states that the inclination of the diagonal compression strut is equal to the mean angle of the shear crack and is given by the Equation 2.26.

$$\cot\theta = \frac{0.85d_s}{d_s - x} \leq 2.50 \quad (2.26)$$

It is important to note here that Equation 2.26 is applicable for stresses at or after the yielding of the reinforcement [31].

where

x : depth of neutral axis of the cracked section of a prestressed concrete beam evaluated using the assumption of zero concrete tensile strength. Moreover, it is assumed that concrete in compression zone is in linear elastic zone.

x = x_o (for reinforced concrete beams without axial load).

d_s : effective shear depth.

$$\frac{x_o}{d} = \alpha_e \rho_l \left(-1 + \sqrt{1 + \frac{2}{\alpha_e \rho_l}} \right) \approx 0.75(\alpha_e \rho_l)^{\frac{1}{3}} \quad (2.27)$$

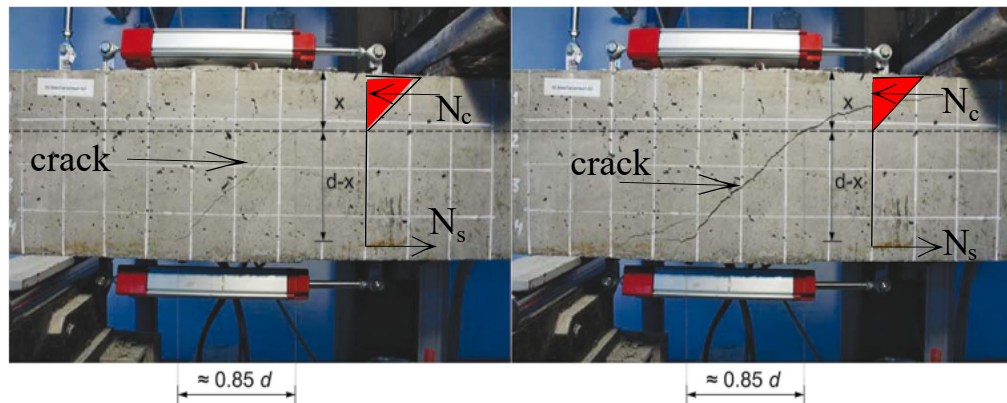


Figure 2.16: Evolution of the critical shear crack (adapted from [15])

Assumptions/ Limitations of Model

The horizontal projection of the first branch of flexural-shear crack is assumed equal to $0.85d$.

4. CFT Model [16]

This theory assumes that the concrete element resists the externally applied shear stress by generating tensile stresses in both transverse and longitudinal reinforcement and compressive stress in concrete. The crack pattern is simply assumed as a series of parallel cracks all inclined at an angle θ to the longitudinal reinforcement. Figure 2.17 shows the summary of the equilibrium, compatibility and constitutive relations according to this theory. The rearrangement of the equations shown in Figure 2.17 for linear elastic reinforcement response give Equation 2.28 to calculate the

diagonal compression strut angle (or the inclination of the principle stress in this case).

$$\tan^4 \theta = \frac{1 + \frac{1}{n\rho_l}}{1 + \frac{1}{n\rho_t}} \quad (2.28)$$

where n : modular ratio = E_s/E_c .

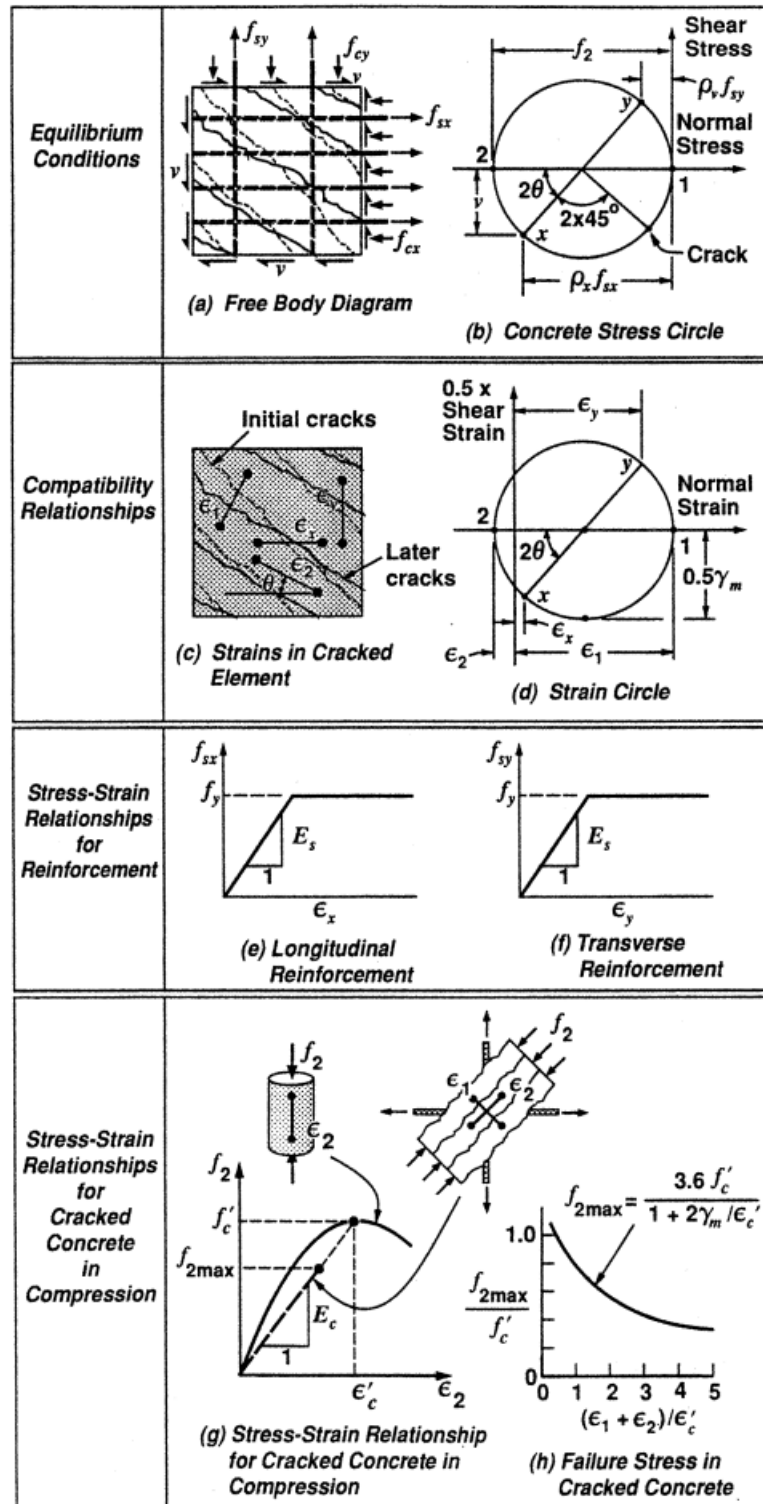


Figure 2.17: Compression Field Theory [4]

Assumptions/ Limitations of Model

The application of the model is limited to situations where reinforcement response is in linear elastic range.

5. NLFEA Model (Ueda et al. Model) [56]

The authors perform NLFEA to find the inclination of the principle compressive stress in shear reinforced concrete beams and propose the Equation 2.29 and Equation 2.30 to evaluate the diagonal compression strut angle (in degrees).

$$\theta = -\alpha(v - v_o)^2 + \theta_o \quad v_o \leq v \leq 1.7v_c \quad (2.29)$$

$$\theta = \theta_1 \left(\frac{1.7v_o}{v} \right)^\beta \quad 1.7v_c \leq v \quad (2.30)$$

$$\theta_o = 3.2 \left(\frac{a}{d} \right) + 40.2 \quad a/d > 1.5 \quad (2.31)$$

$$\theta_1 = -\alpha(1.7v_c - v)^2 + \theta_o \quad (2.32)$$

$$v_o = 0.9v_c \quad (2.33)$$

$$v_c = 0.2f_c^{\frac{1}{3}} (100\rho_t)^{\frac{1}{3}} (1/d)^{\frac{1}{4}} \left(0.75 + \frac{1.4}{a/d} \right) \quad (2.34)$$

$$\alpha = 0.4 \left(\frac{a}{d} \right)^2 + 2.9 \quad (2.35)$$

$$\beta = (0.7 - 32\sqrt{\rho_t\rho_w}) \frac{a}{d} \quad (2.36)$$

where

v is nominal shear stress.

V applied shear force.

v_c is nominal shear stress at first diagonal cracking.

ρ_t longitudinal tensile reinforcement.

a/d shear span ratio (>1.5).

$$v = \frac{V}{bd}$$

Assumptions/ Limitations of Model

The model is applicable for beams with $a/d > 1.5$.

6. Summary of the Diagonal Compression Strut Angle Models

It is stated and experimentally observed that the angle of diagonal compression strut angle is more or less close to the shear crack angle ([4], [65], [41]). The Theorem of Plasticity predicts the diagonal compression strut angle at ULS. A unique value of θ (diagonal compression strut angle) which is independent of the applied shear force is obtained. The predictions given by SMCFT [7] and [16] are based on the compliance with equilibrium and compatibility conditions of diagonally cracked concrete member with orthogonal reinforcement bars. The CFT [16] give a constant value of θ similar to the Theorem of Plasticity model. However, the predictions given by SMCFT [7] and NLFEA model [56] are based on the magnitude of applied shear stress on the beam. Both the models allow for the reduction of the compression strut angle as the applied shear force increases.

2.3. Concrete Contribution to Shear Resistance Models

2.3.1. Force Transfer in a Shear Reinforced Beam

Many design codes in practice use sectional design approach for the shear resistance of reinforced concrete beams. Truss analogy for beams is one such approach which is introduced as early as 1900s. The beam with diagonal shear cracks can be idealized as a truss for analysis and design purposes. Figure 2.18 shows the schematic presentation of various discretized truss components of a reinforced concrete beam. The idealized truss comprises of the diagonal compression strut (of concrete), horizontal concrete compression chord at the top, horizontal tension chord at the bottom (longitudinal tension reinforcement) and vertical ties (stirrups) [41]. The diagonal concrete compression struts transfer the external force to the vertical tension ties. The shear resistance in the truss analogy therefore, primarily comes from the vertical ties (or stirrups). The flexural resistance comes from the horizontal top and bottom chords. While the concrete contribution to the shear resistance is ignored in the conventional models, recently a greater number of design codes recognize this concrete contribution and adopt a combination of shear resistance of steel ties from the truss analogy in combination with an additional term for concrete contribution [4].

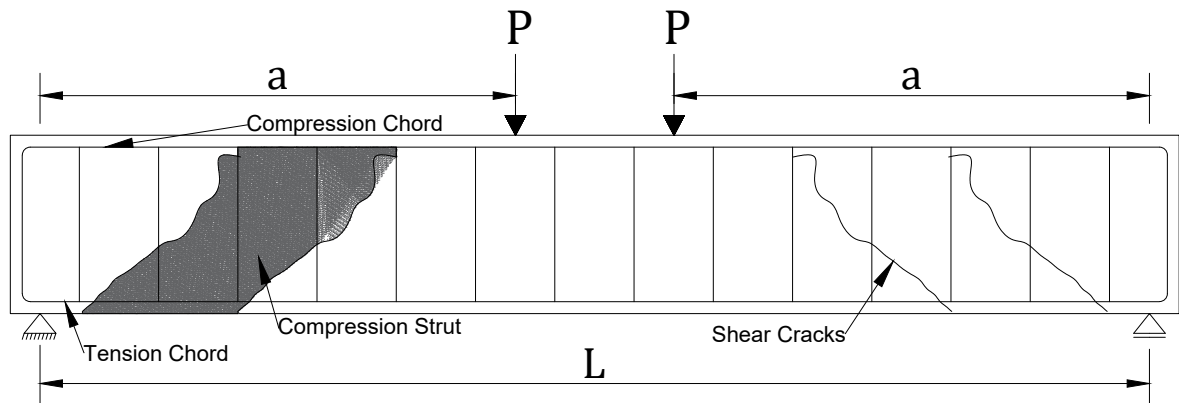


Figure 2.18: Truss analogy for a shear reinforced beam subjected to shear and flexure force

2.3.2. Shear Transfer Action Types

There is a consensus in the literature regarding the application of additive model (i.e total shear resistance as a sum of shear strength contribution from concrete and steel respectively) to calculate the total shear resistance of concrete [4]. The concrete contribution to shear resistance comes from various individual components otherwise called shear transfer actions in this study. The different shear transfer actions are shown in Figure 2.19. The different shear transfer actions of dowel action, aggregate interlock and concrete compression zone can be merged together and represented by a single term V_c . Therefore, the total shear resistance V can be obtained using Equation 2.37.

$$V = V_c + V_s \quad (2.37)$$

where

V_c concrete contribution to shear resistance.

Conventionally, in the experiments the shear resistance contribution from the stirrups is

measured using the strain values in the stirrups obtained with the installed strain gauges. Thereafter, the concrete contribution to the shear resistance is calculated. Figure 2.20 shows the various shear transfer mechanisms comprising the concrete contribution to total shear resistance. The various shear transfer mechanisms comprising the shear resistance are briefly described below.

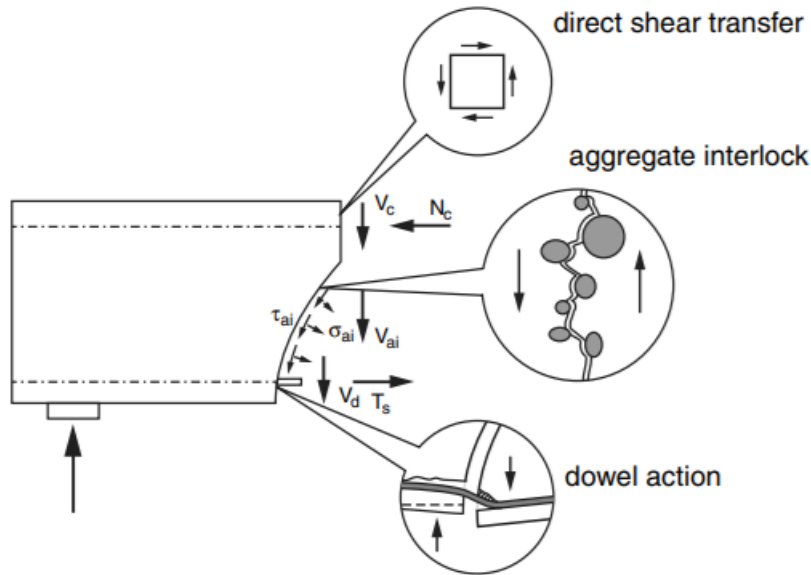


Figure 2.19: Different shear strength transfer mechanisms of a reinforced concrete beam without shear reinforcement Yang [62]

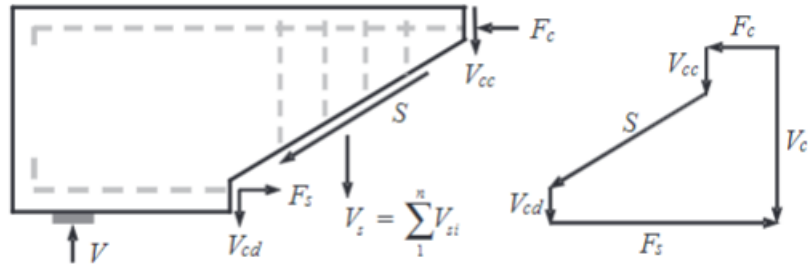


Figure 2.20: Different shear strength components of a reinforced concrete beam with shear reinforcement (Hu and Wu [32])

1. **Aggregate Interlock Effect**

This effect comes into picture due to the protruding aggregates between the two cracked surfaces. The tangential and normal displacements between the two cracked surfaces lead to the development of compressive and normal stresses. The protruding aggregates resist the slipping between the two surfaces and thereby help in transmitting the shear. The magnitude of aggregate interlock effect depends on the crack width. It decreases sharply with increase in crack width. This effect decreases with decrease in the size of aggregate since smaller aggregates implies smoother crack

plane surface. The aggregate interlock effect for a high strength concrete is lower than for a normal strength concrete due to the cracks passing through aggregates (which actually are responsible for bridging the crack surface and provide aggregate interlocking shear resistance in case of normal strength concrete) instead of the cement fine aggregate matrix in high strength concrete.

2. Uncracked Concrete Compression Zone Contribution

The uncracked compression zone of concrete is subjected to shear stress along with compression. The contribution of this zone to the shear resistance depends on the depth of compression zone. For slender beams at ULS, the contribution of compression zone to shear resistance is small owing to its small depth.

3. Dowel Action

This shear resistance mechanism come into action because of the ability of the longitudinal reinforcement to resist shear force perpendicular to its axis. The dowel action provides shear resistance through either bending, shear or kinking action as shown in Figure 2.21.

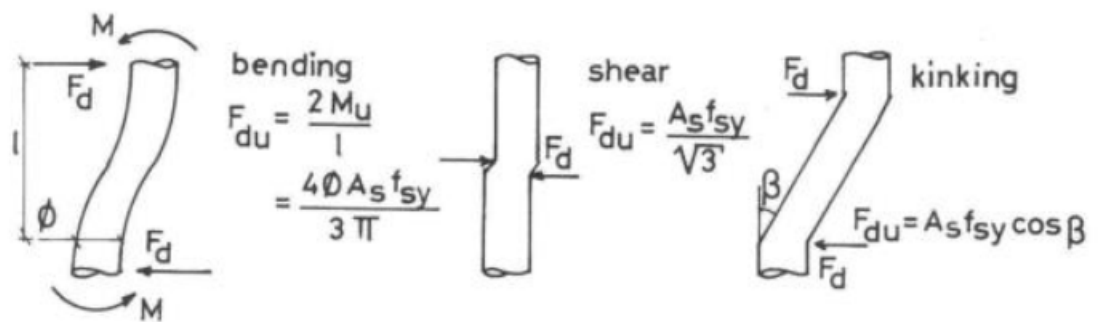


Figure 2.21: Different mechanisms of shear transfer by dowel action [50]

In the above Figure 2.21,

l denotes the free length over which deformations occur in the reinforcement bar. The other symbols have their usual meanings.

4. Residual Tensile Stresses

When the crack width is small ($<0.1\text{mm}$), the cracked concrete still has a residual tensile strength to transmit the shear forces across cracks. However, when the crack width is larger ($>0.1\text{mm}$), the contribution of this shear transfer mechanism is about 10 times smaller than the aggregate interlock effect [63].

5. Axial Resistance of Shear Stirrups

This is one of the most significant shear transfer mechanism in a shear reinforced beam. The shear resistance in this mechanism arises from the component of the stress (in stirrups) perpendicular to the crack plane. Besides carrying the shear force, stirrups also confine the growth of diagonal cracks in beams.

2.3.3. Concrete Contribution to Shear Resistance Models

ASCE-ACI Committee 426 [3] recommends that the concrete resistance to the shear resistance of the shear reinforced concrete beams can be considered identical to the concrete contribution to the shear resistance in case of reinforced concrete beams without shear reinforcement. Thus, this section summarizes numerous approaches to evaluate the concrete contribution to the shear resistance as given by various researchers for the shear reinforced beams as well as models provided to evaluate the shear resistance of reinforced concrete beams without shear reinforcement (in this study the failure load or the ultimate shear resistance of the shear un-reinforced beam is assumed to be equal to the concrete contribution to the shear resistance in case of shear reinforced beams).

1. EC2 Shear Resistance of Shear Un-reinforced Beams Model [19]

Equation 2.38 is proposed to evaluate the shear resistance of shear un-reinforced concrete beams.

$$V_{Rd,c} = [C_{Rd,c} k (100 \rho_l f_{ck})^{\frac{1}{3}} + k_1 \sigma_{cp}] b_w d \quad (2.38)$$

with a minimum value given by Equation 2.39.

$$V_{Rd,c} = (v_{min} + k_1 \sigma_{cp}) b_w d \quad (2.39)$$

where

$$k = 1 + \sqrt{\frac{200}{d}} \leq 2.0 \quad (2.40)$$

$$\rho = \frac{A_{sl}}{b_w d} \leq 0.02 \quad (2.41)$$

A_{sl} Cross sectional area of the longitudinal reinforcement extended to a section $\geq l_{bd} + d$ past the section under consideration.

b_w smallest width of the cross-section in the tensile region.

$\sigma_{cp} = \frac{N_{Ed}}{A_c} < 0.2 f_{cd}$

A_c area of cross-section of concrete (in mm^2).

The recommended values of various parameters are given below.

$C_{Rd,c}$ 0.18/ γ_c .

k_1 0.15.

v_{min} $0.035 k^{\frac{3}{2}} f_{ck}^{\frac{1}{2}}$.

where

Figure 2.22 shows the definition of A_{sl} as specified in EC2 (2004).

The term v_{min} is defined as the minimum mean shear stress at which opening of a flexural shear crack in a shear un-reinforced beam occurs simultaneously with the yielding of the longitudinal tension reinforcement. This term facilitates the calculation of the minimum shear capacity for the members with very low amount of flexural reinforcement [61].

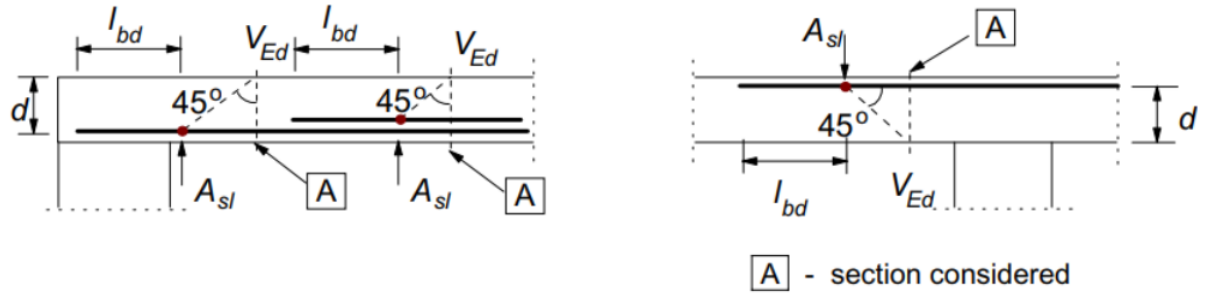


Figure 2.22: The longitudinal reinforcement in Equation 2.41 [19]

In the Figure 2.22, l_{bd} : is the design anchorage length.

Assumptions/ Limitations of Model

The model is valid for beam specimens with longitudinal reinforcement ratio $\leq 2\%$.

2. ACI 318-11 Model [33]

The minimum shear strength of a shear un-reinforced beam can be calculated using the empirical Equation 2.42.

$$V_c = 2\lambda\sqrt{f'_c}b_wd \quad (2.42)$$

Equation 2.42 is obtained by the simplification of Equation 2.43.

$$V_c = \left(1.9\lambda\sqrt{f'_c} + 2500\rho_w\frac{V_u d}{M_u}\right)b_wd \quad (2.43)$$

where

ρ_w longitudinal reinforcement percentage.

V_u factored shear force in lb.

M_u factored moment at section in lb.

It must be noted that the units in this model are in fps (foot-pound-second) system.

Assumptions/ Limitations of Model

(a) It is assumed that the critical section is located at a distance d from the support.

(b) An assumption is made that ratio $2500\rho_w(V_u d/M_u) = 0.1\sqrt{f'_c}$.

3. CCC Model [15]

The concrete contribution to shear resistance in this model is based on the multi-action mechanical model. This model is based on the premise that the shear failure in a shear-reinforced beam is initiated by the concrete compression chord being subjected to the principle stresses reaching the Kupfer's bi-axial failure envelope [35]. The shear resistance provided by concrete comprises of contribution from the compression zone, dowel action and shear transfer across cracks. The Equation 2.44 is proposed to evaluate this contribution to the shear resistance.

$$V_{Rm,c} = V_c + V_w + V_l = 0.3\zeta\frac{x}{d}(f_{cm})^{\frac{2}{3}}b_{v,eff} \quad (2.44)$$

where

V_c the contribution of the compression zone.

V_w the shear transferred by concrete across the crack.

V_l the contribution of longitudinal rebars to shear resistance of concrete through dowel action.

$$\frac{x}{d} = 0.75(\alpha_e \rho_l)^{\frac{1}{3}} \quad (2.45)$$

if $x \leq h_f$

$$b_{v,eff} = b_v = b_w + 2h_f \leq b \quad (2.46)$$

if $x > h_f$

$$b_{v,eff} = b_w + (b_v - b_w) \left(\frac{h_f}{x} \right)^{\frac{3}{2}} \quad (2.47)$$

where

b_v effective width of the compression flange.

b total cross-section width at the flange.

$$b_v = b_w + 2h_f \leq b \quad (2.48)$$

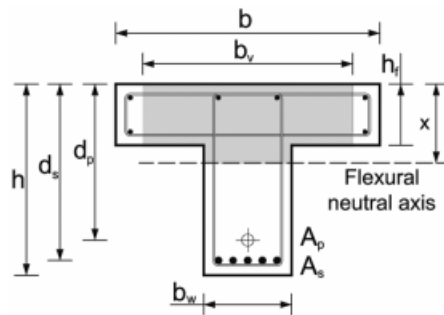


Figure 2.23: Notations for a T beam [15]

The minimum shear strength contribution by concrete can be expressed Equation 2.49.

$$V_{Rm,min} = 0.25 \left(\zeta \frac{x}{d} + \frac{20}{d} \right) (f_{cm})^{\frac{2}{3}} b_w d \quad (2.49)$$

$$\zeta = \frac{2}{\sqrt{1 + \frac{d}{200}}} \left(\frac{d}{a} \right)^{0.2} \geq 0.45 \quad (2.50)$$

According to the model, failure occurs when there is a damage concentration around the so-called critical shear crack with increasing load. As the load is increased, a second branch of crack is opened. This model assumes a linear and parabolic distribution of normal and shear stresses respectively for the concrete compression chord

above the critical shear crack. With the increasing load this second crack branch increases in length and eventually leads to a continuous crack connecting the tip of the first crack branch to the point of application of the external point load. This generation of a through crack marks the shear failure of the beam. Several assumptions are made to develop a simplified expression in this model. The following assumptions are made.

- (a) The diagonal crack spacing is equal to d (effective depth to the longitudinal reinforcement).
- (b) The tensile stress versus crack opening is a linear relationship.
- (c) The mean value of longitudinal reinforcement is assumed as $\rho = 1.5\%$ and the mean shear crack angle is assumed to be $\theta = 36^\circ$.
- (d) The horizontal projection of the critical shear crack is equal to $0.85d$ as observed in the experiments.
- (e) The depth of the neutral axis can be calculated from the cracked section analysis for concrete sections under pure bending.

It should be noted that the model introduces an empirical factor given by Zararis and Papadikis [68] to account for the size effect.

$$Size \ factor = \left\{ 1.2 - 0.2 \frac{a}{d} \right\} \geq 0.65 \quad (2.51)$$

d in m in the Equation 2.51.

Assumptions/ Limitations of Model

- (a) The mean longitudinal reinforcement ratio is assumed equal to 1.5%.
- (b) The diagonal shear crack spacing is assumed equal to d .
- (c) It is assumed that the tensile stress- crack opening curve is linear.
- (d) The mean shear crack angle is assumed equal to 36 degrees.

4. JSCE Model [1]

The design shear strength in this model is based on a conventional 45° truss analogy with an additional contribution from concrete to the shear resistance offered by stirrups. A due consideration is given to the influence of axial forces, effective depth and longitudinal reinforcement on the shear strength contribution from concrete. The empirical Equation 2.52 is proposed to calculate the contribution of concrete to the shear capacity of the reinforced concrete beam.

$$V_{cd} = \beta_d \beta_p \beta_n f_{vcd} b_w d / \gamma_b \quad (2.52)$$

$$f_{vcd} = 0.20 \sqrt[3]{f'_{cd}} \quad (N/mm^2) \text{ where } f_{vcd} \leq 0.72(N/mm^2) \quad (2.53)$$

$$\beta_d = \sqrt[4]{1000/d}, \text{ when } \beta_d > 1.5, \text{ is taken as } 1.5.$$

$$\beta_p = \sqrt[3]{100\rho_v}, \text{ when } \beta_p > 1.5, \text{ is taken as } 1.5.$$

$\beta_n = 1 + 2M_o/M_{ud} = 1 + 4M_o/M_{ud}$ when $\beta_n > 2$, is taken as 2 when $\beta_n < 0$, is taken as 0.

$\rho_v = A_s/bd$.

$\gamma_b = 1.3$ (used generally).

Assumptions/ Limitations of Model

Equation 2.52 is developed from the formula given by Niwa et al. but after neglecting the effect of a/d [46].

5. AASHTO Model [47]

This design procedure assumes that the shear stress is constant over the effective shear depth of the beam d_v . The design method is derived from MCFT [57] which is described in Appendix B. The equilibrium of the forces in the diagonally cracked concrete lead to the strain in the tension and compression flange. The Equation 2.54 is proposed to evaluate the concrete contribution to the shear resistance. It must be noted that the units in this model are based on fps convention.

$$V_c = 0.0316\beta\sqrt{f'_c}b_vd_v \quad (2.54)$$

The concrete contribution V_c comes from the tensile stresses in concrete [47].

where

β factor accounting for influence of diagonal cracking in concrete on shear and tensile resistance.

b_v minimum web width throughout the effective shear depth.

In Equation 2.54 for sections having minimum amount of transverse reinforcement (The minimum amount of transverse reinforcement is given by Equation 2.55).

$$A_v \geq 0.0316\sqrt{f'_c}\frac{b_v s}{f_y} \quad (2.55)$$

where

b_v cross sectional width of the beam adjusted for the presence of pre-stressing ducts (in the present study the effect of pre-stressing is not included).

$$\beta = \frac{4.8}{1 + 750\epsilon_s} \quad (2.56)$$

The simplified equation (considering zero pre-stressing) to obtain the longitudinal strain ϵ_s is given by Equation 2.57).

$$\epsilon_s = \frac{\left(\frac{M}{d} + 0.5V\right)}{E_s A_s} \quad (2.57)$$

where

M moment due to service load at a section at distance d_v from the face of the support.

V shear force due to service load at a section at distance d_v from the face of the support.

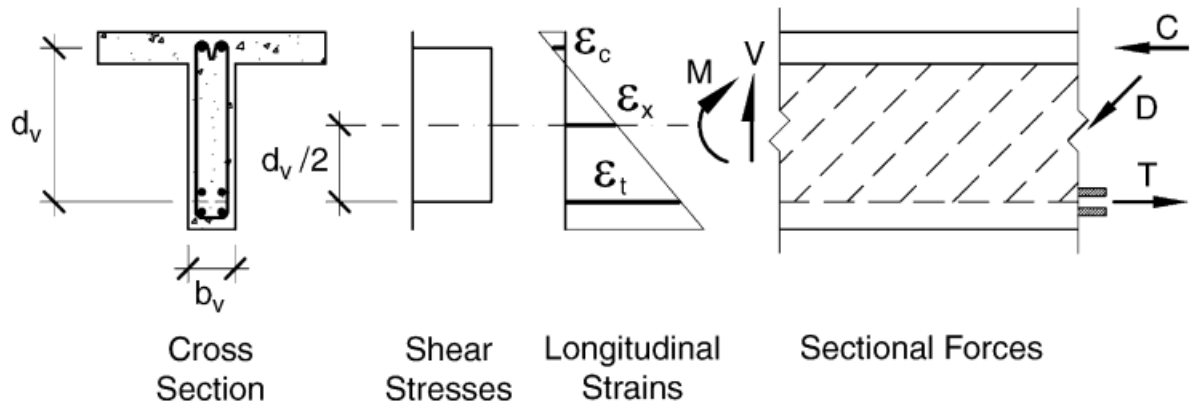


Figure 2.24: Determination of longitudinal strain in the web of a reinforced concrete non-prestressed beam [14]

In Figure 4.21, D refers to the compression force in the strut.

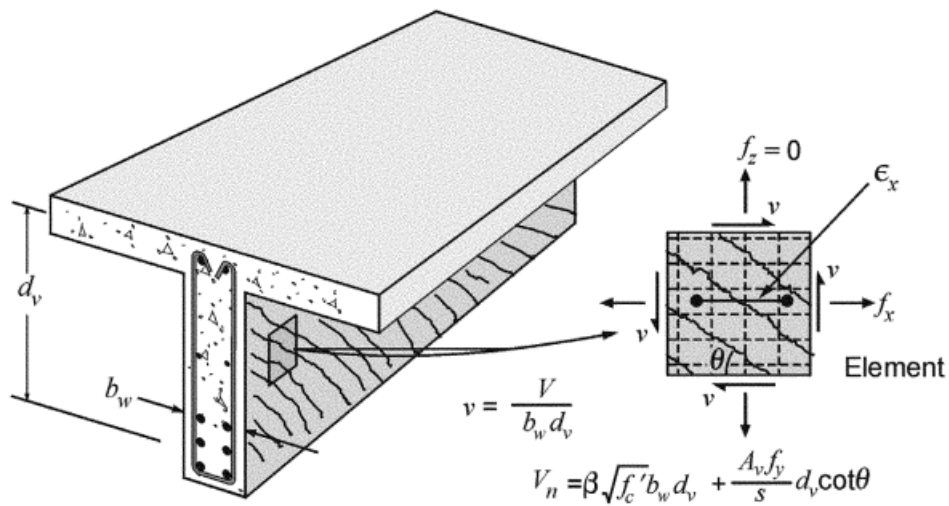


Figure 2.25: Determination of shear strength from AASHTO model [7]

Figure 2.25 shows the contribution of the moment, shear force and axial force in the determination of the axial strain in the longitudinal reinforcement bars.

where

θ angle of the diagonal cracks.

The other symbols used in the above Figure 4.20 have the same meaning as explained above. The subscript “u” indicates ultimate limit state.

It must be noted that the units in this model are in fps system.

Assumptions/ Limitations of Model

It is assumed that the shear stress is constant over effective shear depth.

6. **CSA Model [5]** The shear resistance contribution of concrete using this model is functionally equivalent to the AASHTO model. The Equation 2.58 is proposed to calculate the concrete contribution to shear resistance.

$$V_c = \phi_c \lambda \beta \sqrt{f'_c} b_w d_v \tag{2.58}$$

where

- $\sqrt{f'_c} \not\geq 8 \text{ MPa}$ for beams containing minimum transverse reinforcement.
- β factor to account for shear resistance of cracked concrete.
- f'_c specified compressive strength of concrete.

$$\beta = \frac{0.40}{1 + 1500 \epsilon_x} \tag{2.59}$$

The strain in the longitudinal reinforcement ϵ_x can be calculated using the Equation 2.60.

$$\epsilon_x = \frac{\frac{M_f}{d_v} + V_f - V_p + 0.5N_f - A_p f_{po}}{2(E_s A_s + E_p A_p)} \tag{2.60}$$

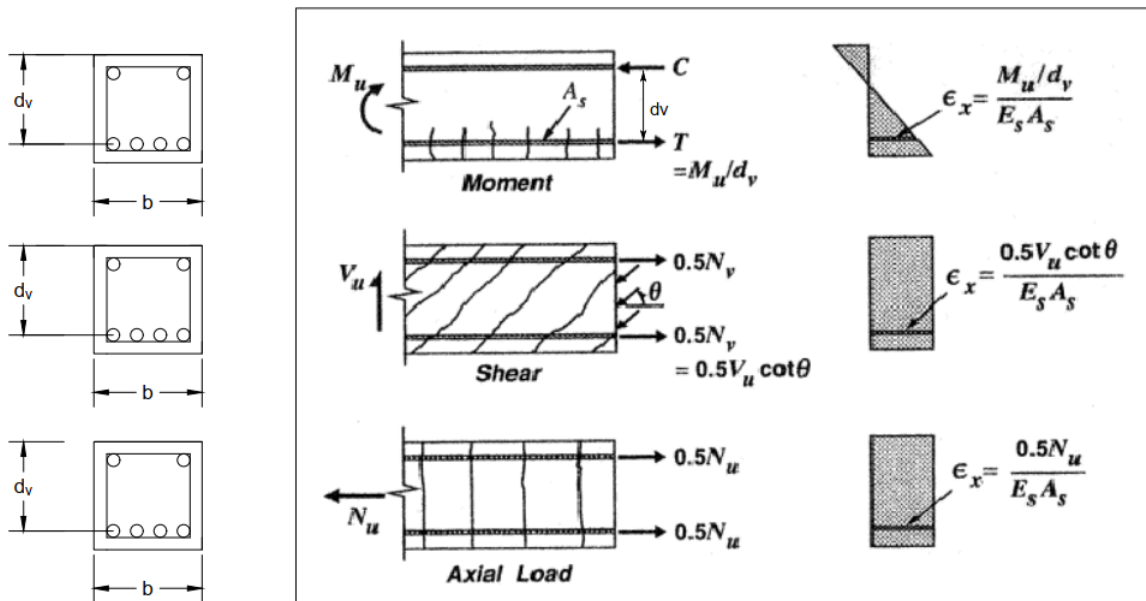


Figure 2.26: Determination of longitudinal strain in the longitudinal reinforcement of a reinforced concrete non-prestressed beam [4].

Assumptions/ Limitations of Model

- (a) The model is applicable only when $\sqrt{f'_c} \not\geq 8 \text{ MPa}$.
- (b) The model is applicable for RC members with minimum shear reinforcement area $A_v = 0.06 \sqrt{f'_c} b_w s / f_y$.

7. Zsutty Model [69]

The author perform regression analysis on a base expression obtained using dimensional analysis. The Equation 2.61 is proposed to calculate the concrete contribution to the shear resistance (Note in this study the shear resistance of shear un-reinforced beams is considered as the equivalent to concrete contribution to shear resistance for comparison purposes).

$$V_u = 2.2 \left[\left(f'_c \rho \frac{d}{a} \right)^{\frac{1}{3}} \right] bd \quad (2.61)$$

Assumptions/ Limitations of Model

?? validated as giving conservative and consistent predictions for $a/d > 2.5$.

8. Niwa et al. Model [46]

The authors perform a regression analysis of experimentally observed shear strength of shear un-reinforced beams. The empirical Equation 2.62 is proposed to evaluate the the shear resistance of shear un-reinforced beams (which in this study is considered as the equivalent of concrete contribution to the shear resistance in case of a shear reinforced beam).

$$V_u = \left[0.2(100f'_c\rho)^{\frac{1}{3}} \left(d^{-\frac{1}{4}} \right) \left(0.75 + 1.4\frac{d}{a} \right) \right] bd \quad (2.62)$$

The term $d^{-\frac{1}{4}}$ accounts for the size effect and is based on the Weibull's weakest link theory.

Assumptions/ Limitations of Model

The model is validated on a limited experimentally dataset.

9. Zararis Model [67]

This model is based on the premise that the failure in shear un-reinforced beams occur due to formation of critical diagonal crack in slender reinforced concrete beam. The critical diagonal crack has two branches. The first branch is an inclined shear crack which is formed in the vicinity of the flexural cracks and is often formed in between the flexural cracks. It is the second branch of the critical diagonal crack (which initiates at the tip of the first branch) which is responsible for the failure of the beam. Figure 2.27 shows the free body diagram of the segment of the beam above the critical diagonal crack [67]. The Equation 2.63 is proposed to calculate the concrete contribution to the shear resistance of the shear reinforced concrete beam.

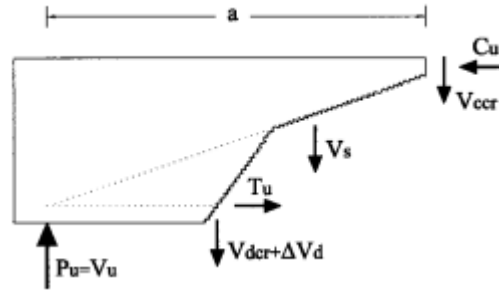


Figure 2.27: Free body diagram of the segment of the beam above the critical diagonal crack [67]

$$V_u = \left[\left\{ 1.2 - 0.2 \left(\frac{a}{d} \right) d \right\} \frac{c}{d} f_{ct} \right] bd \quad (2.63)$$

$$\text{Size factor} = \left\{ 1.2 - 0.2 \left(\frac{a}{d} \right) d \right\} \geq 0.65 \quad (2.64)$$

d is in m in the Equation 2.64.

$$f_{ct} = 0.3(f'_c)^{\frac{2}{3}} \quad (2.65)$$

$$\left(\frac{c}{d} \right)^2 + 600 \frac{\rho + \rho'}{f'_c} \left(\frac{c}{d} \right) - 600 \frac{\rho + \left(\frac{d'}{d} \right) \rho'}{f'_c} = 0 \quad (2.66)$$

where

c depth of the neutral axis.

The model is explained in detail in B.

Assumptions/ Limitations of Model

- (a) It is assumed that $a/d > 2.5$.
- (b) It is assumed that there is no slip in the first branch of the diagonal shear crack.
- (c) It is assumed that the neutral axis depth after shear cracking is same as that for cross-section with flexural cracks.

10. Tureyen et al. Model [54]

This model is based on the premise that the shear failure in a shear un-reinforced beam occurs when the principle tensile stress in concrete above the neutral axis reaches the concrete tensile strength value f_t . The depth of neutral axis is determined using the cracked cross sectional analysis for bending cracks. Figure 2.28 shows that various forces and stresses acting on free body diagram of the beam portion between two cracks. The Equation 2.67 is proposed by Tureyen and Frosch [54] for the shear resistance of a shear un-reinforced beam (considered as concrete contribution to the shear resistance of a shear reinforced beam).

$$V_u = \frac{2}{3} bc \sqrt{f_t^2 + f_t \frac{\sigma_m}{2}} \quad (2.67)$$

where

f_t concrete tensile strength.

$$f_t = 0.5\sqrt{f'_c} \quad (2.68)$$

$$\sigma_m = 0.625\sqrt{f'_c} \quad (2.69)$$

$c = kd$.

$$k = \sqrt{2\rho m + (\rho m)^2} - \rho m \quad (2.70)$$

$m = \frac{E_s}{E_c}$

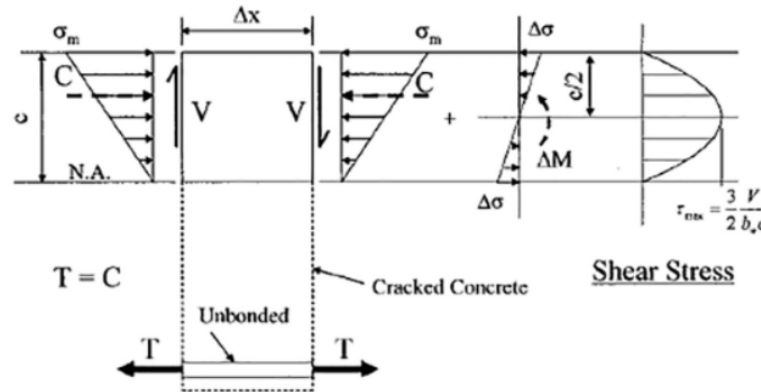


Figure 2.28: The FBD (Free Body Diagram) showing various stresses and forces at a cracked section as considered by Tureyen and Frosch [6]

In the Figure 2.28,

c height of the compression zone.

N.A. neutral axis of the beam.

Δx length of the cracked concrete.

This model is developed for shear unreinforced beams with shear span ratio, $a/d > 2.7$. The model is applicable to only those beams which fail in shear before bending failure and have adequate end anchorage for the longitudinal reinforcement.

Assumptions/ Limitations of Model

(a) It is assumed that $a/d > 2.5$.

(b) It is assumed that the neutral axis depth after shear cracking is same as that for cross-section with flexural cracks.

11. Summary of the Concrete Contribution to Shear Resistance Models

In this section, a review of the various available models to predict the concrete contribution to the total shear resistance of a shear reinforced beam is made. These models are based on either empirical and dimensional analysis or principles of applied

mechanics. It can be seen that all the models except AASHTO Model [47] and CSA Model [5] gives a fixed value of the shear resistance independent of the applied loading conditions. The latter two models are based on the MCFT [57] and incorporate the longitudinal reinforcement strain as a parameter influencing the predicted value. It is also seen that only Niwa et al Model [46] and Zararis Model [68] explicitly account for the size effect in their expressions. It is seen that on a minute scale the concrete contribution to shear resistance can be attributed to various shear transfer mechanisms namely aggregate interlock, concrete un-cracked compression zone, dowel action and residual tensile stresses. However, there is no consensus among researchers as to which transfer mechanism has a dominant contribution.

2.4. Conclusion

In Chapter 2, a detailed review of the various models available in literature to predict shear crack width, shear crack spacing, diagonal compression strut angle and concrete contribution to shear resistance at the ULS is carried out. Table 2.1 presents a summary of the basic principles and some limitations of these models. It is found that the shear crack spacing and shear stirrup strain are the two most important parameters that influence shear crack width.

Majority of the available shear crack spacing models are based on the assumption of parallel diagonal shear cracks. The final crack spacing expression is given as the weighted sum of crack spacing control characteristics in longitudinal and transverse directions. The influence of the bond stress transfer length is evident from the term containing the ratio ϕ/ρ in various crack spacing models. The determination of diagonal compression strut angle is based on the equilibrium of forces in the concrete member in a few models reviewed in this chapter. The other models are derived empirically based on either experimental observations of the shear crack length projections or non linear finite element simulations.

Most of the models give an empirical expression for the calculation of concrete contribution to ultimate shear resistance. However, a few models also give analytical expressions for this contribution based on the assumption that the failure occurs when the tensile stress in concrete reaches a particular predetermined value. The most significant parameters found in various available models which affect concrete contribution to shear resistance are concrete compressive strength, longitudinal and transverse reinforcement ratio and height of the uncracked concrete compressive zone. Most of the reviewed models give a constant value of concrete contribution to shear resistance. However, models based on MCFT are capable to predict the concrete contribution at different stages of loading. In Chapter 3 the predictions of the respective parameters from the various models reviewed in this Chapter are compared with the experimental observations. This facilitates the identification of the models giving predictions close to the experimentally observed values of parameters.

Table 2.1: Basic principles and limitations of the reviewed models

Theory/ Model	Principle	Assumptions / Remarks
Shear Crack Width Models		
EC2 Crack Width Model [19]	Expresses crack width as the product of mean reinforcement strain and the maximum crack spacing. The maximum crack width is obtained as a function of bond transfer length	cracks opens perpendicular to the reinforcement; crack control is limited to the effective height of hidden tensile member
Zakaria et al. Crack Width Model [65]	Expresses crack width as a function of mean shear crack spacing , stirrup strain, transverse and longitudinal reinforcement	comprises empirical constants; stirrup strain to be obtained experimentally
Shear Crack Spacing Models		
EC2 Crack Spacing Model [19]	Expresses crack spacing as a function of clear cover, reinforcement diameter and effective reinforcement ratio	lacks a clear description for transverse reinforcement
fib MC Crack Spacing Model [23]	Expresses crack spacing as a function of slip lengths in longitudinal and transverse direction	shear cracks are assumed parallel to each other at a constant spacing
Zakaria et al. Crack Spacing Model [65]	Expresses crack spacing as a function of relative position of reinforcement in the cross-section, reinforcement spacing, diameter of the reinforcement bars and effective reinforcement ratio in the longitudinal and transverse direction	shear cracks are assumed parallel to each other at a constant spacing

Diagonal Compression Strut Angle Models	Principle	Assumptions Remarks
Theorem of Plasticity [19]	Based on the assumption of simultaneous yielding of stirrups and crushing of the compression strut	constant value of the compression strut angle throughout the shear span
SMCFT Model [7]	based on the simplification of MCFT	failure shear stress = $0.25f'_c$; clamping stress, $f_z = 0$; $s_{xe} = 300mm$ for shear reinforced concrete beams
CCC Model [15]	Based on the experimental observation of horizontal projection of the critical shear crack	horizontal projection of first branch of flexural-shear crack = $0.85d$
CFT Model [4]	The shear stress is resisted by both longitudinal and transverse reinforcement in tension and concrete in compression	limited to reinforcement response in linear elastic zone
NLFEA Model (Ueda et al. Model) [56]	Based on the parametric study using Non Linear Finite Element Analysis	valid for $a/d > 1.5$
Concrete Contribution to Shear Resistance Models	Principle	Assumptions / Remarks
EC2 Concrete Shear Resistance Model [19]	Expresses concrete shear resistance as a function of compressive strength, applied axial force and the longitudinal reinforcement ratio	longitudinal reinforcement ratio $\leq 2\%$
ACI 318-11 Model [33]	States that the concrete contribution to shear in both shear reinforced and unreinforced beams can be taken equal to the load that causes significant shear cracking	critical section is located at distance d from the support ; $2500\rho_w(V_u d/M_u) = 0.1\sqrt{f'_c}$

CCC Model [15]	Concrete contribution to shear resistance comes from uncracked compression chord, dowel action and residual tensile stresses at crack surface	mean longitudinal reinforcement percentage = 1.5%; shear crack spacing = d ; tensile stress-crack opening curve is linear; $\theta_{mean} = 36^\circ$
JSCE Model [1]	Empirical equation that expresses influence of axial forces, effective depth and longitudinal reinforcement ratio on the concrete contribution to shear resistance	equation is developed from formula given by Niwa et al. [46] but neglecting the effect of a/d
AASHTO Model [47]	Based on the MCFT	shear stress constant over effective shear depth
CSA Model [5]	Based on the MCFT	$\sqrt{f'_c}$ not greater than 8 MPa; $A_v = 0.06\sqrt{f'_c}b_ws/f_y$
Zsutty Model [69]	Empirical equation based on dimensional analysis and regressional fitting	model is validated as giving conservative and consistent predictions for $a/d > 2.5$
Niwa et al. Model [46]	Empirical equation to derive shear resistance of shear unreinforced beams with a factor which accounts for size effect	originally validated on a very limited experimental dataset
Zararis Model [67]	States that shear failure occurs because of the formation of the opening of second branch of the critical diagonal crack	$a/d > 2.5$; no slip in the first branch of critical diagonal crack; neutral axis depth same as that obtained for cross section with flexural cracks
Tureyen and Frosch Model [54]	Shear failure in a shear unreinforced beam occurs when the principle tensile stress in the concrete above neutral axis reaches concrete tensile strength	$a/d > 2.7$; neutral axis depth same as that obtained for cross section with flexural cracks

3

Evaluation of the Available Models

“Once we accept our limits, we go beyond them.”

Albert Einstein

This Chapter comprises the performance evaluation of various models reviewed in the Chapter 2 in terms of their prediction accuracy of the respective parameters. The variation of the mean prediction ratios (experimentally observed value to the predicted value) with respect to the various specimen parameters is also included to identify any possible bias with any of these parameters in the models.

THE present Chapter aims at evaluating the accuracy of predictions made by the various available models for shear crack spacing, diagonal compression strut angle and concrete contribution to the shear resistance with respect to the experimental data available in the literature. A comparative assessment of the accuracy of these models and their statistical dependence on the various beam specimen parameters is provided. This motivates a better choice of models for conservative estimates of these parameters. The units for all parameters are in N and mm unless stated otherwise.

3.1. Shear Crack Spacing

3.1.1. Experimental Details

Table 3.1 shows the summary of the key characteristics of the different experiments from literature referred in the study. Zakaria et al. [66] perform experiments to study the factors that impact the shear crack spacing and shear crack width in shear reinforced concrete beams. The shear reinforcement characteristics like the side concrete cover to stirrups, stirrup spacing and stirrup configuration (details of the cross section are shown in Figure 3.2 and Figure 3.3) are the parameters in the experiments. While the authors find the remarkable influence of these parameters on the shear crack spacing and shear crack width, the influence of the loading paths (loading and unloading) is found to be insignificant. Ten simply supported shear reinforced concrete beams are casted to study the effect of the parameters mentioned above. Experiments are performed in three different test series namely series I, II and III. These series are designed to study the effect of shear span ratio, side concrete to stirrups and longitudinal reinforcement ratio. The shear crack spacing is measured perpendicular to the shear cracks at mid depth of the beam as shown in Figure 3.1.

In another study, Hu and Wu [31] quantify shear cracking in reinforced concrete beams tested with a cantilever mechanical scheme. The authors install strain gauges inside the stirrups by cutting them longitudinally and then joining them using Araldite epoxy resin. Figure 3.4 shows the mechanical scheme and the cross section of the beams used in the experiments. In the present analysis, two of the shear reinforced beams titled D10 and R10 respectively are included. Lee et al. [37] studied the effect of high strength stirrups on shear crack spacing and shear crack width in shear reinforced concrete beams. The mechanical scheme and instrumentation details in the experiment are shown in Figure 3.5. Table 3.2 shows the various geometrical parameters for the specimens involved in the present analysis. The range of these parameters is summarized in Table 3.3.

Table 3.1: Key characteristics of specimens referred for shear crack spacing study

Publication	Series	Specimens	Mechanical Scheme	Variable	Method
Zakaria et al. [65]	A1 to C3	10	4- point bending	crack spacing	at mid-height
Hu and Wu [31]	D10, R10	2	cantilever	crack spacing	at mid-height
Lee et al. [37]	B334-120 to B667-200	12	4- point bending	crack spacing	in middle-one third portion

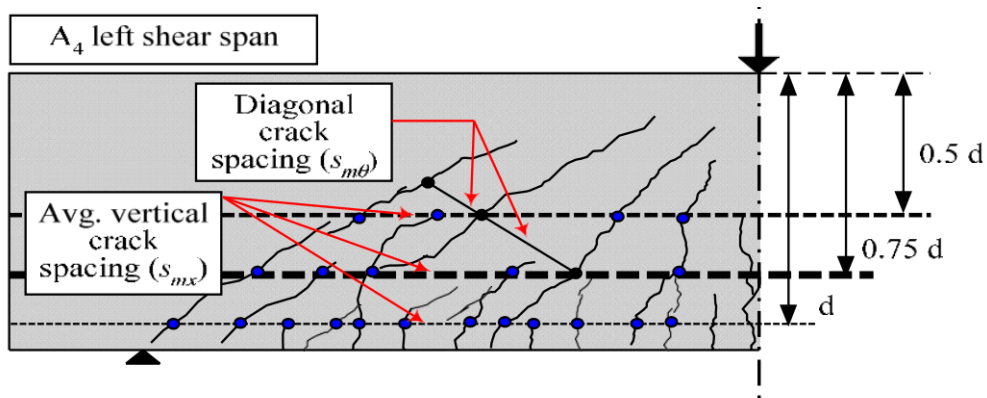


Figure 3.1: The measurement of average shear crack spacing [66]

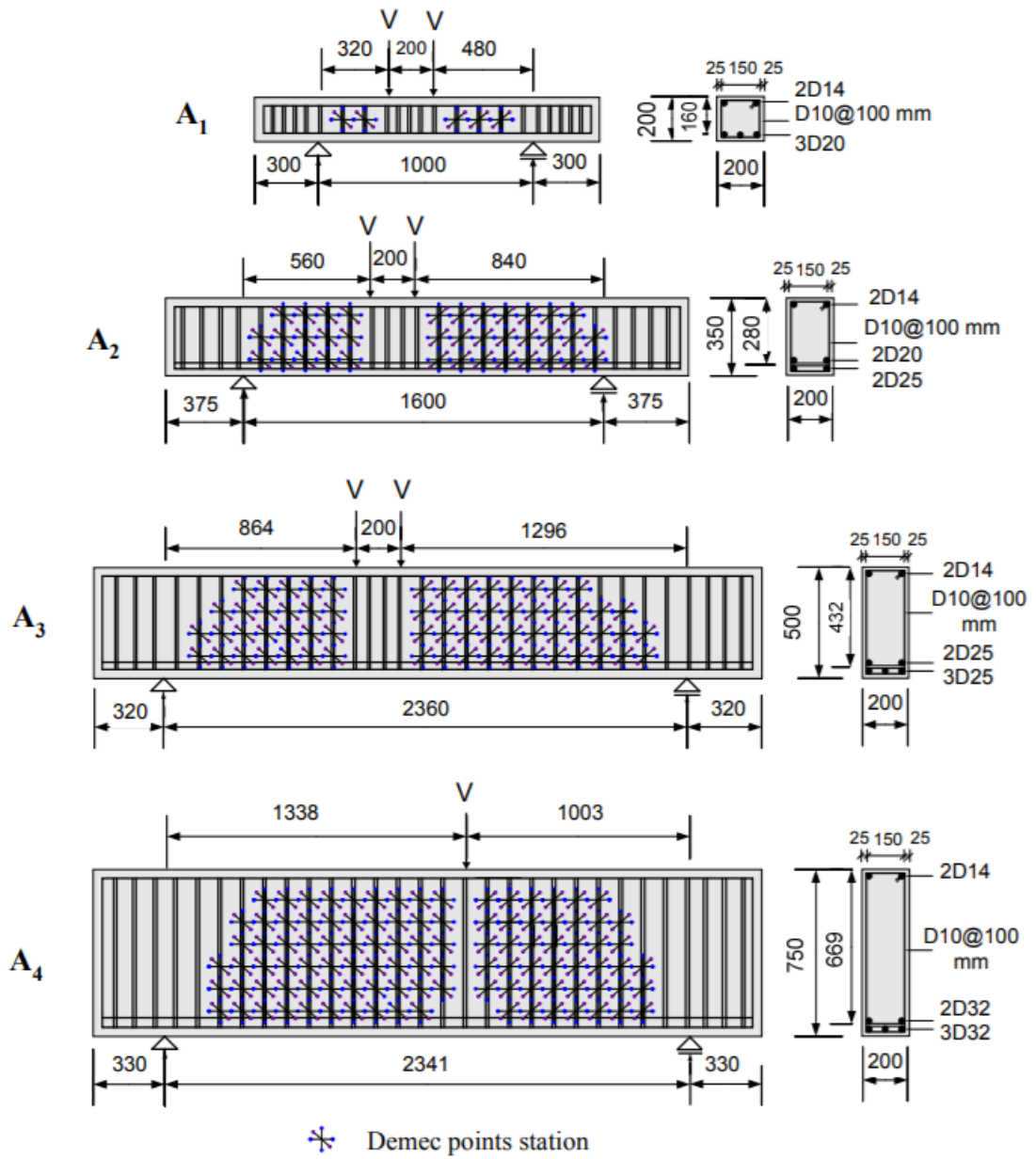


Figure 3.2: The mechanical scheme and cross section details for the reinforced concrete beams in series I [66]

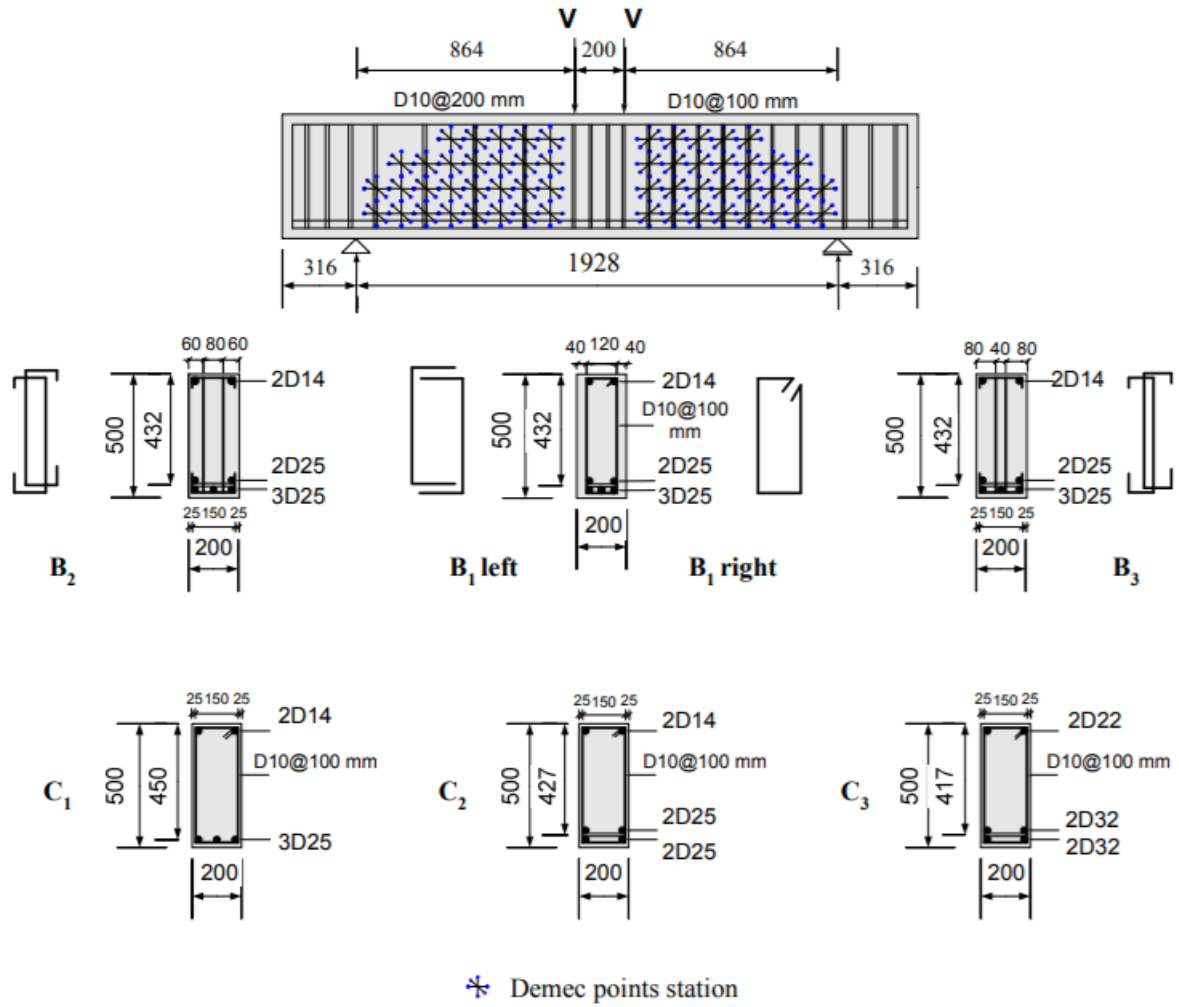


Figure 3.3: The mechanical scheme and cross section details for the reinforced concrete beams in Series II and III [66]

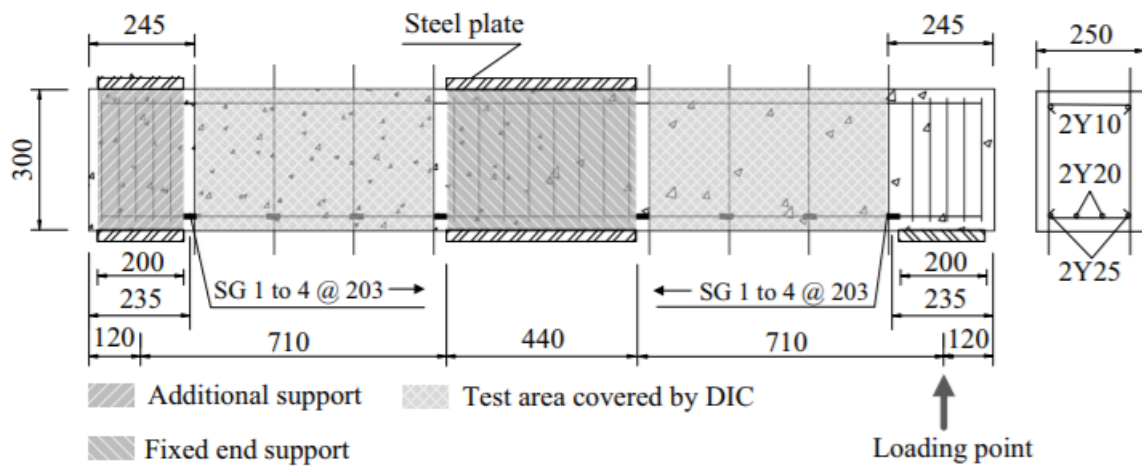


Figure 3.4: The mechanical scheme and cross section details for the reinforced concrete beams [37]

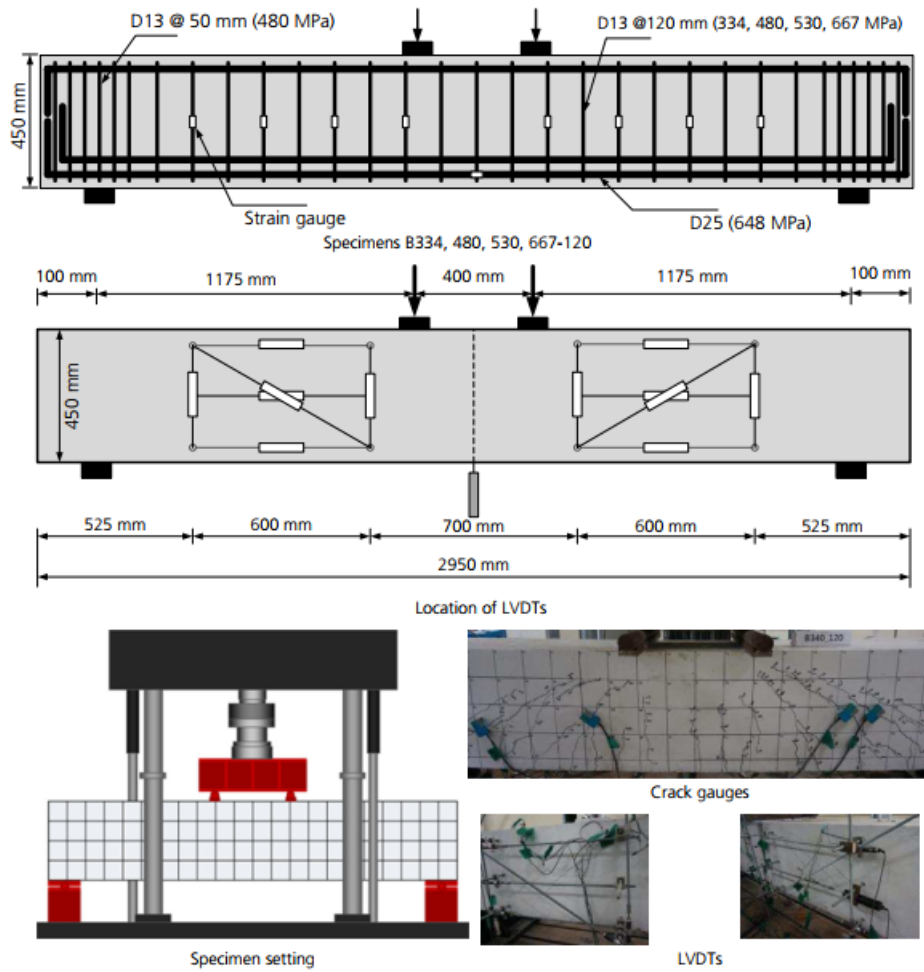


Figure 3.5: The mechanical scheme and cross section details for the reinforced concrete beams [31]

Table 3.2: Geometrical parameters for the different specimens in the test series of Zakaria et al. [66] and Hu and Wu [31]

Specimen	Width (mm)	Height (mm)	ρ_w %	ρ_l %	a/d	d/b
A1 left	200	200	0.72	2.86	2	0.80
A2 left	200	350	0.72	2.83	2	1.40
A3 left	200	500	0.72	2.84	2	2.16
A4 left	200	750	0.72	2.84	2	3.35
B1 left	200	500	0.72	2.84	2	2.16
B2 left	200	500	0.36	2.84	2	2.16
B3 left	200	500	0.36	2.84	2	2.16
C1	200	500	0.72	1.62	2	2.25
C2	200	500	0.72	2.3	2	2.14
C3	200	500	0.72	3.64	2	2.09
D10	250	300	0.41	2.38	2.6	1.08
R10	250	300	0.62	2.38	2.6	1.08
B334-120	350	450	0.60	3.72	3	1.12
B334-160	350	450	0.44	3.72	3	1.12
B334-200	350	450	0.36	3.72	3	1.12
B480-120	350	450	0.60	3.72	3	1.12
B480-160	350	450	0.44	3.72	3	1.12
B480-200	350	450	0.36	3.72	3	1.12
B530-120	350	450	0.60	3.72	3	1.12
B530-160	350	450	0.44	3.72	3	1.12
B530-200	350	450	0.36	3.72	3	1.12
B667-120	350	450	0.60	3.72	3	1.12
B667-160	350	450	0.44	3.72	3	1.12
B667-200	350	450	0.36	3.72	3	1.12

Table 3.3: Range of parameters for the specimens studies for evaluation of available shear crack spacing models

Parameter	Range
a/d	2-3
d/b	0.80-3.34
$\rho_w f_{ym}$ (MPa)	1.33-4.02
ρ_l (%)	1.62-3.72
ρ_w (%)	0.36-0.72
f'_c (MPa)	32.47-50.10

3.1.2. Observations

The shear crack spacing observed from the experiments is compared with the shear crack spacing predictions from the crack spacing models by Zakaria et al. [65], EC2 [19], and fib MC 2010 [23]. The ratio of experimental to calculated shear crack spacing from different models are given in Table 3.4. Table 3.5 shows various statistical parameters of the ratio $s_{avg,exp}/s_{avg,pred}$ for the EC2 model, Zakaria et al model and fib MC model. It can be observed that the Zakaria et al. model show the conservative mean value closest to 1.0

followed by the model given by fib MC model. This indicates that the factors considered in the formulation of these models are the crucial factors influencing the shear crack spacing. These factors are side concrete cover to stirrup, shear and longitudinal reinforcements ratio and diameter of both shear and longitudinal reinforcement. Zakaria et al. observe that the distance of the nearest longitudinal reinforcement from the center of the beam height is more important parameter influencing shear crack spacing than effective concrete cover. This may be a reason for the better correlation of their model as compared to the EC2 model.

However, both EC2 and Zakaria et al. models show higher standard deviation and coefficient of variation as compared to the fib MC model. The similar trend is reflected in the range of the prediction ratio from these models. The over conservative (a higher predicted value of shear crack spacing results in a conservative estimate of shear crack width) shear crack spacing predictions of the fib MC model may be attributed to the fact that the model does not incorporate the effective reinforcement percentage in the formulation unlike the EC2 model and Zakaria et al. model. The statistical dependence of these models is studied by plotting the variation of $s_{avg,exp}/s_{avg,pred}$ against various parameters for each of the three models.

Table 3.4: $s_{avg,exp}/s_{avg,pred}$ values of the different shear crack spacing models

Specimen	$s_{avg,exp}/s_{avg,pred}$		
	EC2 [19]	Zakaria et al. [65]	fib MC [23]
A1 left	0.32	0.28	0.25
A2 left	0.55	0.61	0.56
A3 left	0.74	0.83	0.76
A4 left	0.99	1.10	1.01
B1 left	0.56	0.64	0.80
B2 left	0.53	0.55	0.52
B3 left	0.59	0.55	0.58
C1	0.82	0.91	0.82
C2	0.76	0.85	0.77
C3	0.66	0.74	0.68
D10	0.54	0.54	0.42
R10	0.47	0.40	0.40
B334-120	1.32	1.22	0.55
B334-160	1.09	0.93	0.37
B334-200	1.73	1.32	0.54
B480-120	1.10	1.01	0.46
B480-160	1.49	1.27	0.50
B480-200	1.59	1.21	0.50
B530-120	1.65	1.52	0.69
B530-160	1.71	1.46	0.58
B530-200	1.59	1.21	0.50
B667-120	1.02	0.94	0.43
B667-160	1.09	0.93	0.37
B667-200	1.49	1.13	0.46

Table 3.5: Statistical parameters for $s_{avg,exp}/s_{avg,pred}$ for the different shear crack spacing models

Statistical Variable	$s_{avg,exp}/s_{avg,pred}$		
	EC2 [19]	Zakaria et al. [65]	fib MC 2010 [23]
Mean	1.02	0.92	0.56
Median	1.01	0.93	0.53
SD	0.45	0.34	0.18
COV	0.45	0.36	0.31
Minimum	0.32	0.28	0.25
Maximum	1.73	1.52	1.01
Range	1.41	1.24	0.75

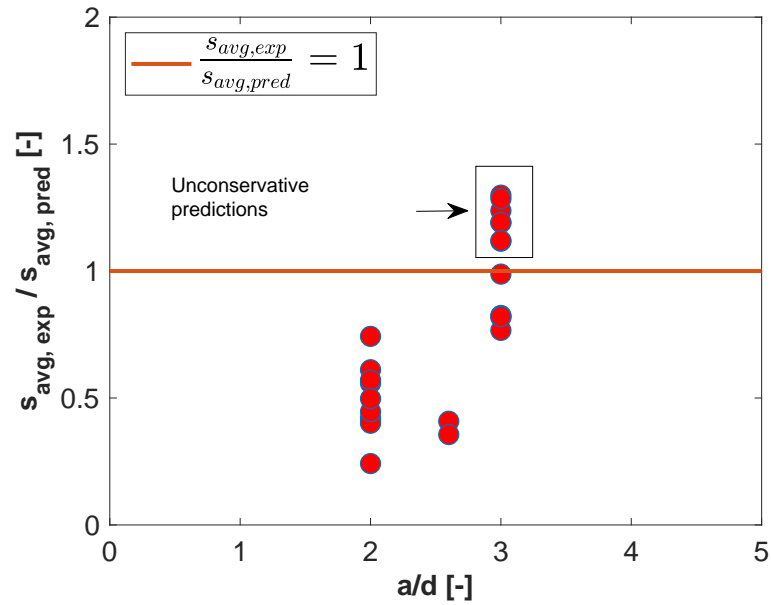


Figure 3.6: The ratio of $s_{avg,exp}/s_{avg,pred}$ versus a/d for the EC2 model [19]

Figure 3.6 shows that EC2 model exhibits a tendency to predict unconservative crack spacing value at higher shear span ratio ($\frac{a}{d} \geq 3$). This may lead to unconservative predictions at higher values of shear span ratios. Similar tendency is shown by Zakaria et al. model (see Figure 3.7).

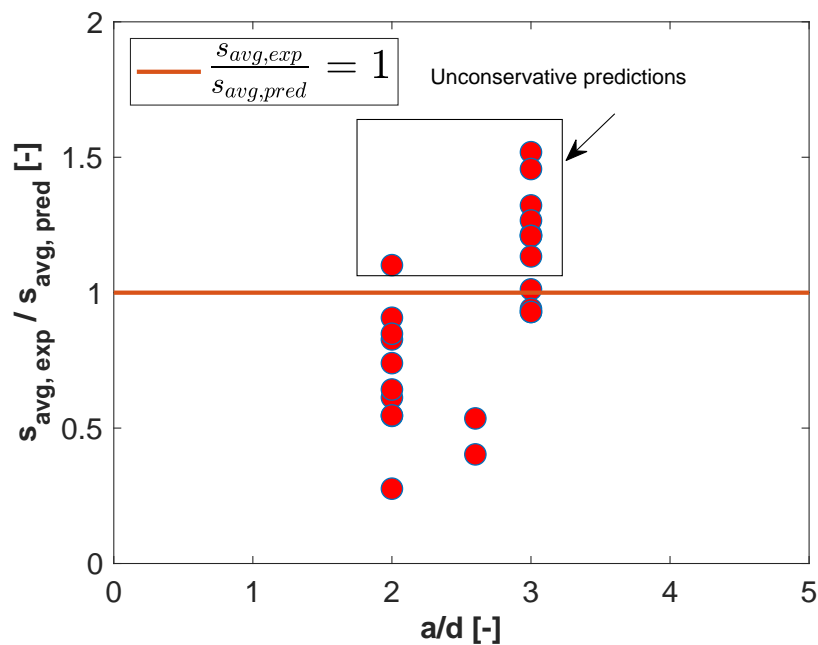


Figure 3.7: The ratio of $s_{avg,exp}/s_{avg,pred}$ versus a/d for the Zakaria et al. model [65]

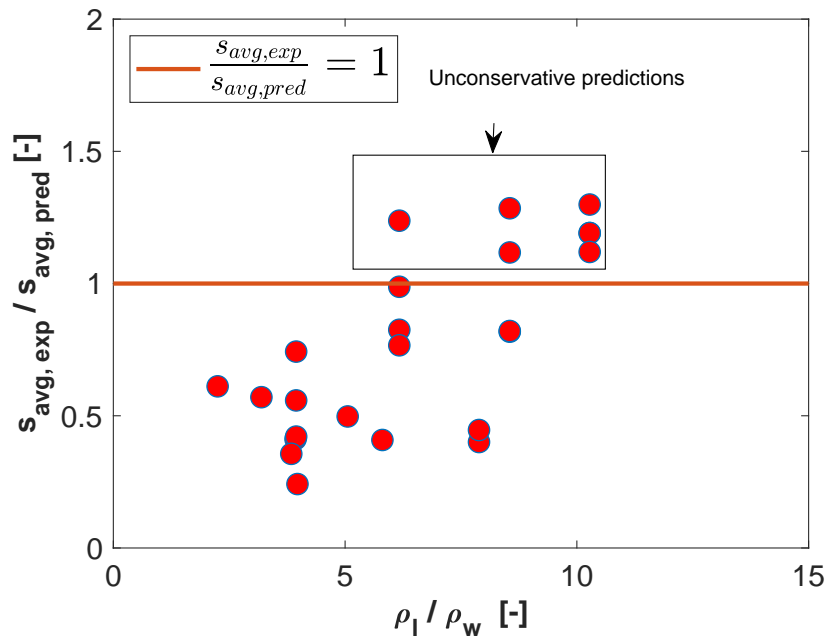


Figure 3.8: The ratio of $s_{avg,exp}/s_{avg,pred}$ versus ρ_l/ρ_w for EC2 model [19]

It can be observed from Figure 3.8 that most of the unconservative predictions ($\frac{s_{exp}}{s_{pred}} > 1.0$) are obtained for higher values of $\frac{\rho_l}{\rho_w}$ ($\frac{\rho_l}{\rho_w} > 6.0$). This may lead to unconservative predictions for relatively lightly shear reinforced beams. Similar tendency is shown by Zakaria et al. model (see Figure 3.9).

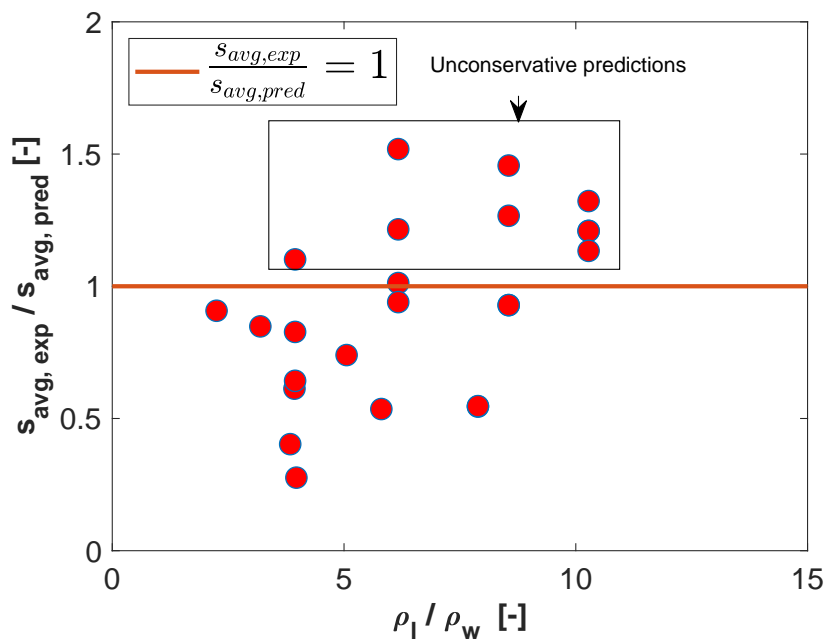


Figure 3.9: The ratio of $s_{avg,exp}/s_{avg,pred}$ versus ρ_l/ρ_w for the Zakaria et al. model [65]

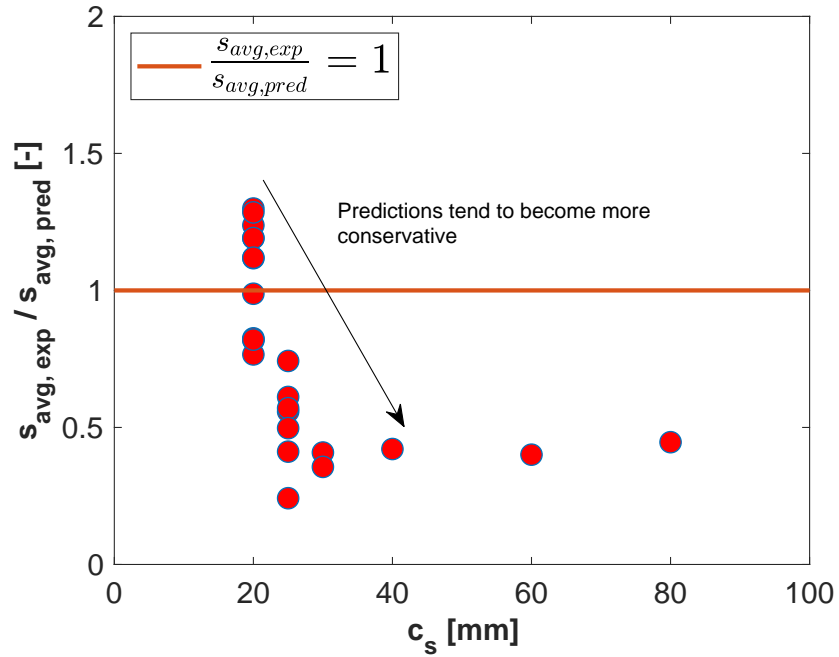


Figure 3.10: The ratio of $s_{avg,exp}/s_{avg,pred}$ versus c_s for the EC2 model [19]

It can be observed from Figure 3.12 that the predictions from EC2 model shows a tendency to decrease and therefore, become more conservative with the increasing values of the side concrete cover to stirrups. The unconservative predictions are observed only for the low value of side concrete cover to stirrups ($c_s = 20mm$). Similar tendency is exhibited by Zakaria et al. model (see Figure 3.13).

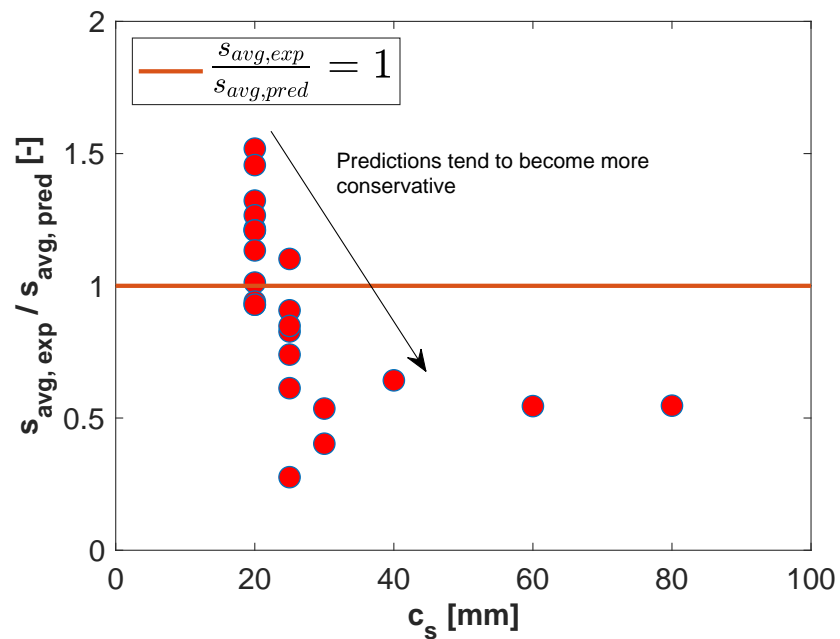


Figure 3.11: The ratio of $s_{avg,exp}/s_{avg,pred}$ versus c_s for Zakaria et al. model [65]

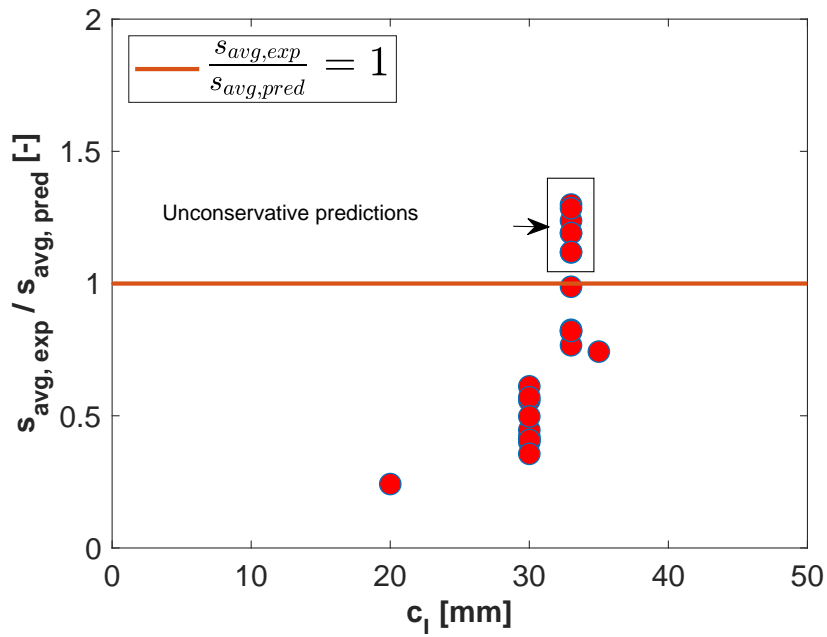


Figure 3.12: The ratio of $s_{avg,exp}/s_{avg,pred}$ versus c_l for the EC2 model [19]

Figure 3.12 shows the tendency of the EC2 model to predict unconservative values for shear crack spacing at higher values of clear cover to the concrete. However, the difference between the values of concrete cover shown in the plots is negligible from execution point of view.

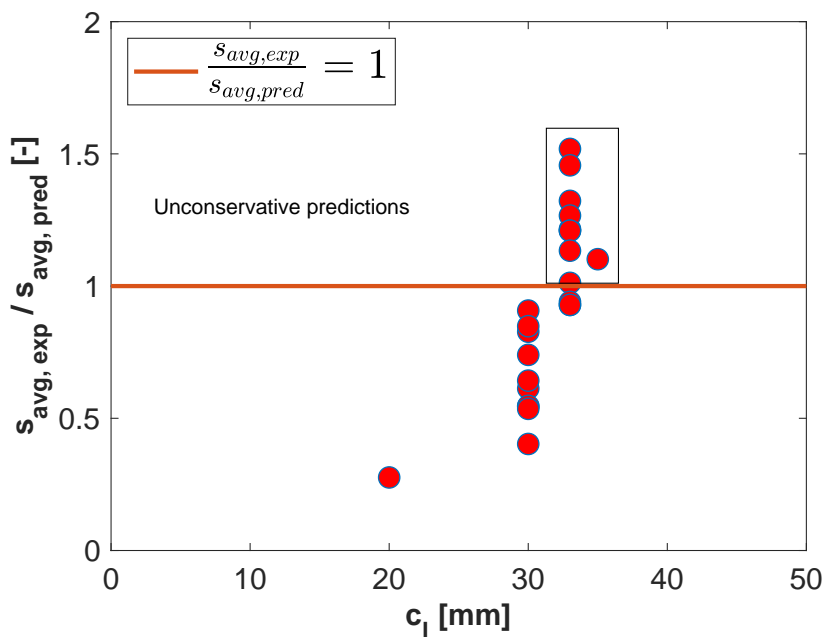


Figure 3.13: The ratio of $s_{avg,exp}/s_{avg,pred}$ versus c_l for Zakaria et al. model [65]

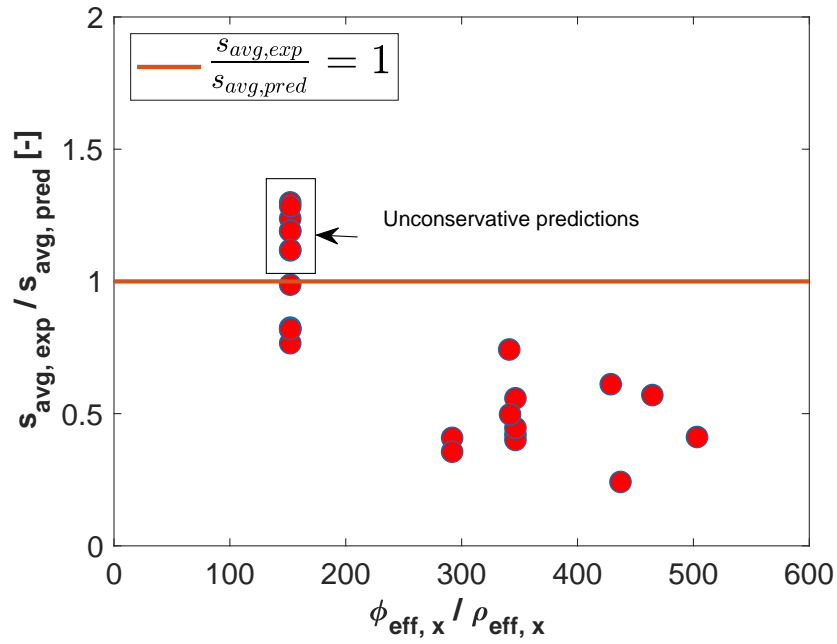


Figure 3.14: The ratio of $s_{avg,exp}/s_{avg,pred}$ versus $\phi_{eff,x}/\rho_{eff,x}$ for the EC2 model [19]

It may be observed from Figure 3.14 and Figure 3.15 that both EC2 and Zakaria et al. model give several unconservative predictions at $\frac{\phi_{eff,x}}{\rho_{eff,x}} = 150$. However, almost all the predictions at values of $\frac{\phi_{eff,x}}{\rho_{eff,x}} > 150$ are found to be conservative.

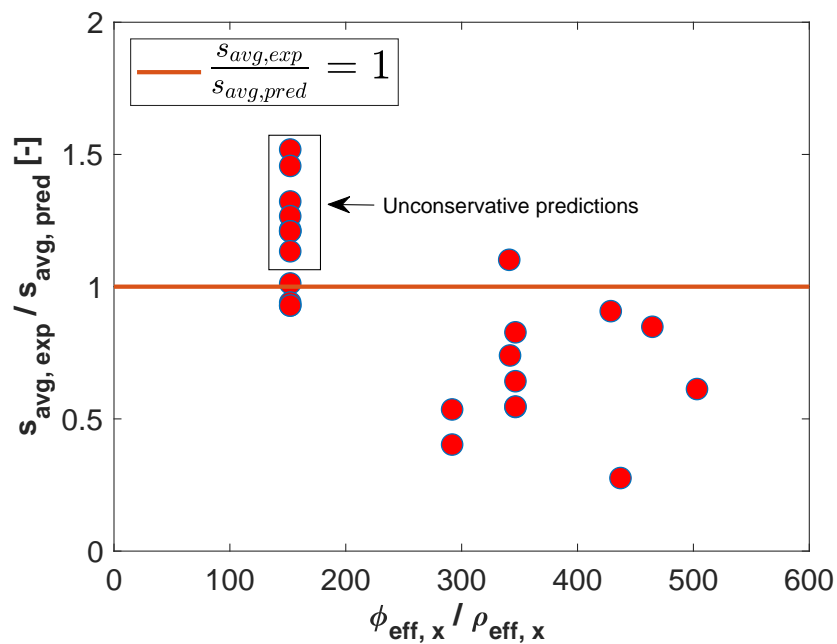


Figure 3.15: The ratio of $s_{avg,exp}/s_{avg,pred}$ versus $\phi_{eff,x}/\rho_{eff,x}$ for Zakaria et al. model [65]

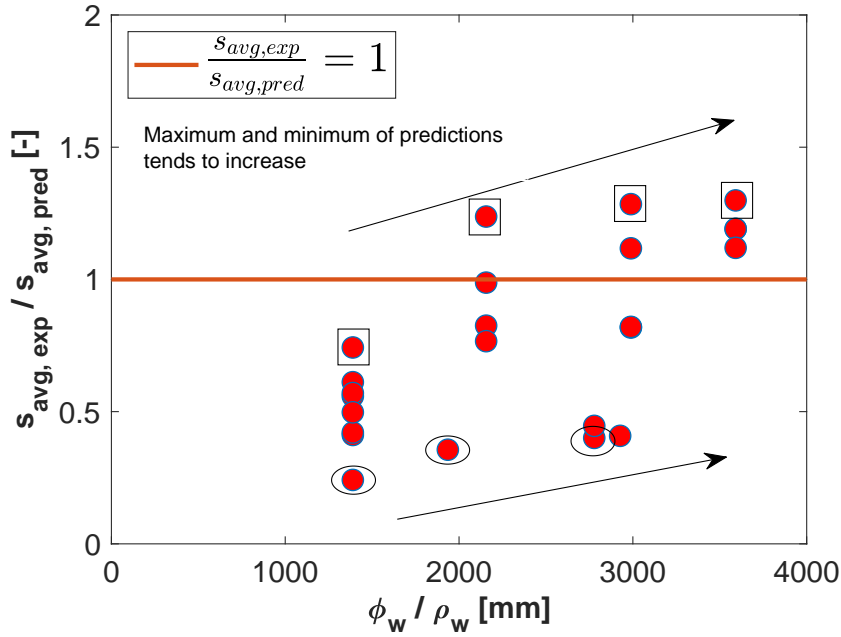


Figure 3.16: The ratio of $s_{avg,exp}/s_{avg,pred}$ versus ϕ_w/ρ_w for the EC2 model [19]

With the increasing values of ϕ_w / ρ_w , EC2 and fib MC models show the tendency to predict unconservative and conservative values (see Figure 3.16 and Figure 3.17). This may indicate the suitability of the fib MC model over EC2 model at values of $\phi_w / \rho_w > 2000$. However, this trend needs to be validated with experimental observations to make sure that it is a factual trend and not a limitation due to the sampling size in this study.

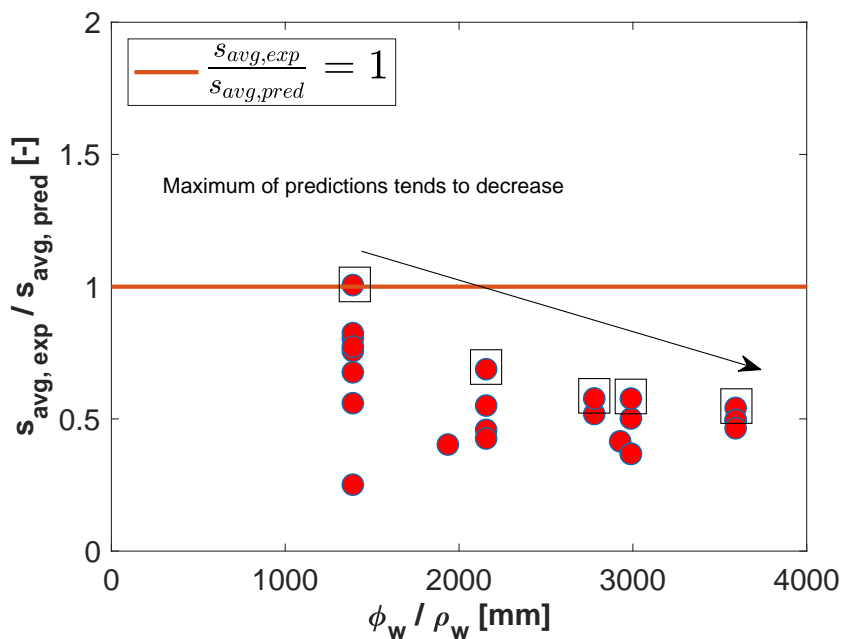


Figure 3.17: The ratio of $s_{avg,exp}/s_{avg,pred}$ versus ϕ_w/ρ_w for fib MC 2010 model [23]

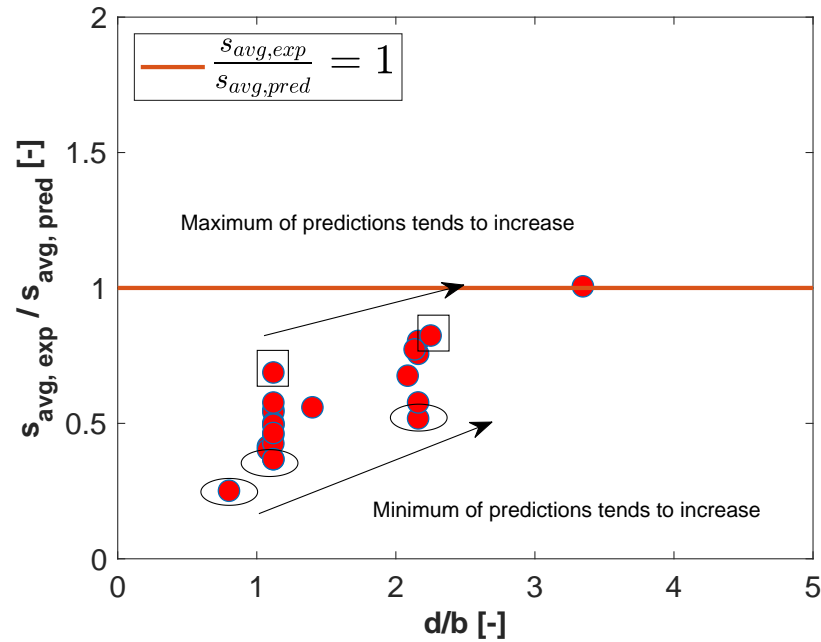


Figure 3.18: The ratio of $s_{avg,exp}/s_{avg,pred}$ versus d/b for fib MC 2010 model [23]

It can be seen from Figure 3.18 that both maximum and minimum of the predictions from the fib MC model tends to increase with the increasing values of d/b . However, all the predictions (except one corresponding to $d/b > 3.0$) are conservative. This trend needs further validation with an experimental dataset to establish if it is a factual trend or a limitation in the sampling.

3.2. Diagonal Compression Strut Angle

3.2.1. Experimental Details

The same set of specimens as described in section 3.1 are used for the analysis of diagonal compression strut angle. Initially, the crack opens parallel to the direction principle strain, however, as the shear force increases the shear crack undergoes rotation and its direction deviates [4]. Thus, the diagonal compression strut angle is the maximum of the diagonal shear crack angle. It may be noted here that although the compression strut angle is not exactly same as shear crack angle but it is similar to it and therefore, a comparison between the values can be made [65].

Table 3.6: Key characteristics of specimens referred for diagonal crack angle study

Publication	Series	Specimens	Mechanical Scheme	Variable	Method
Zakaria et al. [65]	A1-C3	10	4-point bending	crack angle	average angle
Hu and Wu [31]	D10, R10	2	cantilever	crack angle	average angle at mid-height
Lee et al. [37]	B340-120 to B670-200	12	4-point bending	crack angle	average angle in the middle one- third portion along height

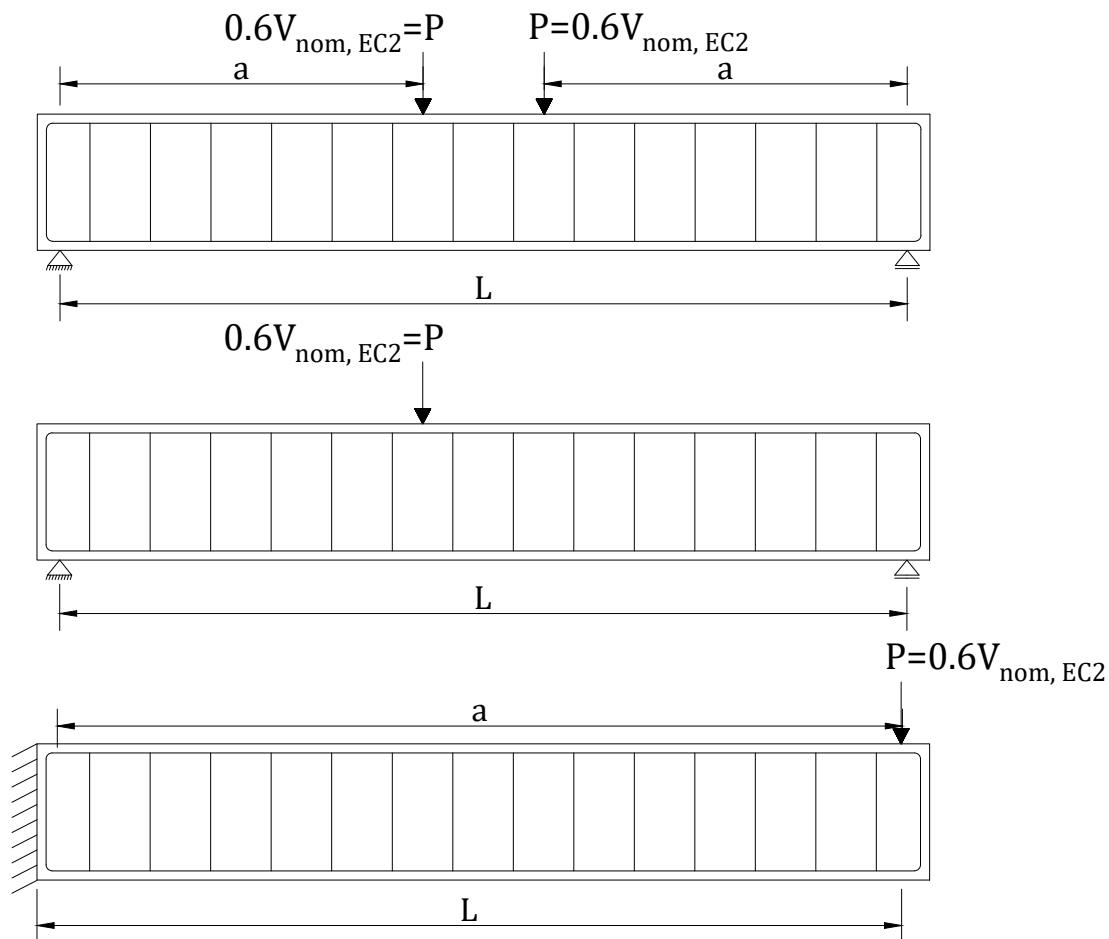


Figure 3.19: The application of service load to the different mechanical schemes considered in the calculation of shear crack angle from different models

Figure 3.19 shows the application of service load (the service load in this study is taken as 60% of the nominal shear resistance calculated from the EC2 VSIM) to different mechanical schemes considered while calculating diagonal compression strut angle from various

models. Note that in SMCFT and NLFEA models, the predicted diagonal compression strut angle is dependent on the magnitude of applied load.

3.2.2. Observations

The experimental values of the shear crack angles are compared with the angle of the compression strut angle calculated using different models. The comparison is summarized in Table 3.8. A total of twenty four set of data points from the previous research studies are analyzed. The experimental observations are made in the stabilized cracking phase i.e., no more shear cracks can be developed with increase in load and the crack pattern is fully-developed. It can be seen that all the models result in a mean prediction ratio greater than 1.0. This means that all predictions are unconservative since the predicted shear crack angle is flatter than the experimentally observed angle. This leads to predicting smaller strains in the stirrups than the actual strains if stirrups are assumed to be smeared across the shear crack. It is observed that the predictions by SMCFT [7] and CFT [31] have the mean values of $\theta_{avg,exp}/\theta_{avg,pred}$ as 1.14 and 1.22 respectively. The SD and COV in case of CFT model are slightly higher than the SMCFT. This is expected since this CFT does not take into account the tensile strength of concrete. It should also be noted that the predictions by CCC model [15] are also close to the experimental values as suggested by the mean, SD and COV values of 1.19, 0.09 and 0.08 respectively.

The crack angle predictions by Theorem of Plasticity are highly biased towards predicting the flatter angles within the range of permissible angles given by the EC2 ($21.8^\circ \leq \theta \leq 45^\circ$) [19]. This is reflected by the mean value of 1.85. Moreover, the model gives rise to relatively high uncertainty in the predictions as is reflected by the SD value of 0.18 and COV of 0.10 respectively which are higher than the corresponding values reported for the SMCFT model predictions and CCC model predictions. The results obtained for the Theorem of Plasticity model in the present analysis are coherent with the observations made by Olalusi [48] who studies the variation of the predicted angle with shear reinforcement parameter $\rho_w f_{ym}$ for EC2-VSIM (Theorem of Plasticity) [19], SMCFT and CCC model [15] (Refer to Figure 3.24). It is observed that the SMCFT gives the most consistent predictions for the angle while Theorem of Plasticity shows bias towards predicting flatter angles even smaller than the lower limit of 21.8 degrees as prescribed in EC2 [19] as shown in Figure 3.24.

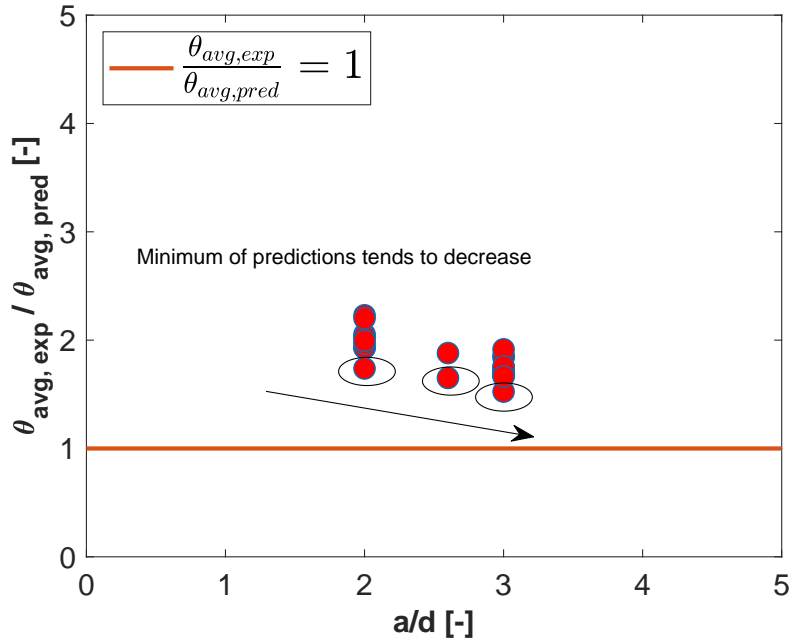


Figure 3.20: The ratio of $\theta_{avg,exp}/\theta_{avg,pred}$ versus a/d for the Theorem of Plasticity [19]

It can be observed from Figure 3.20 that minimum predictions from Theorem of Plasticity model show a tendency to predict lower values with increasing a/d . However, the prediction ratio is greater than 1.0 for all $a/d \leq 3.0$ indicating the model predicts flatter angles than observed in the experiments in the ULS.

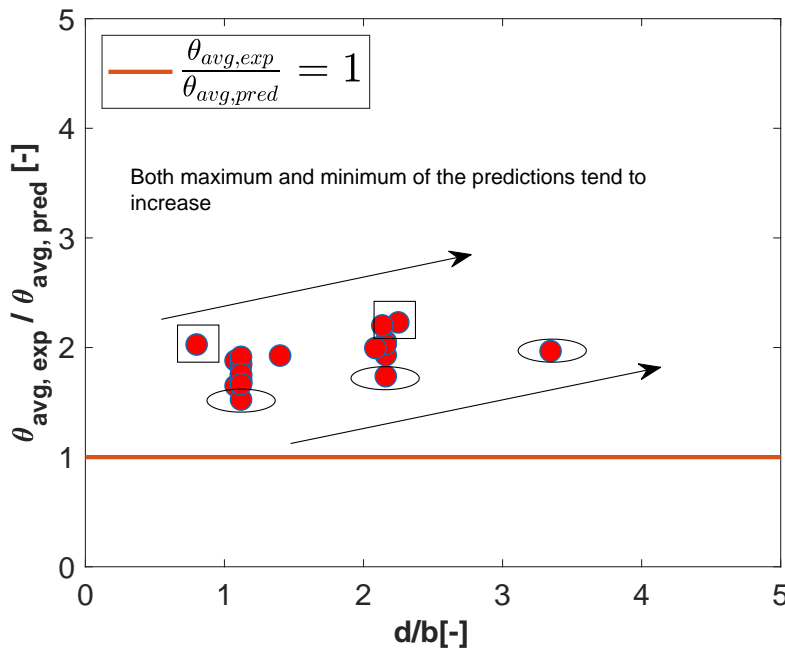


Figure 3.21: The ratio of $\theta_{avg,exp}/\theta_{avg,pred}$ versus d/b for the Theorem of Plasticity [19]

Figure 3.21 shows the variation of the predictions from Theorem of Plasticity model with d/b . It can be seen that both minimum and maximum of the predictions tend to increase

with the increasing d/b . This may result in highly unconservative predictions for slender deep beams.

It can be observed from Figure 3.22 and Figure 3.23 that CFT model and SMCFT model do not show any bias in the prediction for a range of values of $\rho_w f_{ym}$.

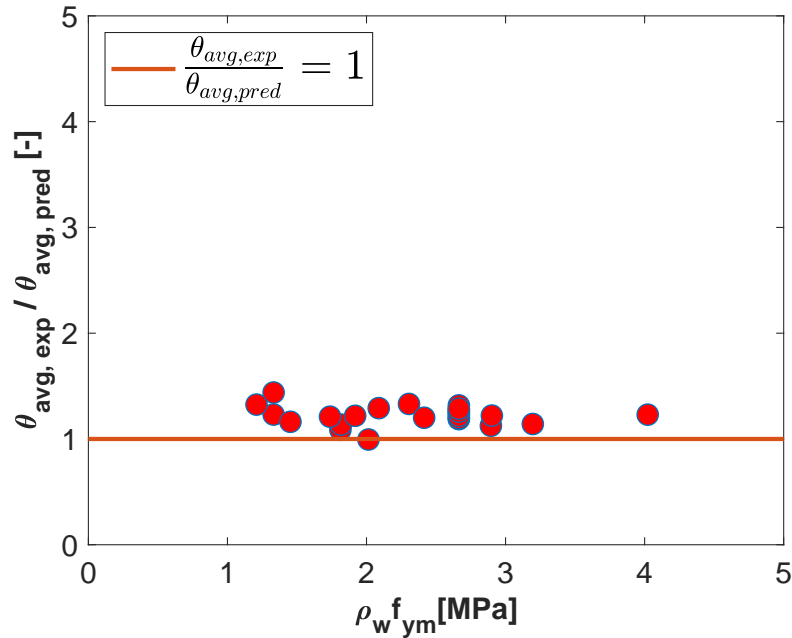


Figure 3.22: The ratio of $\theta_{avg,exp}/\theta_{avg,pred}$ versus $\rho_w f_{ym}$ for the CFT [16]

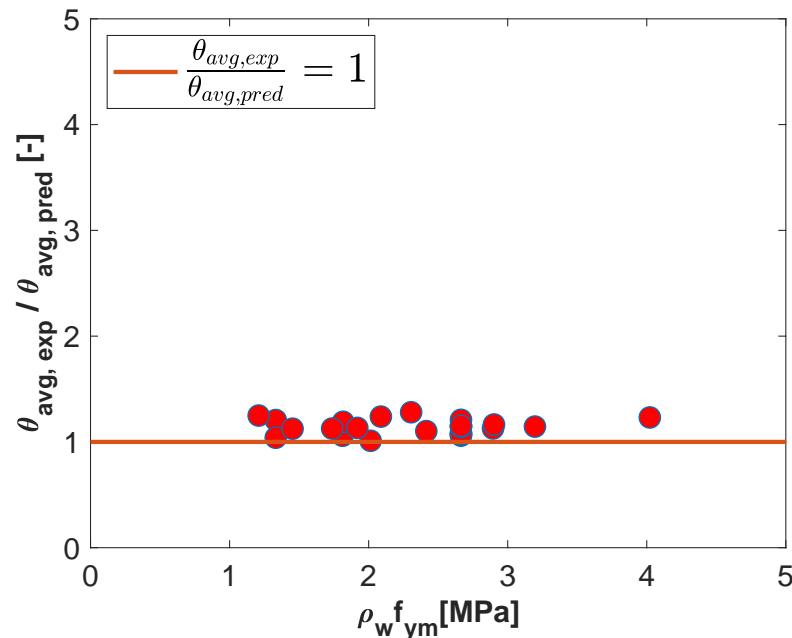


Figure 3.23: The ratio of $\theta_{avg,exp}/\theta_{avg,pred}$ versus $\rho_w f_{ym}$ for the SMCFT [7]

It can be observed from Figure 3.23 that SMCFT model predicts values with a higher dispersion for lower values of $\rho_w f_{ym}$. This model uses half of the longitudinal reinforcement

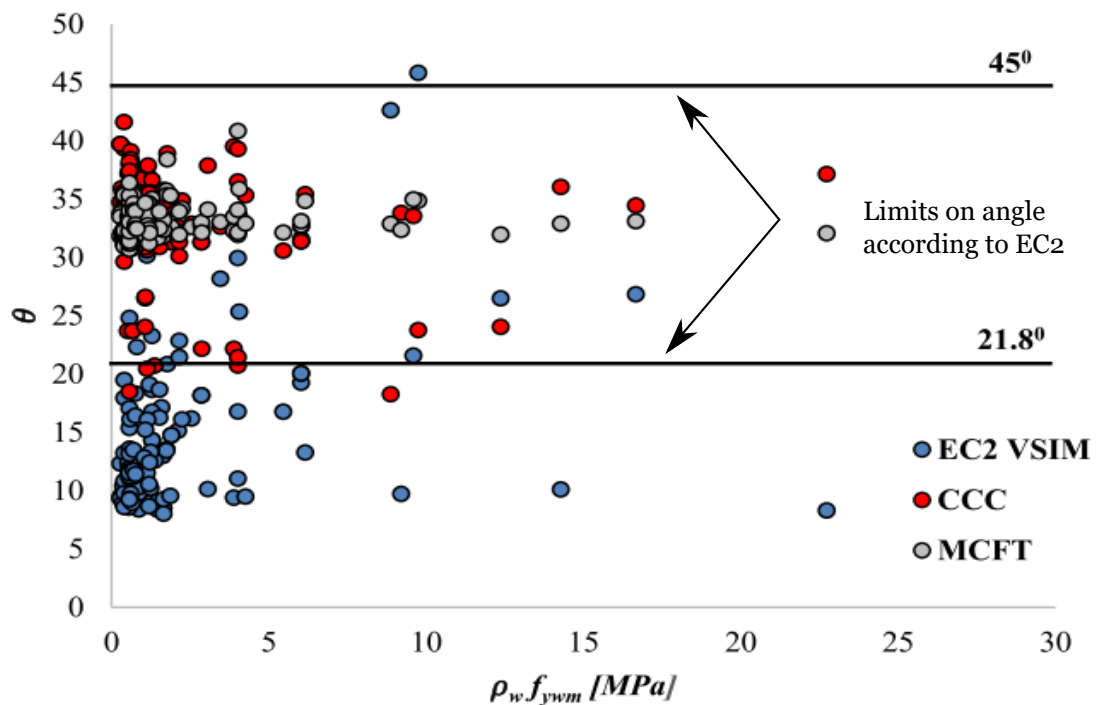
stress as an estimate for the web stress to calculate the shear crack angle. However, the strain varies continuously over the depth. Moreover, the assumption of a linear strain diagram based on the plane section hypothesis may not hold true after cracking. This may be a reason for the observed dispersion in the model predictions. However, a experimental verification is required to establish if it is a factual trend or a limitation of the sampling.

Table 3.7: $\theta_{avg,exp}/\theta_{avg,pred}$ values of the different diagonal compression strut angle prediction models

Specimen	Theorem of Plasticity [19]	$\theta_{avg,exp}/\theta_{avg,pred}$			
		SMCFT [7]	CCC [15]	NLFEA [56]	CFT [16]
A1 left	2.03	1.09	1.27	2.17	1.24
A2 left	1.93	1.06	1.21	1.95	1.19
A3 left	1.93	1.07	1.22	1.93	1.20
A4 left	1.97	1.07	1.24	2.06	1.22
B1 left	2.05	1.14	1.30	2.05	1.27
B2 left	2.03	1.21	1.28	2.75	1.44
B3 left	1.74	1.04	1.10	1.91	1.23
C1	2.23	1.15	1.29	2.46	1.26
C2	2.20	1.21	1.34	2.07	1.32
C3	2.00	1.15	1.33	1.66	1.29
D10	1.65	1.06	1.00	1.19	1.09
R10	1.88	1.19	1.15	1.40	1.14
B334-120	1.53	1.01	1.00	1.20	1.00
B334-160	1.67	1.13	1.10	1.28	1.16
B334-200	1.84	1.25	1.21	1.31	1.32
B480-120	1.72	1.13	1.13	1.46	1.13
B480-160	1.86	1.24	1.22	1.52	1.29
B480-200	1.68	1.13	1.10	1.36	1.21
B530-120	1.75	1.14	1.15	1.47	1.14
B530-160	1.92	1.28	1.26	1.54	1.33
B530-200	1.69	1.13	1.11	1.39	1.22
B667-120	1.70	1.23	1.24	1.60	1.23
B667-160	1.76	1.16	1.16	1.51	1.22
B667-200	1.67	1.10	1.09	1.52	1.20

Table 3.8: Mean, SD and COV of $\theta_{avg,exp}/\theta_{avg,pred}$ for the different compression strut angle prediction models

Statistical Variable	$\theta_{avg,exp}/\theta_{avg,pred}$				
	Theorem of Plasticity [19]	SMCFT [7]	CCC [15]	NLFEA [56]	CFT [16]
Mean	1.85	1.14	1.19	1.70	1.22
Median	1.85	1.14	1.21	1.53	1.22
SD	0.18	0.07	0.10	0.41	0.09
COV	0.10	0.06	0.08	0.27	0.07
Maximum	2.23	1.28	1.34	2.75	1.44
Minimum	1.53	1.01	1.00	1.19	1.00
Range	0.70	0.27	0.34	1.56	0.44

Figure 3.24: The values of θ versus $\rho_w f_{ywm}$ as observed by Oladimeji [48]

3.3. Concrete Contribution to the Shear Resistance

3.3.1. Experimental Details

Table 3.9 shows the summary of the key characteristics of the different experiments from literature referred in the study. The concrete contribution to shear resistance is a crucial parameter because it indicates the load shared by stirrups and therefore, strains in the stirrups for a given applied load. This section describes the experiments referred to compare the results of concrete contribution to the shear strength at ultimate limit state calculated using various models.

Hu and Wu [32] studied the variation in the concrete contribution to shear resistance with

shear span. It is observed that for the RC beams with shear span ratio 2.5 (with deformed bars in shear reinforcement), the concrete contribution is almost comparable from the instance of first diagonal cracking to the first instance of yielding of stirrups (not all the stirrups yield simultaneously). For beams with shear span ratio 3.1, a steep decrement is observed in the concrete contribution to the shear resistance between these two stages (Refer Figure 3.29). According to the ASCE-ACI Committee 426 [4], clause R22.5.1.1 (recommendation also extended to ACI-318-14 [34]), concrete contribution to the shear resistance for both shear reinforced and shear unreinforced beams should be taken as the cracking shear force in the shear unreinforced beam. Therefore, comparison of the predicted concrete contributions from different available models with the concrete contribution to the shear resistance at first diagonal cracking may be relevant and is required to be done.

In the assessment that follows, experiments performed by Hu and Wu [31], Zakaria et al. [66], Hassan et al. [26], Hu and Wu [32], and Munikrishna et al. [44] are referred. The details of the specimens used in the first two researches mentioned are provided in section 3.1 and section 3.2. Hassan et al. [26] assess the behavior of shear reinforced concrete beams with high strength stirrups. Hu and Wu [32] perform a study on the effect of shear span ratio on the concrete and stirrup contribution to the total shear resistance of the reinforced concrete beams for different magnitudes of applied load. Munikrishna et al. performed experimental studies on the shear behavior of reinforced concrete beams with high strength stirrups. The geometrical parameters of the beam specimens are given in Table 3.10. Figure 3.25- Figure 3.28 show the cross section and mechanical scheme of the beam specimens in the experimental work referred in this study.

Table 3.9: Key characteristics of specimens referred for concrete contribution to shear resistance study

Publication	Series	Specimens	Mechanical Scheme	Variable	Method
Zakaria et al. [65]	A1-C3	16	4-point bending	V_{cr}	strain gauges in stirrups
Hassan et al. (2012)	B8, B9	2	3-point bending	V_{cr}	strain gauges in stirrups
Hu and Wu [32]	D2.5, D3.1, R2.5, R3.1	4	cantilever	V_c, V_{cr}	strain gauges in stirrups
Hu and Wu [31]	D10, R10	2	cantilever	V_c, V_{cr}	strain gauges in stirrups
Munikrishna et al. [44]	G1-C60 to G3-M100	9	3-point bending	V_c	strain gauges in stirrups

Table 3.10: Geometrical parameters for the different specimens in the test series of Hu and Wu [32], Hu and Wu [31] and Munikrishna et al. [44] respectively

Specimen	Width (mm)	Height (mm)	ρ_w (%)	ρ_l (%)	a/d	d/b
D2.5	180.0	360.0	0.42	3.27	2.50	1.67
D3.1	180.0	360.0	0.42	3.27	3.10	1.67
R2.5	180.0	360.0	0.64	3.27	2.50	1.67
R3.1	180.0	360.0	0.64	3.27	3.10	1.67
D10	250	300	0.41	2.38	2.6	1.08
R10	250	300	0.62	2.38	2.6	1.08
G1-C60	609.6	711.2	0.11	1.02	3.10	1.06
G1-M80	609.6	711.2	0.09	1.53	3.10	1.06
G1-M100	609.6	711.2	0.07	1.02	3.10	1.06
G2-C60	609.6	711.2	0.11	1.02	3.10	1.06
G2-M80	609.6	711.2	0.09	1.53	3.10	1.06
G2-M100	609.6	711.2	0.07	1.02	3.10	1.06
G3-C60	609.6	711.2	0.31	2.16	3.00	0.75
G3-M80	609.6	711.2	0.25	3.24	3.00	0.75
G3-M100	609.6	711.2	0.2	2.16	3.00	0.75

Table 3.11: Range of parameters for the specimens studies for evaluation of available concrete contribution to shear resistance models

Parameter	Range
a/d	2.5-3.1
d/b	0.75-1.67
$\rho_w f_{ym}$ (MPa)	0.46-2.07
ρ_l (%)	1.02-3.27
ρ_w (%)	0.07-0.64
f'_c (MPa)	32.48-44.00

Table 3.12: Range of parameters for the specimens studies for comparison of concrete cracking shear resistance with predictions from various models

Parameter	Range
a/d	2.5-3.1
d/b	0.80-3.34
$\rho_w f_{ym}$ (MPa)	1.33-2.3.23
ρ_l (%)	1.62-3.64
ρ_w (%)	0.31-0.72
f'_c (MPa)	25-45

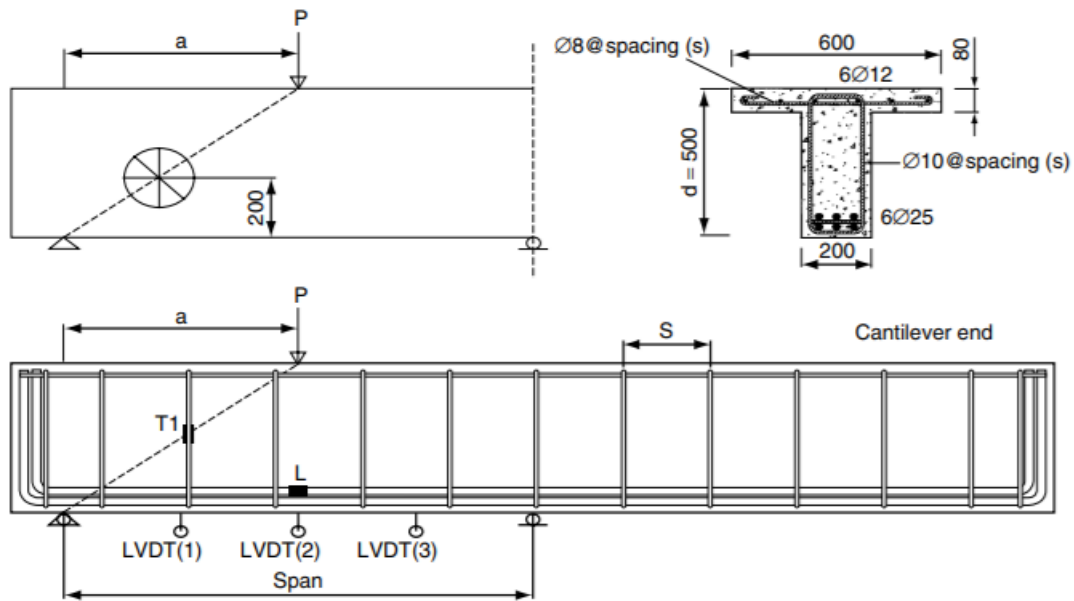


Figure 3.25: The cross section details for the reinforced concrete beams [26]

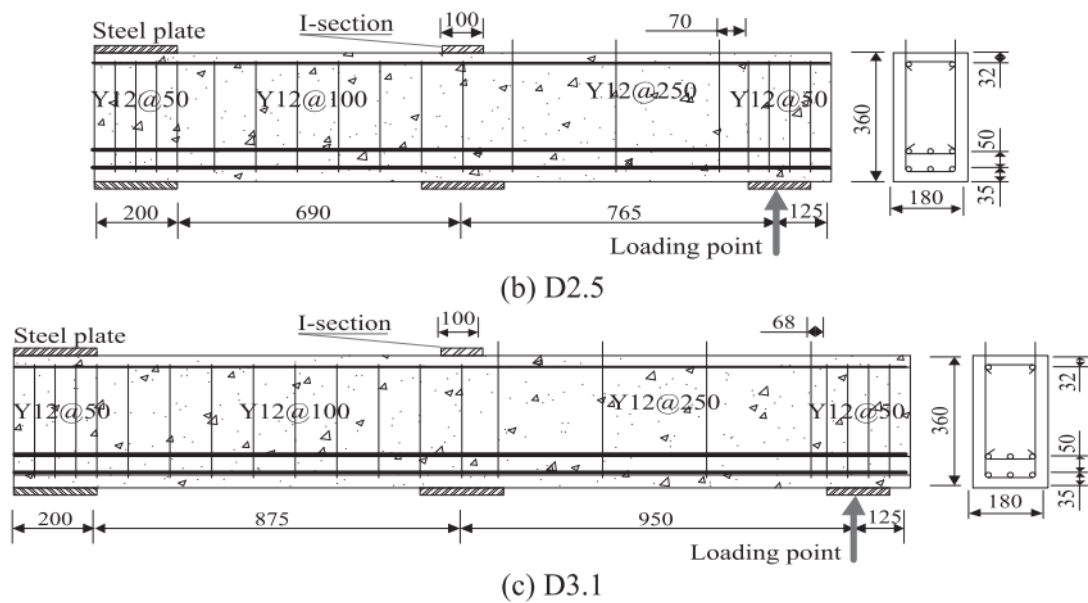
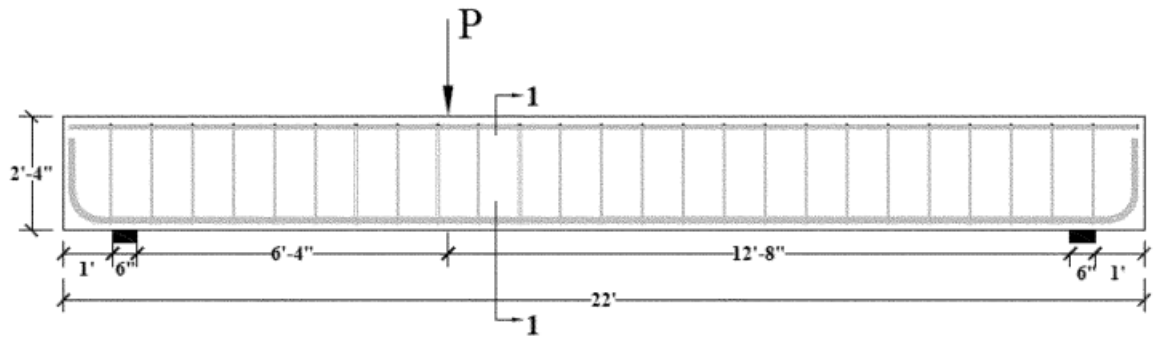
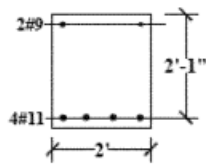


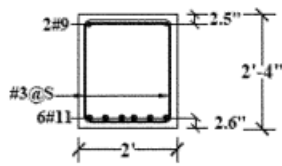
Figure 3.26: The cross section and the mechanical schemes of the reinforced concrete beams [32]



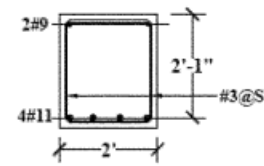
Typ. Sectional Elevation



Section 1-1 for beam G1-M0



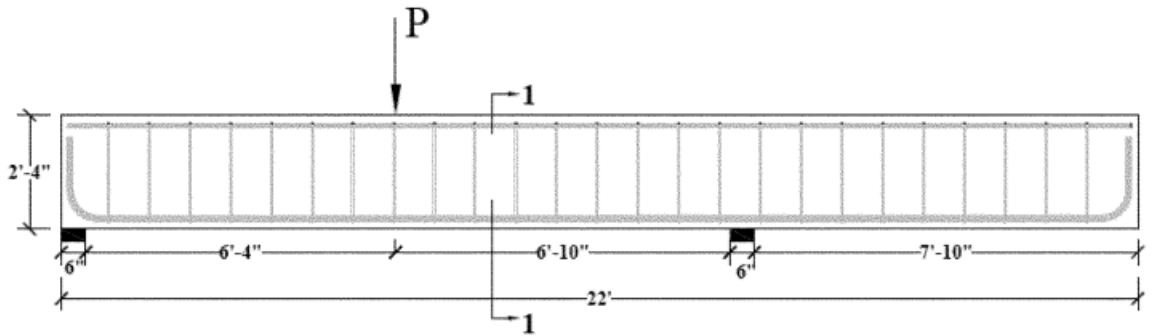
Section 1-1 for beam G1-C60



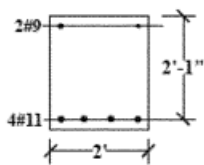
Section 1-1 for beam G1-M80 & G1-M100

Specimen	Spacing, S
G1-M0	-
G1-C60	8"
G1-M80	10"
G1-M100	13"

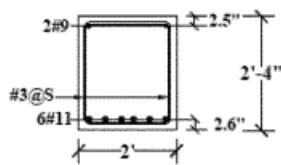
(a)



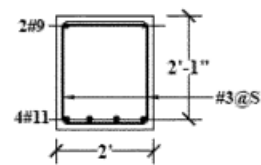
Typ. Sectional Elevation



Section 1-1 for beam G2-M0



Section 1-1 for beam G2-C60



Section 1-1 for beam G2-M80 & G2-M100

Specimen	Spacing, S
G2-M0	-
G2-C60	8"
G2-M80	10"
G2-M100	13"

(b)

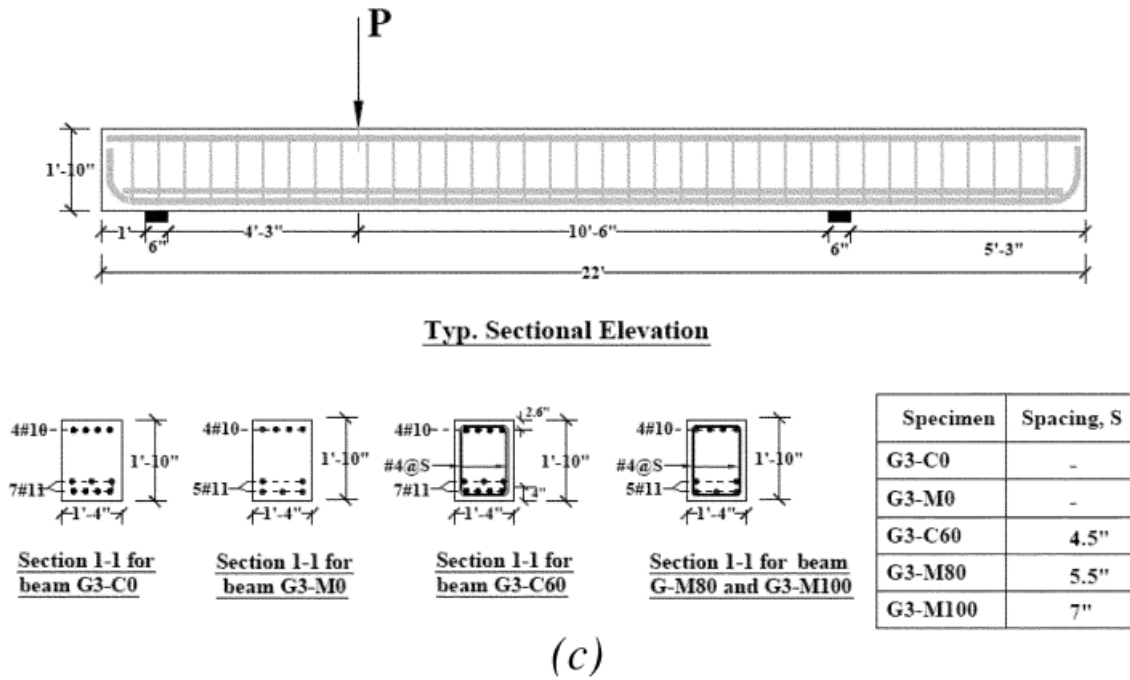


Figure 3.27: The cross section and the mechanical schemes of the RC beams [44]

Note: The dimensions mentioned in the Figure 3.27 are in feet and inches.

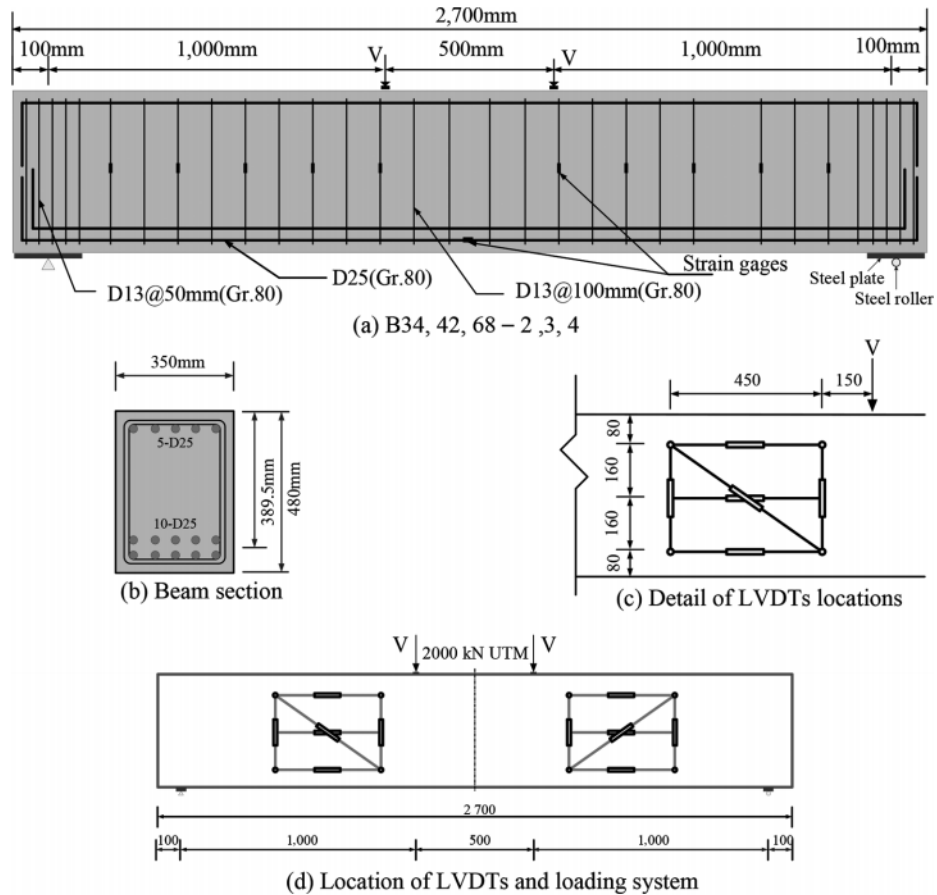


Figure 3.28: The cross section and the mechanical schemes of the RC beams [38]

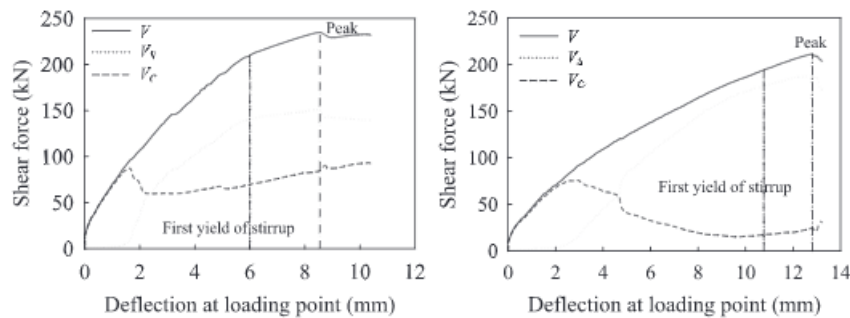


Figure 3.29: The variation of concrete and stirrup contribution to shear resistance for the beam with a/d 2.5 (Left) and 3.1 (Right) respectively [32]

3.3.2. Observations

Table 3.16 and Table 3.17 show the mean, SD and COV of the ratio of experimental to predicted concrete contribution to the ultimate shear resistance. The prediction ratio (experimental to predicted value) of the concrete contribution to shear resistance at ultimate limit state for each specimen using different models is shown in Table 3.16 and Table 3.17. It can be seen that Tureyen and Frosch (2003) [54], Niwa et al. [46], JSCE [1], ACI-318-11 [33] and CCC [15] models give conservative estimates for the concrete contribution to the ultimate

shear resistance. CCC model gives relatively the most accurate (and also conservative) predictions for the concrete contribution to the ultimate shear resistance with the mean value of the experimental to predicted concrete contribution equal to the 1.05. The model also shows relatively better consistency in the predictions with the SD and COV of 0.35 and 0.33 respectively.

Table 3.13 shows the ratio of experimentally observed shear cracking load and predicted concrete shear resistance from the various models. It can be observed that the predicted values are noticeably smaller than the experimentally observed cracking shear resistance (the mean prediction ratio is significantly greater than 1.0). This indicates that generally concrete contribution to shear resistance decreases continuously from instance of first diagonal shear cracking to the ultimate shear failure. Therefore, equating concrete shear resistance at ultimate limit state from the aforementioned models to the first diagonal shear cracking load is assumed to yield a conservative estimate of first diagonal shear cracking load.

Table 3.13: $V_{cr,exp}/V_{c,pred}$ ratio for the concrete contribution to the shear resistance at first diagonal crack by different models

Statistical Variable	$V_{cr,exp}/V_{c,pred}$				
	Tureyen and Frosch [54]	Niwa et al. [46]	JSCE [1]	ACI-318-11 [33]	CCC [15]
Mean	2.19	1.79	2.05	2.38	1.72
Median	2.16	1.74	2.09	2.35	1.75
SD	0.83	0.65	0.76	0.90	0.65
COV	0.38	0.36	0.37	0.38	0.38
Max	4.35	3.25	3.44	4.66	2.93
Min	1.04	0.83	0.89	1.04	0.75
Range	3.31	2.41	2.55	3.62	2.18

Table 3.14: $V_{c,avg,exp}/V_{c,avg,pred}$ ratio for the concrete contribution to the ultimate shear resistance by different models (a)

Specimen	$V_{c,avg,exp}/V_{c,avg,pred}$				
	EC2 [19]	ACI 318-11 [33]	CCC [15]	CSA [5]	JSCE [1]
D10	0.78	1.11	0.82	0.86	0.95
R10	1.10	1.58	1.17	1.22	1.33
D2.5	0.93	1.43	0.99	1.04	1.13
D3.1	0.27	0.41	0.30	0.30	0.32
R2.5	1.61	2.48	1.72	1.81	1.95
R3.1	0.54	0.82	0.59	0.60	0.66
G1-C60	1.05	0.98	1.33	0.61	1.32
G1-M80	0.92	0.98	1.16	0.55	1.16
G1-M100	1.06	0.98	1.32	0.61	1.33
G2-C60	1.05	0.98	1.33	0.61	1.32
G2-M80	0.92	0.98	1.16	0.55	1.16
G2-M100	1.06	0.98	1.32	0.61	1.33
G3-C60	0.77	0.97	0.90	0.85	0.95
G3-M80	0.69	0.98	0.79	0.74	0.84
G3-M100	0.79	0.98	0.89	0.88	0.98

Table 3.15: $V_{c,avg,exp}/V_{c,avg,pred}$ ratio for the concrete contribution to the ultimate shear resistance by different models (b)

Specimen	$V_{c,avg,exp}/V_{c,avg,pred}$				
	AASHTO [47]	Zsutty [69]	Zararis [65]	Niwa et al. [46]	Tureyen & Frosch [54]
D10	0.86	0.78	0.48	0.89	1.11
R10	1.22	1.10	0.66	1.25	1.56
D2.5	1.05	0.90	0.56	1.04	1.30
D3.1	0.30	0.28	0.16	0.33	0.37
R2.5	1.81	1.55	0.96	1.80	2.24
R3.1	0.60	0.56	0.33	0.66	0.75
G1-C60	0.61	0.94	0.91	1.34	1.30
G1-M80	0.55	0.82	0.79	1.17	1.10
G1-M100	0.61	0.94	0.91	1.34	1.31
G2-C60	0.61	0.94	0.91	1.34	1.30
G2-M80	0.55	0.82	0.79	1.17	1.10
G2-M100	0.61	0.94	0.91	1.34	1.31
G3-C60	0.85	0.73	0.54	0.95	0.97
G3-M80	0.74	0.64	0.49	0.84	0.85
G3-M100	0.89	0.74	0.55	0.97	0.99

Table 3.16: Statistical parameters for $V_{c,avg,exp}/V_{c,avg,pred}$ ratio for the concrete contribution to the ultimate shear resistance by different models (a)

Statistical Variable	$V_{c,avg,exp}/V_{c,avg,pred}$				
	EC2 [19]	ACI 318-11 [33]	CCC [15]	CSA [5]	JSCE [1]
Mean	0.90	1.11	1.05	0.79	1.12
Median	0.92	0.98	1.16	0.61	1.16
SD	0.30	0.46	0.35	0.36	0.37
COV	0.33	0.41	0.33	0.46	0.33
Maximum	1.61	2.48	1.72	1.81	1.95
Minimum	0.27	0.41	0.30	0.30	0.32
Range	1.34	2.07	1.42	1.50	1.62

Table 3.17: Statistical parameters for $V_{c,avg,exp}/V_{c,avg,pred}$ ratio for the concrete contribution to the ultimate shear resistance by different models (b)

Statistical Variable	$V_{c,avg,exp}/V_{c,avg,pred}$				
	AASHTO [47]	Zsutty [69]	Zararis [65]	Niwa et al. [46]	Tureyen and Frosch [54]
Mean	0.79	0.84	0.66	1.09	1.17
Median	0.61	0.82	0.66	1.17	1.11
SD	0.36	0.28	0.24	0.35	0.41
COV	0.46	0.33	0.37	0.32	0.35
Max	1.81	1.55	0.96	1.80	2.24
Min	0.30	0.28	0.16	0.33	0.37
Range	1.51	1.27	0.80	1.47	1.87

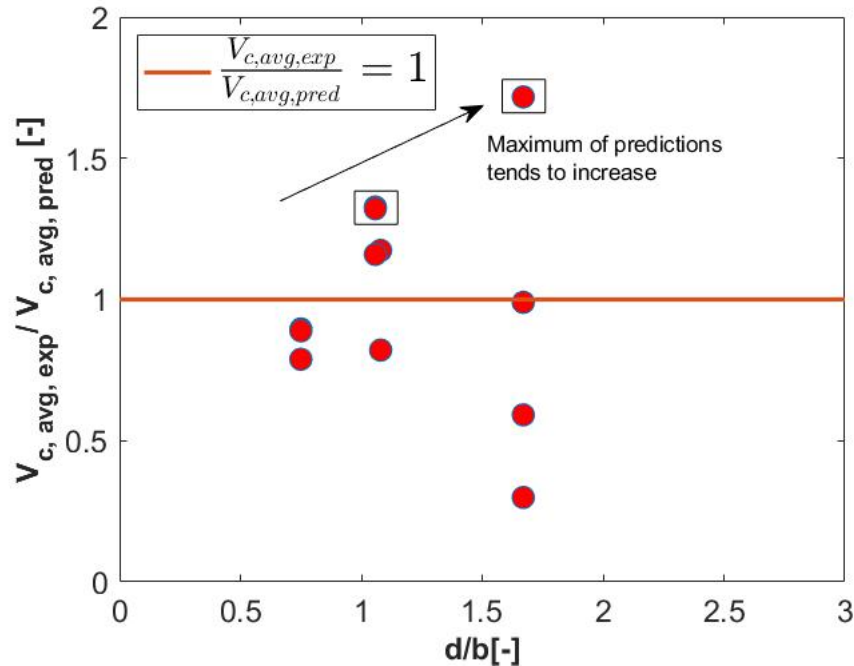


Figure 3.30: $V_{c,avg,exp}/V_{c,avg,pred}$ versus d/b for predictions by CCC model [15]

It can be seen from Figure 3.30 that the maximum of the predictions from the CCC model tends to increase with the increasing d/b . This shows a tendency of the predictions to become increasingly unconservative and thus, this model may give highly unconservative values for deep slender beams. However, a verification with an experimental study may be needed to establish if this observed tendency is factual or a limitation of the sampling.

3.4. Conclusion

In this Chapter, the performance of the different models for diagonal compression strut angle, diagonal crack spacing and concrete contribution to shear resistance is assessed by comparison with experimental observations. The following conclusions are drawn.

1. Zakaria et al. Crack Spacing Model and fib Crack Spacing Model gives conservative estimates of shear crack spacing from shear crack width calculation point of view. The best estimate is given by Zakaria et al Model. Moreover, It is observed that fib MC model predicted over conservative values of shear crack spacing.
2. All the studied shear crack angle models predict unconservative (flatter angles) values (in varying degrees) as compared to the experimental observations. The best estimates are obtained by SMCFT, CCC and CFT models.
3. The best estimate of concrete contribution to shear resistance is obtained using CCC model. It is observed from the experimental data that the predicted value of concrete contribution to shear resistance at ULS can serve as a conservative estimate for the first diagonal shear cracking load.

4

Proposed Models

“Imagination is more important than knowledge.”

Albert Einstein

This Chapter comprises the proposed models for diagonal shear crack width and shear deflection under service loads for the slender ($a/d > 2.5$) shear reinforced concrete beams. The performance of these models is assessed by comparison with experimental values. The results are presented in the form of a prediction ratio (ratio of experimentally observed value to the predicted value) for evaluation in terms of accuracy in predictions. The variation of mean prediction ratio is studied against various experimental specimen parameters to identify any bias in the predictions with respect to any of these parameters. The models are assessed for the accuracy by closeness of the mean prediction ratio (experimentally obtained shear crack width to the predicted shear crack width) to one. Moreover, a sensitivity analysis of the models with respect to the statistical dependence on the various material and mechanical parameters of the beams is assessed. Appendix D provides a solved example for calculation of mean shear crack width and shear deflection using the proposed models.

THIS Chapter explains the theoretical background and performance of the proposed models for calculating mean shear crack width and shear deflection. It may be noted that default units for the various parameters are in N and mm unless stated otherwise. Also, same equations from the models described in Chapter 2 are used in various proposed models but some of these equations are restated here for the ease of readability.

4.1. Concrete and Steel Contribution to Shear Resistance

In Chapter 3, the prediction accuracy of various models available in the literature for shear crack spacing, diagonal compression strut angle and concrete contribution to shear resistance is assessed. Also, in Chapter 3 it is observed that stirrup strain and principle tensile strain in the concrete (in between the cracks) are crucial parameters that influence the shear crack width. In this section, an approach is suggested to make an engineering estimate of the concrete contribution to shear resistance corresponding to the service loads. Firstly, an estimate of the concrete contribution to shear resistance at ULS should be made with CCC [15] model. Based on the discussion in Chapter 3, this concrete contribution V_c can be assumed equal to first diagonal cracking shear force, V_{cr} . Equation 4.18 is proposed by CCC model to evaluate the concrete contribution to shear resistance of the shear reinforced beam at ULS.

Figure 4.1 shows the variation of concrete and steel stirrups contribution to the shear resistance as per experimental observations [32]. It can be seen that the concrete contribution decreases after the first diagonal shear crack occurs (after the first diagonal crack occurs stirrups are activated and begin to take any further load) and only start to increase noticeably again once the stirrups have yielded. In the proposed model, it is assumed that the concrete contribution to the shear resistance decreases linearly (from V_{cr} at the first diagonal crack) to zero (at the applied load equal to V_{nom} according to EC2 [19]) as shown in Figure 4.2. Moreover, in the proposed approach, It is assumed that there is no yielding in stirrups at service loads. Thus, concrete contribution to the shear resistance at the service loading conditions can be obtained using Equation 4.1.

$$V_{c,pred,ser} = V_{cr,CCC} + \frac{(0 - V_{cr,CCC})}{V_{nom} - V_{cr,CCC}} (V_{ser} - V_{cr,CCC}) \quad (4.1)$$

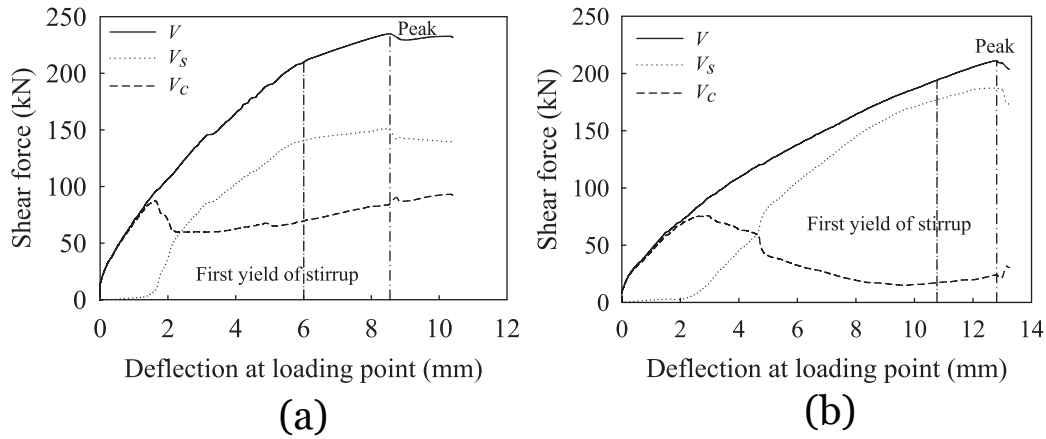


Figure 4.1: Variation of V_c and V_s for two beam specimens with shear span ratio of 2.5 and 3.1 respectively [32]

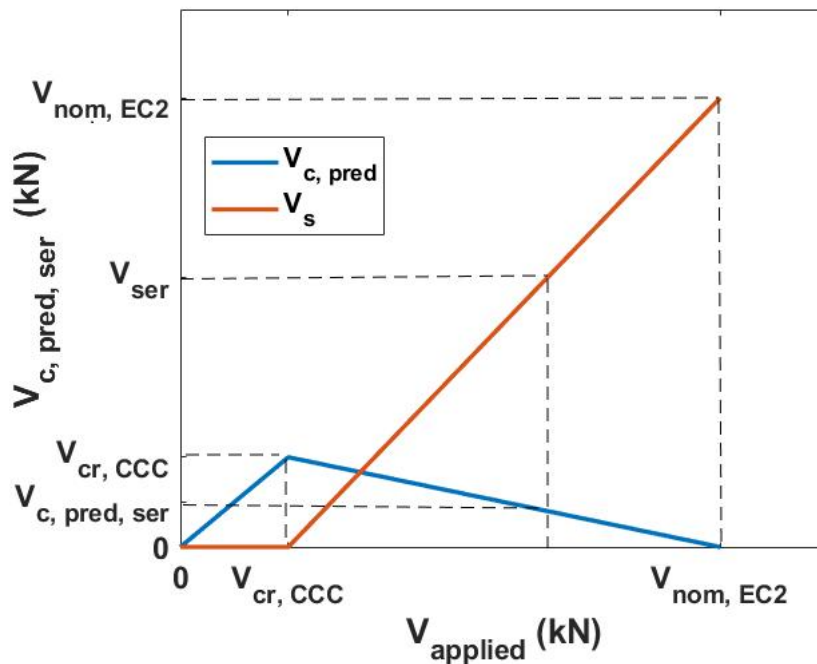


Figure 4.2: Proposed method to calculate V_c at service load condition

Now,

$$V_s = V - V_c \tag{4.2}$$

In the Equation 4.2, V_c at service loading conditions can be obtained by equating it to the $V_{cr,pred,ser}$ as obtained In Equation 4.1.

4.2. Principle Strains and the Stirrups Strain

Hu and Wu [31] found that before the yielding of shear reinforcement (which in the proposed models is also assumed to hold since shear stirrups are not expected to yield un-

der the application of service loads), the measured inclination of the principle stresses are very close to the direction of principle strains. Similar observations are made by Bhide and Collins ([10], [11]) who found that initially the crack formation occurs almost along the direction of principal strains and the crack only rotates later with the increasing value of principle strains. Therefore, in the proposed models in this Chapter, the assumption of co-axiality of principle stress and principle strain is adopted.

Assuming that the transverse reinforcement is uniformly distributed across the crack sur-

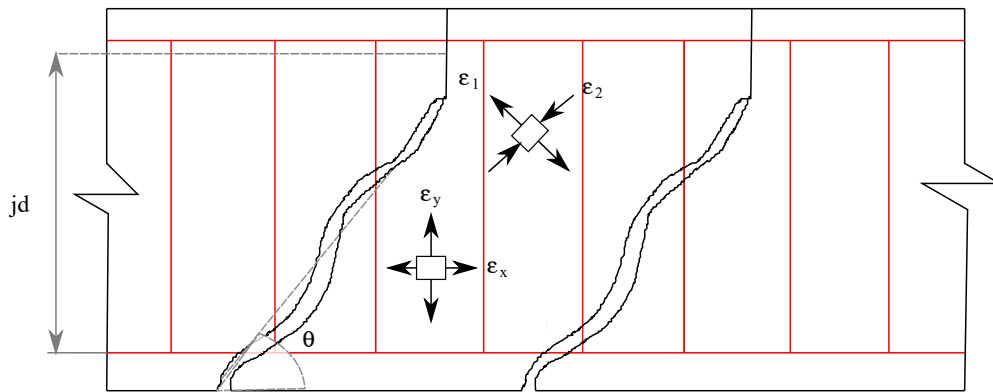


Figure 4.3: The local stress and strain at the crack surface of an RC beam

face and the transverse strain in concrete is equal to the strain in the stirrups, stirrups strain can be given by Equation 4.3 [41].

$$\varepsilon_y = \frac{V_s s}{A_v E_s j d \cot \Theta} \quad (4.3)$$

The force in the diagonal compression strut from Figure 4.3 and Figure 4.4 can be given by Equation 4.4.

$$\sin(\theta) = \frac{V}{V_{strut}} \quad (4.4)$$

Now assuming that the strut is in linear elastic stage under the application of service loads, stress in the strut can be obtained by Equation 4.5.

$$\sigma_{strut} = \frac{V_{strut}}{A_{strut}} \quad (4.5)$$

where,

$$A_{strut} = j d \cos(\theta) b_w \quad (4.6)$$

Thus, principle compressive strain in the diagonal concrete strut can be given by Equation 4.7.

$$\varepsilon_2 = -\frac{V}{j d b_w E_c \sin \Theta \cos \Theta} = -\frac{V_s + V_c}{j d b_w E_c \sin \Theta \cos \Theta} \quad (4.7)$$

where:

θ diagonal compression strut angle.

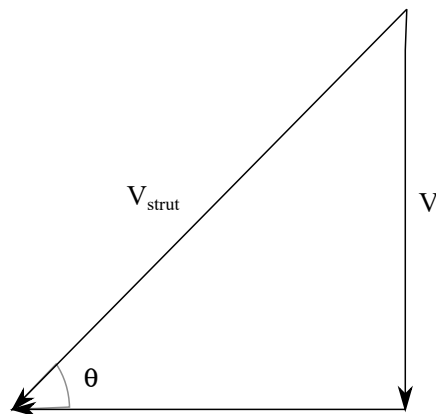


Figure 4.4: The components of the applied shear force along and perpendicular to the diagonal compression strut

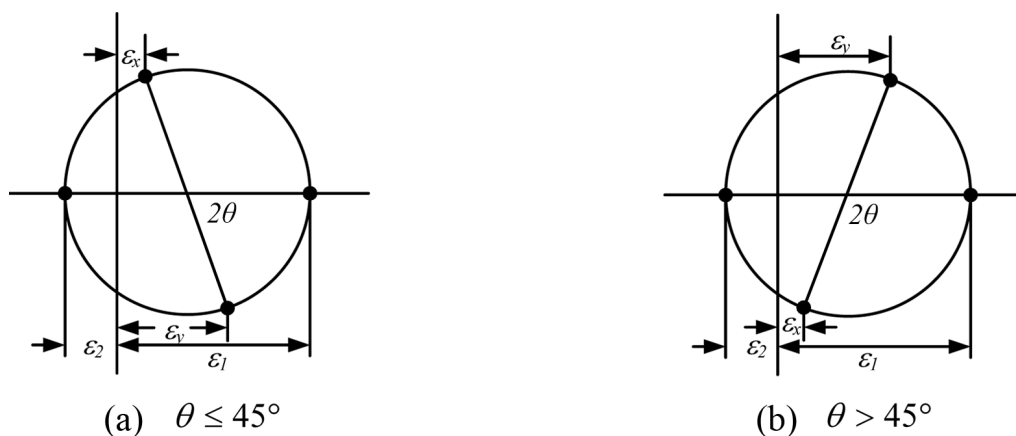


Figure 4.5: The Mohr circle for strains for different values of θ [41]

The relationship in Equation 4.8 between the principle strains can be obtained from the Figure 4.5.

$$\varepsilon_1 = \frac{2(\varepsilon_y + \varepsilon_2)}{|\cos 2\theta| + 1} - \varepsilon_2 \quad (4.8)$$

4.3. Shear Crack Width

In the discussion so far, a calculation strategy to obtain the concrete contribution to shear resistance and subsequently the principle strains and the stirrup strain is proposed. These strain values form the basis of the calculations of mean shear crack width using the models proposed in this section.

4.3.1. Model-IA

This model is adapted from EC2 crack width formula for tensile and flexural cracks. The current EC2 crack spacing model [19] evaluates the crack spacing by virtually transforming the given cross section into the cross section of an equivalent hidden tensile member. In

this model, it is proposed to calculate the shear crack spacing using the current methodology provided in EC2 to calculate crack spacing for members with reinforcement in orthogonal directions. The crack spacing is influenced by the bond transfer length between concrete and reinforcement. The stress in the longitudinal reinforcement is maximum at the location of intersection of longitudinal reinforcement with cracks and gradually the stress is transmitted to concrete over the transfer length. It is assumed that a similar stress distribution holds for stirrups as well (see Figure 4.6 and Figure 4.7). The obtained crack spacing should then be multiplied with the average reinforcement strain (stirrup strain) in between the two diagonal shear cracks.

It is assumed that the influence of longitudinal reinforcement on the shear crack width is taken into account only through its influence in shear crack spacing, $s_{r,max,\theta}$. The shear crack spacing is a function of crack control characteristics of longitudinal and transverse reinforcement (calculated by the parameter $s_{r,max}$ in both directions). The crack spacing control parameter of the longitudinal reinforcement is applicable to the hidden tensile member as shown in Figure 4.8. It is assumed that crack spacing control parameter in transverse direction is also applicable to the hidden tensile member around the stirrups. The crack spacing control parameter in transverse direction is calculated using a definition of the effective area of the hidden tensile member (around stirrups) from the fib MC 2010 [23] as shown in the Figure 4.10. The concrete contribution to shear resistance at ULS (to obtain stirrup force, stress and strain) and the mean shear crack angle are calculated using the CCC model (Equation 4.18 and Equation 4.30 respectively).

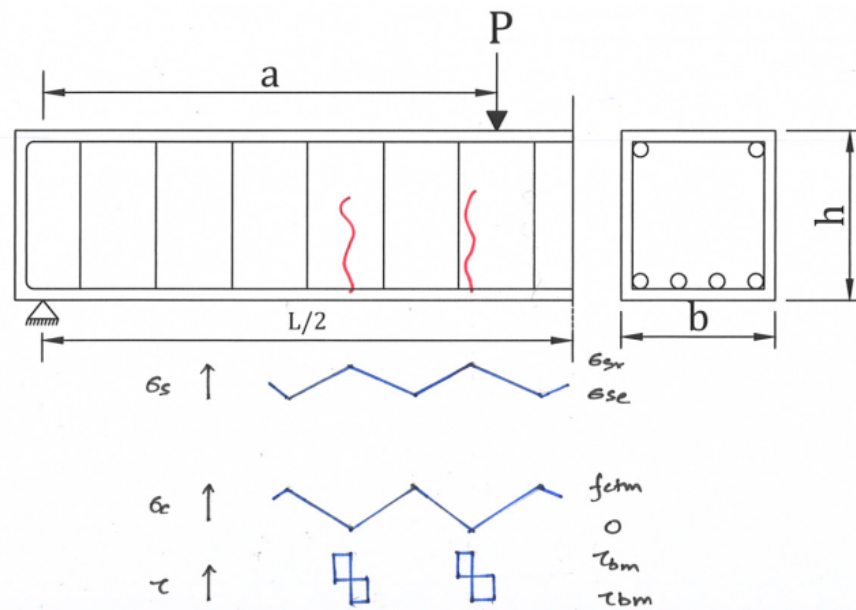


Figure 4.6: Figure showing stress distribution in concrete and longitudinal reinforcement close to flexural cracks

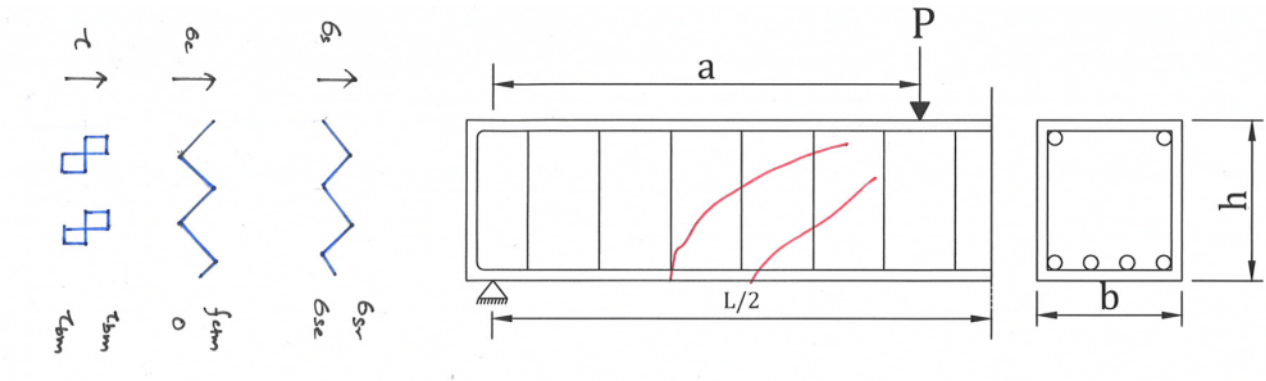


Figure 4.7: Figure showing assumed stress distribution in concrete and longitudinal reinforcement close to shear cracks

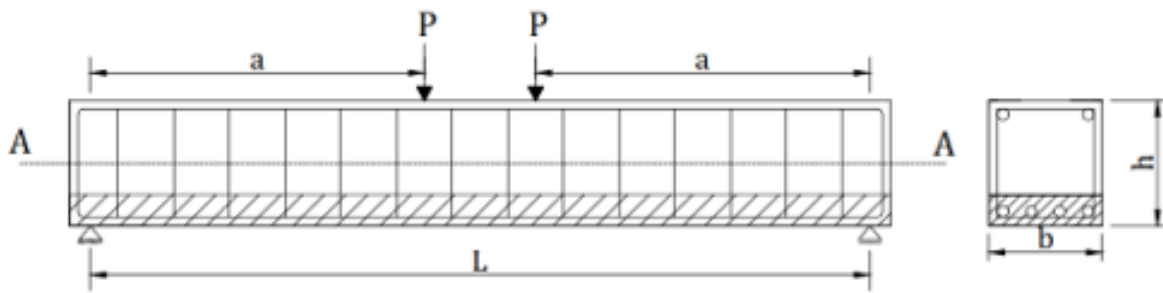


Figure 4.8: Effective area of the hidden tensile member around longitudinal reinforcement as per EC2 [19]

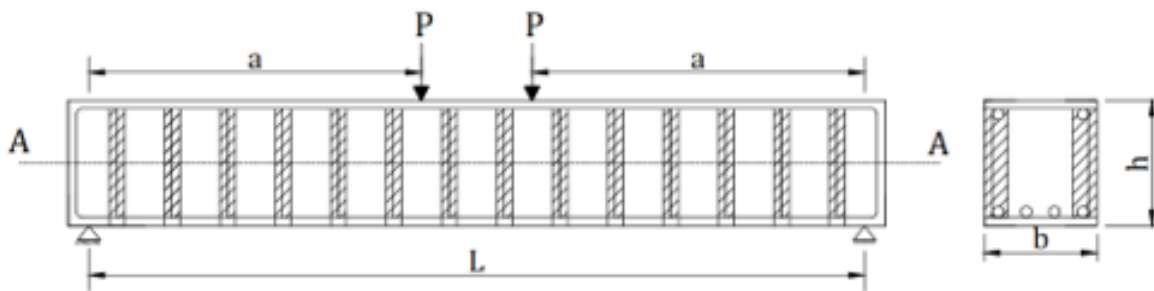
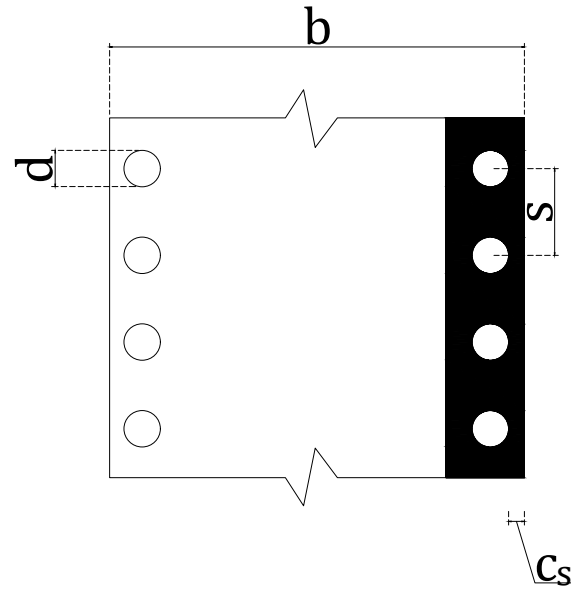


Figure 4.9: Assumed effective area of the hidden tensile member around stirrups.



$$A_{\text{eff}} = \min \{ (2.5 (c_s + d/2))s, 0.5bs \}$$

Figure 4.10: Effective area of the hidden tensile member around stirrups as given in fib MC 2010 [23]

$$A_{y,ef} = \min (2.5(c_s + d_{by}/2)s_y, (b_w/2)s_y) \quad (4.9)$$

The crack width is calculated using the Equation 4.10 given in the EC2 [19].

$$w_k = s_{r,max}(\varepsilon_{sm} - \varepsilon_{cm}) \quad (4.10)$$

$$w_{avg} = s_{r,avg}(\varepsilon_{sm} - \varepsilon_{cm}) \quad (4.11)$$

$$\varepsilon_{sm} - \varepsilon_{cm} = \frac{\sigma_s - k_t \frac{f_{ct,eff}}{\rho_{p,eff}} (1 + \alpha_e \rho_{p,eff})}{E_s} \geq 0.6 \frac{\sigma_s}{E_s} \quad (4.12)$$

where:

σ_s the stress in the stirrup assuming a cracked section.

$\alpha_e = E_s/E_{cm}$.

$\rho_{p,eff} = 0.5A_{sw}/A_{y,eff}$

A_{sw} the cross section area (of both legs) of the stirrups.

$A_{y,eff}$ the area shown in Figure 4.10.

k_t factor that accounts for duration of loading.

= 0.6 for short term loading.

= 0.4 for long term loading.

Limitation of the Current EC2 Crack Width Model

It must be noted that the crack width calculated using Equation 4.10 is characteristic crack width and not mean crack width. This is clear because the mean stirrup strain is multiplied with the maximum diagonal crack spacing in this equation. However, to properly evaluate the prediction accuracy of the crack width model, mean crack width is required since

only mean crack width can be compared directly with the experimental values. Therefore, it is decided to introduce a factor to reduce the maximum shear crack spacing from the EC2 Crack Spacing Model to mean shear crack spacing. In the derivation of the EC2 Crack Spacing Model, the maximum crack spacing corresponds to 2 times the transfer length (for the transfer of forces from reinforcement to concrete) [12]. The minimum crack spacing corresponds to the transfer length. Therefore, it can be assumed that the mean crack spacing corresponds to 1.5 times the transfer length. Therefore, the maximum crack spacing from EC2 Crack Spacing Model in Equation 4.28 is multiplied with (1.5/2) to obtain the mean shear crack spacing.

It must be noted that Equation 4.12 is applicable for the longitudinal tensile reinforcement and nothing is explicitly mentioned about the transverse direction in the current EC2 version. The given Equation 4.12 considers the tension stiffening effect of concrete in between the cracks. The reinforcement stress is maximum at the location of intersection of reinforcement with crack and gradually reduces as stress is transferred to the concrete due to bond slip between reinforcement and concrete over the disturbed area. The stress in concrete is zero at the location of crack and gradually increases along the disturbed area. In the present model, similar mechanism for the transfer of forces from reinforcement to concrete is assumed around stirrups. Therefore, Equation 4.12 is used to evaluate the mean strain in the stirrups as well. Now,

$$\sigma_s = \frac{V_s}{E_s} \quad (4.13)$$

$$V_s = V - V_c \quad (4.14)$$

$$V_c = V_{c,pred,ser} \quad (4.15)$$

$$V_{c,pred,ser} = V_{cr,CCC} + \frac{(0 - V_{cr,CCC})}{V_{nom} - V_{cr,CCC}}(V_{ser} - V_{cr,CCC}) \quad (4.16)$$

$$V_{cr,CCC} = V_{Rm,c} \quad (4.17)$$

The Equation 4.15 is proposed to evaluate this contribution to the shear resistance.

$$V_{Rm,c} = V_c + V_w + V_l = 0.3\zeta \frac{x}{d} (f_{cm})^{\frac{2}{3}} b_{v,eff} \quad (4.18)$$

where

V_c the contribution of the compression zone.

V_w the shear transferred by concrete across the crack.

V_l the contribution of longitudinal rebars to shear resistance of concrete through dowel action.

$$\frac{x}{d} = 0.75(\alpha_e \rho_l)^{\frac{1}{3}} \quad (4.19)$$

if $x \leq h_f$

$$b_{v,eff} = b_v = b_w + 2h_f \leq b \quad (4.20)$$

if $x > h_f$

$$b_{v,eff} = b_w + (b_v - b_w) \left(\frac{h_f}{x} \right)^{\frac{3}{2}} \quad (4.21)$$

where

b_v effective width of the compression flange.
 b total cross-section width at the flange.

$$b_v = b_w + 2h_f \leq b \quad (4.22)$$

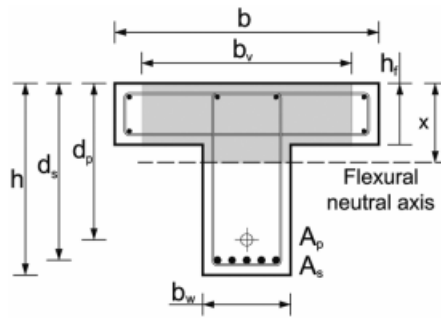


Figure 4.11: Notations for a T beam [15]

The minimum shear strength contribution by concrete can be expressed Equation 4.23.

$$V_{Rm,min} = 0.25 \left(\zeta \frac{x}{d} + \frac{20}{d} \right) (f_{cm})^{\frac{2}{3}} b_w d \quad (4.23)$$

$$\zeta = \frac{2}{\sqrt{1 + \frac{d}{200}}} \left(\frac{d}{a} \right)^{0.2} \geq 0.45 \quad (4.24)$$

The shear crack spacing can be determined using EC2 crack spacing model as follows.

EC2 Crack Spacing Model

1. Reinforcement bars spaced $< 5(c + \phi/2)$ c/c (centre to centre)

This model is derived using the cracking in a tension member model wherein the crack spacing between the two cracks is governed by the transfer length for the forces to get transferred from the steel reinforcement bar to concrete.

According to EC2 [19] if the reinforcement bars are located with respect to each other within a distance of $5(c + \phi/2)$, the crack spacing may be calculated using the Equation 4.25.

$$s_{r,max} = k_3 c + k_1 k_2 k_4 \phi / \rho_{p,eff} \quad (4.25)$$

It is suggested to use ϕ_{eq} where more than one type of reinforcement bar diameters are present. If a section contains n_1 and n_2 reinforcement bars with diameters ϕ_1 and

ϕ_2 respectively, then ϕ_{eq} is calculated using Equation 4.26.

$$\phi_{eq} = \frac{n_1\phi_1^2 + n_2\phi_2^2}{n_1\phi_1 + n_2\phi_2} \quad (4.26)$$

where

c the clear cover to the longitudinal reinforcement.

k_1 coefficient to account for the bond properties of the reinforcement.

= 0.8 for HYSD (High Yield Strength Deformed Bars).

=1.6 for plain reinforcement bars.

k_2 coefficient to account for the type of strain distribution.

=0.5 for flexure.

=1.0 for pure tension.

It may be noted that the recommended values of k_3 and k_4 are 3.4 and 0.425 respectively. The second term on right hand side in the Equation 4.25 arises from the transfer length for the transfer of forces from the reinforcement bars to concrete. The first term on right hand side in the equation effectively provides a lower bound for the maximum crack spacing in case of beams with very high reinforcement ratios.

2. Reinforcement bars spaced $>5(c + \phi/2)$ c/c (centre to centre)

In this case an upper bound to the crack spacing is suggested as given In Equation 4.27.

$$s_{r,max} = 1.3(h - x) \quad (4.27)$$

It may be noted that for a shear stirrup this would mean that if the distance between the legs of the stirrups exceed $5(c_s + \phi_s/2)$ (where c_s and ϕ_s are the side concrete cover to stirrups and shear stirrup diameter respectively) the crack spacing parameter $s_{r,max,y} = 1.3b$ (where b is the cross section width of the beam). The crack spacing in reinforced concrete members where the angle between the axes of principle stresses and the direction of reinforcement $> 15^\circ$ is given by Equation 4.28.

$$s_{r,max} = \frac{1}{\frac{\cos\theta}{s_{r,max,y}} + \frac{\sin\theta}{s_{r,max,z}}} \quad (4.28)$$

$$s_{r,avg} = 0.75s_{r,max} \quad (4.29)$$

where

θ angle between the rebars in y direction and the direction of principle tensile stress (Figure 4.13).

Figure 4.12 shows the orientation of the axes as considered in EC2 crack spacing model.

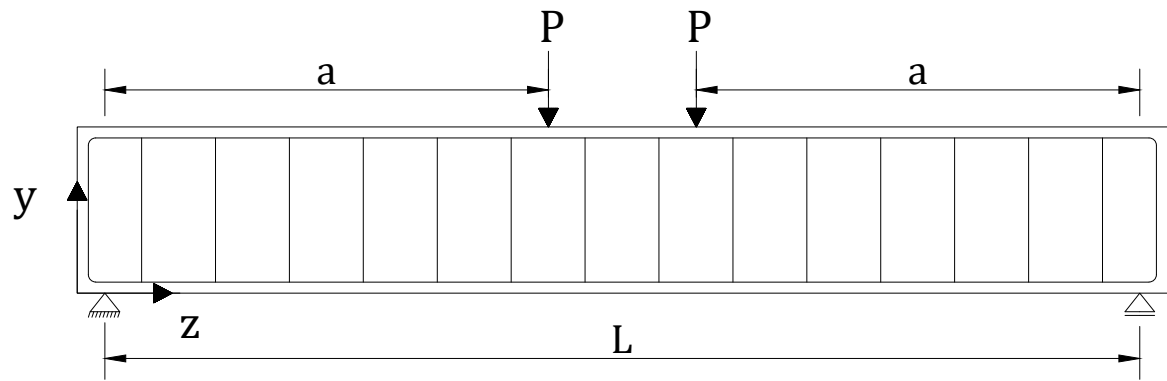


Figure 4.12: The orientation of axes in EC2 [19] crack spacing model

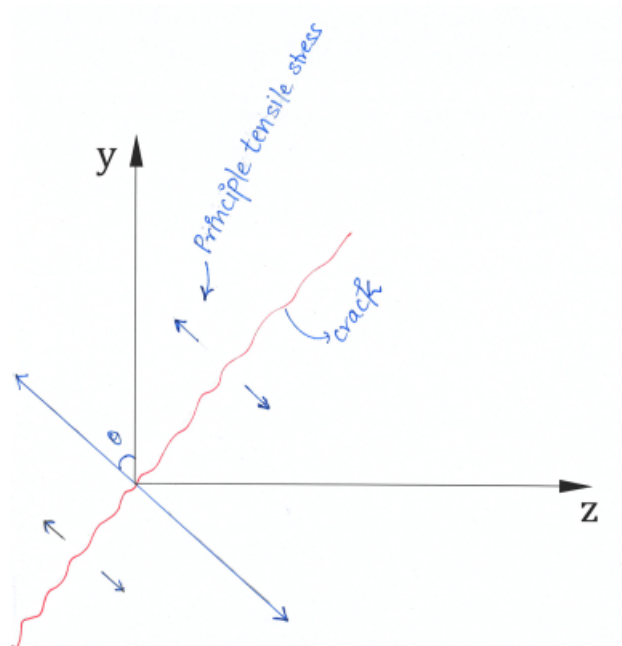


Figure 4.13: The definition of θ in EC2 [19] crack spacing model

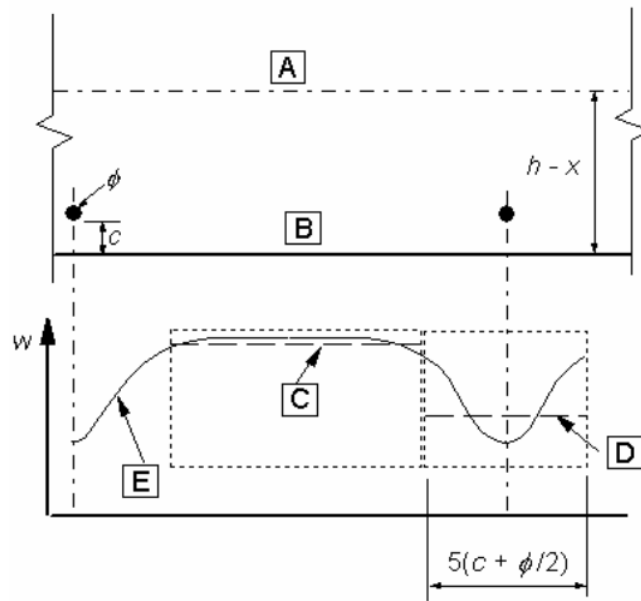


Figure 4.14: Variation of crack width with respect to distance from the reinforcement bars (Adapted from EC2 [19])

Figure 4.14 shows the variation in crack width with respect to the distance from the reinforcement bar.

where

- c* clear cover to the reinforcement bar.
- A* neutral axis of the beam.
- B* concrete tension zone surface.
- C* predictions of the crack spacing Equation 4.27.
- D* predictions of the crack spacing Equation 4.25.
- E* actual crack width on the beam surface.

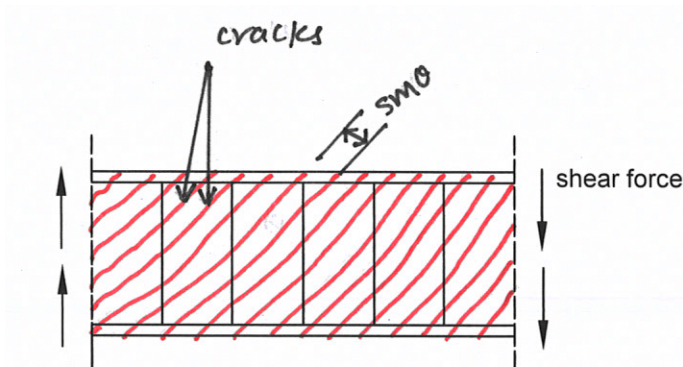


Figure 4.15: Assumed diagonal shear cracks at a constant crack spacing

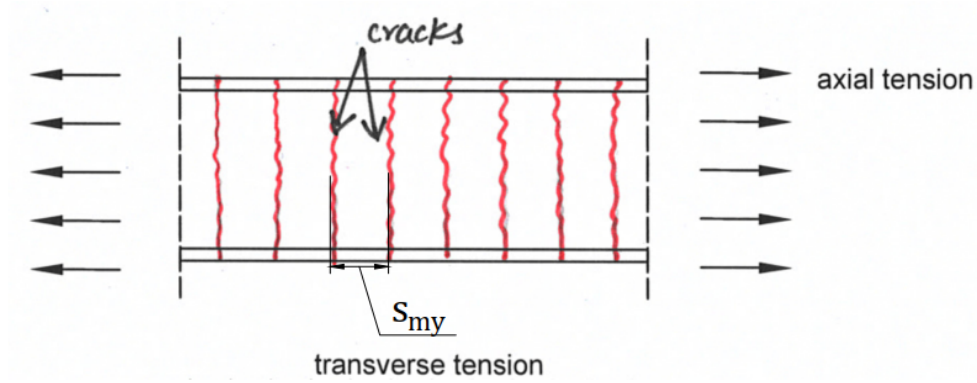


Figure 4.16: Assumed horizontal cracks caused by transverse tension with crack spacing s_{my} in between the two adjacent cracks

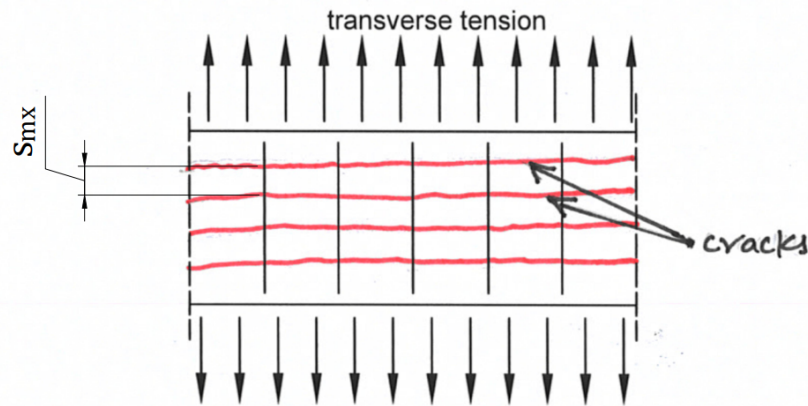


Figure 4.17: Assumed vertical cracks caused by axial tension with crack spacing s_{mx} in between the two adjacent cracks

The angle θ in Equation 4.28 can be calculated using CCC model. The model states that the inclination of the diagonal compression strut (assumed equal to mean shear crack angle in this thesis) is given by the Equation 4.30.

$$\cot\theta = \frac{0.85d_s}{d_s - x} \leq 2.50 \quad (4.30)$$

It is important to note here that the Equation 4.30 is applicable for stresses at or after the yielding of the reinforcement [31].

where

x : depth of neutral axis of the cracked section of a prestressed concrete beam evaluated using the assumption of zero concrete tensile strength. Moreover, it is assumed that concrete in compression zone is in linear elastic zone.

$x = x_o$ (for reinforced concrete beams without axial load).

d_s : effective shear depth.

$$\frac{x_o}{d} = \alpha_e \rho_l \left(-1 + \sqrt{1 + \frac{2}{\alpha_e \rho_l}} \right) \approx 0.75(\alpha_e \rho_l)^{\frac{1}{3}} \quad (4.31)$$

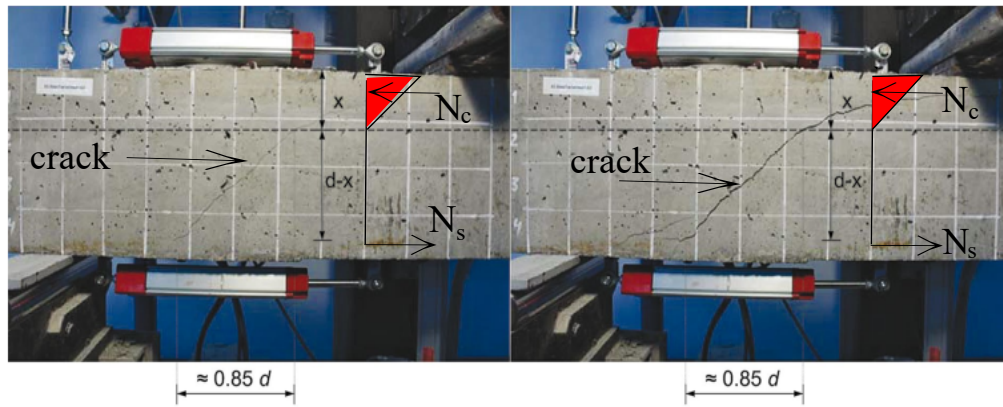


Figure 4.18: Evolution of the critical shear crack (adapted from [15])

Assumptions/ Limitations of Model-IA

1. It is assumed that the bond stress transfer mechanism in transverse direction is similar to the longitudinal direction.
2. It is assumed that the bond slip occurs between stirrup and concrete causing bond stress which allows the transfer of forces from the reinforcement to concrete. The bond stress between reinforcement and concrete is assumed constant throughout the length of disturbed zone.
3. The calculated mean shear crack width is applicable to the hidden tensile member and may not be representative of mean shear crack widths in case of deep slender beams at large distance from reinforcement.
4. Shear cracks are assumed parallel to each other.
5. The angle of shear crack is assumed equal to the mean shear crack inclination from the CCC model which is originally applicable at ULS. The horizontal projection of the first branch of flexural-shear crack is assumed equal to $0.85d$.
6. The concrete contribution to shear resistance at ULS is assumed equal to the value predicted by CCC model. The concrete contribution to shear resistance at ULS in the CCC model is determined after making a few assumptions. It is assumed that the mean longitudinal reinforcement percentage = 1.5%. The shear crack spacing is assumed equal to d and mean shear crack inclination is assumed equal to 36 degrees. Moreover, it is assumed that the tensile stress- crack opening curve is linear.
7. It is assumed that the concrete contribution to shear resistance decreases linearly from first diagonal cracking to the stage of all stirrups yielding.
8. It is assumed that the strain in all stirrups along the shear crack is equal. However, this assumption is not compliant with the experimental observations [31].
9. Shear crack width along the shear crack path is assumed as constant. However, shear crack width is observed to vary along the crack path [66].

10. It is assumed that the shear crack angle is constant throughout the span of the beam. However, it is experimentally observed that the shear crack angle varies along the shear span of the beam ([41], [60]).

4.3.2. Model-IB

This model completely ignores any direct contribution of concrete to the shear resistance under service loading conditions. The model assumes that the entire load is transmitted first to the stirrups and then the concrete is stressed because of the forces in the stirrups. The mean shear crack width can be determined using Equation 4.11. The calculation procedure is same as the Model-IA except that concrete contribution to shear resistance $V_{c,pred,ser}$ is equal to zero in Equation 4.16. Moreover, the mean shear crack angle in Equation 4.28 is calculated using CFT [16] instead of CCC model [15] since in the former model concrete tensile resistance is not considered and this makes the model relatively more compatible with zero concrete contribution (zero concrete contribution ($V_c = 0$)) assumption. The mean shear crack angle can be determined using Equation 4.32.

$$\tan^4\theta = \frac{1 + \frac{1}{n\rho_l}}{1 + \frac{1}{n\rho_t}} \quad (4.32)$$

Assumptions/ Limitations of Model-IB

1. It is assumed that the bond stress transfer mechanism in transverse direction is similar to the longitudinal direction.
2. It is assumed that the bond slip occurs between stirrup and concrete causing bond stress which allows the transfer of forces from the reinforcement to concrete. The bond stress between reinforcement and concrete is assumed constant throughout the length of disturbed zone.
3. The calculated mean shear crack width is applicable to the hidden tensile member and may not be representative of mean shear crack widths in case of deep slender beams.
4. Shear cracks are assumed parallel to each other.
5. It is assumed that the strain in all stirrups along the shear crack is equal. However, this assumption is not compliant with the experimental observations [31].
6. The shear crack angle is determined using CFT instead of CCC model. The expression used for the calculation of this angle is applicable to reinforcement structural response in linear elastic zone only and therefore, no stirrup yielding should occur under the application of service loads.
7. Shear crack width along the shear crack path is assumed as constant. However, shear crack width is observed to vary along the crack path [66].
8. It is assumed that the shear crack angle is constant throughout the span of the beam. However, it is experimentally observed that the shear crack angle varies along the shear span of the beam ([41], [60]).

4.3.3. Model-IIA

This is a semi-empirical model based on harmonization of crack width model given by Zakaria et al. [65] and the stirrup strain obtained in Equation 4.3. The concrete contribution to shear resistance at ULS comes from CCC model and the concrete contribution to shear resistance at service loads can be determined using Equation 4.16. The Equation 4.33 can be used to calculate the crack width [65].

$$w_{avg} = K(c_s)^a \left(\frac{1}{\rho_w}\right)^b \left(\frac{1}{\rho_t}\right)^c s_{m\theta-avg} \varepsilon_w \quad (4.33)$$

$$K = 0.112 k_s k_t \quad (4.34)$$

$$w_{max} = k_{max} w_{avg} \quad (4.35)$$

where

K	constant to account for the stirrup type.
k_s	= 1.0 for shear stirrups with conventional closed hook (135°).
k_s	= 1.2 for shear stirrups comprising of two U-shaped lap spliced parts.
k_t	constant to account for the type of shear stirrup rebar.
k_t	= 1.0 for HYSD (High Yield Strength Deformed) bars.
k_t	= 1.2 for plain reinforcement bars.
ρ_w	= $A_w / b_w s_y$.
a, b and c	empirical constants.
a	=0.05
b	=0.207
c	=0.252
k_{max}	correlation factor. =1.4

$$\varepsilon_s = \frac{\sigma_s}{E_s} \quad (4.36)$$

The stirrup stress σ_s can be determined using Equation 4.13-Equation 4.24 given in Model-IA. The description of the Zakaria et al. crack width model is provided in 2.2.2. The value of stirrup strain ε_w can now be substituted from Equation 4.36 into Equation 4.33 to obtain the shear crack width. The original model proposed by Zakaria et al. [65] is based on the following observations made by authors in an experimental program[66].

1. Shear crack width increases proportionately with increase in shear crack spacing and shear stirrup strain.
2. The shear crack width to shear crack spacing ratio decreases with increase in the transverse and longitudinal reinforcement ratio. The ratio also increases with increase in side concrete cover to stirrups.

3. The shear crack width to shear crack spacing ratio is also influenced by the type of reinforcement bars (deformed or plane reinforcement bars).

The empirical constants are incorporated into Equation 4.33 for calculating mean shear crack width to account for the influence of stirrups type, longitudinal and transverse reinforcement ratio and side concrete cover to stirrups. The shear crack spacing expression used in the model is formulated based on the observations in a previously carried out experimental study [66]. The background of the shear crack spacing model is the harmonization of CEB-FIP MC 1978 [18], CEB-FIP MC 1990 [8] and Collins and Mitchell Model [17]. The shear crack spacing is expressed as a weighted mean of crack control characteristics of both longitudinal and transverse reinforcements after taking into consideration the shear crack angle. The mean shear crack spacing $s_{m\theta-avg}$ in Equation 4.33 can be determined using Zakaria et al. crack spacing model which gives Equation 4.37 for determining the mean shear crack spacing.

$$s_{m\theta-avg} = \frac{1}{\frac{\sin\theta}{s_{m,x}} + \frac{\cos\theta}{s_{m,y}}} \quad (4.37)$$

$$s_{m,x} = 2 \left(c_x + \frac{s_x}{10} \right) + k_1 k_2 \frac{d_{bx}}{\rho_x} \quad (4.38)$$

$$s_{m,y} = 2 \left(c_s + \frac{s_y}{10} \right) + k_1 k_2 \frac{d_{by}}{\rho_y} \quad (4.39)$$

$$\rho_x = \frac{A_s + A_{ps}}{A_{cx,ef}} \quad (4.40)$$

$$A_{cx,ef} = 2.5(h - d_e)b_w \quad (4.41)$$

$$d_e = \frac{A_s d + A_{ps} d_p}{A_s + A_{ps}} \quad (4.42)$$

$$\rho_y = \frac{0.5A_w}{A_{cy,ef}} \quad (4.43)$$

$$A_{cy,ef} = \min(2.5(c_s + d_{by}/2)s_y, (b_w/2)s_y) \quad (4.44)$$

where

$$s_y \leq 15d_{by}.$$

k_1 factor to account for the bond characteristics of the reinforcement.

= 0.4 for HYSD bars.

= 0.8 for plain reinforcement bars.

k_2 factor to account for the shape of the stress distribution.

= 0.125 for in flexure.

= 0.25 for the pure tension.

Figure 4.19 shows the various crack spacing parameters used in this model.

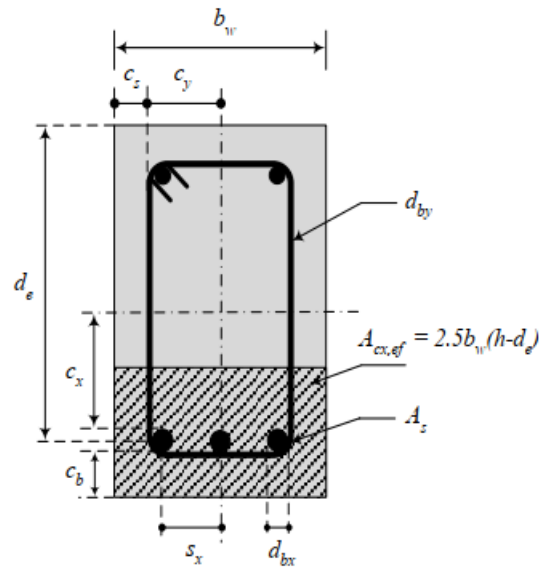


Figure 4.19: Various geometrical parameters used in the shear crack spacing model [65]

The angle θ in Equation 4.37 can be determined using Equation 4.30.

Assumptions/ Limitations of Model-IIA

1. It is assumed that the bond stress transfer mechanism in transverse direction is similar to the longitudinal direction.
2. Shear cracks are assumed parallel to each other.
3. The angle of shear crack is assumed equal to the mean shear crack inclination from the CCC model which is originally applicable at ULS. The horizontal projection of the first branch of flexural-shear crack is assumed equal to $0.85d$.
4. Shear crack width along the shear crack path is assumed as constant. However, shear crack width is observed to vary along the crack path [66].
5. It is assumed that the shear crack angle is constant throughout the span of the beam. However, it is experimentally observed that the shear crack angle varies along the shear span of the beam ([41], [60]).
6. The concrete contribution to shear resistance at ULS is assumed equal to the value predicted by CCC model. The concrete contribution to shear resistance at ULS in the CCC model is determined after making a few assumptions. It is assumed that the mean longitudinal reinforcement percentage = 1.5%. The shear crack spacing is assumed equal to d and mean shear crack inclination is assumed equal to 36 degrees. Moreover, it is assumed that the tensile stress- crack opening curve is linear.
7. It is assumed that the concrete contribution to shear resistance decreases linearly from first diagonal cracking to the stage of all stirrups yielding.
8. It is assumed that the strain in all stirrups along the shear crack is equal. However, this assumption is not compliant with the experimental observations [31].

9. The model comprises several empirical constants.
10. The model is applicable only for deformed shear stirrups and not for specimens with plain reinforcement bars.
11. Model is only applicable for reinforcements in elastic stage.

4.3.4. Model-IIB

This model completely ignores any direct contribution of concrete to the shear resistance under service loading conditions. The model assumes that the entire load is transmitted first to the stirrups and then the concrete is stressed because of the forces in the stirrups. The mean shear crack width can be determined using Equation 4.33. The calculation procedure is same as the Model-IIA except that concrete contribution to shear resistance $V_{c,pred,ser}$ is equal to zero in (Equation 4.16). Moreover, the mean shear crack angle in Equation 4.38 is calculated using CFT [16] instead of CCC model [15] since in the former model concrete tensile resistance is not considered and this makes the model relatively more compatible with zero concrete contribution (zero concrete contribution ($V_c = 0$)) assumption. The mean shear crack angle can be determined using Equation 4.32.

Assumptions/ Limitations of Model-IIB

1. Shear cracks are assumed parallel to each other.
2. It is assumed that the strain in all stirrups along the shear crack is equal. However, this assumption is not compliant with the experimental observations [31].
3. The model comprises several empirical constants.
4. The model is applicable only for deformed shear stirrups and not for specimens with plain reinforcement bars.
5. Model is only applicable for reinforcements in elastic stage.
6. The shear crack angle is determined using CFT instead of CCC model. The expression used for the calculation of this angle is applicable to reinforcement structural response in linear elastic zone only and therefore, no stirrup yielding should occur under the application of service loads.
7. Shear crack width along the shear crack path is assumed as constant. However, shear crack width is observed to vary along the crack path [66].
8. It is assumed that the shear crack angle is constant throughout the span of the beam. However, it is experimentally observed that the shear crack angle varies along the shear span of the beam ([41], [60]).

4.3.5. Model-IIIA

This model is based on the assumption that average shear crack width can be expressed as the product of mean principle tensile strain in concrete (in and between the cracks) and the spacing between shear cracks (Equation 4.45) the cracks are assumed parallel to

each other and inclined to the longitudinal reinforcement at an angle given by the CCC model (Equation 4.30). The concrete contribution to shear resistance at ULS and at service loads can be calculated using the same procedure and equations used for Model-IA. The principle tensile strain ε_1 can be calculated using Equation 4.8. This principle strain should then be multiplied with the shear crack spacing (Equation 4.37) from the model given by Zakaria et al. which is also used in Model-IIA.

$$w_{avg} = \varepsilon_1 s_\theta \quad (4.45)$$

Assumptions/ Limitations of Model-IIIA

1. It is assumed that the mean principle tensile strain in cracked concrete is absorbed within all the cracks.
2. It is assumed that the bond stress transfer mechanism in transverse direction is similar to the longitudinal direction. The bond stress between reinforcement and concrete is assumed constant throughout the length of disturbed zone.
3. The calculated mean shear crack width is applicable to the hidden tensile member and may not be representative of mean shear crack widths in case of deep slender beams.
4. Shear cracks are assumed parallel to each other.
5. The angle of shear crack is assumed equal to the mean shear crack inclination from the CCC model which is originally applicable at ULS. The horizontal projection of the first branch of flexural-shear crack is assumed equal to $0.85d$.
6. The concrete contribution to shear resistance at ULS is assumed equal to the value predicted by CCC model. The concrete contribution to shear resistance at ULS in the CCC model is determined after making a few assumptions. It is assumed that the mean longitudinal reinforcement percentage =1.5%. The shear crack spacing is assumed equal to d and mean shear crack inclination is assumed equal to 36 degrees. Moreover, it is assumed that the tensile stress- crack opening curve is linear.
7. It is assumed that the concrete contribution to shear resistance decreases linearly from first diagonal cracking to the stage of all stirrups yielding.
8. It is assumed that the strain in all stirrups along the shear crack is equal. However, this assumption is not compliant with the experimental observations [31].
9. Shear crack width along the shear crack path is assumed as constant. However, shear crack width is observed to vary along the crack path [66].
10. It is assumed that the shear crack angle is constant throughout the span of the beam. However, it is experimentally observed that the shear crack angle varies along the shear span of the beam ([41], [60]).

4.3.6. Model-IIIB

This model completely ignores any direct contribution of concrete to the shear resistance under service loading conditions. The model assumes that the entire load is transmitted first to the stirrups and then the concrete is stressed because of the forces in the stirrups. The mean shear crack width can be determined using Equation 4.47. The calculation procedure is same as the Model-IIIA except that concrete contribution to shear resistance $V_{c,pred,ser}$ is equal to zero in (Equation 4.16). Moreover, the mean shear crack angle in Equation 4.29 is calculated using CFT [16] instead of CCC model [15] since in the former model concrete tensile resistance is not considered and this makes the model relatively more compatible with zero concrete contribution (zero concrete contribution ($V_c = 0$)) assumption. The mean shear crack angle can be determined using Equation 4.32.

Assumptions/ Limitations of Model-IIIB

1. It is assumed that the strain in all stirrups along the shear crack is equal. However, this assumption is not compliant with the experimental observations [31].
2. The shear crack angle is determined using CFT instead of CCC model. The expression used for the calculation of this angle is applicable to reinforcement structural response in linear elastic zone only and therefore, no stirrup yielding should occur under the application of service loads.
3. Shear crack width along the shear crack path is assumed as constant. However, shear crack width is observed to vary along the crack path [66].
4. It is assumed that the shear crack angle is constant throughout the span of the beam. However, it is experimentally observed that the shear crack angle varies along the shear span of the beam ([41], [60]).

4.3.7. Model-IV

This model is also based on the assumption that average shear crack width can be expressed as the product of principle tensile strain in concrete (in and between the cracks) and the spacing between shear cracks (Equation 4.47). All the cracks are assumed parallel to each other and inclined to the longitudinal reinforcement at an angle given by the CSA model based on SMCFT (Equation 4.46). The concrete contribution to shear resistance at ULS (to obtain the mean principle tensile strain in cracked concrete) is also calculated using the CSA model (instead of CCC model) wherein this contribution is expressed as the capacity of the beam web (under tensile stress) to resist shear (Equation 4.48). This contribution decreases with increase in the longitudinal strain in the web. The mean principle tensile strain ε_1 can be calculated using Equation 4.8. This strain is calculated using the additive model for shear resistance, truss analogy for diagonally cracked RC beam and Mohr's strain circle similar to the procedure followed in Model-IIIA. This principle strain should then be multiplied with the shear crack spacing (Equation 4.37) from the model given by Zakaria et al. which is also used in Model-IIA. The mean shear crack angle in the calculation of mean shear crack spacing can be determined using the expression for diagonal

compression strut angle given by Equation 4.46. It may be noted that the angle θ in Equation 4.46 is in degrees.

$$\theta = 29 + 7000\epsilon_x \tag{4.46}$$

$$w_{avg} = \epsilon_1 s_\theta \tag{4.47}$$

$$V_c = \phi_c \lambda \beta \sqrt{f'_c} b_w d_v \tag{4.48}$$

where

$\sqrt{f'_c} \not\geq 8 \text{ MPa}$ for beams containing minimum transverse reinforcement.

β factor to account for shear resistance of cracked concrete.

f'_c specified compressive strength of concrete.

$$\beta = \frac{0.40}{1 + 1500\epsilon_x} \tag{4.49}$$

The strain in the longitudinal reinforcement ϵ_x can be calculated using Equation 4.50.

$$\epsilon_x = \frac{\frac{M_f}{d_v} + V_f - V_p + 0.5N_f - A_p f_{po}}{2(E_s A_s + E_p A_p)} \tag{4.50}$$

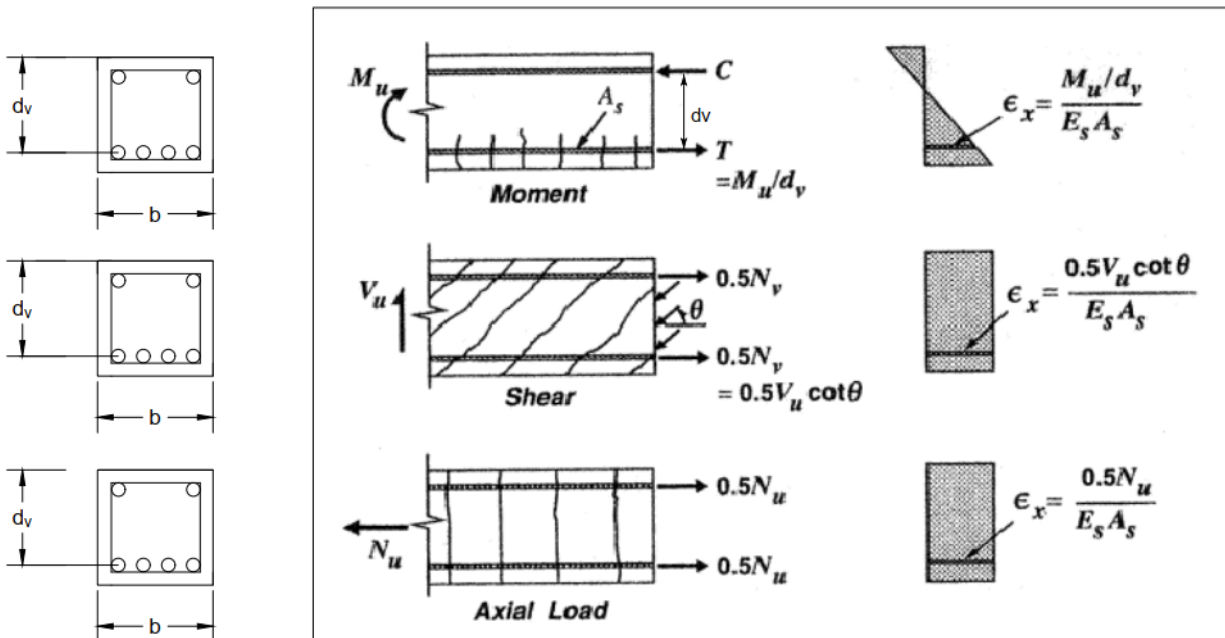


Figure 4.20: Determination of longitudinal strain in the longitudinal reinforcement of a reinforced concrete non-prestressed beam [4].

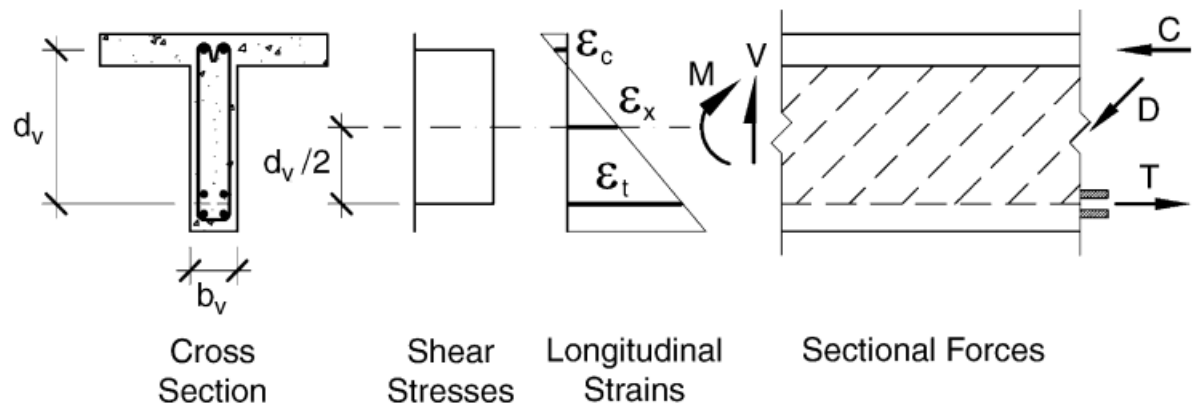


Figure 4.21: Determination of longitudinal strain in the web of a reinforced concrete non-prestressed beam [14]

Assumptions/ Limitations of Model-IV

1. Shear cracks are assumed parallel to each other.
2. The angle of shear crack is assumed equal to the mean shear crack inclination from the SMCFT. The theory assumes that clamping stress in transverse directions are zero. The failure shear stress is assumed equal to $0.25f_c$. And the shear crack spacing is assumed equal to $300mm$.
3. The concrete contribution to shear resistance at ULS is assumed equal to the value predicted by CSA model which is based on SMCFT. The concrete contribution to shear resistance at ULS in the SMCFT is determined after making a few assumptions. The maximum value of $\sqrt{f_c} \not\geq 8MPa$. This theory can be used for RC beams which have a minimum transverse reinforcement area equal to $0.06\sqrt{f_c}b_ws/f_y$. Moreover, the web longitudinal strain is assumed equal to half the maximum strain in the longitudinal tension reinforcement.
4. It is assumed that the concrete contribution to shear resistance decreases linearly from first diagonal cracking to the stage of all stirrups yielding.
5. It is assumed that the strain in all stirrups along the shear crack is equal. However, this assumption is not compliant with the experimental observations [31].
6. Shear crack width along the shear crack path is assumed as constant. However, shear crack width is observed to vary along the crack path [66].
7. It is assumed that the shear crack angle is constant throughout the span of the beam. However, it is experimentally observed that the shear crack angle varies along the shear span of the beam ([41], [60]).

4.3.8. Model-V

This model is adapted from handbook for EC2 developed by Swedish Concrete Association (Betongföreningen, 2010). According to the handbook, the reinforcement stresses in a plane stress state can be calculated by establishing equilibrium of the tensile stresses in the reinforcement with compressive stress and shear stress in the uncracked concrete. It is assumed that the cracked concrete can not take any tensile force. The reinforcement stresses in the two directions may be calculated with Equation 4.51 and Table D.9. The mean principle tensile strain should then be multiplied with the mean shear crack spacing obtained from Zakaria et al. shear crack spacing model (using Equation 4.37) to obtain the mean shear crack width.

$$\sigma_{sx} = \frac{\sigma_x \left(\frac{x}{2h} \right) + \tau_{xy} \cot \theta}{\frac{A_{sx}}{b_w h}} \quad (4.51)$$

$$\sigma_{sy} = \frac{\sigma_y + \tau_{xy} \tan \theta}{\frac{A_{sy}}{b_w s}} \quad (4.52)$$

$$\epsilon_y = \frac{\sigma_s}{E_s} \quad (4.53)$$

Once the strain in the stirrups is known, the mean principle tensile strain in concrete can be found with Equation 4.8 and Equation 4.7. In case the compressive stress in concrete on the top and bottom extreme fibers are σ_{c1} and σ_{c2} respectively then the stress in the longitudinal reinforcement can be obtained using Equation 4.54.

$$\sigma_{sx} = \frac{\left(\frac{\sigma_{c1} + \sigma_{c2}}{2} \right) + \tau_{xy} \cot \theta}{\frac{A_{sx}}{b_w h}} \quad (4.54)$$

where

σ_{c1} compressive stress in the extreme top fiber of the beam.

τ_{xy} maximum shear stress in concrete.

A_{sx} cross-section area of the longitudinal reinforcement.

A_{sy} combined cross-section area of both legs of a 2-legged stirrup.

x height of the compression zone.

b_w web width of the beam.

h height of the beam cross-section.

s stirrup spacing.

σ_{sx} is reinforcement stress in the x-direction.

σ_{sy} is the reinforcement in the y-direction.

ρ_x is reinforcement ratio in the x- direction ($A_{sx}/b_w h$).

ρ_y is the reinforcement ratio in the y- direction ($A_{sy}/b_w s$).

θ diagonal compression strut angle with respect to the longitudinal axis of the beam.

It is proposed to use θ given by the CFT in case of RC beams. In case of PC beams, the angle may be adopted and its value can be given using the proposed Equation 4.55 [51].

$$\theta_p = \theta \left[1 - \left(\frac{\sigma_{pc}}{f_c} \right)^{0.7} \right] \quad (4.55)$$

where

θ_p shear crack angle in case of PC (Prestressed Concrete) beams.

θ shear crack angle in case of RC beams.

σ_{pc} prestressing force divided by cross-section area of the beam.

f_c compressive strength of concrete.

Derivation of Reinforcement Stresses in Longitudinal and Transverse Directions

The proposed equations for the stresses in longitudinal and transverse reinforcements in the model can be obtained from equilibrium of forces in the longitudinal and transverse directions respectively.

From Figure 4.22, considering equilibrium in horizontal direction $\sum H = 0$ we can write Equation 4.56.

$$\sigma_{sx} A_{sx} = \frac{\sigma_{c1}}{2} (b_w x) + \tau_{yx} (l b_w) \quad (4.56)$$

$$\Rightarrow \sigma_{sx} = \frac{\frac{\sigma_{c1}}{2} (b_w x) + \tau_{yx} (l b_w)}{A_{sx}} \quad (4.57)$$

$$\Rightarrow \sigma_{sx} = \frac{\frac{\sigma_{c1}}{2h} (x) + \tau_{yx} (\frac{l}{h})}{\frac{A_{sx}}{b_w h}} \quad (4.58)$$

Now, $l/h = \cot(\theta)$

$$\Rightarrow \sigma_{sx} = \frac{\frac{\sigma_{c1}}{2h} (x) + \tau_{yx} \cot(\theta)}{\rho_x} \quad (4.59)$$

where:

ρ_x longitudinal reinforcement percentage.

Similarly,

From Figure 4.23, considering equilibrium in vertical direction $\sum V = 0$ we can write Equation 4.60.

$$\sigma_{sy} \left(\frac{l}{s} \right) A_{sy} = \sigma_y (l b_w) + \tau_{xy} (h b_w) \quad (4.60)$$

$$\Rightarrow \sigma_{sy} = \frac{\sigma_y (l b_w) + \tau_{xy} (h b_w)}{A_{sy} \left(\frac{l}{s} \right)} \quad (4.61)$$

$$\Rightarrow \sigma_{sy} = \frac{\sigma_y + \tau_{xy} (\frac{h}{l})}{\frac{A_{sy}}{b_w s}} \quad (4.62)$$

$$\Rightarrow \sigma_{sy} = \frac{\sigma_y + \tau_{xy} \tan(\theta)}{\rho_w} \quad (4.63)$$

where

ρ_w transverse reinforcement percentage.

Now let us assume that the entire cross-section of the beam is under non uniform compression due to the influence of prestressing. The equilibrium of forces in the longitudinal direction can be written as Equation 4.64.

$$\sigma_{sx} A_{sx} = \frac{\sigma_{c1} + \sigma_{c2}}{2} (b_w x) + \tau_{yx} (l b_w) \tag{4.64}$$

$$\Rightarrow \sigma_{sx} = \frac{\frac{\sigma_{c1} + \sigma_{c2}}{2} (b_w x) + \tau_{yx} (l b_w)}{A_{sx}} \tag{4.65}$$

$$\Rightarrow \sigma_{sx} = \frac{\frac{\sigma_{c1} + \sigma_{c2}}{2h} (x) + \tau_{yx} (\frac{l}{h})}{\frac{A_{sx}}{b_w h}} \tag{4.66}$$

Now, $l/h = \cot(\theta)$

$$\Rightarrow \sigma_{sx} = \frac{\frac{\sigma_{c1} + \sigma_{c2}}{2h} (x) + \tau_{yx} \cot(\theta)}{\rho_x} \tag{4.67}$$

where

l length of the reinforced element under consideration.

ρ_x longitudinal reinforcement percentage.

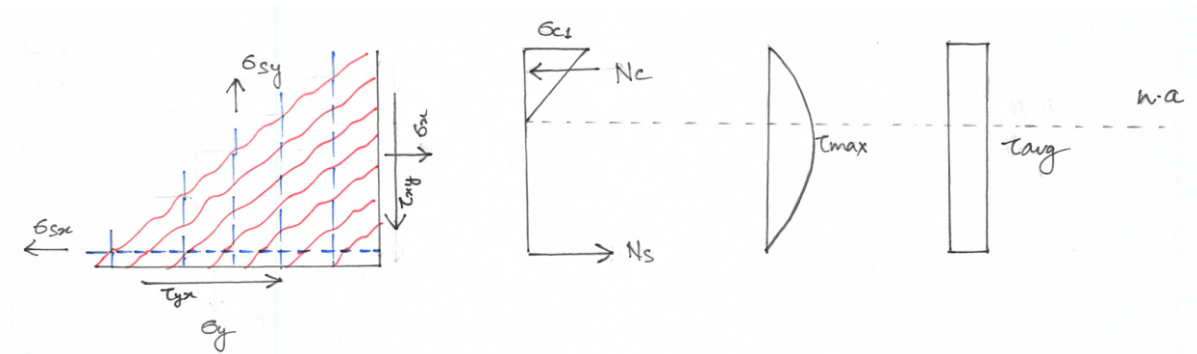


Figure 4.22: Stresses in the reinforcement and cracked concrete

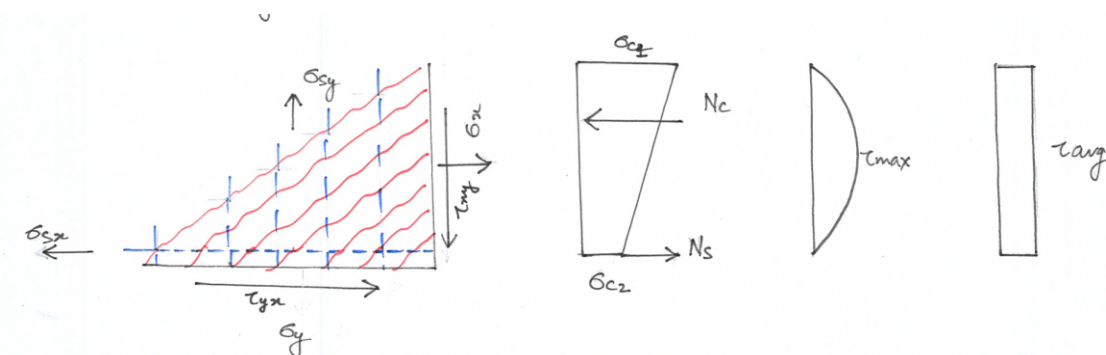


Figure 4.23: Stresses in the reinforcement and concrete under varying compressive stress along the depth

Assumptions/ Limitations of Model-V

1. It is assumed that the bond stress transfer mechanism in transverse direction is similar to the longitudinal direction.
2. The calculated mean shear crack width is applicable to the hidden tensile member and may not be representative of mean shear crack widths in case of deep slender beams.
3. Shear cracks are assumed parallel to each other.
4. The angle of shear crack is predicted from CFT. This theory is used to predict the mean shear crack angle for this model because the CFT also does not consider the tensile strength of concrete.
5. It is assumed that concrete cannot resist any tensile force after cracking.
6. It is assumed that the bond exist between longitudinal reinforcement and concrete which causes shear stress to occur in concrete below the neutral axis.
7. Clamping stress in the transverse direction are assumed zero.
8. The shear stress distribution in concrete before and after cracking is assumed to be the same.
9. It is assumed that the strain in all stirrups along the shear crack is equal. However, this assumption is not compliant with the experimental observations [31].
10. Shear crack width along the shear crack path is assumed as constant. However, shear crack width is observed to vary along the crack path [66].
11. It is assumed that the shear crack angle is constant throughout the span of the beam. However, it is experimentally observed that the shear crack angle varies along the shear span of the beam ([41], [60]).

4.3.9. Results

In this subsection, assessment of the performance of the various models presented in subsection 4.3.1- subsection 4.3.6 is done. In order to evaluate the accuracy of these models, a comparison is made with the experimental values of mean shear crack width for 26 different beam specimens from literature.

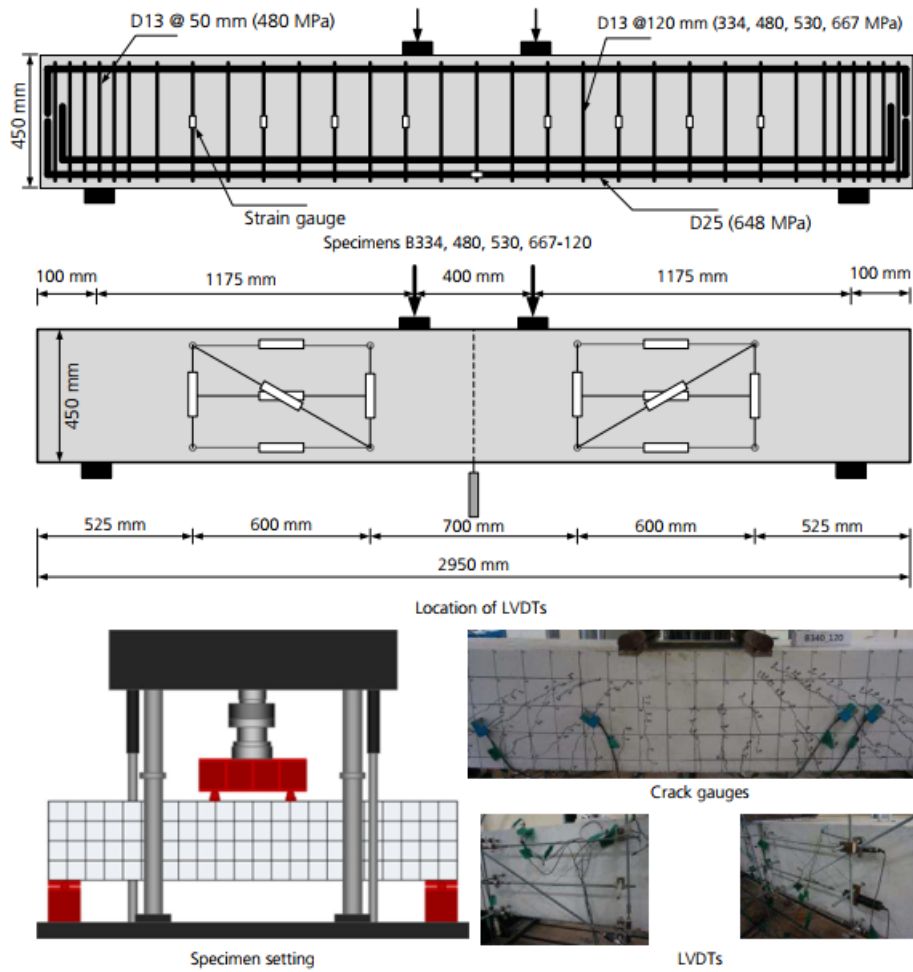


Figure 4.24: Experimental setup for the shear crack width study [37]

Table 4.1: Key characteristics of experiments and specimens referred for diagonal crack width study

Paper	Specimens	Mechanical Scheme	Variable	Method
Munikrishna et al. [44]	3	3-point bending	w_{avg}, w_{max}	LVDTs, crack gauges
Lee et al. [38]	12	4-point bending	w_{avg}	crack comparator, pressure gauge
Lee et al. [37]	11	4-point bending	w_{avg}, w_{max}	LVDTs

Table 4.1 show the key characteristics of the experiments referred in this analysis. The mechanical schemes and the cross section details of these experimental studies ([44], [38]) are shown in Figure 3.28 and Figure 3.27 respectively. The corresponding details of the experi-

mental study of Lee et al. [37] are shown in Figure 4.24. The various geometrical parameters of the corresponding beam specimens in these studies are provided in Table 4.2.

Table 4.2: Range of parameters for the specimens studies for comparison of shear crack widths with predictions from various models

Parameter	Range
a/d	2.56- 3.00
d/b	1.12- 1.13
$\rho_w f_{ym}$ (MPa)	0.96- 4.83
ρ_l (%)	2.00- 4.00
ρ_w (%)	0.20- 0.70
f'_c (MPa)	33.60- 68.40

Table 4.3: Mean shear crack width prediction ratios of the models proposed

Specimen	$w_{avg,exp}/w_{avg,pred}$							
	Model - IA	Model -IB	Model - IIA	Model - IIB	Model - IIIA	Model - IIIB	Model - IV	Model - V
G3-C60	1.08	0.99	0.65	0.60	0.53	0.51	0.52	0.28
G3-M80	0.88	0.81	0.50	0.46	0.40	0.39	0.40	0.18
G3-M100	0.96	0.98	0.43	0.43	0.37	0.42	0.36	0.20
B34-3	1.56	1.10	1.05	0.75	0.92	0.59	0.88	0.38
B34-5	2.53	1.82	2.05	1.49	1.35	0.92	1.30	0.56
B42-2	1.48	0.96	1.18	0.76	0.86	0.51	0.81	0.36
B42-3	1.67	1.20	1.46	1.06	0.96	0.64	0.90	0.41
B42-4	1.40	1.04	1.22	0.91	0.80	0.55	0.76	0.34
B42-5	1.58	1.15	1.28	0.94	0.83	0.58	0.79	0.35
B42-6	1.75	1.39	1.20	0.95	0.80	0.63	0.76	0.34
B68-2	1.86	1.02	1.47	0.80	1.05	0.54	0.91	0.48
B68-3	1.60	1.13	1.40	0.99	0.89	0.60	0.80	0.40
B68-4	1.43	1.11	1.25	0.97	0.79	0.58	0.73	0.36
B68-5	1.83	1.22	1.47	0.98	0.93	0.61	0.83	0.42
B68-6	1.92	1.41	1.31	0.96	0.85	0.64	0.76	0.38
B334-120	2.97	1.69	1.88	1.06	1.23	0.66	0.78	0.53
B334-160	3.44	1.00	1.86	0.54	1.35	0.37	0.46	0.58
B480-120	2.29	1.54	1.45	1.04	0.94	0.65	0.69	0.40
B480-160	3.20	2.04	1.74	1.11	1.20	0.76	0.80	0.52
B480-200	5.62	2.95	2.63	1.38	1.89	1.00	1.06	0.81
B530-120	3.57	2.36	2.25	1.69	1.45	1.04	1.09	0.63
B530-160	4.70	3.25	2.55	1.76	1.75	1.21	1.24	0.76
B530-200	3.60	2.19	1.68	1.03	1.20	0.75	0.76	0.52
B667-120	5.09	3.51	3.40	2.63	2.19	1.63	1.64	0.95
B667-160	4.74	3.55	2.57	2.02	1.76	1.39	1.35	0.76
B667-200	2.45	1.83	1.15	0.86	0.81	0.62	0.60	0.35

Table 4.3 show the values of prediction ratio (ratio of experimentally observed mean crack width to the predicted mean crack width) for the various models.

Table 4.4: Statistical parameters for the predictions of proposed models to evaluate the average diagonal crack width

Statistical Parameter	Model -IA	Model -IB	Model -IIA	Model -IIB	Model -IIIA	Model -IIIB	Model -IV	Model -V
Mean	2.51	1.66	1.58	1.08	1.08	0.72	0.85	0.47
Median	1.89	1.30	1.45	0.97	0.94	0.63	0.79	0.41
SD	1.35	0.83	0.69	0.50	0.45	0.31	0.30	0.19
COV	0.54	0.50	0.44	0.46	0.41	0.42	0.35	0.40
Max	5.62	3.55	3.40	2.63	2.19	1.63	1.64	0.95
Min	0.88	0.81	0.43	0.43	0.37	0.37	0.36	0.18
Range	4.74	2.74	2.97	2.20	1.82	1.26	1.29	0.77

Table 4.4 shows the various statistical parameters based on the prediction of shear crack width using the proposed models. It can be observed that conservative mean crack width predictions are made by Models-IIIB, IV and V. The predictions of Model-I, which is based on the EC2 crack width model, are highly unconservative than the experimental values. It can be observed from Table 4.4 that the maximum of prediction ratio of all the models lead to an unconservative prediction of mean shear crack width except Model-V. However, mean of the prediction ratio from the Models- IIIB, IV and V gives conservative estimates

of mean shear crack width. It can be seen that Model- V give the least SD (equal to 0.19) among all the models. However, Model IV showed the least COV among all the models. The maximum of the prediction ratio from this model is 0.95. On an absolute scale SD and COV for even Models- IIIB and IV (models which provide a conservative estimate of mean shear crack width) are high with values 0.31 and 0.30 respectively for the two models respectively. Moreover, the maximum of the prediction ratio is greater than 1.0 for Models IIIB and Model IV indicating that there is a probability of unconservative predictions of mean shear crack width calculated using these models. On comparing the value of stresses (during calculations) in stirrups from different models, it is found that Model-V predicted higher stresses in the stirrups than Model-I (A and B) and Model-II (A and B).

Model-IA which is based on the substitution of stirrup force from the truss analogy in the conventional EC2 shear crack width model for flexural and tensile cracks resulted in the most unconservative predictions. This may be due to the difference in the calculated and actual stirrup stresses. In the proposed methodology to calculate the stirrup strains, it is assumed that the stirrup strain is equal in all the stirrups. However, experimentally it is observed that the stirrup strain is not equal [31]. Another reason for the discrepancy in the calculation of shear stirrup strain may be the flatter angles (as compared to the actual shear crack angle) predicted by diagonal compression strut angle models. This is reinforced by the fact that even after assuming zero contribution (in Model-IB and Model-IIB) of the concrete to the shear resistance, the mean calculated shear crack width is smaller than the experimentally observed mean shear crack width.

Model-IA shows the highest SD. A significant portion of this SD may be due to the variation in the predicted values of concrete contribution from the CCC model as the SD is reduced in Model-IB (wherein the concrete contribution to shear resistance is considered as zero). Model-IIA which is based on the substitution of stirrup strain in the semi-empirical diagonal crack width calculation model by Zakaria et al. [65] also resulted in unconservative results with a high degree of dispersion indicated by the high values of SD and COV. It is seen in Chapter 3 that the mean shear crack spacing prediction from the Zakaria et al. crack spacing model is conservative. Therefore, the unconservative predictions for shear crack width may be attributed to unconservative values of stirrup strain and (or) the uncertainty in the regression parameters. However, it is clear from the predictions of Model-IIB that the variation in Model-IIA largely comes from the dispersion in the predicted concrete contribution to shear resistance (since $V_{c,pred,ser} = 0$ in Model-IIB and the mean of the prediction ratio for Model-IIB is 1.08 while it is 1.58 for Model-IIA). Model-IIIB shows a mean value of the prediction ratio equal to 0.72. The reason for the conservative estimate is assuming that the concrete contribution to the shear resistance is zero and due to the ability of the model to properly account for the inclination of the cracks with respect to the stirrups (multiplication of principle strains in cracked reinforced concrete instead of shear stirrup strain with shear crack spacing). Conservative estimates are also obtained from Model-IV and Model-V with a mean of the prediction ratio equal to 0.85 and 0.47 respectively. Similar to Model- IIIB, these models also express the crack width in terms of the mean principle tensile strain in the cracked concrete. The value of concrete resistance factor ϕ_c is taken as 1.0 in the original formulation of the Model-IV. An alternate analysis with $\phi_c = 0.65$ (recommended value in CSA-2004 [5]) is also performed. The mean and SD for the alternate analysis are found to be 0.79 and 0.30 respectively. The concrete contribution to shear re-

sistance at the stirrup yielding in Model-IV is estimated using the CSA model which is based on SMCFT.

Table 4.5: Average crack width prediction ratios of the models propose with a shear crack angle equal to 45 degrees

Specimen	$w_{avg,exp}$	$w_{avg,exp}/w_{avg,pred}$						
		Model- IA	Model-IB	Model- IIA	Model- IIB	Model - IIIA	Model - IIIB	Model- IV
G3-C60	0.25	0.74	0.54	0.46	0.38	0.28	0.23	0.27
G3-M80	0.23	0.52	0.37	0.31	0.25	0.18	0.14	0.17
G3-M100	0.37	0.67	0.49	0.30	0.24	0.20	0.16	0.19
B34-3	0.30	0.91	0.66	0.63	0.52	0.37	0.30	0.35
B34-5	0.53	1.52	1.08	1.23	0.98	0.55	0.44	0.53
B42-2	0.22	0.91	0.66	0.72	0.53	0.36	0.26	0.34
B42-3	0.36	1.01	0.73	0.90	0.73	0.40	0.33	0.38
B42-4	0.35	0.77	0.60	0.75	0.63	0.34	0.28	0.32
B42-5	0.36	0.97	0.70	0.78	0.62	0.35	0.27	0.33
B42-6	0.56	1.07	0.77	0.73	0.59	0.34	0.27	0.33
B68-2	0.23	1.19	0.70	0.94	0.55	0.47	0.27	0.41
B68-3	0.37	1.03	0.73	0.89	0.68	0.40	0.30	0.36
B68-4	0.46	0.84	0.63	0.80	0.66	0.36	0.29	0.33
B68-5	0.38	1.17	0.80	0.94	0.65	0.42	0.29	0.38
B68-6	0.57	1.23	0.87	0.84	0.59	0.39	0.27	0.35
B334-120	0.20	1.85	1.00	1.17	0.70	0.53	0.31	0.34
B334-160	0.12	2.14	0.61	1.16	0.33	0.58	0.16	0.19
B480-120	0.28	1.23	0.86	0.90	0.69	0.41	0.31	0.31
B480-160	0.35	1.99	1.09	1.08	0.68	0.52	0.32	0.35
B480-200	0.49	3.50	1.65	1.64	0.80	0.82	0.39	0.46
B530-120	0.50	1.81	1.34	1.40	1.11	0.63	0.49	0.49
B530-160	0.62	2.93	1.66	1.59	1.07	0.76	0.51	0.54
B530-200	0.40	2.24	1.16	1.05	0.60	0.52	0.29	0.33
B667-120	0.88	2.61	2.04	2.12	1.74	0.95	0.77	0.76
B667-160	0.89	2.52	1.76	1.60	1.23	0.76	0.58	0.59
B667-200	0.42	1.49	0.88	0.72	0.50	0.35	0.24	0.26

It is seen in section 3.2 that the predictions from all the diagonal compression strut angle (or shear crack angle) prediction models are slightly unconservative as all the models predicted flatter values of the compression strut angle value (i.e., prediction ratio greater than 1.0) than the experimentally observed values. Moreover, since it is known that the plane with the maximum shear stress is inclined at 45 degrees to the longitudinal axis of the beam before first shear cracking, an additional analysis for all the models with the shear crack angle assumed equal to 45 degrees is performed. It should be noted that the actually shear crack angle would definitely be lesser than this value on account of rotation of the crack angle with post- shear cracking. However, this higher assumed value of shear crack angle will give higher predicted forces in the stirrups and is therefore, a conservative approach. Table 4.5 shows the values of prediction ratio (ratio of experimentally observed mean crack width to the predicted mean crack width) for the various models with the assumed value of shear crack angle equal to 45 degrees. Table 4.6 shows the statistical parameters for the predictions of proposed models to evaluate the average diagonal crack width with a shear crack angle equal to 45 degrees. It can be seen that the mean of the prediction ratio decreases significantly for all the models. All the models except Model-IA gives conservative predictions of the mean shear crack width. Similarly, reduction in SD

and Range are also observed for all the models. This is expected because an assumption of 45 degree angle of the shear crack angle results in higher values of strains in the stirrups and the mean principle tensile strain in the cracked concrete which leads to higher predicted value of mean crack width. It can be seen that the maximum value of the predictions from Models-IIIA, IIIB and IV becomes less than 1.0. The mean value of the predictions from these models is also less than 1.0 as shown in Table 4.6. This indicates enhanced probability of the models to give conservative estimates of mean shear crack width. Although, mean of the predictions from Model-IIA shows the closest and conservative value to 1.0, however, the maximum of the predictions from this model is 2.12 which indicates a probability that the predictions from this model may be unconservative as well. The mean and SD of the predictions from Model- IV with $\phi_c = 0.65$ are found to be 0.35 and 0.13 respectively. The calculation of mean shear crack width from Model-V with an assumption of the mean shear crack angle of 45 degrees causes stresses much larger than the yield strength in the stirrups and therefore, the results are omitted in Table 4.6 and Table 4.5 (since stirrups are not expected to yield at service loads). It is observed that with an assumption of mean shear crack angle of 45 degrees Model-V gives over-conservative results (relatively very high values of predicted mean shear crack width as compared to the experimental crack widths) and therefore is not suitable for application in design practice.

Table 4.6: Statistical parameters for the predictions of proposed models to evaluate the mean diagonal crack width with a shear crack angle equal to 45 degrees

Statistical Parameter	Model -IA	Model -IB	Model -IIA	Model -IIB	Model -IIIA	Model -IIIB	Model -IV
Mean	1.49	0.94	0.99	0.69	0.47	0.33	0.37
Median	1.21	0.79	0.90	0.64	0.41	0.29	0.34
SD	0.77	0.43	0.42	0.32	0.19	0.14	0.13
COV	0.52	0.46	0.43	0.46	0.40	0.42	0.35
Max	3.50	2.04	2.12	1.74	0.95	0.77	0.76
Min	0.52	0.37	0.30	0.24	0.18	0.14	0.17
Range	2.98	1.66	1.81	1.49	0.77	0.63	0.59

Table 4.7: The ratio of the experimentally obtained maximum crack width to the average crack width for the reinforced concrete beam specimens [38]

Specimen	$w_{avg,exp}$	$w_{max,exp}$	$w_{max,exp}/w_{avg,exp}$
B34-3	0.30	0.80	2.69
B34-5	0.53	0.74	1.40
B42-2	0.22	0.63	2.88
B42-3	0.36	0.81	2.26
B42-4	0.35	1.05	2.97
B42-5	0.36	1.05	2.92
B42-6	0.56	1.68	2.99
B68-2	0.23	0.60	2.63
B68-3	0.37	1.06	2.91
B68-4	0.46	1.59	3.43
B68-5	0.38	0.84	2.24
B68-6	0.57	1.19	2.10

The principle tensile strains tend to concentrate at certain weakest locations along the critical diagonal crack as the load increases. This causes a deviation between the values of mean shear crack width and the maximum crack width [31]. Table 4.7 shows the value of the maximum crack width to average crack width as observed experimentally in the test series by Lee et al. [38]. It can be seen that the ratio varies from 1.40 for specimen B34-5 to 3.43 for specimen B68-4. The mean value of w_{max}/w_{avg} is found to be 2.61. Various researchers find different value of this ratio in their experiments and they adopt different ratios to conservatively predict the maximum crack width from the average crack widths. Hu and Wu [31] observe in their experiments that the maximum crack width to average crack width ratio is about 1.5. Deluce et al. [22] suggest the value of this ratio to be 1.57 while Lee et al. [36] and Voo et al. [59] assume the value of this ratio as 1.7. It should be noted that the maximum value of $w_{max,exp}/w_{avg,exp}$ equal to 3.43 may not be the true representative of the actual relation between these two values. Ideally, we may want to have a relation between the characteristic maximum crack width and the average crack width. In this study, we have a limited set of data points, therefore, such a relation can not be reliably stated.

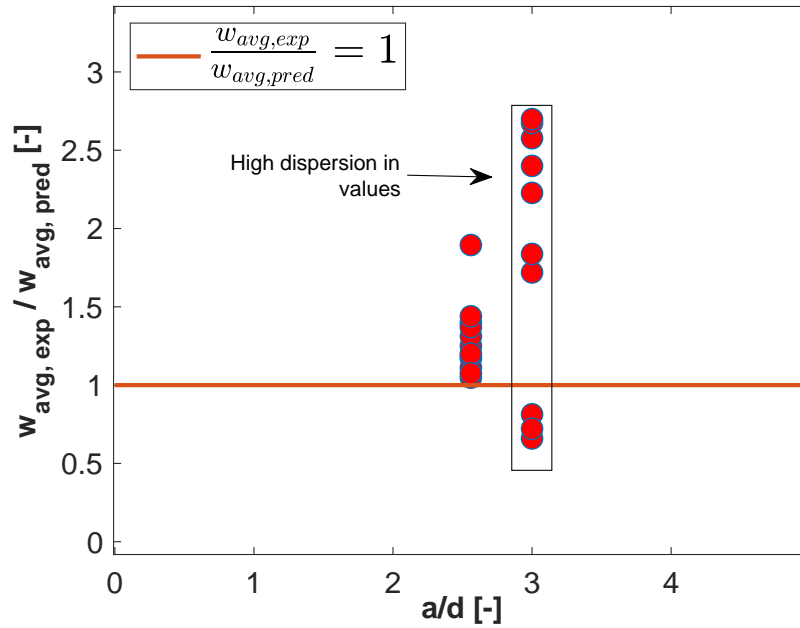


Figure 4.25: The ratio of $w_{avg,exp}/w_{avg,pred}$ versus a/d for the proposed Model-IA.

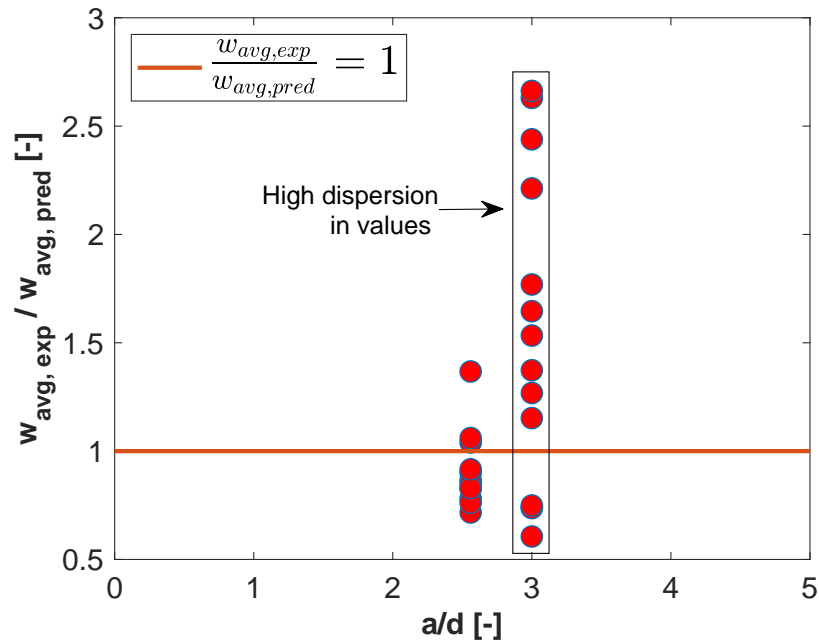


Figure 4.26: The ratio of $w_{avg,exp}/w_{avg,pred}$ versus a/d for the proposed Model-IB.

It can be observed from Figure 4.25 that prediction from Model-IA shows high dispersion for $a/d = 3$ as compared to $a/d = 2.56$. Moreover, a bias towards giving unconservative predictions can be seen at $a/d = 3$ as compared to $a/d = 2.56$. Similar tendency to predict higher dispersion for $a/d = 3.0$ as compared to $a/d = 2.56$ is observed in all the models (see Figure 4.26- Figure 4.31).

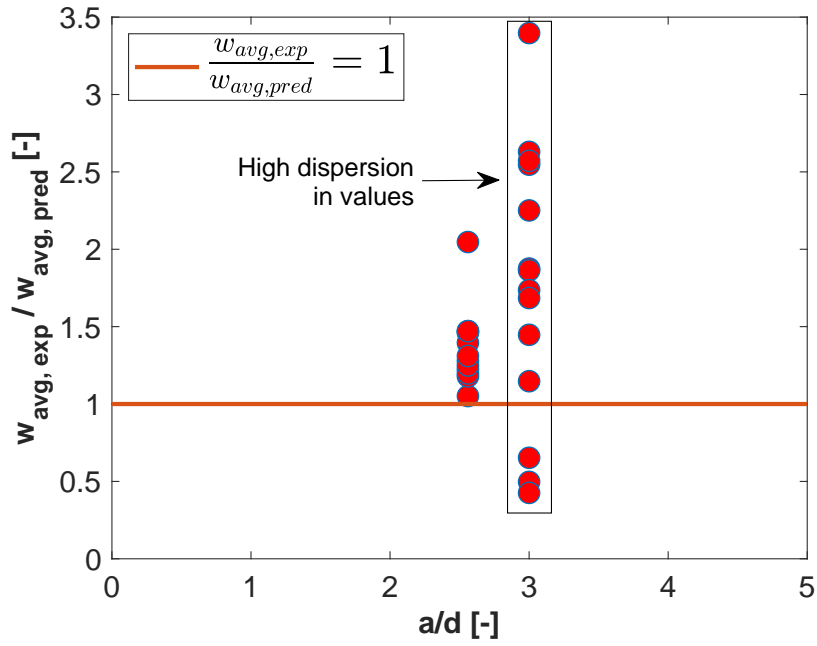


Figure 4.27: The ratio of $w_{avg,exp}/w_{avg,pred}$ versus a/d for the proposed Model-IIA

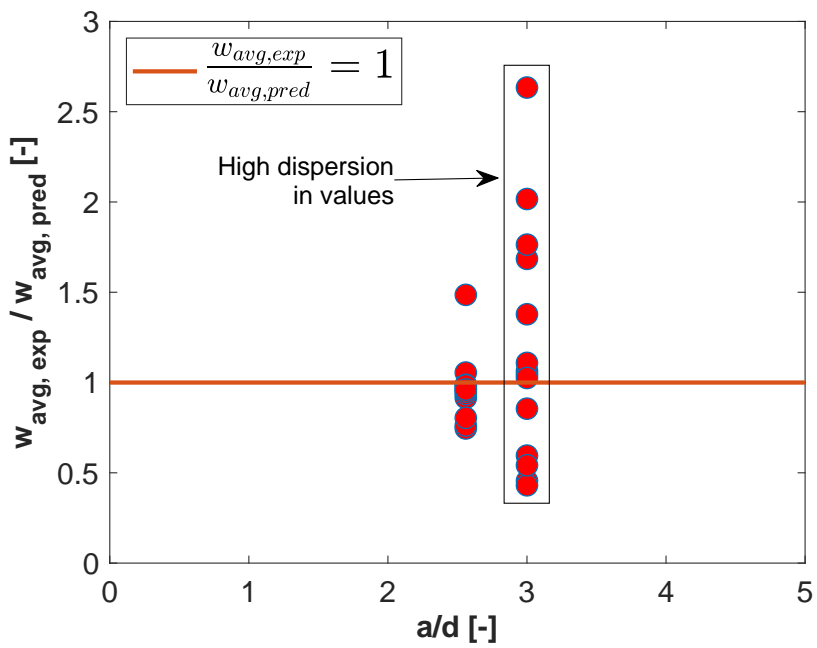


Figure 4.28: The ratio of $w_{avg,exp}/w_{avg,pred}$ versus a/d for the proposed Model-IIB

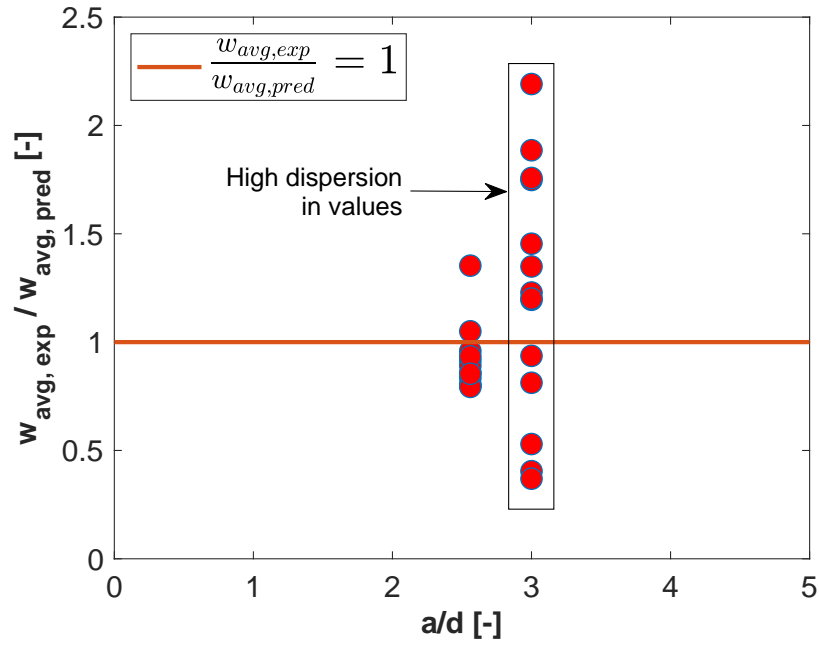


Figure 4.29: The ratio of $w_{avg,exp} / w_{avg,pred}$ versus a/d for the proposed Model-III A

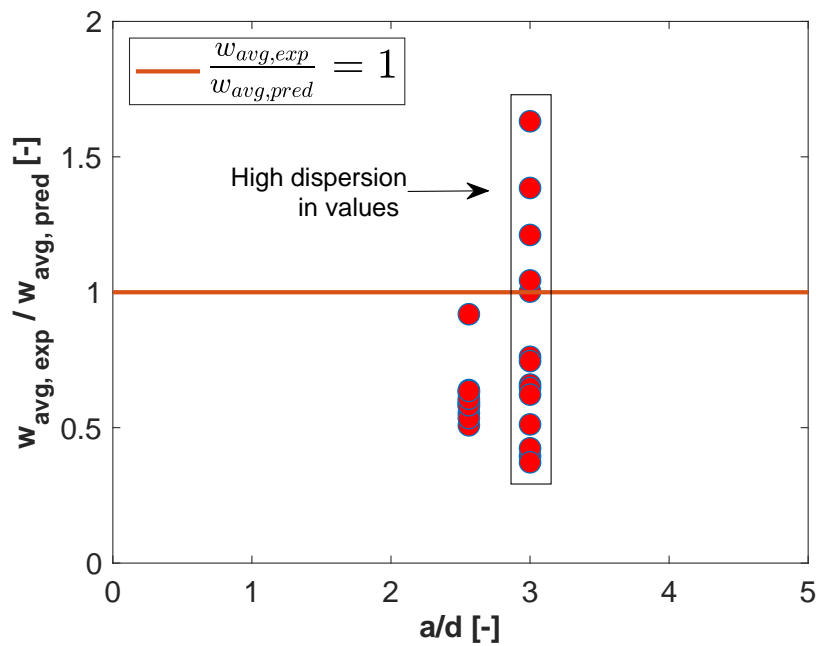


Figure 4.30: The ratio of $w_{avg,exp} / w_{avg,pred}$ versus a/d for the proposed Model-III B

It can be seen from Figure 4.30 that 5 out of 26 predictions are unconservative (i.e. prediction ratio > 1.0).

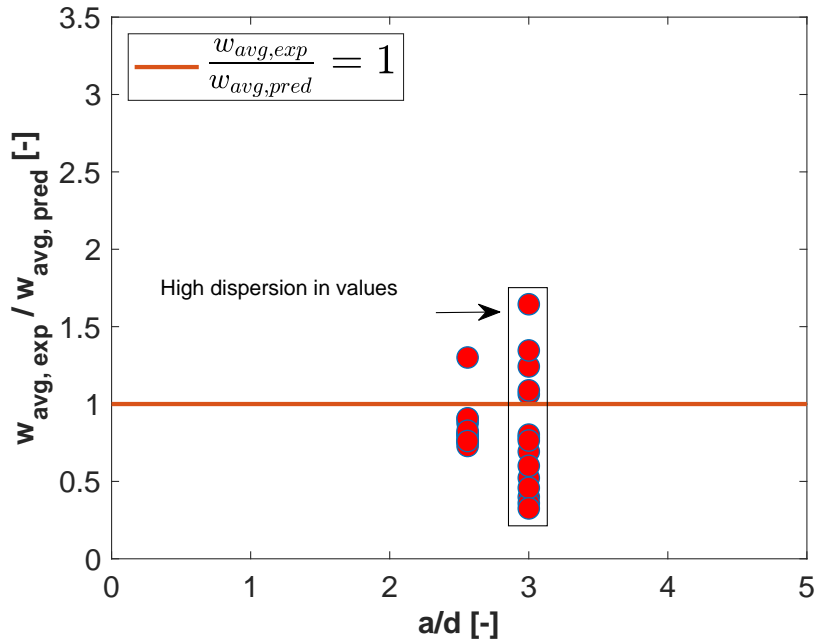


Figure 4.31: The ratio of $w_{avg,exp} / w_{avg,pred}$ versus a/d for the proposed Model-IV

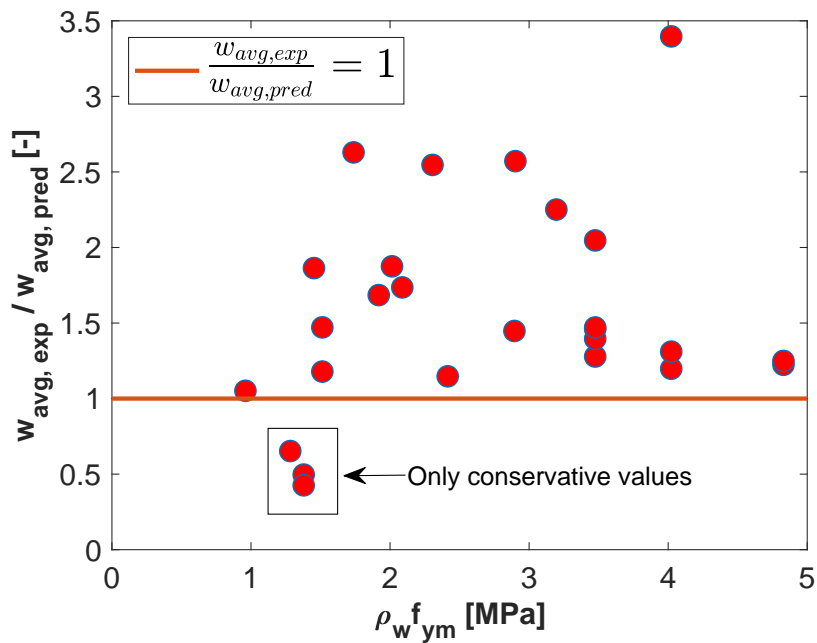


Figure 4.32: The ratio of $w_{avg,exp} / w_{avg,pred}$ versus $\rho_w f_{ym}$ (MPa) for the proposed Model-IIA

It can be observed from Figure 4.32 that 23 out of 26 predictions from Model-IIA are unconservative. Therefore, this model is not suitable to make predictions for the average shear crack width under service loads.

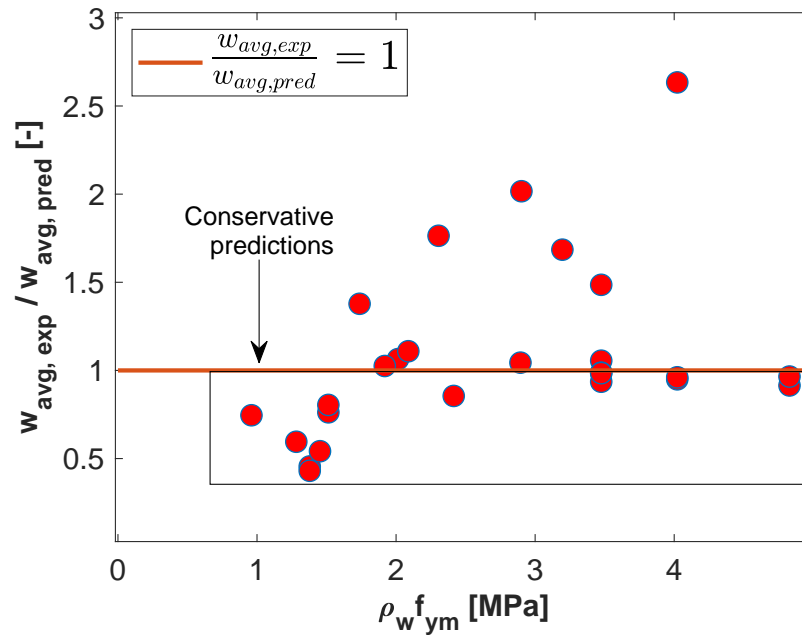


Figure 4.33: The ratio of $w_{avg,exp}/w_{avg,pred}$ versus $\rho_w f_{ym}$ (MPa) for the proposed Model-IIB

Figure 4.33 shows the prediction ratio for various beam specimens according to Model-IIB. It can be seen that the predictions are roughly uniformly distributed around a mean value of 1.0. Although, the mean of the prediction ratios is 1.08, there are a large number of unconservative predictions.

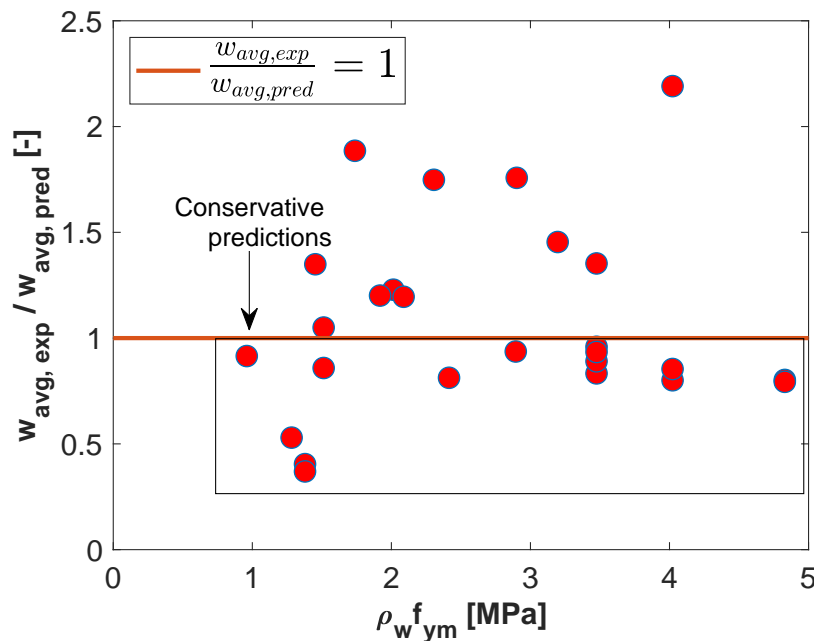


Figure 4.34: The ratio of $w_{avg,exp}/w_{avg,pred}$ versus $\rho_w f_{ym}$ (MPa) for the proposed Model-III A

Figure 4.34 shows that the predictions from Model-III A are roughly uniformly distributed around a mean value of prediction ratio = 1.0. 11 out of 26 predictions are found unconservative.

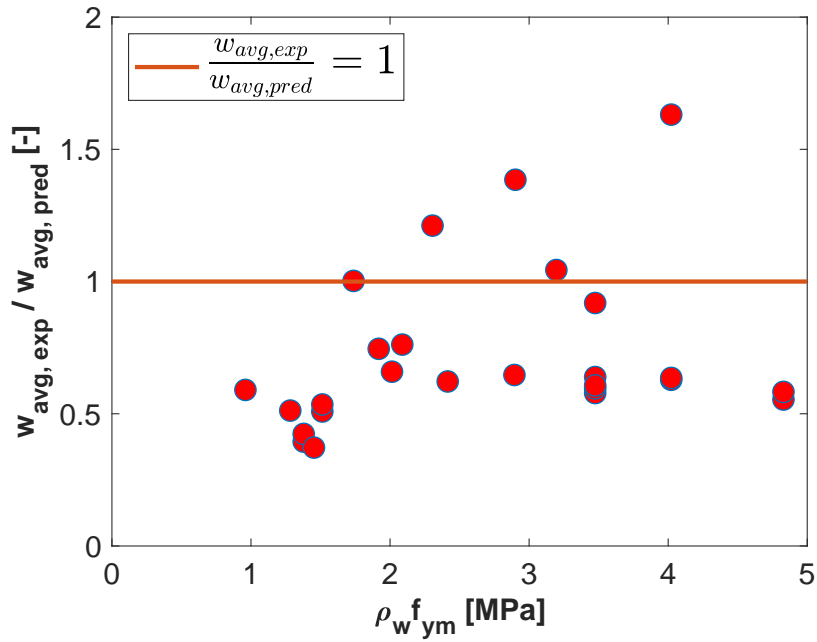


Figure 4.35: The ratio of $w_{avg,exp}/w_{avg,pred}$ versus $\rho_w f_{ym}$ (MPa) for the proposed Model-III B

Figure 4.35 show that there is no particular bias in the predictions of the Model-III B with respect to the shear reinforcement parameter $\rho_w f_{ym}$.

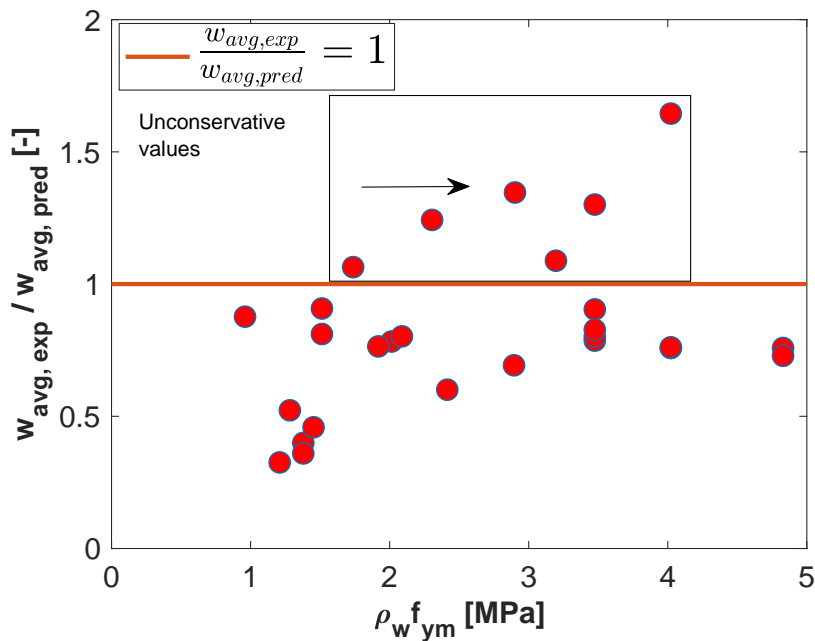


Figure 4.36: The ratio of $w_{avg,exp}/w_{avg,pred}$ versus $\rho_w f_{ym}$ (MPa) for the proposed Model-IV

It can be seen from Figure 4.36 that Model-IV gives 6 unconservative predictions out of the total 26 specimens referred in the analysis. Moreover, it can be noticed that the predictions do not exhibit any bias with respect to $\rho_w f_{ym}$.

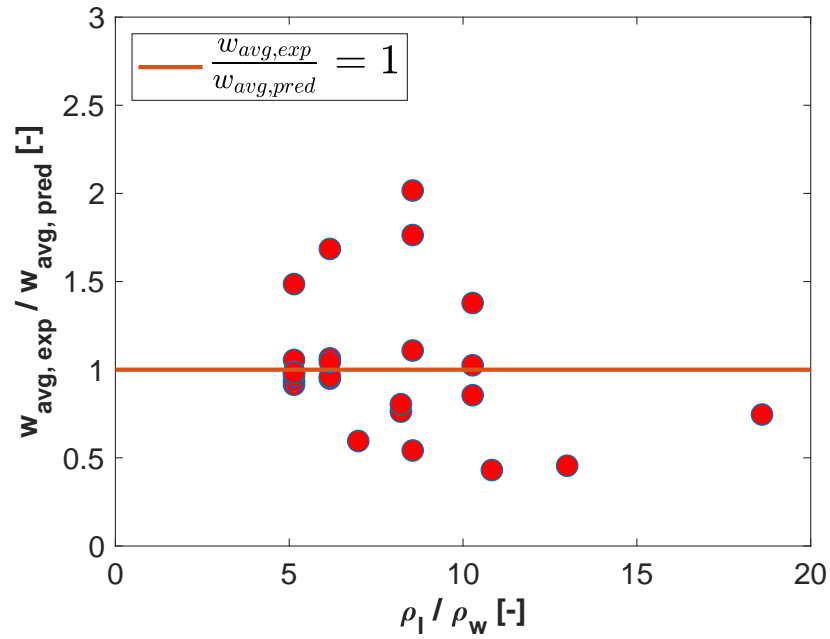


Figure 4.37: The ratio of $w_{avg,exp}/w_{avg,pred}$ versus ρ_l/ρ_w for the proposed Model-IIB

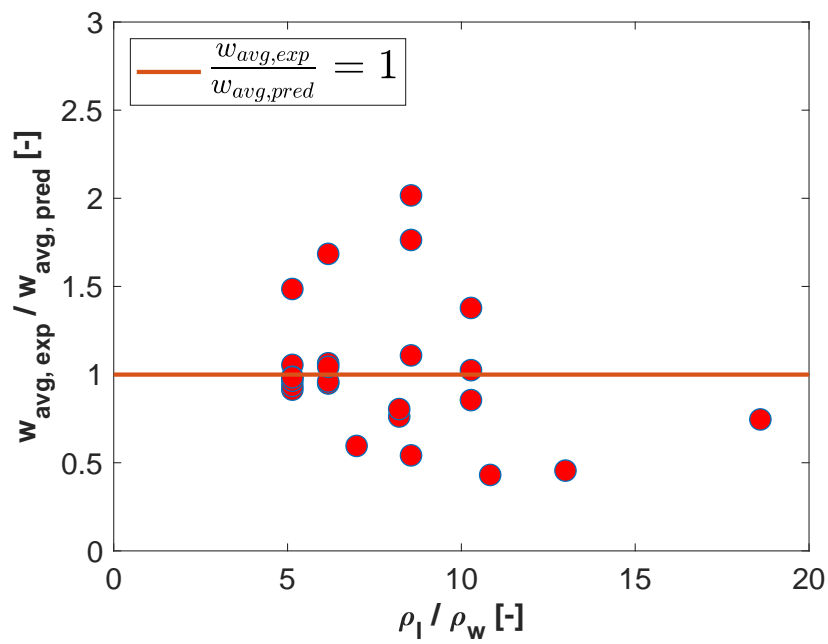


Figure 4.38: The ratio of $w_{avg,exp}/w_{avg,pred}$ versus ρ_l/ρ_w for the proposed Model-IIIA

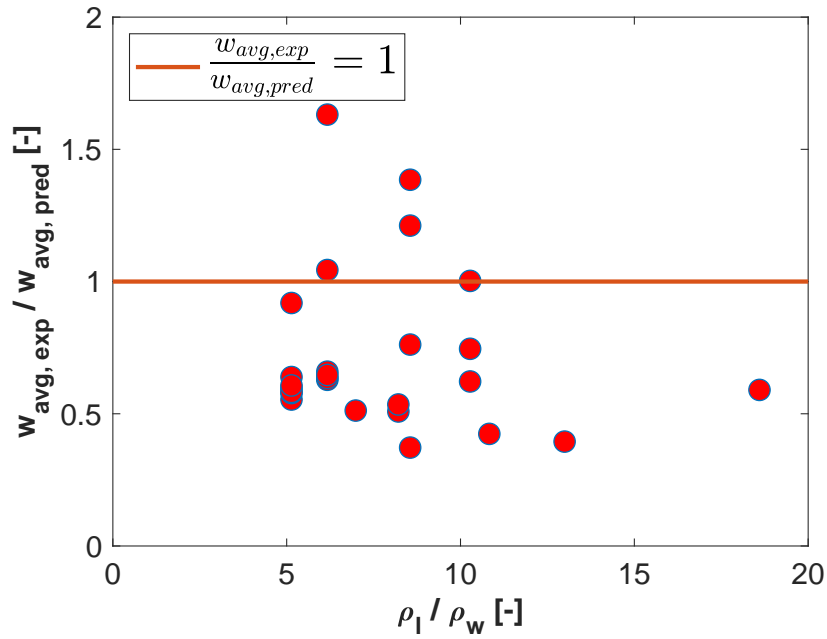


Figure 4.39: The ratio of $w_{avg,exp}/w_{avg,pred}$ versus ρ_l/ρ_w for the proposed Model-III B

It can be observed from figures Figure 4.37- Figure 4.40 that there is no bias in the predictions of Model-IIB, Model-IIIA and Model-IIIB with respect to ρ_l/ρ_w .

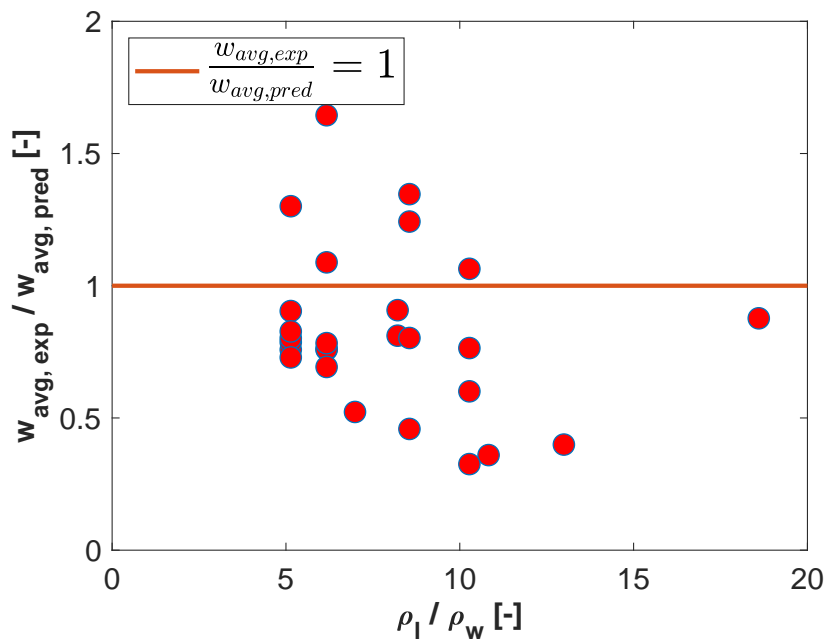


Figure 4.40: The ratio of $w_{avg,exp}/w_{avg,pred}$ versus ρ_l/ρ_w for the proposed Model-IV

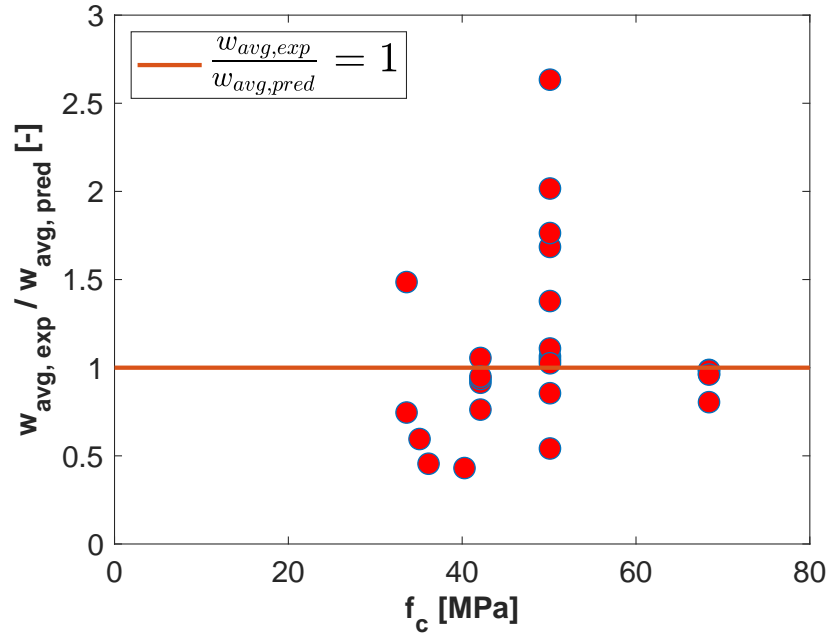


Figure 4.41: The ratio of $w_{avg,exp}/w_{avg,pred}$ versus $f_c(MPa)$ for the proposed Model-IIB

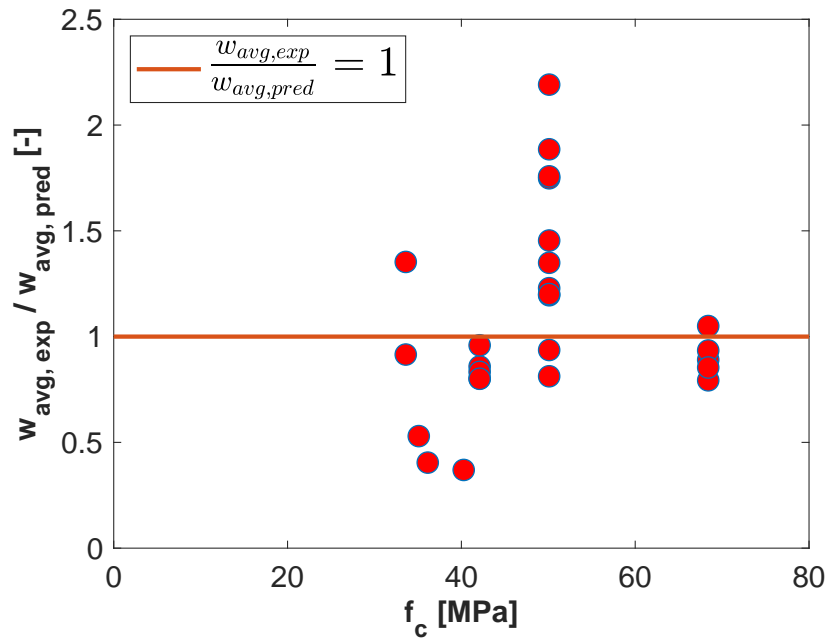


Figure 4.42: The ratio of $w_{avg,exp}/w_{avg,pred}$ versus $f_c(MPa)$ for the proposed Model-III A

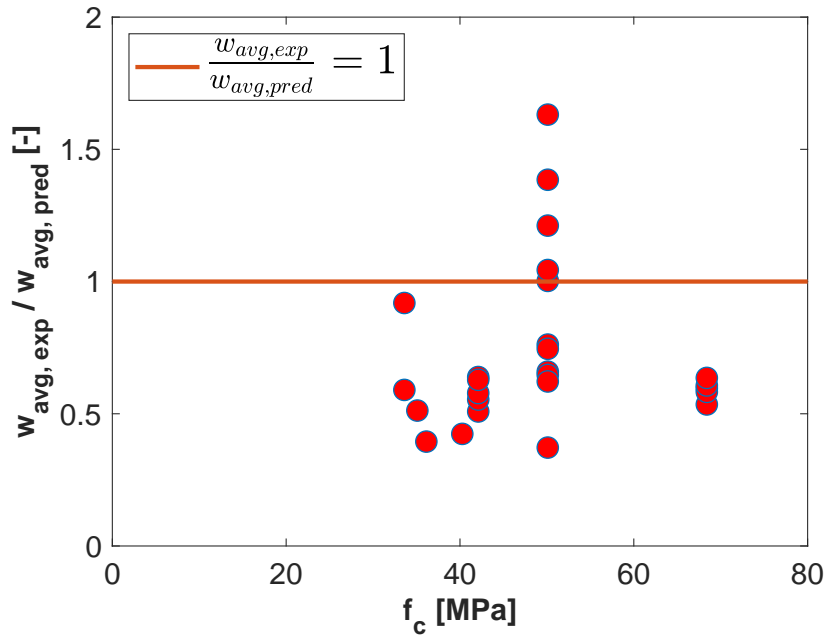


Figure 4.43: The ratio of $w_{avg,exp}/w_{avg,pred}$ versus $f_c(MPa)$ for the proposed Model-III B

It can be observed from Figure 4.41- Figure 4.43 that there is no bias in the predictions of Model-IIB, Model-IIIA and Model-IIIB with respect to f_c .

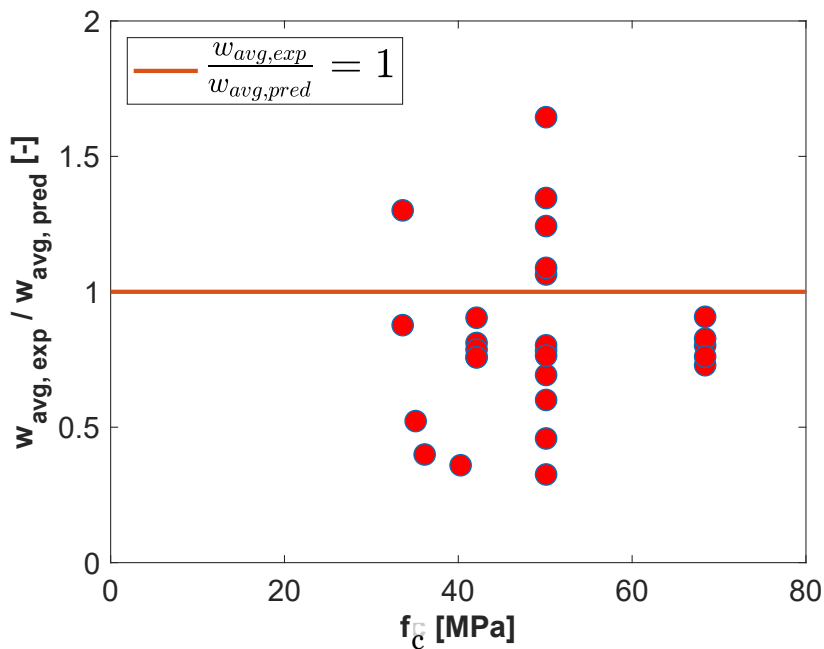


Figure 4.44: The ratio of $w_{avg,exp}/w_{avg,pred}$ versus $f_c(MPa)$ for the proposed Model-IV

It can be observed from Figure 4.44 that there is no bias in the predictions of Model-IV with respect to f_c .

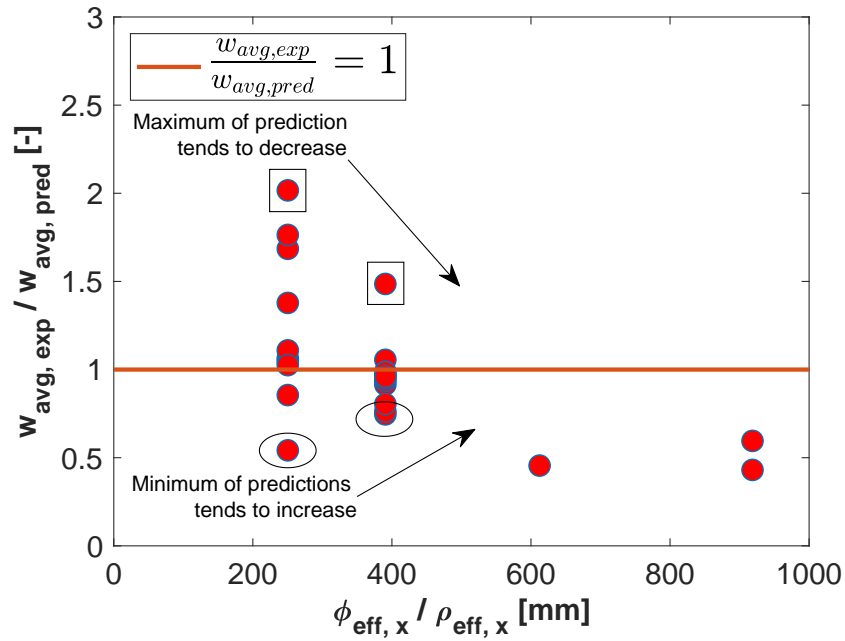


Figure 4.45: The ratio of $w_{avg,exp}/w_{avg,pred}$ versus $\phi_{eff,x}/\rho_{eff,x}$ for the proposed Model-IIB

Figure 4.45 shows that the maximum and minimum of the prediction ratios from Model-IIB show a tendency to decrease and increase respectively with the increase in the $\phi_{eff,x}/\rho_{eff,x}$. This may lead to the predictions converging to values close to 1.0 at higher values of $\phi_{eff,x}/\rho_{eff,x}$ and may lead to more accurate predictions. However, this hypothesis needs further validation based on an experimental study to test whether it is actual or a limitation of the sampling. Similar tendency of the maximum of predictions is observed for the Model-IIIB (see Figure 4.46).

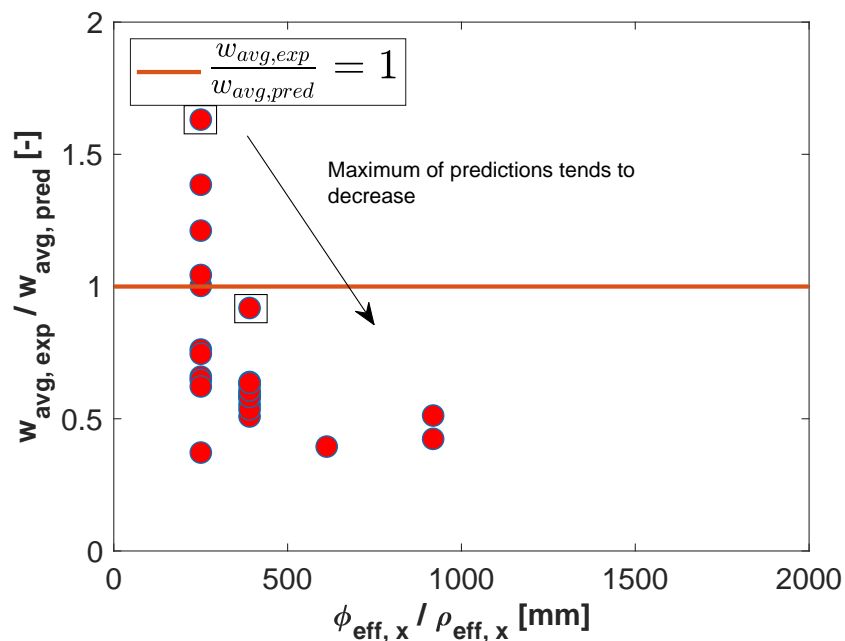


Figure 4.46: The ratio of $w_{avg,exp}/w_{avg,pred}$ versus $\phi_{eff,x}/\rho_{eff,x}$ for the proposed Model-IIIB

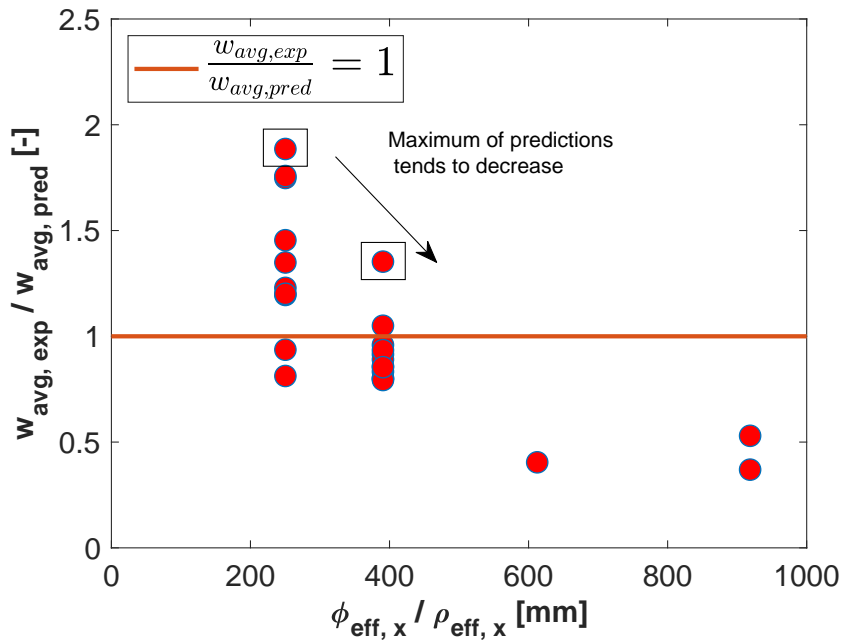


Figure 4.47: The ratio of $w_{avg,exp}/w_{avg,pred}$ versus $\phi_{eff,x}/\rho_{eff,x}$ for the proposed Model-III

Figure 4.47 shows that the maximum of the prediction ratios from Model-III shows a tendency to decrease with the increase in the $\phi_{eff,x}/\rho_{eff,x}$. This may lead to the predictions converging to values close to 1.0 at higher values of $\phi_{eff,x}/\rho_{eff,x}$ and may lead to more accurate predictions. However, this hypothesis needs further validation based on an experimental study to test whether it is factual or a limitation of the sampling.

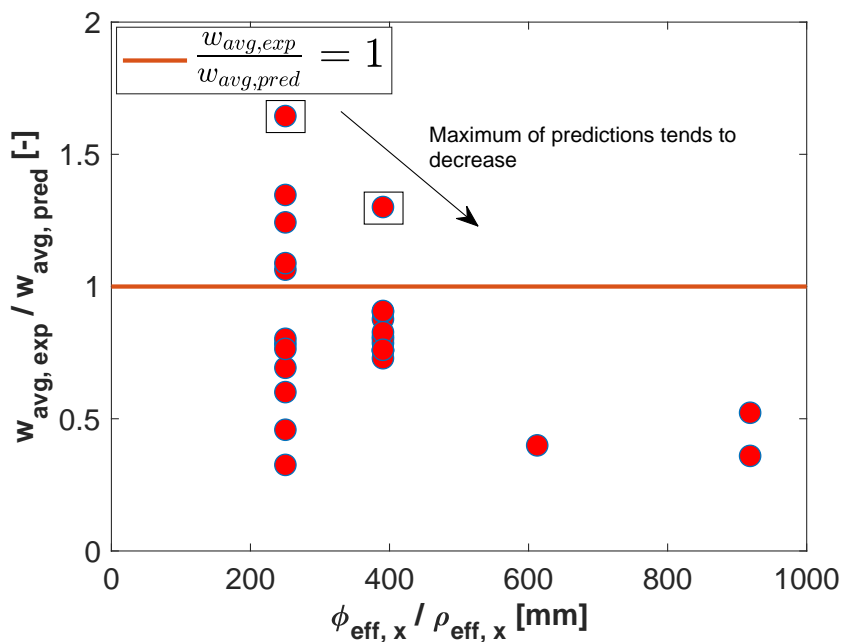


Figure 4.48: The ratio of $w_{avg,exp}/w_{avg,pred}$ versus $\phi_{eff,x}/\rho_{eff,x}$ for the proposed Model-IV

Figure 4.48 shows that the maximum of the prediction ratios from Model-IV shows a tendency to decrease with the increase in the $\phi_{eff,x}/\rho_{eff,x}$. This may lead to the predictions

converging to values close to 1.0 at higher values of $\phi_{eff,x}/\rho_{eff,x}$ and may lead to more accurate predictions. However, this hypothesis needs further validation based on an experimental study to test whether it is factual or a limitation of the sampling.

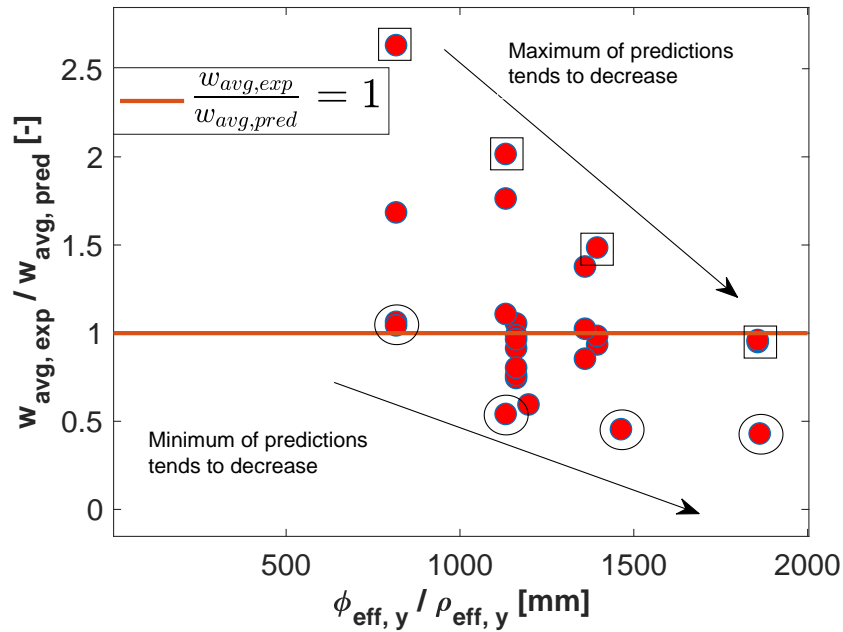


Figure 4.49: The ratio of $w_{avg,exp}/w_{avg,pred}$ versus $\phi_{eff,y}/\rho_{eff,y}$ for the proposed Model-IIB

It can be observed from Figure 4.49 that both maximum and minimum of the prediction ratios from Model-IIB showed a tendency to decrease with the increase in $\phi_{eff,y}/\rho_{eff,y}$. This may lead to the conservative predictions at higher values of $\phi_{eff,y}/\rho_{eff,y}$. However, this hypothesis needs further validation based on an experimental study to test whether it is actual or a limitation of the sampling.

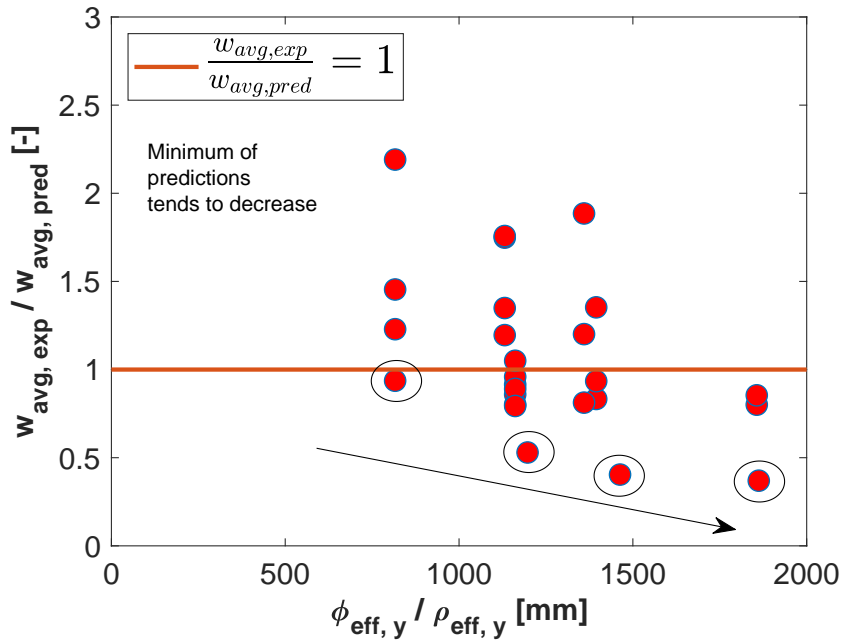


Figure 4.50: The ratio of $w_{avg,exp}/w_{avg,pred}$ versus $\phi_{eff,y}/\rho_{eff,y}$ for the proposed Model-III A

It can be seen from Figure 4.50 that the minimum of the prediction ratio from Model-III A shows a tendency to decrease with the increasing $\phi_{eff,y}/\rho_{eff,y}$. However, the maximum do not show any particular trend and remain significantly greater than 1.0 over the range of $\phi_{eff,y}/\rho_{eff,y}$. Therefore, any comment on the nature of conservatism in the predictions from this model requires verification with an experimental study.

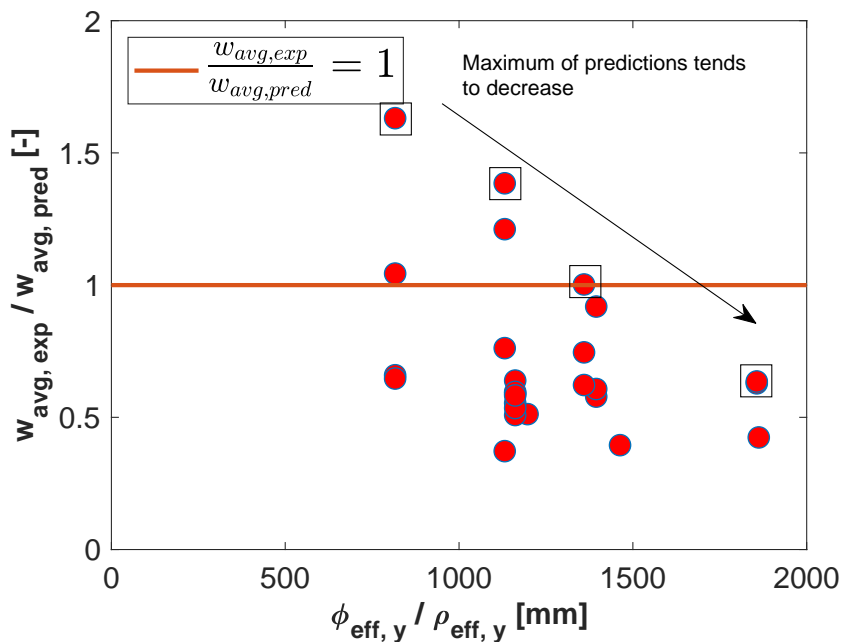


Figure 4.51: The ratio of $w_{avg,exp}/w_{avg,pred}$ versus $\phi_{eff,y}/\rho_{eff,y}$ for the proposed Model-III B

Figure 4.51 shows that the maximum of the prediction ratios from Model-III B shows a tendency to decrease with the increase in the $\phi_{eff,y}/\rho_{eff,y}$. This may lead to conservative

predictions at higher values of $\phi_{eff,y}/\rho_{eff,y}$. However, this hypothesis needs further validation based on an experimental study to test whether it is factual or a limitation of the sampling.

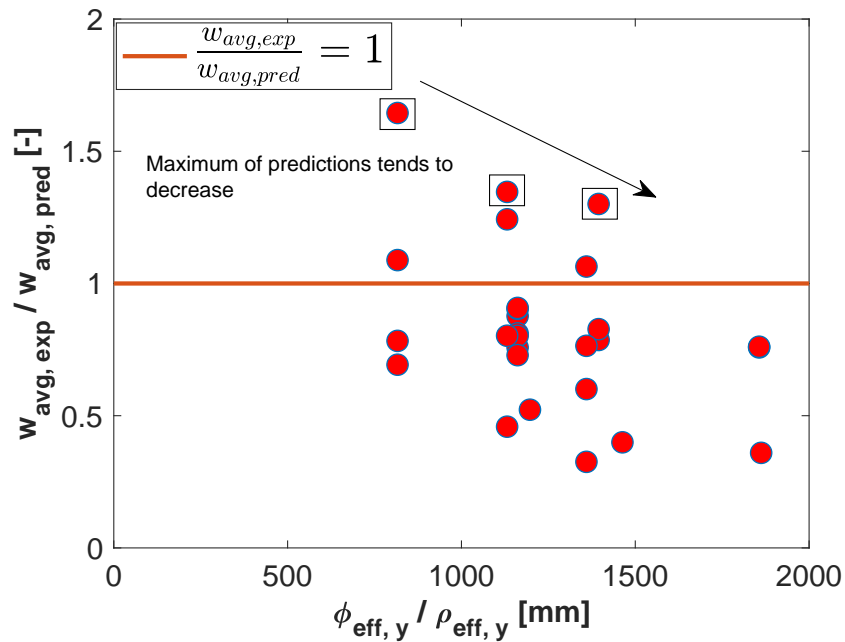


Figure 4.52: The ratio of $w_{avg,exp}/w_{avg,pred}$ versus $\phi_{eff,y}/\rho_{eff,y}$ for the proposed Model-IV

Figure 4.52 shows that the maximum of the prediction ratios from Model-IV show a tendency to decrease with the increase in the $\phi_{eff,y}/\rho_{eff,y}$. This may lead to conservative predictions at higher values of $\phi_{eff,y}/\rho_{eff,y}$. However, this hypothesis needs further validation based on an experimental study to test whether it is factual or a limitation of the sampling.

4.4. Shear Deflection

THUS far we have discussed various models for predicting shear crack width. This model is based on predicting the shear deflection under service loads based on shear stiffness. The shear stiffness can be calculated as a function of shear stiffness at the first diagonal crack and subsequent degradation of the shear stiffness until shear failure (which is assumed to be marked by the yielding of the shear stirrups ([28], [41])). The shear force versus shear strain behavior of the RC beam under service loads is observed to be linearly elastic until the appearance of the first diagonal crack. The shear stiffness of the beam in the elastic stage can be obtained using the method of elasticity ([28], [49]).

$$K_{v,e} = G_c A_v \approx 0.42 E_c A_v \quad (4.68)$$

$$A_v = b_w d_v \quad (4.69)$$

The shear stiffness of the truss at the yielding can be expressed using Equation 4.70.

$$K_{v,y} = \frac{V_y}{\gamma} = \frac{V_y}{\delta_s / d_v \cot \Theta_s} = \frac{n \rho_v E_c A_v \cot^2 \Theta_s}{1 + n \rho_v \csc^4 \Theta_s} \quad (4.70)$$

where

ρ_v shear stirrup ratio.

V_y force at which the stirrups yield and can be expressed by Equation 4.71 [49].

where

$V_{cr} = V_{cr,CCC}$

ρ_v shear reinforcement ratio.

f_{vy} yield strength of stirrups.

θ minimum inclination of the crack angle given by Equation 4.72 [49].

$$V_y = V_{cr} + b d_v \rho_v f_{vy} \cot \theta \quad (4.71)$$

$$\theta = \tan^{-1} \left[\left(\frac{0.77 + \frac{0.66}{n \rho_s}}{4 + \frac{1}{n \rho_v}} \right) \right] \quad (4.72)$$

where

ρ_v longitudinal reinforcement ratio.

It may be noted that shear stiffness of the truss at yielding is given by Equation 4.70 if $\theta \geq \arctan(d_v/a)$. Otherwise, shear stiffness of the truss model is given by Equation 4.73 [49].

$$K_{vc} = \frac{n \rho_v E_c A_v \cot^2 \alpha}{1 + 4 n \rho_v (1 + 0.39 \cot^2 \alpha)} \quad (4.73)$$

where

$\alpha = \arctan(d_v/a)$

He et al. [28] suggested the use of lower bound Theorem of Plasticity to calculate the diagonal compression strut angle. However, based on the discussion in Chapter 3, it is clear that CFT give comparatively more accurate predictions of diagonal compression strut angle than the Theorem of Plasticity. It should be noted that it is proposed that under service loading conditions, the concrete and steel reinforcement can be assumed to behave linearly and therefore, θ_s can be given by Equation 4.74 ([49], [16]).

$$\Theta_s = \arctan \left[\left(\frac{1 + \frac{1}{n\rho_s}}{1 + \frac{1}{n\rho_v}} \right)^{0.25} \right] \quad (4.74)$$

where

ρ_s shear reinforcement percentage.

ρ_v longitudinal reinforcement percentage.

He et al. [28] mention three different approaches to model the degradation of the shear stiffness from the point of first diagonal cracking to the ultimate shear failure (here considered as the yielding of the shear stirrups). The three idealized models are described in the Figure 4.53. In this MSc thesis, the original models are adapted by using a different definition of the mean shear crack angle and first diagonal cracking load than the originally proposed models. It is proposed to calculate the mean shear crack angle from CFT (Equation 4.74) instead of lower bound Theorem of Plasticity (while evaluating yield shear stiffness in Equation 4.70) and use CCC model (Equation 4.18) to calculate the first diagonal cracking load instead of empirical equation given in ACI 318-11 [33].

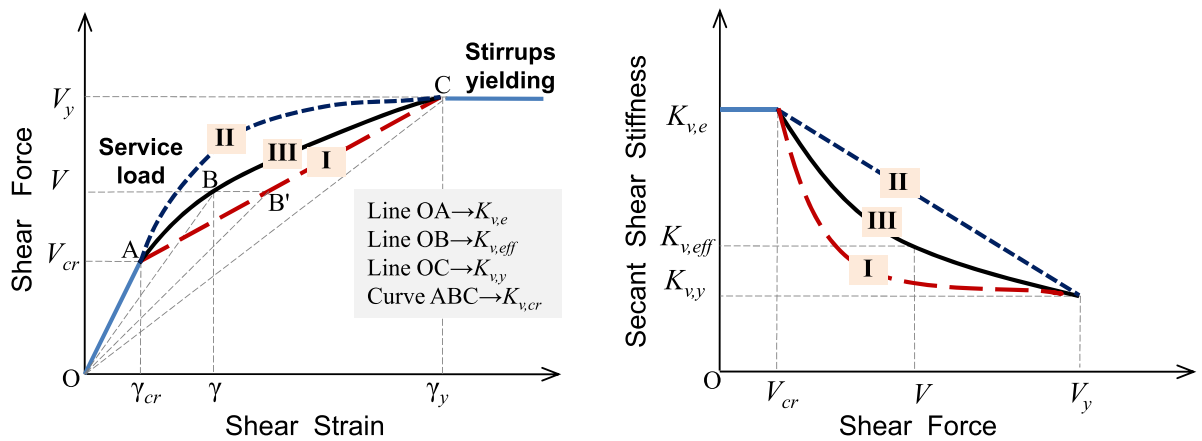


Figure 4.53: The three idealized models for prediction of shear stiffness degradation [28]

These models are described below.

1. Model-I (Linear Tangent Stiffness Model)

In this model it is assumed that the shear stress-strain response is linear between points A and C (which marks the instance of first diagonal crack and ultimate shear failure (yielding of the shear stirrups)). The slope of the graph at any point in between

A and C is given by Equation 4.75.

$$K_{v,cr}^{Model-I} = \frac{V_y - V_{cr}}{\gamma_y - \gamma_{cr}} = \frac{V_y - V_{cr}}{\frac{V_y}{K_{v,y}} - \frac{V_{cr}}{K_{v,e}}} \quad (4.75)$$

Now, the effective shear stiffness at any point B' between A and C (corresponding to the applied shear force V is given by the slope of the line OB').

$$K_{v,eff}^{Model-I} = \frac{V}{\frac{V_{cr}}{K_{v,e}} + \left(\frac{V_y}{K_{v,y}} - \frac{V_{cr}}{K_{v,e}}\right) \frac{V - V_{cr}}{V_y - V_{cr}}} \quad (4.76)$$

2. Model-II (Linear Secant Stiffness Model)

In this model the effective shear stiffness is assumed to be linearly decreasing from $K_{v,e}$ to $K_{v,y}$ as the load increases from the first diagonal cracking to the ultimate shear failure. Hence, the effective stiffness may be given by Equation 4.77.

$$K_{v,eff}^{Model-II} = \frac{V_y - V}{V_y - V_{cr}} K_{v,e} + \frac{V - V_{cr}}{V_y - V_{cr}} K_{v,y} \quad (4.77)$$

3. Model-III (Hybrid Stiffness Model)

In this model the effective shear stiffness between the points A and C is taken as the mean of the effective shear stiffness calculated using Model-I and Model-II and is given by Equation 4.78. Therefore,

$$K_{v,eff}^{Model-III} = \frac{V_y - V}{V_y - V_{cr}} K_{v,e} + \frac{V - V_{cr}}{V_y - V_{cr}} K_{v,y} \quad (4.78)$$

4. Model-IV (Adapted He et al. Model)

He et al.[28] introduced simplifications in Model-III and derived the expression for the effective shear stiffness given in Equation 4.79 [28].

$$K_{v,eff} = \left[\frac{(1 - \sqrt[3]{\rho_v})(-8\lambda_v^3 + 16\lambda_v^2 - 11\lambda_v)}{3} + 1 \right] \quad (4.79)$$

It should be kept in mind that the effective shear stiffness is a function of the applied shear force in all the proposed models. It may be noted that in the original model proposed by the authors an assumption of mean diagonal shear crack angle equal to 45 degrees is made for the evaluation of yield shear force V_y . Moreover, the first diagonal shear cracking load is calculated using the empirical expression given in ACI 318-11 [33]. In the adapted model, It is proposed to calculate the mean shear crack angle from CFT (Equation 4.74) and use CCC model (Equation 4.18) to calculate the first diagonal cracking load instead of empirical equation given in ACI 318-11 [33]. However, the assumption that the ratio of yield shear stiffness to the elastic shear stiffness is equal to third root of shear reinforcement ratio from the original He et al. model is retained in the adapted model. Once the effective shear stiffness $K_{v,eff}^{Model-i}$ is calculated, the shear strain corresponding to an applied shear force V

can be obtained by Equation 4.80.

$$\gamma = \begin{cases} \frac{V}{K_{v,e}}, & \text{if } V \leq V_{cr} \\ \frac{V}{K_{v,eff}}, & \text{if } V_{cr} \leq V_y \end{cases} \quad (4.80)$$

The shear deflection at any point in the span can be found Equation 4.81.

$$\Delta_v = \int_0^L \gamma(x) \bar{V} dx \quad (4.81)$$

Figure 4.54 graphically illustrates the method to obtain the shear deflection for the typical loading configurations of a 4-point bending beam and uniformly distributed loaded beam respectively.

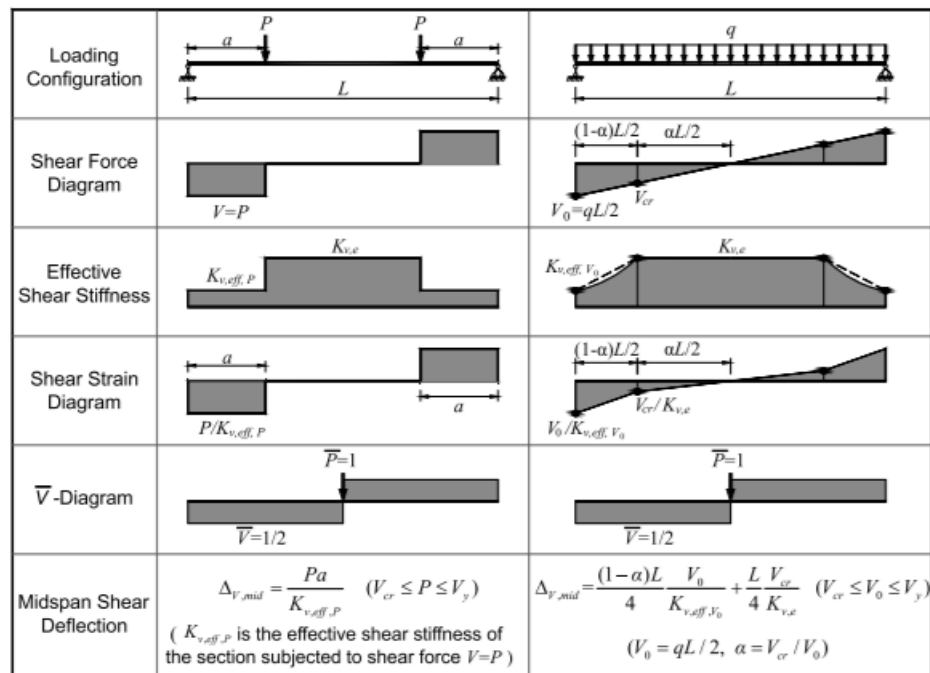


Figure 4.54: Illustrations for calculation of shear deformation for typical load configurations [28]

4.4.1. Experimental Details

Hansapinyo et al. [25] perform a study for shear deflections in shear reinforced concrete beams. The elongation of shear stirrups and longitudinal reinforcement bars is measured using electronic wire strain gauges. The surface deformation of concrete is measured using electronic transducers. The deflection of beam is also measured using displacement transducers. The shear deflection is separated from total deflection by subtracting flexural deflection. Two different methods are deployed to calculate the shear deflection.

1. Adding the total shear deflection of different panels (the beam is discretized in a set of panels and shear deformation of each panel is measured using strain transformation law on the measured strains at 45 degrees to the axis of the beam).
2. Subtracting flexural deflection from total deflection. The flexural deflection is calculated by double integration of beam curvature along the span. The curvature is alternatively also calculated using measured axial strains at different depths along the height of the beam cross-section.

Similarly, Wang et al. [60] perform a series of tests on beams with slenderness ratio < 3.0 to study the degradation of shear stiffness post diagonal-cracking. The total deflection is measured using LVDTs (Linear Variable Differential Transformer). The flexural deflection is calculated using equation given in ACI 318-08 [2] and subtracted from total deflection to obtain the shear deflection.

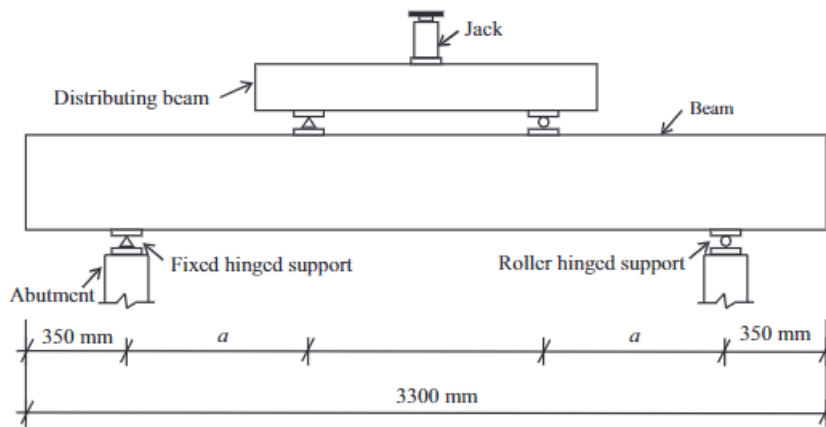


Fig. 1. Dimensions of RC beam and loading mode.

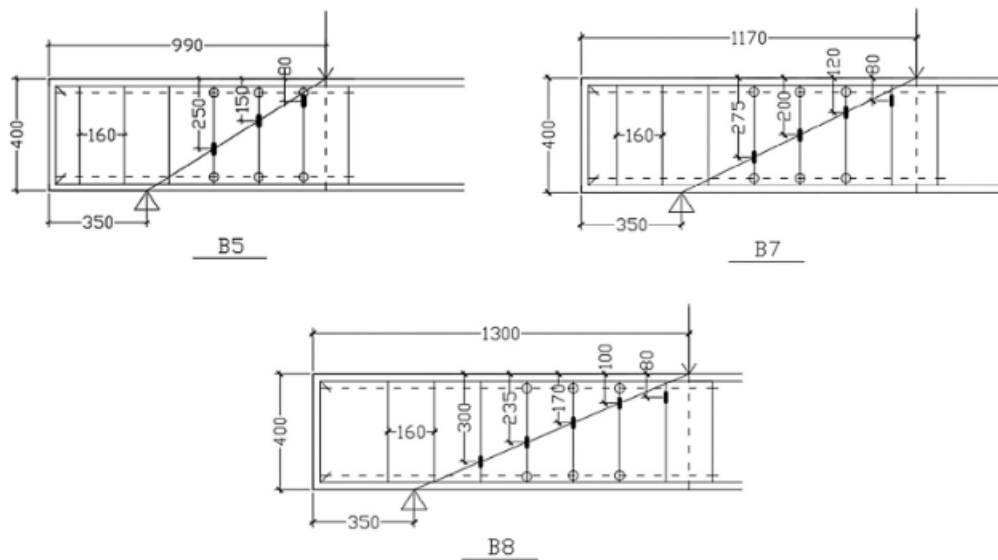


Figure 4.55: Mechanical scheme and instrumentation for specimens [60]

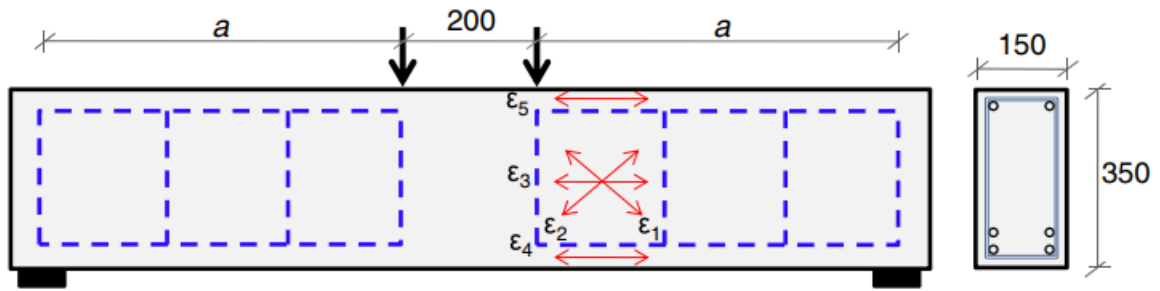


Figure 4.56: Mechanical scheme and instrumentation for specimens [25]

Table 4.8: Summary of specimens analyzed for shear deflection study

Publication	Series	Specimens	Mechanical Scheme	Instrumentation Method
Wang et al.[60]	B3, B8 and B9	3	4-point bending	Strain gauges, LVDT
Hansapinyo et al. [25]	S1, S2, S3 and S4	4	4-point bending	Strain gauges, PI Type electronic transducers

Table 4.8 shows the key characteristics of the experimental work referred in this study.

Table 4.9: Range of parameters for the specimens studies for comparison of shear deflection with predictions from various models

Parameter	Range
a/d	2.60-3.50
d/b	1.81-2.05
$\rho_w f_{ym}$ (MPa)	0.73-1.74
ρ_l (%)	0.70-4.26
ρ_w (%)	0.13-0.47
f'_c (MPa)	24.20-50.00

4.4.2. Results

In this subsection, an assessment of the performance of the various prediction models proposed in section 4.4 is done.

Table 4.10: Shear-Deflection Results from various models

Specimen	Load-Level	Shear Deflection Experiment (mm)	%(Shear-to flexure) Deflection	$\delta_{avg,exp}/\delta_{avg,pred}$			
				Model-I	Model-II	Model-III	Model-IV
B3	0.5V	1.11	0.32	0.72	5.39	3.06	2.78
B8	0.5V	0.82	0.25	0.40	3.69	2.05	1.89
B9	0.5V	0.93	0.22	0.51	5.64	3.08	2.85
B3	0.6V	2.00	0.47	0.90	1.00	3.52	3.23
B8	0.6V	1.48	0.37	0.44	1.00	2.02	2.08
B9	0.6V	1.74	0.35	0.62	1.00	3.44	3.27
B3	0.7V	2.56	0.51	0.88	1.00	2.73	3.24
B8	0.7V	2.15	0.47	0.46	1.00	1.23	2.18
B9	0.7V	2.22	0.38	0.59	1.00	2.30	3.21
S1	0.5V	0.68	0.32	1.13	3.35	2.24	1.98
S2	0.5V	1.25	0.25	1.44	4.42	2.93	2.51
S3	0.5V	0.86	0.30	0.90	3.38	2.14	1.80
S4	0.5V	0.66	0.28	0.68	3.31	1.99	1.74
S1	0.6V	1.00	0.38	1.11	3.38	2.24	1.77
S2	0.6V	1.45	0.23	1.15	3.49	2.32	1.83
S3	0.6V	1.14	0.33	0.85	2.73	1.79	1.72
S4	0.6V	1.00	0.36	0.68	2.93	1.81	1.73
S1	0.7V	1.39	0.44	1.16	3.16	2.16	1.83
S2	0.7V	2.25	0.30	1.35	3.60	2.48	2.17
S3	0.7V	1.75	0.23	1.03	2.30	1.66	2.08

Table 4.10 shows the prediction ratios for the various models at different load levels. Here V is the nominal shear resistance calculated using EC2 [19]. It can be seen that the percentage of shear deflection to the total deflection in the referred studies is large. It is found that on an average shear deflection are as high as 33.83% of the flexural deflections. The percentage varies from 22.13% for specimen B9 at 0.5V to 51.2 % for specimen B3 at 0.7V. It can be seen that the percentage of shear deflection increases with increase in the applied shear load.

Table 4.11: Statistical parameters for the $\delta_{s,exp}/\delta_{s,pred}$ by different models

Statistical Parameter	Model I	Model II	Model III	Model IV (He et al.) [28]
Mean	0.85	2.84	2.36	2.29
Median	0.87	3.24	2.24	2.08
SD	0.31	1.46	0.60	0.58
COV	0.36	0.51	0.25	0.25
Max	1.44	5.64	3.52	3.27
Min	0.40	1.00	1.23	1.72
Range	1.04	4.64	2.29	1.54

Table 4.11 shows the various statistical parameters for the proposed models for shear deflection. It can be seen that Model-I gives the most accurate predictions for the shear deflection with a mean and median value of 0.85 and 0.87 respectively. However, the maxi-

imum prediction ratio is 1.44 indicating a probability for unconservative predictions. The SD and COV for this model are 0.31 and 0.36 respectively which are significantly smaller as compared to other models. It may be noted that all other models in this study are found to give unconservative predictions. This may be attributed to the inability of these models to capture the rate of shear stiffness degradation post diagonal shear cracking. Model-IV also gives unconservative predictions with significant dispersion in the values as indicated by high values of SD. This may be due to two reasons. First, since Model-IV is also based on the hybrid stiffness model, it inherently incorporates the effect of secant stiffness model. Second, the model uses the assumption that the ratio of yield shear stiffness to elastic shear stiffness is third root of shear reinforcement ratio, $(\rho_w)^{\frac{1}{3}}$, may not always be applicable. Based on the results obtained above, a study for the sensitivity of the predictions to the various beam specimen parameters is done for Model-I and Model-IV.

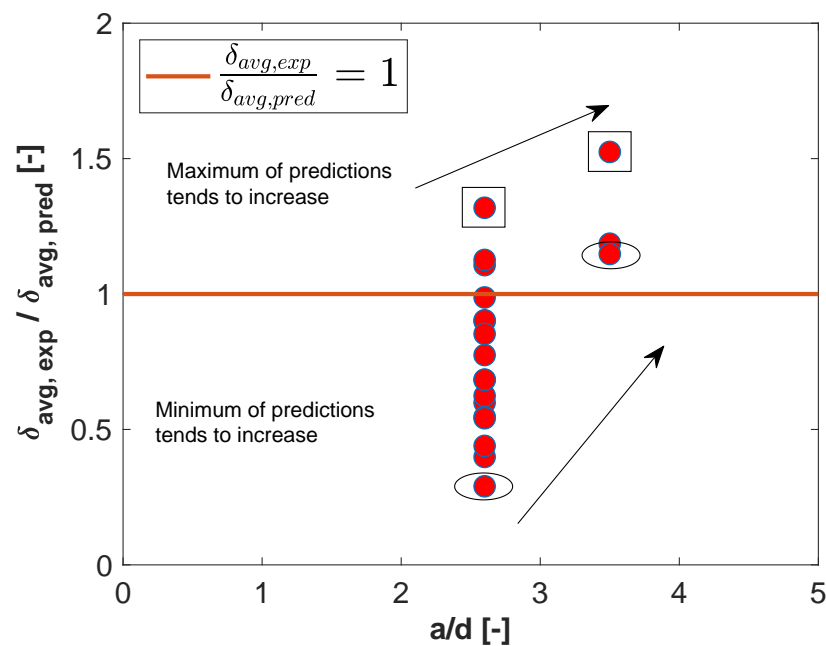


Figure 4.57: The ratio of $\delta_{s,exp}/\delta_{s,pred}$ versus a/d for shear deflection Model-I

Figure 4.57 shows that Model I exhibits a tendency to make higher predictions with a higher maximum at $a/d = 3.5$ as compared to $a/d = 2.5$. This indicates the possibility of unconservative predictions at higher slenderness ratios. However, this hypothesis needs further validation with an experimental study to test whether it is a fact or only a limitation of the sample size in the study.

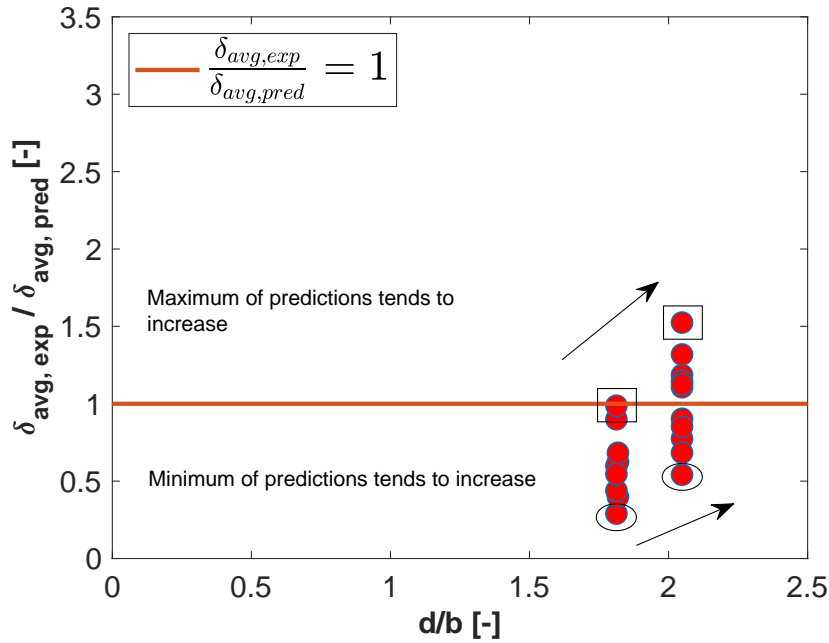


Figure 4.58: The ratio of $\delta_{s,exp}/\delta_{s,pred}$ versus d/b for shear deflection Model-I.

Figure 4.58 shows the variation of the prediction ratio with d/b for Model-I. It can be seen that both the maximum and minimum of the prediction ratio tend to increase with the increasing values of d/b . This indicates that the predictions from this model tends to become less conservative at higher values of d/b . Thus, this model may consistently give unsafe predictions for deep slender beams for $d/b > 2$.

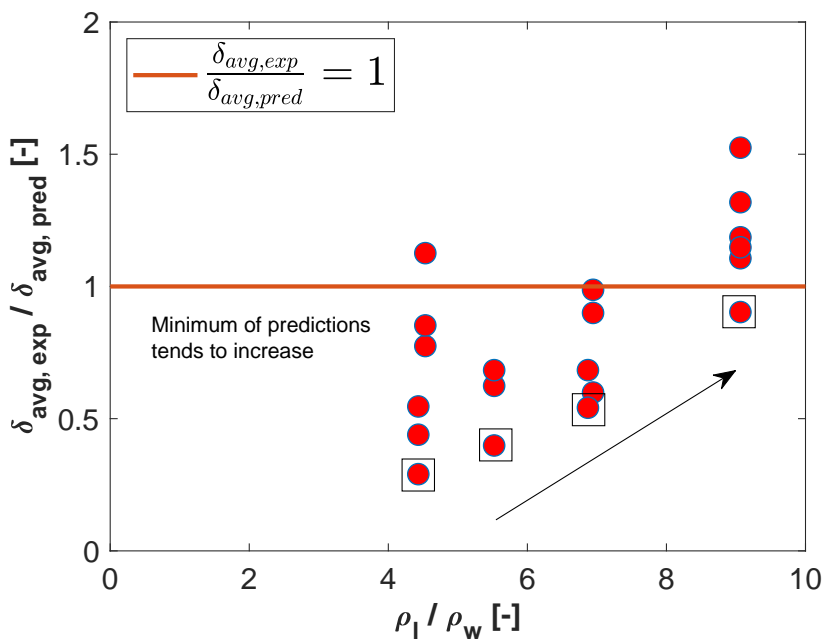


Figure 4.59: The ratio of $\delta_{s,exp}/\delta_{s,pred}$ versus ρ_l/ρ_w for shear deflection Model-I

It can be observed from Figure 4.59 that the minimum of the predictions from Model-I shows a tendency to increasingly predict unconservative values for higher values of ρ_l/ρ_w .

Five out of six unconservative predictions from the model occur at ρ_l/ρ_w equal to 9.06. This indicates that the application of this model may not be suitable for beams with very high longitudinal reinforcement ratio as compared to the shear stirrups ratio. However, further validation with an experimental study is needed for this observation to establish if it is factual or a limitation of the sample size in the study.

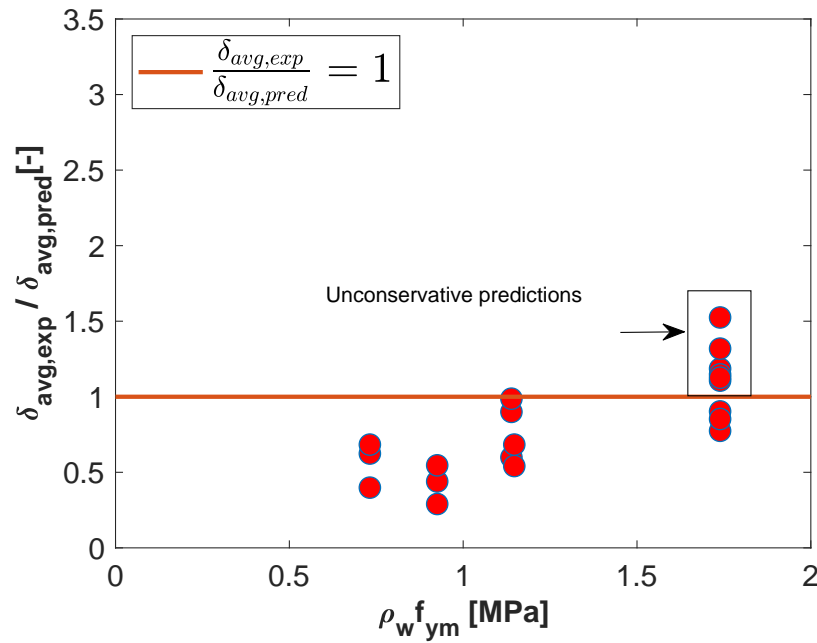


Figure 4.60: The ratio of $\delta_{s,exp}/\delta_{s,pred}$ versus $\rho_w f_{ym}$ (MPa) for shear deflection Model-I.

It can be seen from Figure 4.60 that all the unconservative predictions for Model-I occur corresponding to highest value of $\rho_w f_{ym}$ in the study. This indicates that this model may not be suitable to predict shear deflections for heavily shear reinforced beams. This may be due to the inability of the linear shear force deflection curve to capture the rate of stiffness degradation in shear reinforced beams.

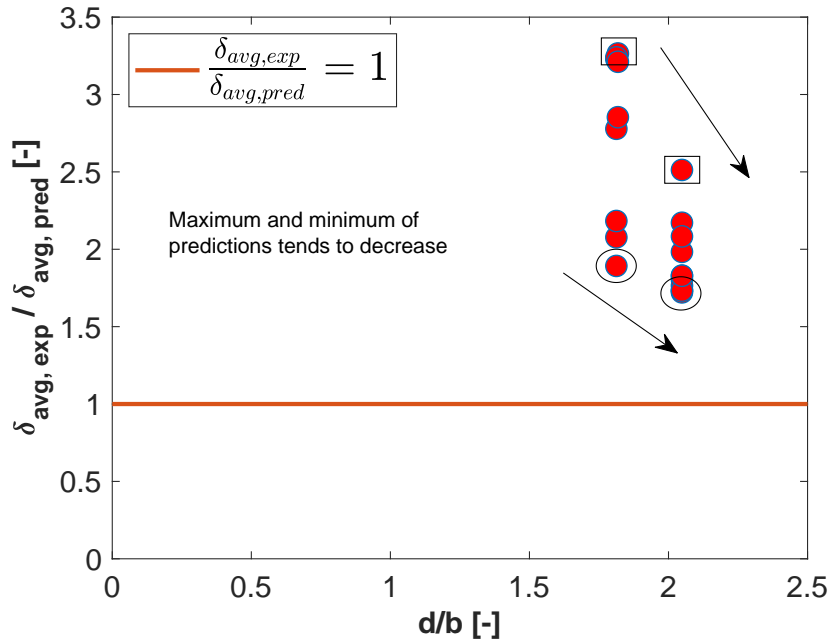


Figure 4.61: The ratio of $\delta_{s,exp}/\delta_{s,pred}$ versus d/b for Model-IV

Figure 4.61 shows that both maximum and minimum of the prediction ratio from Model-IV shows a tendency to decrease with the increase in the d/b . However, the prediction ratio remained significantly higher than 1.0 for the highest value of $d/b = 2.05$ in the study. An experimental study is required to establish if this trend is factual and whether the same trend continues for even higher values of d/b . In the latter case, Model-IV may be used to predict shear deflections for very deep slender beams.

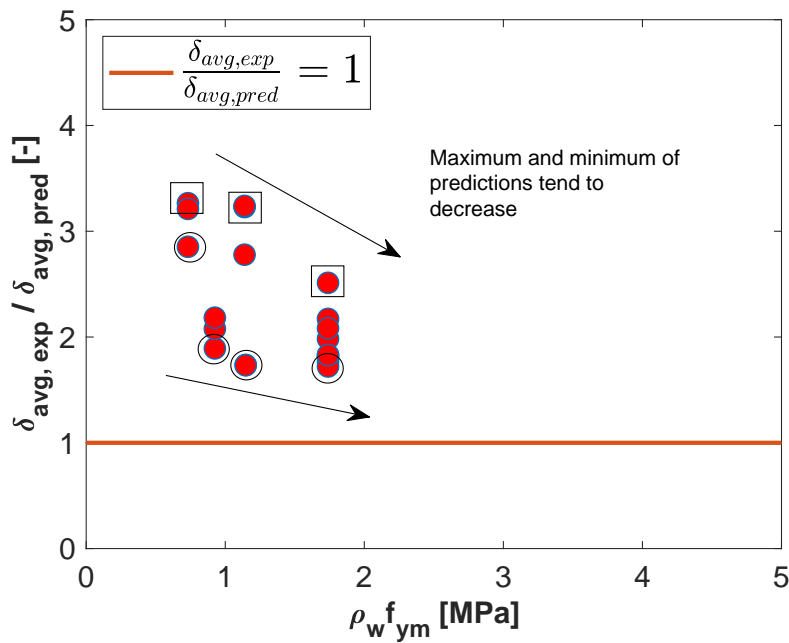


Figure 4.62: The ratio of $\delta_{s,exp}/\delta_{s,pred}$ versus $\rho_w f_{ym}$ (MPa) for Model-IV

It is clear from the Figure 4.62 that both maximum and minimum of the prediction ratio from Model-IV shows a tendency to decrease with the increase in the $\rho_w f_{ym}$. However, the prediction ratio remained significantly higher than 1.0 for the highest value of $\rho_w f_{ym}$ equal to 1.74 in the study. An experimental study is required to establish if this trend is factual and whether the same trend continues for even higher values of $\rho_w f_{ym}$. In the latter case, the Model-IV may be used to predict shear deflections for heavily shear-reinforced beams.

4.5. Overview of the Proposed Shear-Crack Width and Shear Deflection Models

In this Chapter, several models are proposed to evaluate the shear crack width and shear deflection for slender reinforced concrete beams. The basic concept behind the proposed shear crack width models is to evaluate the shear crack spacing and stirrup strain or mean principle tensile strain in the cracked concrete depending on the proposed shear crack width model under consideration. It is proposed that a conservative estimate of the first diagonal shear cracking resistance can be made by assuming it equal to the concrete contribution to shear resistance at ULS (in this thesis it is assumed as a state when all stirrups yield). This assumption is made based on the experimental observation for variation of concrete contribution to shear resistance (after subtracting contribution of stirrups from the applied shear force) with the applied shear force. For slender RC beams, the concrete contribution to shear resistance decreases continuously from the instance of first diagonal shear crack to ULS. It is assumed that the concrete contribution to shear resistance is 100 percent of the applied shear force at first diagonal shear cracking and 0% of the applied shear force at ULS. The total shear resistance is calculated using EC2 expression for shear resistance of shear reinforced concrete beams. The contribution of stirrups to the shear resistance at service loads is the difference between the applied service shear force and corresponding concrete contribution to shear resistance.

It is well-known that the angle of shear crack as well as the angle of diagonal compression strut changes continuously as the applied shear force increases. However, based on reported findings in the literature, this difference is found to be small [31]. Therefore, principle stress and principle strains are assumed co-axial in the proposed models. As stated earlier, the additive model of shear resistance (i.e., total shear resistance is the sum of shear resistance contribution of concrete and stirrups) is used in the proposed models. The diagonally cracked beam is analyzed with the truss analogy.

The principle stress in the diagonal compression strut and strains in stirrups and mean principle tensile strain in the cracked concrete could be obtained once the concrete and stirrup contribution to the shear resistance are known. The mean principle tensile in cracked concrete is determined using Mohr's circle. The obtained stirrup strain (or alternatively mean principle tensile strain in the cracked concrete depending on the shear crack width model under consideration) is used along with shear crack spacing to obtain shear crack width using various proposed models. Five different models are proposed to evaluate the shear crack width in slender reinforced concrete beams under the application of service loads (in this thesis service load is assumed equal to 60% of the nominal shear resistance of a shear reinforced beam according to EC2). The first three models have two variants (A and B) and the variant B of these models are identical to first variant except for the fact that the concrete contribution to shear resistance is assumed equal to zero in variants B. The con-

crete contribution to shear resistance at ULS is determined using CCC model in the first three models.

The first model is adapted form of the current EC2 model to evaluate the crack width. The current model predicts crack width for a flexural or tensile member using mean reinforcement strain and maximum crack spacing. This model is extended to predict shear crack width using mean stirrup strain and the average shear crack spacing (shear crack spacing is calculated using the EC2 model for crack spacing in members with orthogonal reinforcements).

The second model is adapted mean shear crack width model given by Zakaria et al. [65]. The stirrups strain obtained using the methodology described previously is proposed to be substituted in the original expression given by the Zakaria et al. [65].

The third model proposed to determine the mean shear crack width as a product of the mean principle tensile strain in the diagonally cracked concrete and the shear crack spacing obtained from Zakaria et al. model [65].

The fourth model is based on the determination of the concrete contribution to shear resistance using SMCFT. The mean principle tensile strain in the cracked concrete is determined using the previously described methodology. This strain is then multiplied with the mean shear crack spacing obtained from the Zakaria et al. shear crack spacing model [65].

The fifth and the last model for shear crack width determination is adapted from the Swedish handbook for EC2 [9] and the EC2 model for the determination of crack width. This model established equilibrium between the reinforcement stresses and the stresses in concrete to determine the stirrup strains. It is assumed that the cracked concrete can not take any tensile stress. Figure 4.63 shows the strains in different directions in reinforced concrete elements in between the cracks. The various shear transfer actions comprising the concrete contribution to shear resistance are shown in Figure 4.64. Figure 4.65 shows the basic approach behind the proposed models for shear crack width prediction.

In this Chapter, four simplistic models are also proposed for the determination of shear deflection in slender reinforced concrete beams. All the four models required determination of effective shear stiffness and then using this effective stiffness and the applied shear force to determine the shear strain and shear deflection using Virtual- Work theorem. The first model is based on the assumption that the shear stress- strain graph is linear between the stages of first diagonal shear cracking and all stirrups yielding. The second model is based on the assumption that the effective shear stiffness decreases linearly between the stages of first diagonal shear cracking and all stirrups yielding (or ULS in this thesis). The third model evaluates the effective shear stiffness of the diagonally cracked beam as the mean of the effective shear stiffness from the first two models. The fourth model is the adapted form of shear deflection model given by He et al. [28]. In the original model given by He et al., It is assumed that the shear cracks are inclined at an angle of 45 degrees while determining the shear force corresponding to yielding of all the stirrups. Secondly, an additional assumption is introduced that the ratio of yield shear stiffness to the elastic shear stiffness is equal to third root of shear reinforcement ratio. The second assumption is retained in the proposed Model- IV (adapted He et al. Model) as well, however, the mean shear crack angle is calculated using the CFT. Figure 4.66 shows an overview of the calculation steps to evaluate potential shear deflection in slender reinforced concrete beams using the proposed models in this MSc thesis.

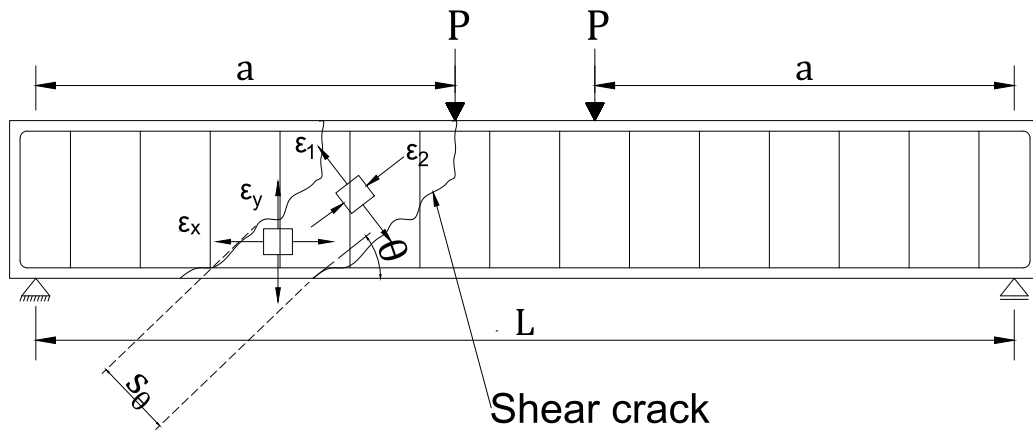


Figure 4.63: Strains in the reinforced concrete element in between the cracks

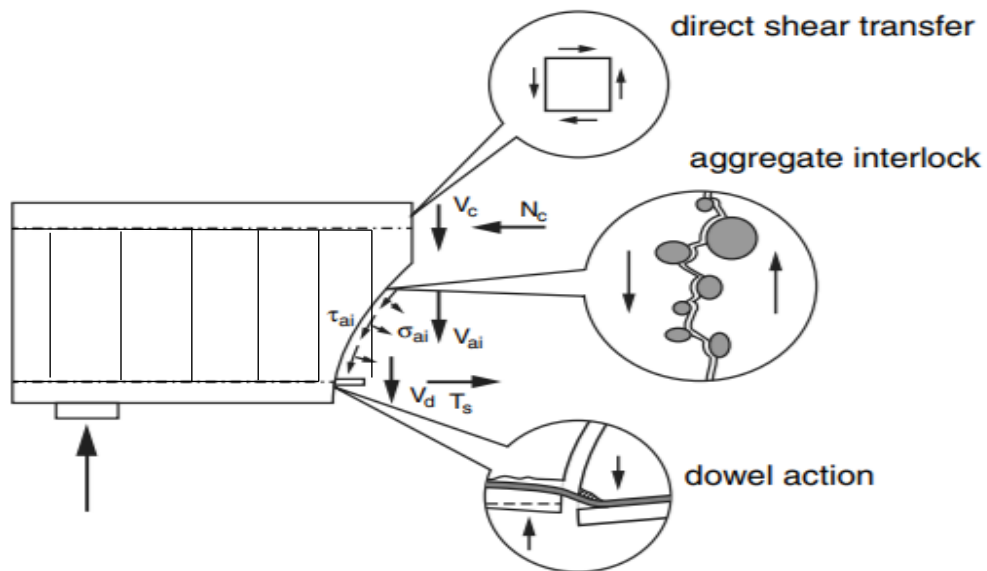


Figure 4.64: Various shear transfer mechanisms (Adapted from Yang et al. [62])

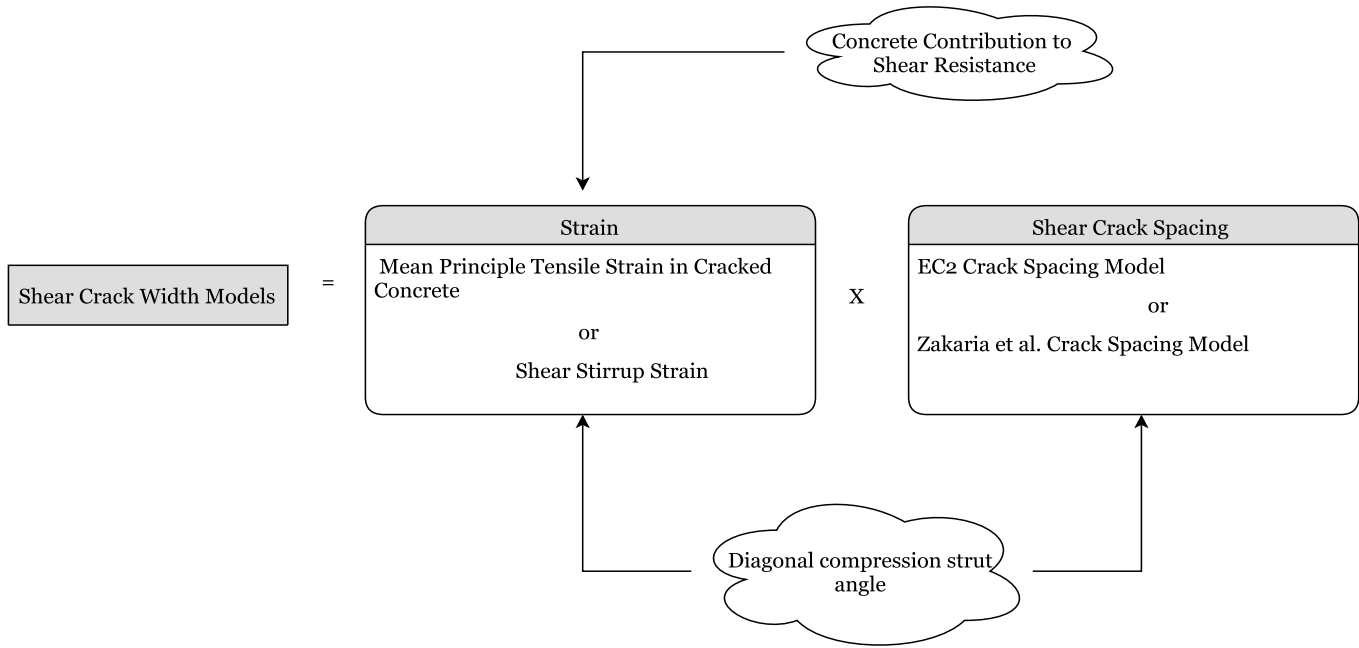


Figure 4.65: Basic approach behind the proposed models for average shear crack width prediction

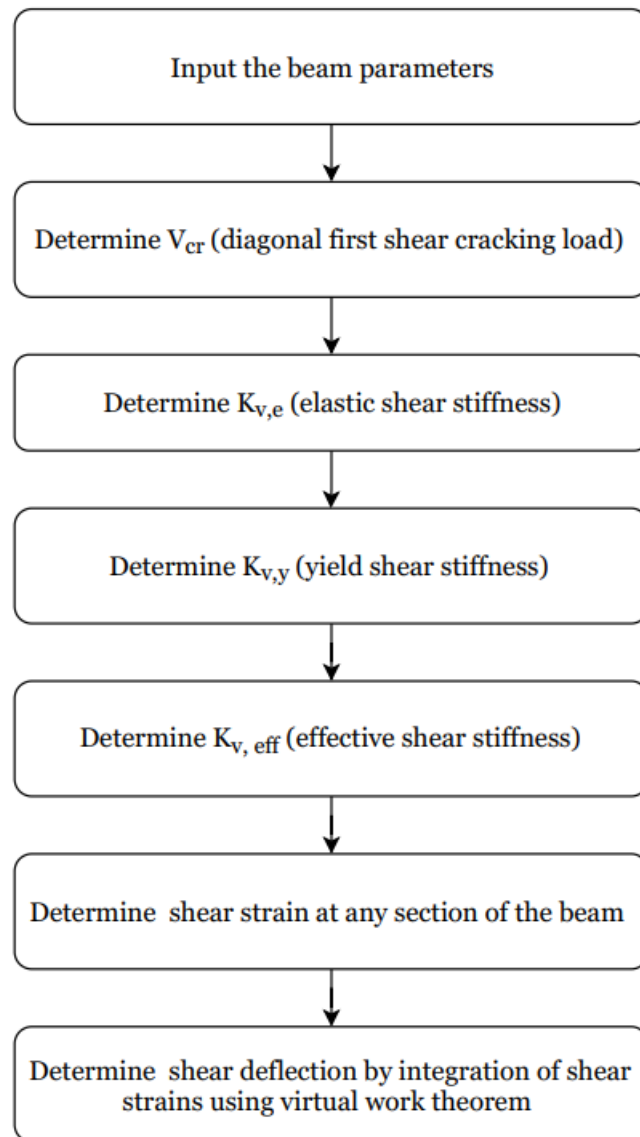


Figure 4.66: Flowchart showing general calculation methodology of the proposed models for shear deflection.

4.6. Conclusion

In this Chapter, five different models for mean shear crack width and four different models for shear deflection in slender reinforced concrete beams are proposed and evaluated. It must be noted that the performance of these models is assessed in comparison to a limited data available from the experiments. Therefore, the following inferences are applicable to the studied specimens and their validity as generic conclusions needs to be established using a detailed experimental study covering wide range of parameters.

1. Model-I (A and B) (adapted EC2 model), Model-II (A and B) (adapted Zakaria et al. model) and Model-IIIA (expressing diagonal shear crack width as the product of principle tensile strain and shear crack spacing) give unconservative predictions of the

shear crack width. One of the possible reasons is identified as the difference in the estimated and actual shear stirrup strain. It is found that the assumption of equal strain in all the stirrups may not be conservative from shear crack width calculation point of view. Another reason for the unconservative predictions may be the fact that the diagonal compression strut angle models used for prediction of mean shear crack angle may have resulted in flatter predictions for the shear crack angles as seen in subsection 3.2.2.

2. All the B variants of the Models (IB, IIB and IIIB) based on the assumption of no direct contribution of concrete to shear resistance give relatively conservative and consistent predictions for the mean shear crack width. This indicates that the prediction of concrete contribution to shear resistance using the proposed methodology has significant scatter.
3. All models except Model-IA give conservative predictions for the mean shear crack width when the mean shear crack angle is assumed as 45 degrees. It is also seen that this assumption leads to significant reductions in the SD in the predictions of Models-IIIA, IIIB and IV.
4. Shear crack width Models III-A, III-B, IV and V show relatively small number of unconservative predictions as well as lower SD as compared to Models-IA, IB, IIA and IIB. This implies that mean principle tensile strain in cracked concrete may be a more accurate parameter than shear stirrup strain to calculate mean shear crack width.
5. Although, the mean prediction ratio from shear crack width Model-IIB and Model-IIIA have a mean value equal to 1.08 (close to 1.0), yet a significant number of estimates (out of the total number of estimates) are unconservative. Thus, unless certain modification is introduced in these models, their usage is susceptible to give unconservative estimates.
6. Model-IV seems to perform well both in its original formulation as well as with the assumption of mean shear crack angle equal to 45 degrees. This also indicates that SMCFT seems to be better than other approaches in predicting the concrete contribution to shear resistance and mean shear crack angle at service loads. Another model that seems to give relatively better predictions is Model-V which is based on the assumption of zero concrete tensile strength post shear cracking. Both Model-IV and Model-V use the shear crack spacing predictions from Zakaria et al. shear crack spacing model indicating that this model seems to give conservative yet relatively accurate estimations of the mean shear crack spacing under service loads. Model-IIIB which is based on the assumption of zero concrete contribution to shear resistance and also comprising mean shear crack spacing from Zakaria et al. model in its formulation follows Model-IV and Model-V in terms of accuracy and consistency of predictions as indicated by the mean, SD and COV values. All the three (Model-IIIB, IV and V) express crack width as the product of mean principle tensile strain in cracked concrete and the diagonal shear crack spacing. This supports the inference that mean principle tensile strain in cracked concrete is a relatively better parameter

than stirrup strain while calculating mean shear crack width.

7. It is found that only Model-I out of all the four models for shear displacement prediction gives conservative estimates for shear deflection. Thus, it indicates that only this model is able to capture the degradation in the shear stiffness post- diagonal cracking.

5

Conclusions and Recommendations

“The important thing is to not stop questioning. Curiosity has its own reason for existing.”

Albert Einstein

This Chapter comprises the conclusions drawn after the analysis of results of the available and proposed models for mean shear crack width and shear deflection. A set of recommendations are made for future explorations to develop robust shear crack width and shear deflection prediction models.

THIS Chapter presents the conclusions of contributions made with this MSc thesis work and presents a list of recommendations for future research.

5.1. Conclusions

In this MSc thesis project various approaches to predict shear crack width and shear deflection are assessed. The performance of the developed approaches is evaluated by comparison with a limited dataset available in the literature. It may be noted here that the inferences are drawn based on the observations of analysis using this limited dataset. Therefore, the following conclusions need to be further validated using a detailed experimental studies covering wide range of parameters before being accepted for slender reinforced concrete beams in general.

1. An engineering model is proposed to predict the concrete contribution to shear resistance corresponding to the service loads. This model assumes that the first diagonal shear cracking load can be estimated conservatively by considering it as equal to the concrete contribution to shear resistance at the instance of shear stirrup yielding. This assumption is supported by results from previous experiments [31]. The first diagonal shear cracking load (the resistance until first diagonal cracking is assumed to be the concrete resistance only) is assumed to decay linearly to zero at instance of shear stirrup yielding. Thus, concrete contribution to shear resistance corresponding to service loads can be made by linear interpolation. This model can be used in practice in absence of a more reliable and accurate model.
2. There can be large differences in the experimentally observed stirrup strain and the calculated stirrup strain based on an assumption of equal strains in all stirrups. The experimental strain in some stirrups can be greater than the others and the absolute value of strain in such stirrups can be greater than that calculated using the assumption of equal strain in all the stirrups. This assumption may lead to unconservative predictions of the stirrup strain values at service loads.
3. The mean principle tensile strain in the cracked concrete is a more accurate strain parameter than the shear stirrup strain from the shear crack width calculation point of view. This is also in compliance with the background of SMCFT [7] and CFT [16].
4. The models (Models-IIIB, IV and V) are proposed in this MSc thesis to predict the mean shear crack width. The models express shear crack width as a product of mean principle tensile strain in cracked concrete and the shear crack spacing. In the absence of a more reliable and accurate model, these models can be used to estimate mean shear crack width for slender reinforced concrete beams ($a/d > 2.5$). Model IIIB assumes no direct contribution of concrete to shear resistance. Model-IV is based on SMCFT and determines concrete contribution to shear resistance from SMCFT. Model-V assumes that concrete cannot take any tensile stress post diagonal shear cracking and the compressive stress and shear stress in concrete are in equilibrium with the reinforcement stresses.
5. The assumption of mean shear crack angle equal to 45 degrees leads to conservative mean shear crack width predictions.

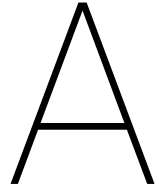
6. The assumption of zero concrete contribution to shear resistance leads to relatively conservative predictions of mean shear crack width from the models and seems to reduce the SD in the predictions of mean shear crack width.
7. The variation of shear stiffness degradation post-diagonal shear cracking can be conservatively predicted by assuming a linear tangent shear stiffness between the instance of first diagonal cracking and shear stirrup yielding. In other words, the shear stiffness degradation behaviour can be modelled by assuming that shear-force strain behaviour of a cracked reinforced concrete beam is a straight line between the instance of first diagonal cracking and shear stirrup yielding. In the absence of a more reliable and efficient method to predict the shear deflection, the proposed Model-I (Linear Tangent Stiffness Model) can be used. It must however be noted that while the mean of the predictions is 0.85 and a high SD of 0.31 is obtained. Moreover, the wider application of the model in design practice requires validation with an experimental study.

5.2. Future Recommendations

During the course of this MSc thesis, a number of following aspects are highlighted which can serve as recommendations for the future work.

1. In this thesis, it is assumed that the concrete contribution to the shear resistance decreases linearly from first diagonal cracking to zero at the stirrup yielding. It can be interesting to study the actual variation of this contribution for a range of beam specimen parameters.
2. It is found that the shear crack angle is not constant throughout the shear span of the beam ([41], [60]). In this thesis, an assumption of a constant value of the shear crack angle is made. It may be interesting to study the variation of the shear crack angle in the shear span to develop a more refined model for shear crack width and shear deflection prediction.
3. The scope of this MSc thesis project is limited to the development of shear crack width and shear deflection models under static loads. However, that the effect of dynamic loads, creep and relaxation may enhance the shear crack width and shear deflection in RC members. Therefore, modification of the proposed models or development of new models considering these load effects can be an interesting study.
4. It is found that the current EC2 model does not provide an estimate for the crack width outside the hidden tensile member. This may lead to significant deviation in the predictions in case of deep beams. A study with regards to the influence of depth of reinforced concrete beam on the diagonal crack width may be an interesting research to address this issue.

Appendices



Appendix A

This Appendix includes the review of the shear crack width and shear deflection models performed by Zakaria et al. [65]. The original table in the publication is reproduced here and for more details reader is recommended to refer the publications referred in the paper [65].

A.1. Crack Width Models-Review

Models	Proposed Equations	Definition of Parameters
CEP-FIP model 1978 ¹⁷⁾	$w_k = 1.7k_w w_{avg}; \quad w_{avg} = s_{rm} \varepsilon_w$ $s_{rm} = 2 \left(c_s + \frac{s_y}{10} \right) + k_1 k_2 \frac{d_{by}}{\rho_y}$	w_k is the characteristic shear crack width; w_{avg} is the average shear crack width; k_w denotes a correction coefficient to take account of the effect of the slope of the stirrups on the spacing of the cracks [$k_w = 1.2$ for vertical stirrups ($\alpha = 90^\circ$), $k_w = 0.8$ for inclined stirrups ($\alpha = 45^\circ - 60^\circ$)]; α is the angle between shear reinforcement and longitudinal axis of the member; ε_w is the shear reinforcement strain; s_{rm} is the average crack spacing as discussed in CEB-FIP Model Code 1978 ^{17), 21)} .
CEP-FIP model 1990 ¹⁸⁾	$w_k = l_{s,max} \varepsilon_w; \quad w_{avg} = s_{m\theta} \varepsilon_w$ $l_{s,max} = \frac{1}{\frac{\sin \theta}{l_{sx,max}} + \frac{\cos \theta}{l_{sy,max}}}$	w_k is the characteristic shear crack width; w_{avg} is the average shear crack width; $l_{s,max}$ is the maximum shear crack spacing; $s_{m\theta}$ is the average shear crack spacing; ε_w is the shear reinforcement strain; $l_{sx,max}$ is the maximum vertical crack spacing; $l_{sy,max}$ is the maximum horizontal crack spacing; definitions of $s_{m\theta}$, $l_{sx,max}$ and $l_{sy,max}$ are given in CEB-FIP Model Code 1990 ^{18), 21)} .
Hassan et al. model ²⁰⁾	$w_{avg} = \frac{d_{by} k_1 k_2 S}{1000 k_{fc} k_p}$ $k_p = \left(\frac{\rho_w}{0.004} \right)^{1.3} \quad k_{fc} = \left(\frac{f_c}{19.6} \right)^{2/3}$	w_{avg} is the average shear crack width; d_{by} is the shear reinforcement diameter; k_p is a coefficient that takes into account the effect of shear reinforcement ratio (ρ_w); k_{fc} is a coefficient that takes into account the effect of compressive strength of concrete (f_c); ε_w is the shear reinforcement strain; S is the modified slip, and $k_1 = 2.4$, $S = 4 \times 10^3 \varepsilon_w + 20 \times 10^6 (\varepsilon_w)^2$ for plain bar $k_1 = 2.0$, $S = 8 \times 10^3 \varepsilon_w + 2 \times 10^6 (\varepsilon_w)^2$ for deformed bar $k_2 = 1.2$ for vertical stirrup, $k_2 = 1.0$ for inclined stirrup
Fukuyama et al. model ¹³⁾	$w_{avg} = 0.9 d_e \frac{\varepsilon_w}{\sqrt{2}}$	w_{avg} is the average shear crack width; d_e is the effective depth of the beam section; ε_w is the shear reinforcement strain.

Figure A.1: Overview of the available crack width models [65]

Piyamahant model ¹⁴⁾	$w_{avg} = \frac{2d_{by}S}{(f_c'/20)^{2/3}}$ $S = \varepsilon_w(6 + 3500\varepsilon_w)$	w_{avg} is the average shear crack width; d_{by} is the shear reinforcement diameter; S is the normalized slip; f_c' is the compressive strength of concrete; ε_w is the shear reinforcement strain.
Shinomiya and Watanabe model ¹⁵⁾	$w_{avg} = l_{av}\varepsilon_w$ $l_{av} = 2\left(\frac{c_s + c_a}{2} + \frac{s}{10}\right) + 0.1\frac{d_{by}}{\rho_y}$	w_{avg} is the average shear crack width; l_{av} is the average crack spacing; c_s is the side concrete cover to the shear reinforcement; $c_a = (s_y - d_{by})/2$; s_y is the shear reinforcement spacing; d_{by} is the diameter of shear reinforcement; s is the distance between stirrup legs ($s = b_w - 2c_s - d_{by}$); ρ_y is the ratio of the amount of transverse reinforcement to the effective concrete area ($\rho_y = A_w/[(2c_a + d_{by})b_w]$); b_w is the beam width; ε_w is the shear reinforcement strain.
Witchukreangkrai et al. model ⁹⁾	$w_{avg} = 0.75k_w k_p s_{m\theta} \varepsilon_w$ $k_w = \left(\frac{0.004}{\rho_w}\right)^{2/3} \quad k_p = \left(\frac{1}{1 + \sigma_{c,ps}/f_c'}\right)$	w_{avg} is the average shear crack width; k_w is a coefficient that takes into account the effect of shear reinforcement ratio (ρ_w); k_p is a coefficient takes into account the effect of compressive stress at centroid of concrete section due to prestress ($\sigma_{c,ps}$); f_c' is the compressive strength of concrete; ε_w is the shear reinforcement strain; $s_{m\theta}$ is the average shear crack spacing which can be calculated as given in the previous work ^{9), 21)} .
De Silva et al. model ¹⁰⁾	$w_{avg} = k_w s_{m\theta} \varepsilon_w$ $s_{m\theta} = \frac{1}{\frac{\sin \theta}{s_{mx}} + \frac{\cos \theta}{s_{my}}}$	w_{avg} is the average shear crack width; k_w is a coefficient that represents the effect of the shear reinforcement angle [$k_w = 1.2$ for vertical stirrups ($\alpha = 90^\circ$), $k_w = 0.8$ for inclined stirrups ($\alpha = 45^\circ - 60^\circ$)]; α is the angle between shear reinforcement and longitudinal axis of the member; ε_w is the shear reinforcement strain; $s_{m\theta}$ is the average shear crack spacing as given in the previous studies ^{10), 21)} .

Figure A.2: Overview of the available crack width models [65]

B

Appendix B

This Appendix includes a brief description about the different types of shear failure modes observed in reinforced concrete beams. This is followed by a description about the background of the MCFT. Thereafter, a more elaborate discussion on the background of one of the concrete contribution to shear resistance models is presented.

B.1. Types of Shear Failure

1. Flexural Shear Failure

In this failure mode (shown in Figure B.1) a flexural crack initiates normal to the longitudinal reinforcement in the tensile zone at the outermost fiber (the outermost fiber is exposed to maximum normal stress and zero shear stress). As the applied load increases the crack propagates upwards and is exposed to increasing shear stress besides a normal stress. Thus the principle stress acting on the crack cause a rotation of the crack. The failure is characterized by the excessive crack opening.

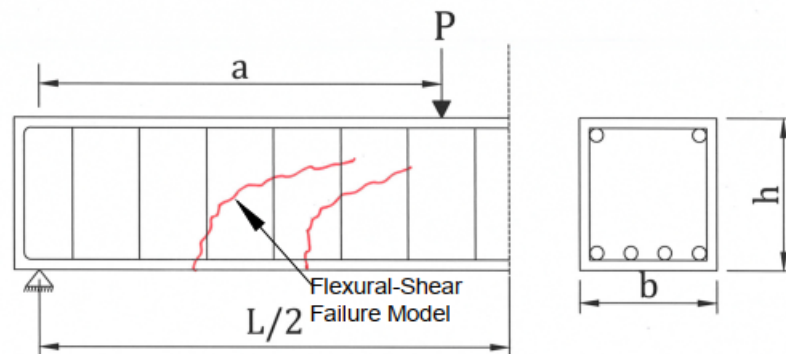


Figure B.1: Flexural Shear Failure Mode

2. Shear Tension Failure

This type of failure is characterized by the cracking of the beam web due to high principle tensile stress (shown in Figure B.2). This mode of failure is commonly observed in pre-stressed beams with thin webs (for example hollow core slabs). The thin

web exposed to high principle tensile stresses crack opens due to a bi-axial tension-compression state. Such a failure is brittle in nature and dangerous because of the absence of warning before failure. The D (Disturbed) regions of the beam close to the support are vulnerable to this type of failure mode.

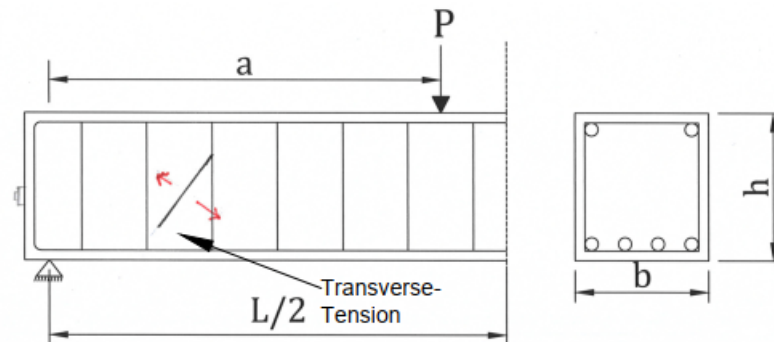


Figure B.2: Shear Tension Failure Mode

3. Web crushing Failure

This type of failure (shown in Figure B.3) occurs when the compressive strength of the web is exceeded before the yielding of shear stirrups (this failure mode is commonly observed in over-shear reinforced beams). This is a typical failure mode in the vicinity of the applied load near the top flange of a I beam. The crack is initiated in the web and then proceed bi-directionally towards the support as well as the loading point.

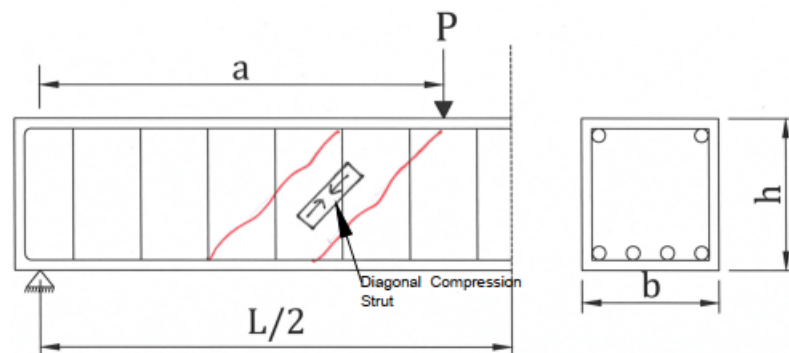


Figure B.3: Web Crushing Failure Mode

4. Shear Stirrup Yielding Failure

This failure mode is characterized by the yielding of shear stirrups (shown in Figure B.4). This is a ductile failure mode and therefore, a warning is visible before the ultimate failure of the reinforced concrete beam. Such a failure mode has a large number of smeared cracks distributed throughout the shear span of the beam.

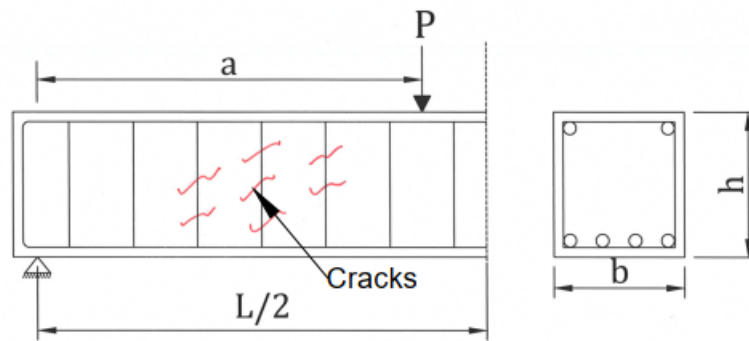


Figure B.4: Shear Stirrup Yielding Failure Mode

MCFT [57]

This theory is based on the assumption that response of a cracked concrete element under the application of in plane stresses (shear force, axial force and bending moment) can be represented with a series of parallel smeared cracks. The crack angle is expressed in terms of the longitudinal strain and therefore, the crack rotates with the change in the external load. According to this theory, concrete can be subjected to the compression and shear stresses but no tensile stresses are allowed at the crack surface. However, concrete in between the cracks can take tensile stresses.

The cracked concrete is treated separately as a new material with its own constitutive model. The model evaluates the shear resistance of the concrete element by simultaneous solution for the equilibrium, compatibility and constitutive relationships in terms of mean stress and strains. The mean stress and strains are the mean values for the cracked concrete and concrete in between the cracks. The principle stress and strains are assumed to be co-axial though experimentally it is found that these can be inclined to each other at an angle of up to 10° in case of members with orthogonal reinforcement. The model expresses the mean crack width as a product of mean principle tensile strain and crack spacing.

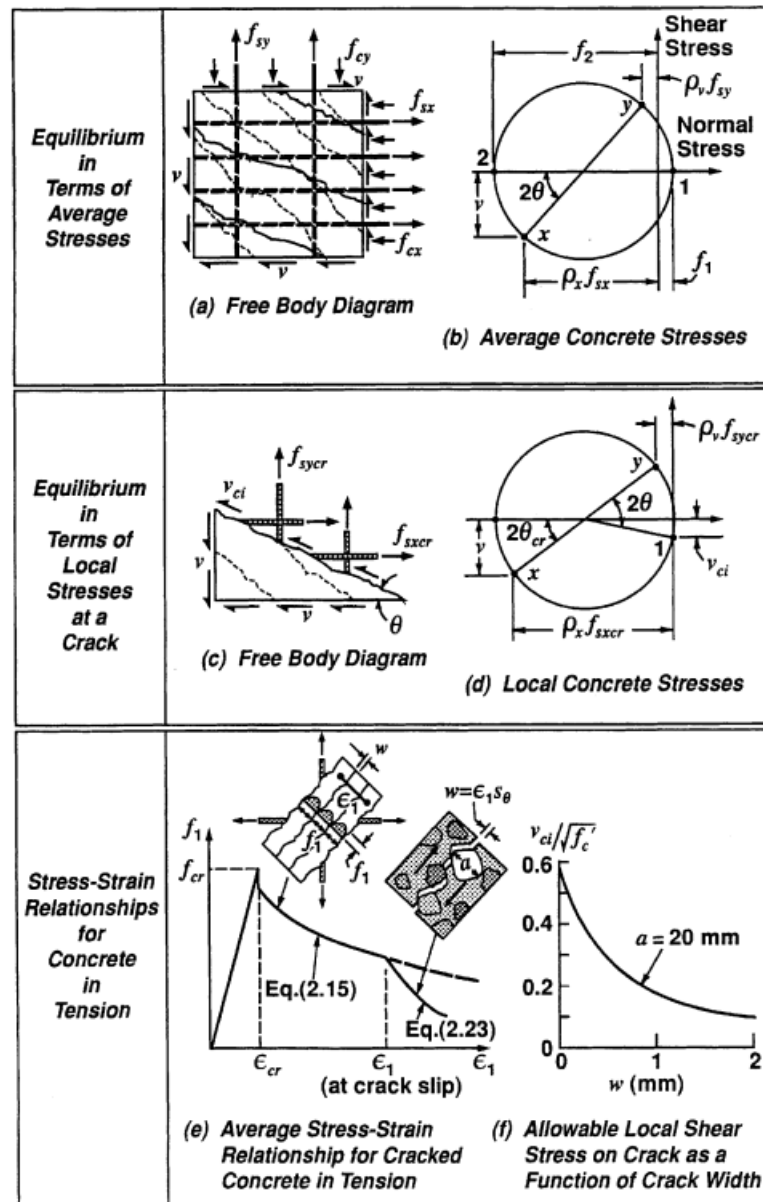


Figure B.5: Various relations of the MCFT [4]

B.2. Zararis (2003) Model for Concrete Contribution to Shear Resistance

B.2.1. Shear-Unreinforced Beams

THE Zararis and Papadakis [68] model for a shear unreinforced beam is based on the premise that the failure in shear unreinforced beams occur due to formation of critical diagonal crack in slender reinforced concrete beam. The critical diagonal crack has two branches. The first branch is an inclined shear crack which is formed in the vicinity of the flexural cracks and is often formed in between the flexural cracks. It is the second branch of the critical diagonal crack (which initiates at the tip of the first branch) which is responsible for the failure of the beam. Conventionally, this type of failure in slender beams is named

“diagonal tension failure” [68]. The model is originally proposed for the beams with slenderness ratio greater than 2.5.

It is assumed that the crack opening of the first branch is perpendicular to its direction. Due to this assumption, there are no aggregate interlock forces acting on this crack branch surface. The only forces considered to act on this branch of crack are dowel forces and axial tension force in the longitudinal reinforcement as shown in Figure B.6 below.

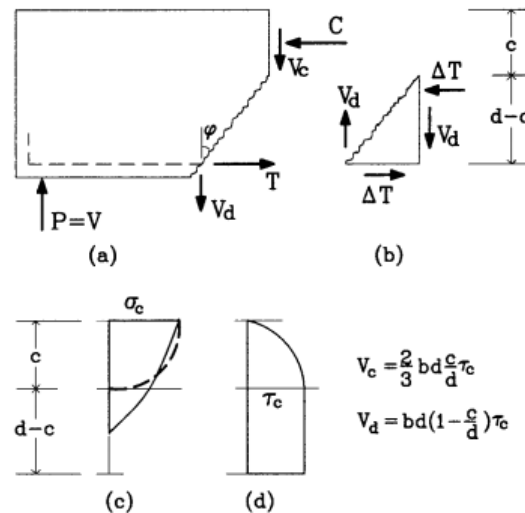


Figure B.6: (a); Free body diagram with the first branch of the diagonal crack (b) Free body diagram of the triangular concrete element below the first branch of the diagonal crack (c) Distribution of normal compressive stress along the beam depth (d) Distribution of the shear stress along the beam depth [68].

where

σ_c	normal stress in the concrete compression zone
c	depth of compression zone above the tip of first branch of diagonal crack
d	effective depth of the longitudinal reinforcement
τ	shear stress in the compression zone
ΔT	compressive force in the triangular element below the tip of the first branch of the diagonal crack due to transfer of compressive stresses from the top fibre to the area below the crack tip
C	Normal force in the compression zone
T	axial force in the longitudinal reinforcement
V_d	the shear force carried by the longitudinal reinforcement
ϕ	angle of the crack from the vertical
b	width of the beam cross section

The authors report that the calculated depth of the compression zone above the inclined shear crack is the same as that above the flexural crack and the same fact is reflected in the observation of the cracked specimens. It is assumed that the neighboring inclined cracks are parallel to each other. The Figure B.6 1(c) and 1(d) shows the considered normal and shear stress distribution respectively. It is shown using the condition for mechanical equilibrium of the portion of beam between the first inclined crack and the loading point that the resultant forces generate splitting stresses across the line of action of resultant compressive force (resultant of applied load and compressive force in the concrete compression

zone) as shown in Figure B.7. Based on the theorem of elasticity and an assumed possible arrangement of the forces (in the portion between the first shear crack branch and the loading point) the stress distribution along the second branch of diagonal crack is obtained as shown in Figure B.8.

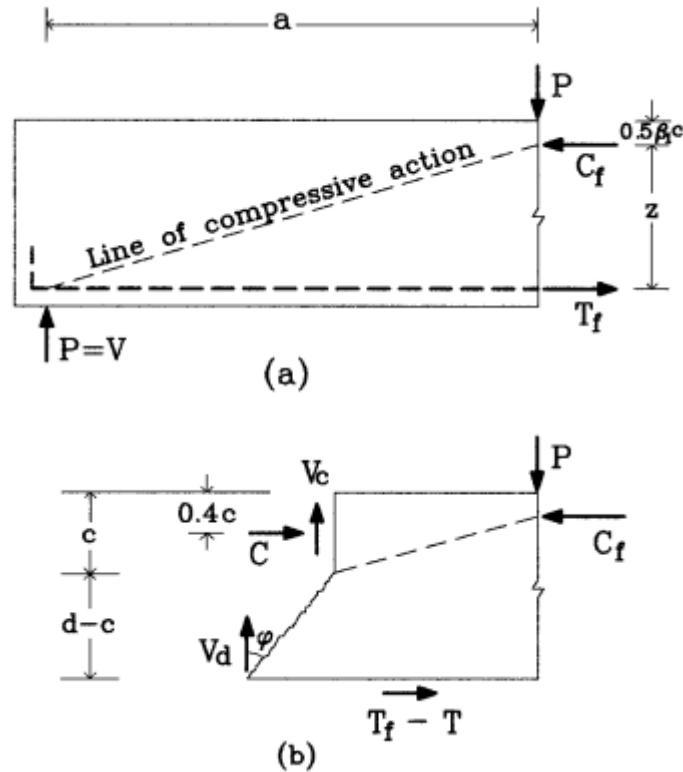


Figure B.7: (a) Line of Action of the resultant compressive force (b) Portion of the beam containing the dashed line along which diagonal splitting occurs [68].

where

P Applied external concentrated load

C_f Normal concrete force in the region of pure flexure

T_f Force in the longitudinal reinforcement in the region of pure flexure

z internal lever arm between the compression and tension forces in the region of pure flexure

β factor to convert compression zone depth to an to the depth with rectangular stress block

a shear span

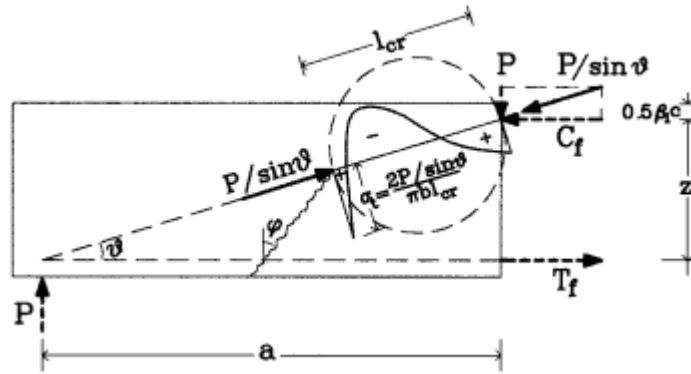


Figure B.8: Normal stresses along the second branch of diagonal crack [68]

where

l_{cr} length of second branch of critical diagonal shear crack The ultimate shear stress (including the size effect) at which the normal tensile stress is found to exceed the split tensile strength is found using Equation B.1

$$v_u = \frac{V_u}{bd} = \left(1.2 - 0.2 \frac{a}{d}\right) \frac{c}{d} f_{ct} \tag{B.1}$$

where

$$\left(1.2 - 0.2 \frac{a}{d}\right) \geq 0.65 \tag{B.2}$$

B.2.2. Beams Reinforced with Stirrups:

Zararis [67] find that the crack pattern for the shear failure of the shear reinforced and shear unreinforced beams are found to be similar. According to the model, the opening of the second branch of the diagonal crack causes an increase of the shear force in the longitudinal reinforcement. The shear force in the above model for shear unreinforced beams is the shear at the initiation of the cracking of the second branch of diagonal cracking. However, it is shown that after the first branch of diagonal cracking, stirrups also come into the picture and begin to take load which causes a slight increase in the shear force of the longitudinal reinforcement. Therefore, the ultimate shear failure load for a shear unreinforced beam is equal to the shear resistance at the beginning of the opening of the second branch of diagonal crack, the contribution from the stirrups and an additional contribution from the change in the shear force of longitudinal reinforcement. The ultimate shear resistance is therefore expressed using Equation B.3.

$$V_u = V_{cr} + V_s + \Delta V_d \tag{B.3}$$

Based on an approximation of the transfer length l_t shown in Figure B.10 equal to $0.5 \cdot d$ and the condition of force equilibrium, the following expression for the additional shear force in the longitudinal reinforcement is obtained using Equation B.4.

$$\Delta V_d = 0.5 \rho_v f_{vy} b d \tag{B.4}$$

A detailed derivation of the intermediate variables in the model can be found elsewhere ([68], [67]). Figure B.9 shows the the free body diagram of the segment of the beam above

the critical diagonal crack, where

C_u normal force in the concrete compression zone

V_s shear force in the stirrups

V_{dcr} shear force in the longitudinal reinforcement

P_u Applied external load

T_u axial force in the longitudinal reinforcement

V_{ccr} Shear force in the second branch of the critical diagonal crack after stirrups are activated

ΔV_d increment of the shear force in the longitudinal reinforcement

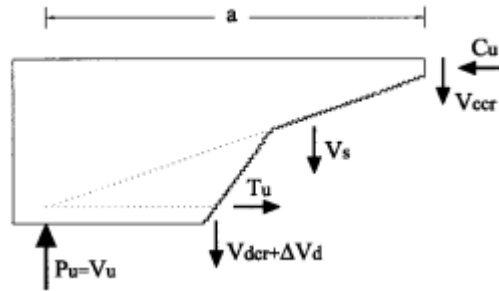


Figure B.9: The free body diagram of the segment of the beam above the critical diagonal crack[67]

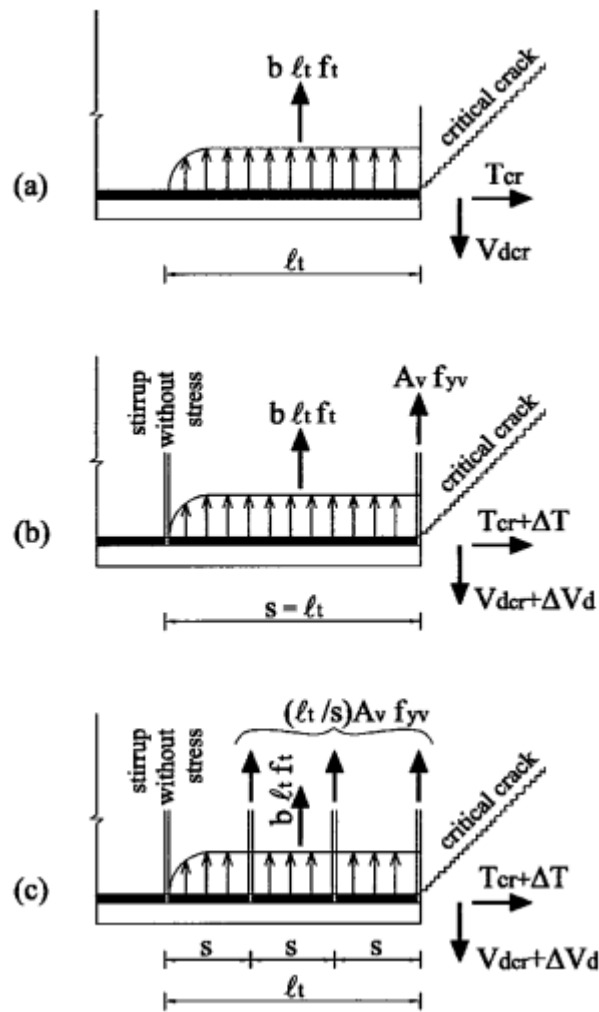


Figure B.10: Forces in the longitudinal reinforcement cover region susceptible to horizontal splitting as the second branch of the diagonal crack opens (a) no stirrups (b) stirrup spacing = transfer length for stresses from longitudinal reinforcement to concrete (c) stirrup spacing less than " l_t " [67]

C

Appendix C

This Appendix presents the observations regarding the nominal shear resistance calculated using the EC2 nominal shear resistance for shear unreinforced beams compared with the experimental values.

C.1. Nominal Shear Capacity from EC2 VSIM Model

Table C.1: Nominal shear capacity as calculated from EC2 VSIM (Variable Strut Inclination Method) and experimental observations.

Publication	Specimen	$\rho_w f_{ym}$	V_{exp}	$V_{EC2,nom}$	$V_{exp}/V_{EC2,nom}$
Hu et al. [31]	D10	1.8122	218.1	275.2279	0.792434
	R10	1.8166	236.9	275.8961	0.858657
Munikrishna et al. [44]	G1-C60	0.45507	560.473	421.1726	1.330744
	G1-M80	0.49644	569.369	442.176	1.287652
	G1-M100	0.48265	573.817	425.1692	1.34962
	G2-C60	0.45507	560.473	421.1726	1.330744
	G2-M80	0.49644	569.369	442.176	1.287652
	G2-M100	0.48265	573.817	425.1692	1.34962
	G3-C60	1.28247	609.403	943.2981	0.646034
	G3-M80	1.379	649.437	1029.052	0.631102
	G3-M100	1.379	653.885	1010.676	0.646978
Lee et al. [38]	B34-2	2.41816	403.16	743.8676	0.541978
	B34-3	3.4752	679.5	877.0823	0.774728
	B34-4	4.82908	714.25	984.876	0.725218
	B34-5	2.8944	674.3	816.1858	0.82616
	B34-6	3.02151	575	830.4211	0.69242
	B42-2	2.41816	665.15	743.8676	0.894178
	B42-3	3.4752	801.25	982.3184	0.815672
	B42-4	4.82908	800.55	1114.401	0.718368
	B42-5	2.8944	691.4	890.3672	0.776534

	B42-6	3.02151	673.3	927.2161	0.726152
	B68-2	2.41816	800.95	743.8676	1.076737
	B68-3	3.4752	870.55	1069.031	0.814336
	B68-4	4.82908	914.7	1386.58	0.659681
	B68-5	2.8944	798.35	890.3672	0.896653
	B68-6	3.02151	701.9	929.4684	0.755163
Lee et al. [36]	S20-1	1.4532	374.1	245.2275	1.525522
	S20-2	1.6659	401.7	281.1206	1.428924
	S20-3	1.9023	441.7	321.0131	1.375956
	S20-4	2.2503	502.5	346.7907	1.449001
	S30-3	0.87	600.2	305.37	1.965484
	S30-4	0.87	620.8	305.37	2.032944
	S30-5	1.74	893.1	610.74	1.462324
	S30-6	1.74	893.7	610.74	1.463307
	S35-1	1.4532	451.6	245.2275	1.841555
	S35-2	1.6659	489.3	281.1206	1.740534
	S35-3	1.9023	516	321.0131	1.607411
	S35-4	2.2503	507	379.7381	1.335131
	S40-2	1.894	795.8	471.1088	1.689206
	S40-3	2.422	1073.9	602.4422	1.782578
	S40-4	2.7765	1133.4	690.6197	1.641135
	S40-5	3.1705	1183.4	730.0351	1.621018
	S40-6	3.7505	981.1	780.3292	1.25729
	S50-2	1.894	1174.4	471.1088	2.492842
	S50-3	2.422	1281.7	602.4422	2.127507
	S50-4	2.7765	1313.5	690.6197	1.901915
	S50-5	3.1705	1420.2	788.6222	1.800862
	S50-6	3.7505	1517.3	889.755	1.705301
	S80-2	1.894	1336.3	471.1088	2.8365
	S80-3	2.422	1444.9	602.4422	2.398404
	S80-4	2.7765	1566.5	690.6197	2.268253
	S80-5	3.1705	1674.8	788.6222	2.123704
	S80-6	3.7505	1736.8	932.89	1.861741
Zakaria et al. [66]	A1 left	2.664	285.4	192.9002	1.479522
	A1 right	2.664	285.4	192.9002	1.479522
	A2 left	2.664	470.2	337.5754	1.392874
	A2 right	2.664	470.2	337.5754	1.392874
	A3 left	2.664	720	520.8306	1.382407
	A3 right	2.664	720	520.8306	1.382407
	A4 left	2.664	1196.5	806.5641	1.483453
	A4 right	2.664	1196.5	806.5641	1.483453
	B1 left	2.664	715	520.8306	1.372807
	B1 right	2.664	715	520.8306	1.372807
	B2 left	1.332	540.7	260.4153	2.076299
	B2 right	2.664	540.7	520.8306	1.038149

	B3 left	1.332	522.4	260.4153	2.006027
	B3 right	2.664	522.4	520.8306	1.003013
	C1	2.664	551.4	542.5319	1.016346
	C2	2.664	600.8	514.8025	1.167049
	C3	2.664	760.3	502.7463	1.512294
Piyamhant []	0.035-S	0.1225	187.5	39.47295	4.750088
	0.035-N	0.1225	187.5	39.47295	4.750088
	0.05-S	0.168	190.8	54.65485	3.490999
	0.05-N	0.168	190.8	54.65485	3.490999
	0.065-S	0.2205	187.8	71.05131	2.64316
	0.065-N	0.2205	187.8	71.05131	2.64316
	0.08-S	0.2765	226.6	88.81413	2.551396
	0.08-N	0.2765	226.6	88.81413	2.551396
T.K.Hassan [26]	B0	1.57	370.5	353.25	1.048832
	B2	2.51	570	482.9043	1.180358
	B3	3.14	608	525.0758	1.157928
	B5	2.51	456	482.9043	0.944286
	B6	3.14	484.5	525.0758	0.922724
	B8	2.51	391.88	482.9043	0.811507
	B9	3.14	427.5	706.5	0.605096
	B10	2.51	566	564.75	1.002213
	B11	3.14	618	706.5	0.874735

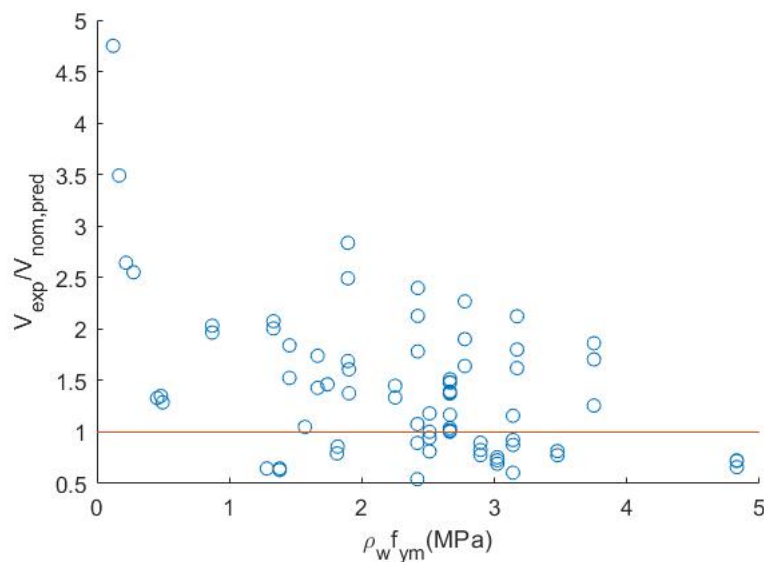


Figure C.1: Prediction of total shear resistance from EC2-VSIM versus experimental observations.

It is reported in the literature that the current EC2-VSIM model give very conservative results at low values of shear reinforcement percentage [1-6]. This model is based on the lower bound Theorem of Plasticity and considers the shear strength resistance as solely the contribution from stirrups without any contribution of concrete. The shear resistance is

given in Equation C.1

$$V_{Rm,s} = \frac{A_{sw} z f_{ym} \cot \theta}{s} \quad (C.1)$$

where

A_{sw} the cross-section area of stirrups

z flexural lever-arm = $0.9d$

f_{ym} mean yield strength of the stirrups

θ diagonal compression strut angle

s spacing between the stirrups

resistance is limited by the capacity of the compression strut to prevent premature crushing of the concrete web in compression.

The shear

$$V_{Rd,max} = \frac{A_{sw}}{s} z f_{yw} \cot \theta \quad (C.2)$$

where

$$21.8^\circ \leq \theta \leq 45^\circ \quad (C.3)$$

The strut inclination angle is calculated assuming that the stirrups yield at the same instant as that of the concrete compression strut crushing.

$$\theta = \sin^{-1} \sqrt{\frac{A_{sw} f_{ym}}{b \alpha_{cw} s v_1 f_{cm}}} \quad (C.4)$$

where the lower limit of the angle is imposed to ensure that the crack width in serviceability limit state can be controlled as recommended by Thurlimann [7].

$$v = 0.6 \left(1 - \frac{f_{cm}}{250} \right) \quad (C.5)$$

The reduction factor accounting for long term effects on concrete is assigned a value of one in this report [8]. Olalusi [9] performs a parametric assessment of the prediction of shear strength using EC2 VSIM model and compared the values with the compilation of the experimental results database for slender shear reinforced RC beams by Reineck et al. [10]. It is found that the EC2-VSIM Model fails to capture the trend of shear strength over the range of parameters and is more conservative than Compression Chord Capacity and MCFT (R2k) predictions which capture the trend better. The shear span ratio of the beams in the database is >2.40 and only the beams that fail in shear compression or the diagonal tension mode are considered (thus removing the beams that failed in flexure mode from the database. The $V_{exp}/V_{EC2,nom}$ is found to be in some cases as high as 3.2 for $\rho_w f_{ym} \leq 1$. While for $2 \leq \rho_w f_{ym} \leq 4$, the same ratio went < 1 indicating the inconsistency in the prediction of the shear strength by EC2 Model. Moreover, it is reported that the prediction of compression strut angle from the EC2-VSIM model are biased towards the smaller angle value limit in the range of theta recommended by EC2. However, MCFT gives the most consistent prediction of the compression strut angle. The Table C.1 lists the total shear resistance predictions for 87 beam specimens from the various experiments referred in this study. From Figure D.1, it is clear that the EC2 VSIM method give extremely conservative estimates of the shear strength of RC beams with $\rho_w f_{ym} \leq 1$. It can be observed from the

scatter plots that EC2 VSIM (Variable Strut Inclination Method) provides inconsistent predictions for the shear strength over the range of values of $\rho_w f_{ym}$.



Appendix D

This Appendix includes solved examples for the proposed mean shear crack width and shear deflection models in this MSc thesis. The examples intend to inform the reader about the sequence in which intermediate parameters should be calculated to calculate the mean shear crack width or shear deflection using the proposed models.

D.1. Shear Crack Width Calculation

This section comprises of the examples for the calculation of mean shear crack width using the proposed models in this MSc thesis. The mean shear crack width is calculated for the specimen named B334-120 from an experimental study [37]. The beam specimen input parameters required for the calculation are tabulated in Table D.1.

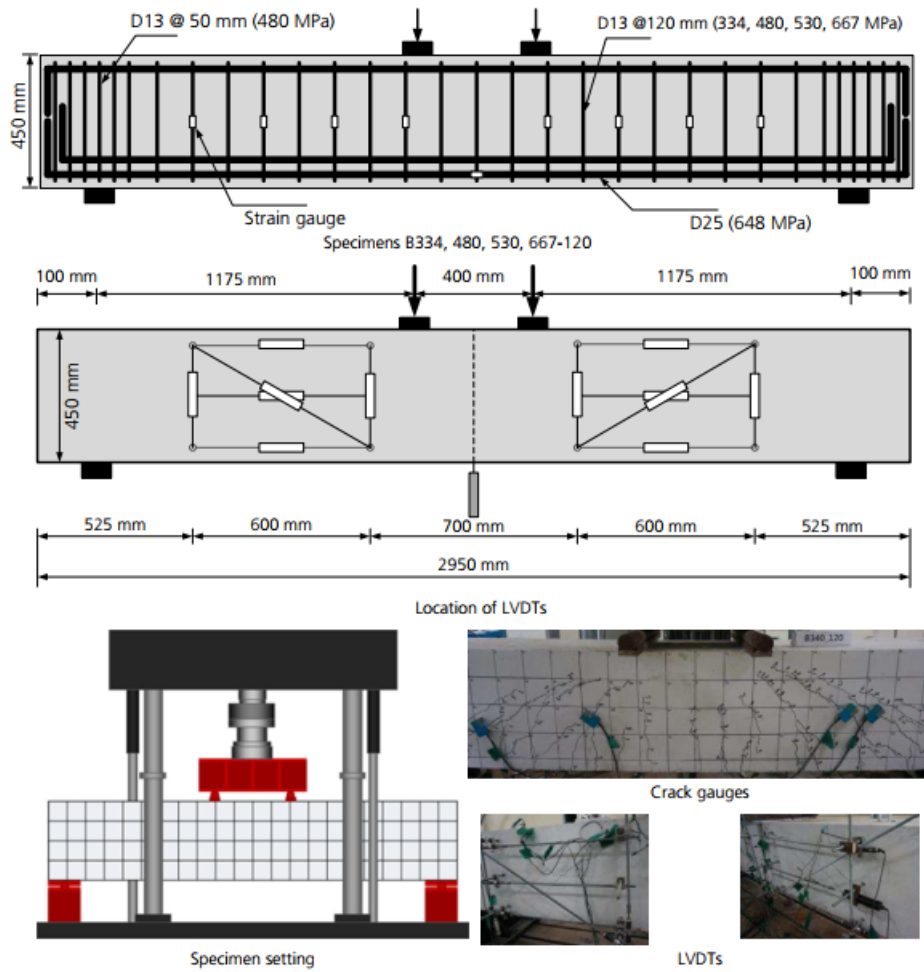


Figure D.1: Experimental setup for the shear crack width study [37]

Table D.1: Input parameters for the specimen B334-120 selected for mean shear crack width calculation from various models.

Parameter	Value
V_{max}	566.4 kN
b	350 mm
h	450 mm
d_v	352.5 mm
l	2.95m
s	120 mm
A_{sw}	253.26 mm ²
ρ_l	3.72%
ρ_w	0.603%
f_{cm}	50.1 MPa
f_{yk}	334 MPa
$E_{s,l}$	200000 MPa (Assumed)
$E_{s,w}$	200000 MPa (Assumed)
a/d	3.0

D.1.1. Model-IA

Table D.2: Calculation of the shear crack width according to the proposed model-IA

Parameter	Formula	Value
$f_{ct,eff}$	f_{ctm}	4.07 MPa
α_e	$\alpha_e = \frac{E_s}{E_c}$	5.6
$\rho_{p,eff}$	$\rho_{p,eff} = 0.5 \frac{A_{sw}}{A_{y,eff}}$	0.016
$V_{cr,CCC}$	$V_{cr,CCC} = V_{Rm,c} = 0.3\zeta \frac{x}{d} (f_{cm})^{\frac{2}{3}} b_{v,eff}$	232.028 kN
V_{nom}	$V_{Rd,s} = \frac{A_{sw} z f_{yd} \cot \theta}{s}$	621.2 kN
V_{ser}	$V_{ser} = 0.6 V_{nom}$	372.72 kN
$V_{c,pred,ser}$	$V_{c,pred,ser} = V_{cr,CCC} + \frac{(0 - V_{cr,CCC})}{V_{nom} - V_{cr,CCC}} (V_{ser} - V_{cr,CCC})$	148.147 kN

V_s	$V_s = V - V_c$	224.573 kN
σ_s	$\sigma_s = \frac{V_s}{E_s}$	188.181 MPa
$\epsilon_{sm} - \epsilon_{cm}$	$\epsilon_{sm} - \epsilon_{cm} = \frac{\sigma_s - k_t \frac{f_{ct,eff}}{\rho_{p,eff}} (1 + \alpha_e \rho_{p,eff})}{E_s} \geq 0.6 \frac{\sigma_s}{E_s}$	$0.565 \cdot 10^{-3}$
$s_{r,max,y}$	$s_{r,max} = k_3 c_s + k_1 k_2 k_4 \phi_w / \rho_{pw,eff}$	345.493 mm
$s_{r,max,z}$	$s_{r,max} = k_3 c_l + k_1 k_2 k_4 \phi_l / \rho_{pl,eff}$	138.051 mm
x	$x = 0.75d(\alpha_e \rho_l)^{\frac{1}{3}}$	184.128 mm
θ	$\cot \theta = \frac{0.85d_s}{d_s - x} \leq 2.50$	0.557
$s_{r,max}$	$s_{r,max} = \frac{1}{\frac{\cos \theta}{s_{r,max,y}} + \frac{\sin \theta}{s_{r,max,z}}}$	159.026 mm
$s_{r,avg}$	$s_{r,avg} = 0.75 s_{r,max}$	119.269 mm
w_{avg}	$w_{avg} = s_{r,avg}(\epsilon_{sm} - \epsilon_{cm})$	0.067 mm

D.1.2. Model-IB

Table D.3: Calculation of the shear crack width according to the proposed model-IB

Parameter	Formula	Value
$f_{ct,eff}$	f_{ctm}	4.07 MPa
α_e	$\alpha_e = \frac{E_s}{E_c}$	5.6
$\rho_{p,eff}$	$\rho_{p,eff} = 0.5 \frac{A_{sw}}{A_{y,eff}}$	0.016
$V_{cr,CCC}$	$V_{cr,CCC} = V_{Rm,c} = 0.3\zeta \frac{x}{d} (f_{cm})^{\frac{2}{3}} b_{v,eff}$	232.028 kN
V_{nom}	$V_{Rd,s} = \frac{A_{sw} z f_{yd} \cot \theta}{s}$	621.2 kN
V_{ser}	$V_{ser} = 0.6 V_{nom}$	372.72 kN
$V_{c,pred,ser}$	$V_{c,pred,ser} = V_{cr,CCC} + \frac{(0 - V_{cr,CCC})}{V_{nom} - V_{cr,CCC}} (V_{ser} - V_{cr,CCC})$	0 kN
V_s	$V_s = V - V_c$	372.719 kN
σ_s	$\sigma_s = \frac{V_s}{E_s}$	330.550 MPa
$\epsilon_{sm} - \epsilon_{cm}$	$\epsilon_{sm} - \epsilon_{cm} = \frac{\sigma_s - k_t \frac{f_{ct,eff}}{\rho_{p,eff}} (1 + \alpha_e \rho_{p,eff})}{E_s} \geq 0.6 \frac{\sigma_s}{E_s}$	$0.992 \cdot 10^{-3}$
$s_{r,max,y}$	$s_{r,max} = k_3 c_s + k_1 k_2 k_4 \phi_w / \rho_{pw,eff}$	345.493 mm
$s_{r,max,z}$	$s_{r,max} = k_3 c_l + k_1 k_2 k_4 \phi_l / \rho_{pl,eff}$	138.051 mm

x	$x = 0.75d(\alpha_e\rho_l)^{\frac{1}{3}}$	184.128 mm
θ	$\cot\theta = \frac{0.85d_s}{d_s - x} \leq 2.50$	0.583
$s_{r,max}$	$s_{r,max} = \frac{1}{\frac{\cos\theta}{s_{r,max,y}} + \frac{\sin\theta}{s_{r,max,z}}}$	156.124 mm
$s_{r,avg}$	$s_{r,avg} = 0.75s_{r,max}$	117.093 mm
w_{avg}	$w_{avg} = s_{r,avg}(\epsilon_{sm} - \epsilon_{cm})$	0.118 mm

D.1.3. Model-IIA

Table D.4: Calculation of the shear crack width according to the proposed model-IIA

Parameter	Formula	Value
$V_{cr,CCC}$	$V_{cr,CCC} = V_{Rm,c} = 0.3\zeta \frac{x}{d} (f_{cm})^{\frac{2}{3}} b_{v,eff}$	232.028 kN
V_{nom}	$V_{Rd,s} = \frac{A_{sw} z f_{ywd} \cot \theta}{s}$	621.2 kN
V_{ser}	$V_{ser} = 0.6 V_{nom}$	372.72 kN
$V_{c,pred,ser}$	$V_{c,pred,ser} = V_{cr,CCC} + \frac{(0 - V_{cr,CCC})}{V_{nom} - V_{cr,CCC}} (V_{ser} - V_{cr,CCC})$	148.147 kN
V_s	$V_s = V - V_c$	224.573 kN
σ_s	$\sigma_s = \frac{V_s}{E_s}$	188.181 MPa
ϵ_w	$\epsilon_w = \frac{V_s s}{A_v E_s j d \cot \theta}$	$0.941 \cdot 10^{-3}$
$s_{r,max,x}$	$s_{m,x} = 2 \left(c_x + \frac{s_x}{10} \right) + k_1 k_2 \frac{d_{bx}}{\rho_x}$	302.297 mm
$s_{r,max,y}$	$s_{m,y} = 2 \left(c_s + \frac{s_y}{10} \right) + k_1 k_2 \frac{d_{by}}{\rho_y}$	145.615 mm
x	$x = 0.75 d (\alpha_e \rho_l)^{\frac{1}{3}}$	184.128 mm
θ	$\cot \theta = \frac{0.85 d_s}{d_s - x} \leq 2.50$	0.557

$$S_{m\theta-avg} = \frac{1}{\frac{\sin\theta}{S_{m,x}} + \frac{\cos\theta}{S_{m,y}}}$$

 $S_{m\theta-avg}$

131.965 mm

$$w_{avg} = K(c_s)^a \left(\frac{1}{\rho_w}\right)^b \left(\frac{1}{\rho_t}\right)^c S_{m\theta-avg} \epsilon_w$$

 w_{avg}

0.106 mm

D.1.4. Model-IIB

Table D.5: Calculation of the shear crack width according to the proposed model-IIB

Parameter	Formula	Value
$V_{cr,CCC}$	$V_{cr,CCC} = V_{Rm,c} = 0.3\zeta \frac{x}{d} (f_{cm})^{\frac{2}{3}} b_{v,eff}$	232.028 kN
V_{nom}	$V_{Rd,s} = \frac{A_{sw} z f_{yw} d \cot \theta}{s}$	621.2 kN
V_{ser}	$V_{ser} = 0.6 V_{nom}$	372.72 kN
$V_{c,pred,ser}$	$V_{c,pred,ser} = V_{cr,CCC} + \frac{(0 - V_{cr,CCC})}{V_{nom} - V_{cr,CCC}} (V_{ser} - V_{cr,CCC})$	0 kN
V_s	$V_s = V - V_c$	372.719 kN
σ_s	$\sigma_s = \frac{V_s}{E_s}$	330.550 kN
ϵ_w	$\epsilon_w = \frac{V_s s}{A_v E_s j d \cot \theta}$	$1.6 \cdot 10^{-3}$
$s_{r,max,x}$	$s_{m,x} = 2 \left(c_x + \frac{s_x}{10} \right) + k_1 k_2 \frac{d_{bx}}{\rho_x}$	302.297 mm
$s_{r,max,y}$	$s_{m,y} = 2 \left(c_s + \frac{s_y}{10} \right) + k_1 k_2 \frac{d_{by}}{\rho_y}$	145.615 mm
θ	$\tan^4 \theta = \frac{1 + \frac{1}{n \rho_l}}{1 + \frac{1}{n \rho_t}}$	0.583
$s_{m\theta-avg}$	$s_{m\theta-avg} = \frac{1}{\frac{\sin \theta}{s_{m,x}} + \frac{\cos \theta}{s_{m,y}}}$	132.381 mm

$$w_{avg} = K(c_s)^a \left(\frac{1}{\rho_w}\right)^b \left(\frac{1}{\rho_t}\right)^c s_{m\theta-avg} \varepsilon_w$$

w_{avg}

0.187 mm

D.1.5. Model-III A

Table D.6: Calculation of the shear crack width according to the proposed model-III A

Parameter	Formula	Value
$V_{cr,CCC}$	$V_{cr,CCC} = V_{Rm,c} = 0.3\zeta \frac{x}{d} (f_{cm})^{\frac{2}{3}} b_{v,eff}$	232.028 kN
V_{nom}	$V_{Rd,s} = \frac{A_{sw} z f_{ywd} \cot \theta}{s}$	621.2 kN
V_{ser}	$V_{ser} = 0.6 V_{nom}$	372.72 kN
$V_{c,pred,ser}$	$V_{c,pred,ser} = V_{cr,CCC} + \frac{(0 - V_{cr,CCC})}{V_{nom} - V_{cr,CCC}} (V_{ser} - V_{cr,CCC})$	148.147 kN
V_s	$V_s = V - V_c$	224.573 kN
σ_s	$\sigma_s = \frac{V_s}{E_s}$	188.181 MPa
ϵ_w	$\epsilon_w = \frac{V_s s}{A_v E_s j d \cot \Theta}$	$0.941 \cdot 10^{-3}$
ϵ_2	$\epsilon_2 = -\frac{V}{j d b_w E_c \sin \Theta \cos \Theta} = -\frac{V_s + V_c}{j d b_w E_c \sin \Theta \cos \Theta}$	$-0.19 \cdot 10^{-3}$
ϵ_1	$\epsilon_1 = \frac{2(\epsilon_y + \epsilon_2)}{ \cos 2\Theta + 1} - \epsilon_2$	$1.2 \cdot 10^{-3}$
$s_{m,x}$	$s_{m,x} = 2 \left(c_x + \frac{s_x}{10} \right) + k_1 k_2 \frac{d_{bx}}{\rho_x}$	302.297 mm
$s_{m,y}$	$s_{m,y} = 2 \left(c_s + \frac{s_y}{10} \right) + k_1 k_2 \frac{d_{by}}{\rho_y}$	145.615 mm

x	$x = 0.75d(\alpha_e\rho_l)^{\frac{1}{3}}$	184.128 mm
θ	$\cot\theta = \frac{0.85d_s}{d_s - x} \leq 2.50$	0.557
$s_{m\theta-avg}$	$s_{m\theta-avg} = \frac{1}{\frac{\sin\theta}{s_{m,x}} + \frac{\cos\theta}{s_{m,y}}}$	131.965 mm
w_{avg}	$w_{avg} = \epsilon_1 s_{m\theta-avg}$	0.162 mm

D.1.6. Model-IIIB

Table D.7: Calculation of the shear crack width according to the proposed model-IIIB

Parameter	Formula	Value
$V_{cr,CCC}$	$V_{cr,CCC} = V_{Rm,c} = 0.3\zeta \frac{x}{d} (f_{cm})^{\frac{2}{3}} b_{v,eff}$	232.0128 kN
V_{nom}	$V_{Rd,s} = \frac{A_{sw} z f_{ywd} \cot \theta}{s}$	621.2 kN
V_{ser}	$V_{ser} = 0.6 V_{nom}$	372.72 kN
$V_{c,pred,ser}$	$V_{c,pred,ser} = V_{cr,CCC} + \frac{(0 - V_{cr,CCC})}{V_{nom} - V_{cr,CCC}} (V_{ser} - V_{cr,CCC})$	0 kN
V_s	$V_s = V - V_c$	372.719 kN
σ_s	$\sigma_s = \frac{V_s}{E_s}$	330.550 kN
ϵ_w	$\epsilon_w = \frac{V_s s}{A_v E_s j d \cot \Theta}$	$1.6 \cdot 10^{-3}$
ϵ_2	$\epsilon_2 = -\frac{V}{j d b_w E_c \sin \Theta \cos \Theta} = -\frac{V_s + V_c}{j d b_w E_c \sin \Theta \cos \Theta}$	$0-0.184 \cdot 10^{-3}$
ϵ_1	$\epsilon_1 = \frac{2(\epsilon_y + \epsilon_2)}{ \cos 2\Theta + 1} - \epsilon_2$	$1.2 \cdot 10^{-3}$
$s_{m,x}$	$s_{m,x} = 2 \left(c_x + \frac{s_x}{10} \right) + k_1 k_2 \frac{d_{bx}}{\rho_x}$	302.297 mm
$s_{m,y}$	$s_{m,y} = 2 \left(c_s + \frac{s_y}{10} \right) + k_1 k_2 \frac{d_{by}}{\rho_y}$	145.615 mm

x	$x = 0.75d(\alpha_e \rho_l)^{\frac{1}{3}}$	184.128 mm
θ	$\tan^4 \theta = \frac{1 + \frac{1}{n \rho_l}}{1 + \frac{1}{n \rho_t}}$	0.583
$s_{m\theta-avg}$	$s_{m\theta-avg} = \frac{1}{\frac{\sin \theta}{s_{m,x}} + \frac{\cos \theta}{s_{m,y}}}$	132.381 mm
w_{avg}	$w_{avg} = \epsilon_1 s_{m\theta-avg}$	0.303 mm

D.1.7. Model-IV

Table D.8: Calculation of the shear crack width according to the proposed model-IV

Parameter	Formula	Value
$V_{cr,CSA}$	$V_{cr,CSA} = V_{Rm,c} = 0.3\zeta \frac{x}{d} (f_{cm})^{\frac{2}{3}} b_{v,eff}$	87.213 kN
V_{nom}	$V_{Rd,s} = \frac{A_{sw} z f_{ywd} \cot \theta}{s}$	621.2 kN
V_{ser}	$V_{ser} = 0.6 V_{nom}$	372.719 kN
$V_{c,pred,ser}$	$V_{c,pred,ser} = V_{cr,CSA} + \frac{(0 - V_{cr,CSA})}{V_{nom} - V_{cr,CSA}} (V_{ser} - V_{cr,CSA})$	40.583 kN
V_s	$V_s = V - V_c$	332.136 kN
σ_s	$\sigma_s = \frac{V_s}{E_s}$	278.313 kN
ϵ_w	$\epsilon_w = \frac{V_s s}{A_v E_s j d \cot \Theta}$	$1.39 \cdot 10^{-3}$
ϵ_2	$\epsilon_2 = -\frac{V}{j d b_w E_c \sin \Theta \cos \Theta} = -\frac{V_s + V_c}{j d b_w E_c \sin \Theta \cos \Theta}$	$-0.188 \cdot 10^{-3}$
ϵ_1	$\epsilon_1 = \frac{2(\epsilon_y + \epsilon_2)}{ \cos 2\Theta + 1} - \epsilon_2$	$1.85 \cdot 10^{-3}$
$s_{m,x}$	$s_{m,x} = 2 \left(c_x + \frac{s_x}{10} \right) + k_1 k_2 \frac{d_{bx}}{\rho_x}$	302.297 mm
$s_{m,y}$	$s_{m,y} = 2 \left(c_s + \frac{s_y}{10} \right) + k_1 k_2 \frac{d_{by}}{\rho_y}$	145.615 mm

ϵ_x	$\epsilon_x = \frac{\frac{M_f}{d_v} + V_f - V_p + 0.5N_f - A_p f_{p0}}{2(E_s A_s + E_p A_p)}$	$2.0 \cdot 10^{-3}$
θ	$\theta = 29 + 7000\epsilon_x$	0.75
$s_{m\theta-avg}$	$s_{m\theta-avg} = \frac{1}{\frac{\sin\theta}{s_{m,x}} + \frac{\cos\theta}{s_{m,y}}}$	137.408 mm
w_{avg}	$w_{avg} = \epsilon_1 s_{m\theta-avg}$	0.255 mm

D.1.8. Model-V

Table D.9: Calculation of the shear crack width according to the proposed model-V

Parameter	Formula	Value
τ_{xy}	$\tau_{xy} = 1.5 \frac{V_{ser}}{bd}$	2.71 MPa
σ_{sy}	$\sigma_{sy} = \frac{\sigma_y + \tau_{xy} \tan \theta}{\frac{A_{sy}}{b_w s}}$	449.43 MPa
ϵ_w	$\epsilon_w = \frac{V_s s}{A_v E_s j d \cot \Theta}$	$1.5 \cdot 10^{-3}$
ϵ_2	$\epsilon_2 = -\frac{V}{j d b_w E_c \sin \Theta \cos \Theta} = -\frac{V_s + V_c}{j d b_w E_c \sin \Theta \cos \Theta}$	$-0.17 \cdot 10^{-3}$
ϵ_1	$\epsilon_1 = \frac{2(\epsilon_y + \epsilon_2)}{ \cos 2\Theta + 1} - \epsilon_2$	$2.84 \cdot 10^{-3}$
$s_{m,x}$	$s_{m,x} = 2 \left(c_x + \frac{s_x}{10} \right) + k_1 k_2 \frac{d_{bx}}{\rho_x}$	302.29 mm
$s_{m,y}$	$s_{m,y} = 2 \left(c_s + \frac{s_y}{10} \right) + k_1 k_2 \frac{d_{by}}{\rho_y}$	145.61 mm
θ	$\tan^4 \theta = \frac{1 + \frac{1}{n \rho_l}}{1 + \frac{1}{n \rho_t}}$	0.58
$s_{m\theta-avg}$	$s_{m\theta-avg} = \frac{1}{\frac{\sin \theta}{s_{m,x}} + \frac{\cos \theta}{s_{m,y}}}$	132.38 mm
w_{avg}	$w_{avg} = \epsilon_1 s_{m\theta-avg}$	0.37 mm

D.2. Shear Crack Deflection Calculation

This section comprises of the examples for the calculation of shear deflection using the proposed models in this MSc thesis. The mean shear deflection is calculated for the specimen named S1 from a previous experimental study [25]. The beam specimen input parameters required for the calculation are tabulated in Table D.10.

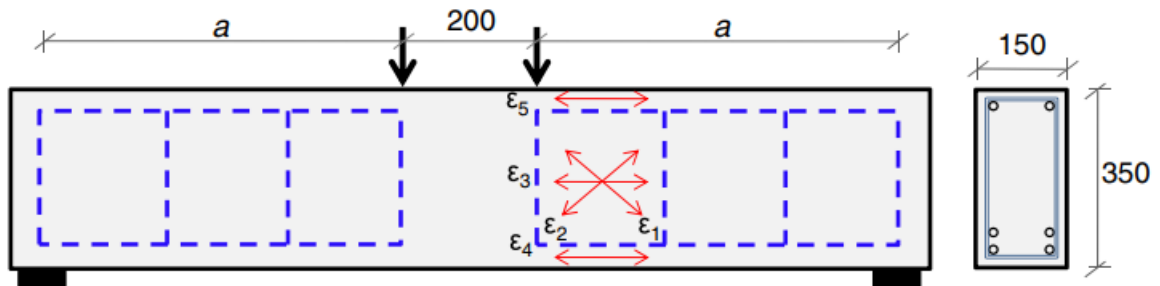


Figure D.2: Mechanical scheme and instrumentation for specimens [25]

Table D.10: Input parameters for the specimen S1 selected for shear deflection calculation from various models.

Parameter	Value
V_{ser}	107.495 kN
b	150 mm
h	350 mm
d_v	276.534 mm
l	1.797m
s	80 mm
A_{sw}	56.4 mm ²
ρ_l	4.26%
ρ_w	0.47%
f_{cm}	33 MPa
f_{yk}	370 MPa
$E_{s,l}$	200000 MPa (Assumed)
$E_{s,w}$	200000 MPa (Assumed)
a/d	2.6

D.2.1. Model-I

Table D.11: Calculation of the shear deflection according to the proposed model-I

Parameter	Formula	Value
V_y	$V_y = V_{cr} + bd_v \rho_v f_{vy} \cot \theta$	204.957 kN
V_{cr}	$V_{cr} = V_{cr,CCC} = V_{Rm,c} = 0.3 \zeta \frac{x}{d} (f_{cm})^{\frac{2}{3}} b_{v,eff}$	71.594 kN
K_{ve}	$K_{v,e} = G_c A_v \approx 0.42 E_c A_v$	$5.48 \cdot 10^8 \text{ N/mm}$
K_{vy}	$K_{v,y} = \frac{V_y}{\gamma} = \frac{V_y}{\delta_s / d_v \cot \Theta_s} = \frac{n \rho_v E_c A_v \cot^2 \Theta_s}{1 + n \rho_v \csc^4 \Theta_s}$	$0.834 \cdot 10^8 \text{ N/mm}$
$K_{v,eff}^{Model-I}$	$K_{v,eff}^{Model-I} = \frac{V}{\frac{V_{cr}}{K_{v,e}} + \left(\frac{V_y}{K_{v,y}} - \frac{V_{cr}}{K_{v,e}} \right) \frac{V - V_{cr}}{V_y - V_{cr}}}$	$1.14 \cdot 10^8 \text{ N/mm}$
Δ_v	$\Delta_v = \int_0^L \gamma(x) \bar{V} dx$	0.9 mm

D.2.2. Model-II

Table D.12: Calculation of the shear deflection according to the proposed model-II

Parameter	Formula	Value
V_y	$V_y = V_{cr} + bd_v \rho_v f_{vy} \cot \theta$	204.957 kN
V_{cr}	$V_{cr} = V_{cr,CCC} = V_{Rm,c} = 0.3 \zeta \frac{x}{d} (f_{cm})^{\frac{2}{3}} b_{v,eff}$	71.594 kN
K_{ve}	$K_{v,e} = G_c A_v \approx 0.42 E_c A_v$	$5.48 \cdot 10^8 \text{ N/mm}$
K_{vy}	$K_{v,y} = \frac{V_y}{\gamma} = \frac{V_y}{\delta_s / d_v \cot \Theta_s} = \frac{n \rho_v E_c A_v \cot^2 \Theta_s}{1 + n \rho_v \csc^4 \Theta_s}$	$0.834 \cdot 10^8 \text{ N/mm}$
$K_{v,eff}^{Model-I}$	$K_{v,eff}^{Model-I} = \frac{V}{\frac{V_{cr}}{K_{v,e}} + \left(\frac{V_y}{K_{v,y}} - \frac{V_{cr}}{K_{v,e}} \right) \frac{V - V_{cr}}{V_y - V_{cr}}}$	$3.48 \cdot 10^8 \text{ N/mm}$
Δ_v	$\Delta_v = \int_0^L \gamma(x) \bar{V} dx$	0.29 mm

D.2.3. Model-III

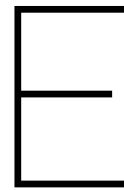
Table D.13: Calculation of the shear deflection according to the proposed model-III

Parameter	Formula	Value
V_y	$V_y = V_{cr} + bd_v \rho_v f_{vy} \cot \theta$	204.957 kN
V_{cr}	$V_{cr} = V_{cr,CCC} = V_{Rm,c} = 0.3 \zeta \frac{x}{d} (f_{cm})^{\frac{2}{3}} b_{v,eff}$	71.594 kN
K_{ve}	$K_{v,e} = G_c A_v \approx 0.42 E_c A_v$	$5.48 \cdot 10^8 \text{ N/mm}$
K_{vy}	$K_{v,y} = \frac{V_y}{\gamma} = \frac{V_y}{\delta_s / d_v \cot \Theta_s} = \frac{n \rho_v E_c A_v \cot^2 \Theta_s}{1 + n \rho_v \csc^4 \Theta_s}$	$0.834 \cdot 10^8 \text{ N/mm}$
$K_{v,eff}^{Model-I}$	$K_{v,eff}^{Model-I} = \frac{V}{\frac{V_{cr}}{K_{v,e}} + \left(\frac{V_y}{K_{v,y}} - \frac{V_{cr}}{K_{v,e}} \right) \frac{V - V_{cr}}{V_y - V_{cr}}}$	$2.31 \cdot 10^8 \text{ N/mm}$
Δ_v	$\Delta_v = \int_0^L \gamma(x) \bar{V} dx$	0.44 mm

D.2.4. Model-IV

Table D.14: Calculation of the shear deflection according to the proposed model-I

Parameter	Formula	Value
V_y	$V_y = V_{cr} + bd_v\rho_v f_{vy} \cot\theta$	204.957 kN
V_{cr}	$V_{cr} = V_{cr,CCC} = V_{Rm,c} = 0.3\zeta \frac{x}{d} (f_{cm})^{\frac{2}{3}} b_{v,eff}$	71.594 kN
K_{ve}	$K_{v,e} = G_c A_v \approx 0.42 E_c A_v$	$5.48 \cdot 10^8 \text{ N/mm}$
K_{vy}	$K_{v,y} = \frac{V_y}{\gamma} = \frac{V_y}{\delta_s/d_v \cot\Theta_s} = \frac{n\rho_v E_c A_v \cot^2\Theta_s}{1 + n\rho_v \csc^4\Theta_s}$	$0.834 \cdot 10^8 \text{ N/mm}$
$K_{v,eff}^{Model-I}$	$K_{v,eff}^{Model-I} = \frac{V}{\frac{V_{cr}}{K_{v,e}} + \left(\frac{V_y}{K_{v,y}} - \frac{V_{cr}}{K_{v,e}}\right) \frac{V-V_{cr}}{V_y-V_{cr}}}$	$1.81 \cdot 10^8 \text{ N/mm}$
Δ_v	$\Delta_v = \int_0^L \gamma(x) \bar{V} dx$	0.56 mm



Appendix E- Integral Design Management Perspective

E.1. Introduction

This Appendix is written in partial fulfilment of the requirements to obtain the IDM (Integral Design Management) annotation at the Delft University of Technology. The annotation is designed for students aiming at combining technical knowledge with engineering management skills and preparing the graduates for future roles in multidisciplinary engineering practices. In this Appendix, a discussion is made about the implications of the proposed technical structural design methodology on the other aspects of an infrastructure project like quality, risk-management, maintenance time and cost-estimation of the project.

Section E.2 describes the design steps of a cantilever balanced bridge and evaluation of mean shear crack widths and shear deflection with the proposed models in this thesis. The proposed models facilitate the design of right amounts of shear reinforcement to keep the crack widths under the permissible limits specified in the practical design codes.

E.3 defines quality in project management and comment on the implications of the proposed models on the project quality. The cost to achieve this quality is discussed. The section E.4 and section E.5 discuss the effects of the modified design method using the proposed models on the time to maintenance and cost range estimates for the project. The section E.6 presents a risk register with a description of three crucial risks inherent in the application of conventional design method. The proposed design methods are used as a risk response and post-risk response assessment is also made. The section E.7 and section E.8 present the conclusions of the discussion in the Appendix and a critical reflection on the personal experience of the author while pursuing the IDM annotation at the Delft University of Technology.

E.2. Cantilever Balanced Bridge

An inspection in 2001 reveals extensive cracks in the web of concrete hollow box girders of Grondal bridge in Stockholm, Sweden just after two years of putting the bridge in service (Figure 1.1). After some time, similar problem is reported in the Alvik bridge in Stockholm [29]. The concerned authorities decide to temporarily close the bridges fearing the risk of shear failure. The bridges are designed in accordance with the Swedish codes. However,

later it is found that the designs have inadequate shear reinforcement in serviceability limit state. It is observed that the crack width kept on increasing along with an increase in the number of cracks [24]. In general, the average crack width is found to be in the range of 0.1-0.3 mm whereas the maximum crack width is found in the range of 0.4-0.5 mm which is considered to pose problems concerning durability and serviceability of the structure [29]. Now, the original details of the sections of these bridges are not available and therefore, in Figure E.2, a hypothetical case with an assumed main and side spans is considered and a cantilevered balanced bridge cross section is designed using simplified assumptions and thumb rules to assess the applicability of the proposed mean shear crack width model. Figure E.1 shows the schematic diagram of the designed cantilever balanced bridge along with an approach bridge. The section A-A is considered at the hammer head while the section B-B is considered at the center of the main span.

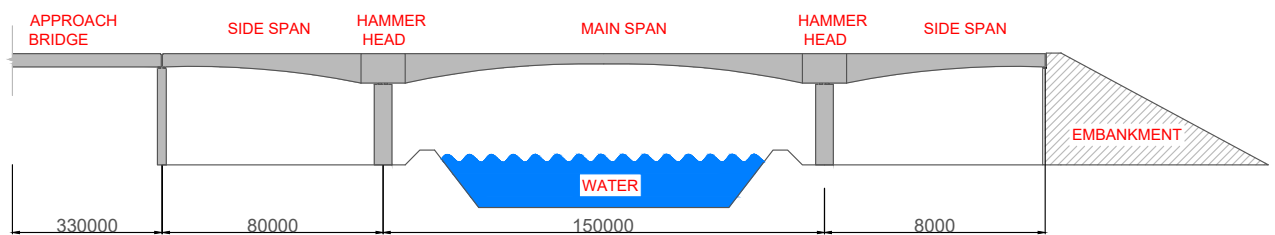


Figure E.1: Schematic diagram of the cantilever balanced bridge and approach bridge

In this section, a cantilever balanced bridge cross-section is designed using simplifying assumptions and thumb rules. The main span of the bridge is 150m and the two side spans are 80m wide. The cast in-situ segments and travelling formwork are used. The approach bridge of length 330m is connected to the bridge (see Figure E.1). The characteristic strength of concrete and steel reinforcement is 50MPa and 500MPa respectively. The structure is designed for Euro Code Consequence Class 3 and Load Model 1. The carriage way comprises in each direction of two traffic lanes, a hard strip and hard shoulder, and parapets on each side.

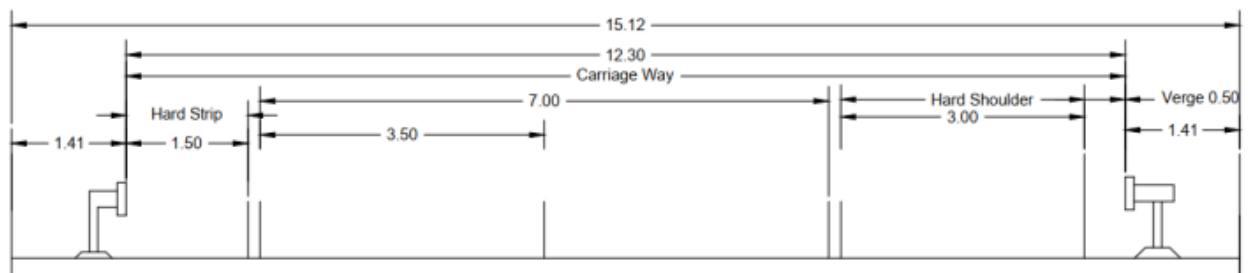


Figure E.2: Schematic representation of carriage-way of the designed cantilever balanced bridge

Figure E.2 shows the schematic diagram of the carriage way of the bridge. Figure E.3 shows a typical box girder cross-section used in the cantilever balanced bridge construction. The various parameters marked in the diagram are to be determined. The main span of the bridge is 150m. Based on the thumb rule $\frac{L}{h} = 22$. This means the required minimum height

of the girder, $h_{min} = 6.8m$.

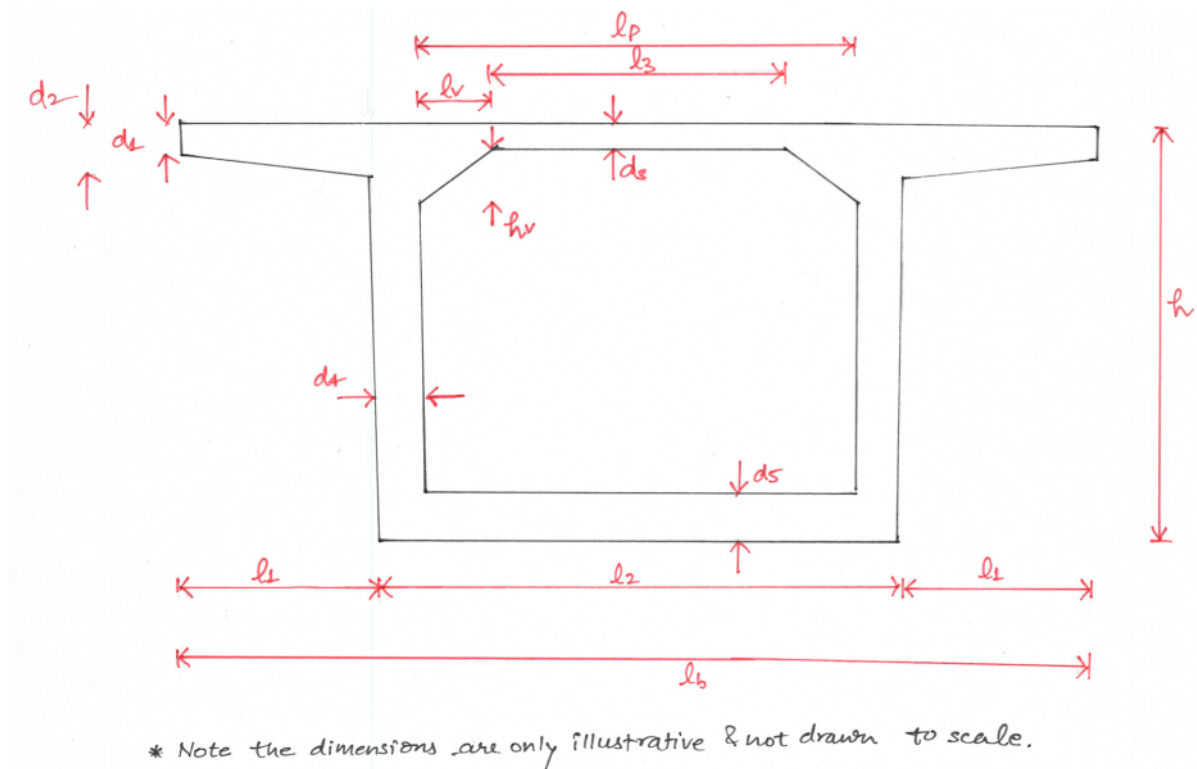


Figure E.3: Schematic representation of RC beam as beam on elastic foundation [43]

Determination of Box-Girder Cross Section

$$\frac{L}{h} = 22$$

$$\Rightarrow h_{min} = 6.81$$

$$\Rightarrow h_{provided} = 7.0m$$

$$l_1 = 2.5 \text{ to } 3.5m$$

Let us assume $l_1 = 3.5m$

Based on the thumb rules in design practice [64]

$$\frac{l_1}{l_2} = 0.45$$

$$\Rightarrow l_2 = 8.0m$$

Determination of d_4

$$\begin{aligned}
 d_4 \text{ (required)} &\geq 350 \text{ mm} \\
 d_4 &= 2(c_c + \phi_{stirrup} + \phi_{main}) + \phi_{p-hose} + \phi_{duct-main} \\
 \Rightarrow d_4 \text{ (required)} &= 382 \text{ mm} \\
 d_4 &= 2 X_r \\
 X_r &= 167.5 \text{ mm} \\
 d_4 \text{ (provided)} &= 400 \text{ mm}
 \end{aligned}$$

Determination of d_1

$$\begin{aligned}
 d_1 \text{ (required)} &\geq 250 \text{ mm} \\
 d_1 &= 2(c_c + \phi_{stirrup} + \phi_{main}) + \phi_{duct-trans} + \phi_{duct-main} \\
 \Rightarrow d_1 \text{ (required)} &= 324 \text{ mm} \\
 \Rightarrow d_1 \text{ (provided)} &= 350 \text{ mm}
 \end{aligned}$$

Determination of d_2

$$\begin{aligned}
 \frac{d_1}{d_2} &= 0.75 \\
 \Rightarrow d_2 \text{ (required)} &= 466.67 \text{ mm} \\
 \Rightarrow d_2 \text{ (provided)} &= 475 \text{ mm}
 \end{aligned}$$

Taking $l_1 = 3.5 \text{ m}$,

$$\Rightarrow l_p = 7.2 \text{ m}$$

Determination of d_3

$$\begin{aligned}
 d_3 \text{ (required)} &\geq 250 \text{ mm} \\
 d_3 \text{ (required)} &\geq \frac{l_p}{30} \\
 d_3 &= 2(c_c + \phi_{stirrup} + \phi_{main}) + \phi_{duct-trans} + \phi_{duct-main} \\
 \Rightarrow d_3 \text{ (provided)} &= 350 \text{ mm}
 \end{aligned}$$

Now, the height of haunch should be equal to d_3 , therefore, $h_v = 350\text{mm}$.

Determination of l_v

$$\frac{l_v}{l_p} \leq 0.20$$

$$\Rightarrow l_v (\text{provided}) = 1.4\text{m}$$

Using l_v and l_p ,

$$l_3 = l_p - 2l_v$$

$$\Rightarrow l_3 (\text{provided}) = 4.4\text{m}$$

d_5 at the section A-A (at the location of hammer) can be taken as 1000mm . Figure E.3 shows the typical section of a box girder cross section.

Determination of the BM above the main support

As the name suggests, the mechanical scheme of the cantilever balanced bridge is a cantilever beam with a fixed end. The self weight intensity at section A-A

$$q_{A-A} = \gamma_c A_{A-A} \Rightarrow q_{A-A} = 467.43\text{kN/m} \quad (\text{E.1})$$

where

γ_c weight density of the reinforced concrete.

A_{A-A} cross-section area of the section A-A.

A_{B-B} cross-section area of the section B-B.

Let us assume a linear decrement of the load from section A-A to section B-B.

$$q_{B-B} = \gamma_c A_{B-B} \Rightarrow q_{B-B} = 261.43\text{kN/m} \quad (\text{E.2})$$

Figure E.4 shows the linear variation of the weight between the section A-A and section B-B.

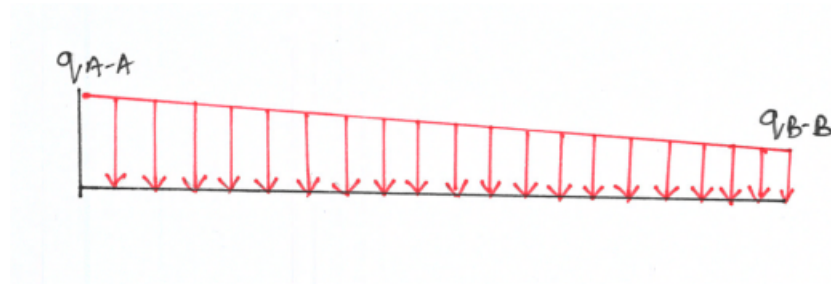


Figure E.4: Variable self-weight intensity along the span

Now,

$$M_{A-A} = \frac{q_{B-B}}{2} \left(\frac{L}{2} - \frac{w_{pier}}{2} \right)^2 + \frac{1}{2} (q_{A-A} - q_{B-B}) \left(\frac{L}{2} - \frac{w_{pier}}{2} \right) \frac{1}{3} \left(\frac{L}{2} - \frac{w_{pier}}{2} \right) \quad (E.3)$$

where

w_{pier} top width of the pier.

$$\Rightarrow M_{A-A} = 903825.20 \text{ kN/m}$$

Determination of the SF above the main support

The SF at the cross section A-A is

$$V_{A-A} = \frac{q_{B-B}}{2} \left(\frac{L}{2} - \frac{w_{pier}}{2} \right) + \frac{1}{2} (q_{A-A} - q_{B-B}) \left(\frac{L}{2} - \frac{w_{pier}}{2} \right) \quad (E.4)$$

$$\Rightarrow V_{A-A} = 26968.37 \text{ kN}$$

Number of prestressing strands

Assuming that the stress at the top fiber of the box girder is equal to 3 MPa (thumb rule to assume that the compressive stress at the top fiber after the including the effect of asphalt load and traffic load)

Therefore,

$$\sigma_t = -\frac{P}{A} - P \frac{e_p}{W_t} + \frac{M_{A-A}}{W_t} = -3000 \text{ kN/m}^2 \quad (E.5)$$

$$e_p = y_t - c_c - \phi_{main} - \phi_{stirrup} - \frac{\phi_{duct-main}}{2} \quad (E.6)$$

$$y_t = 3.61 \text{ m}$$

$$e_p = 3.44 \text{ m}$$

where

e_p	eccentricity of the prestressing cable.
y_t	distance of the top extreme fiber of the cross-section from centroid.
c_c	clear cover to the main reinforcement.
ϕ_{main}	diameter of the longitudinal reinforcement.
$\phi_{stirrup}$	diameter of the transverse reinforcement.
$\phi_{duct-main}$	diameter of the duct of the longitudinal prestressing cable.
$\phi_{duct-trans}$	diameter of the duct of the transverse prestressing cable.

$$\Rightarrow P = 180910.15kN$$

Assuming application of prestressing steel F_{ep} 1860 for which,

$$\sigma_{pw} = \sigma_{pi} * 0.85$$

where

σ_{pw}	residual prestressing force after short term prestressing losses.
σ_{pi}	initial prestressing force before prestressing losses.

$$\sigma_{pw} = 1395 * 0.85 = 1185.75MPa$$

Total required area of the prestressing strands (A_p) to achieve the required prestress at permissible stress levels is :

$$A_p = \frac{P}{\sigma_{pw}} \quad (E.7)$$

$$\Rightarrow A_p = 152570.23mm^2$$

Assuming (12, ($\phi 15.7mm$) strands are being used,

Number of cables (required) =84

Number of cables (adopted)= 85

The c/c spacing b/w prestressing cable = $\frac{15000}{85}=176.47$ mm

Figure E.5 shows the side and the top view layouts of the prestressing cables in the cantilevered balanced bridge.

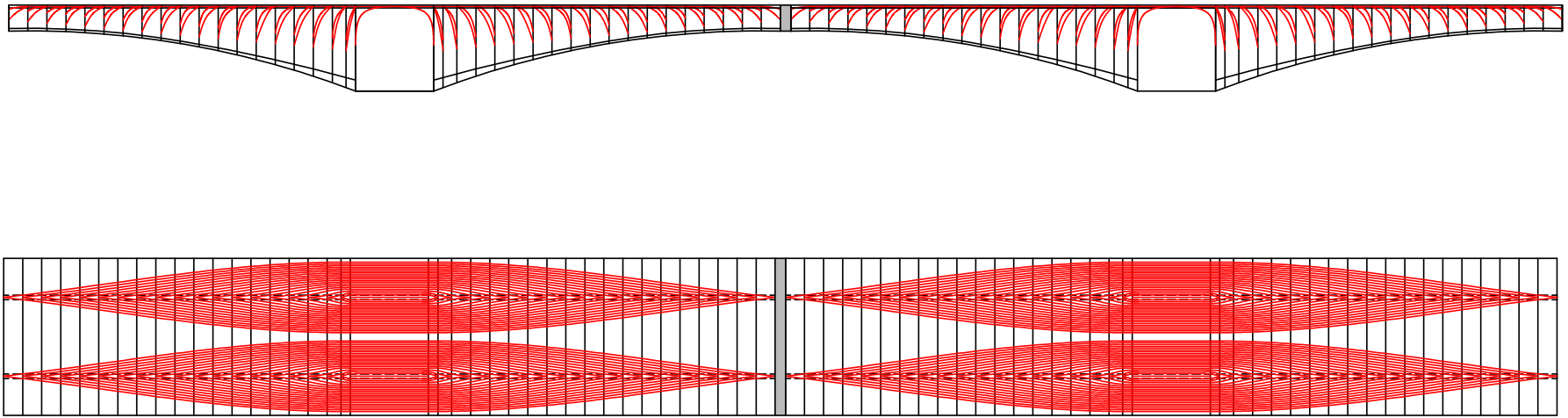


Figure E.5: Side and Top view layout of the prestressing cables

Check for bottom flange thickness at ULS

Let us assume a max strain of $1.75 * 10^{-3}$ in the bottom flange to prevent the possibility of brittle failure while checking the axial resistance provided by the bottom flange at ULS.

1st Iteration

Assuming,

$$\sigma_{pu} = \frac{0.95 f_{pk}}{\gamma_s} = 1606.45 MPa \quad (E.8)$$

σ_{pu} maximum permissible stress in the prestressing strands.

f_{pk} yield strength of the prestressing strands.

γ_s factor of safety for the stress in the prestressing strands.

Now,

$$\sigma_{pm\infty} = \frac{P}{A_p} = 1182.41 mm^2$$

$\sigma_{pm\infty}$ maximum applied prestressing stress in the strands.

$$\Delta N_p = A_p (\sigma_{pu} - \sigma_{pm\infty}) = 64863.48 kN \quad (E.9)$$

Now,

$$\alpha b f_{cd} x_u = P_{m\infty} + \Delta N_p \quad (E.10)$$

x_u depth of the compression zone.

$$x_u = \frac{P_{m\infty} + \Delta N_p}{\alpha b f_{cd}} = 819.24$$

Now,

$$\Delta \varepsilon_p = \left(\frac{d_p - x_u}{x_u} \right) \varepsilon_w = 1.30 * 10^{-2} \quad (E.11)$$

where,

$$d_p = h - \phi_{main} - \phi_{stirrup} - \frac{\phi_{duct-main}}{2} = 6891.5$$

Figure E.6 shows the stress-strain relationship for the pre-stressing strands used in this case.

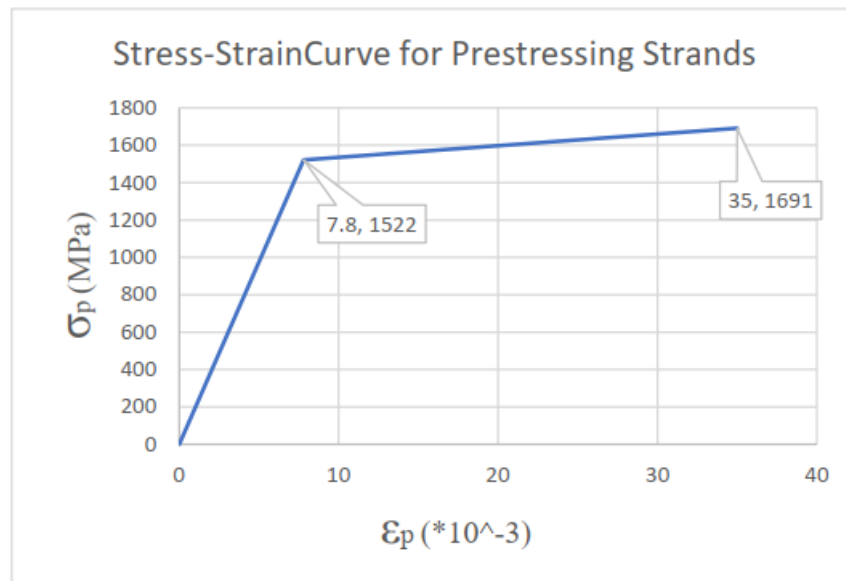


Figure E.6: Stress-strain relationship for the prestressing strands

Now ,

$$\Rightarrow \sigma_{pu} = 1554.12 \text{ MPa} \quad (\text{E.12})$$

2nd Iteration

Let's assume $\sigma_{pu} = 1554.12 \text{ MPa}$

$$\Rightarrow \Delta N_p = 56871.54 \text{ kN}$$

$$\Rightarrow x_u = 792.60 \text{ mm}$$

$$\Rightarrow \epsilon_u = 1.35 \cdot 10^{-2}$$

ϵ_u maximum strain in the prestressing strands at the ULS.

$$\Rightarrow \sigma_{pu}(\text{graph}) = 1557.20 \text{ MPa} \approx \sigma_{pu}(\text{assumed})$$

\Rightarrow the iteration is stopped & $x_u = 792.60 \text{ mm}$

Check for Moment Resistance

Figure E.7 shows the cross-section forces acting at ULS.

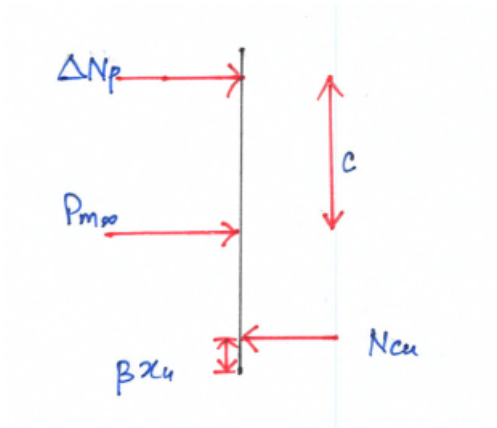


Figure E.7: Cross-section forces at ULS

$$M_{Rd} = P_{m\infty}(h - y_t - \beta x_u) + \Delta N_p(h - \beta x_u - c - \phi_{st} - \phi_{main} - \frac{\phi_{duct-main}}{2}) \quad (E.13)$$

where

h total height of the girder cross-section

$c = y_t$ distance of centroid from the top

Now,

$$M_{Rd} = 882890.710 \text{ kNm}$$

$$M_{Ed} = 1.4M_{A-A} - P_{m\infty}e_p \quad (E.14)$$

$$\Rightarrow M_{Ed} = 642293.91 \text{ kNm}$$

Now,

$$M_{Rd} > M_{Ed}$$

\Rightarrow Moment resistance capacity is sufficient at the section A-A

Check for Shear Resistance

Since the height of the box-girder section decreases linearly from section A-A to section B-B, the inclination in the bottom flange of the box girder leads to a vertical component of the concrete compression force. This vertical component resists external shear force and therefore, enhances the shear resistance of the box girder. Figure E.8 shows the variation in the height of the box girder between section A-A and section B-B.

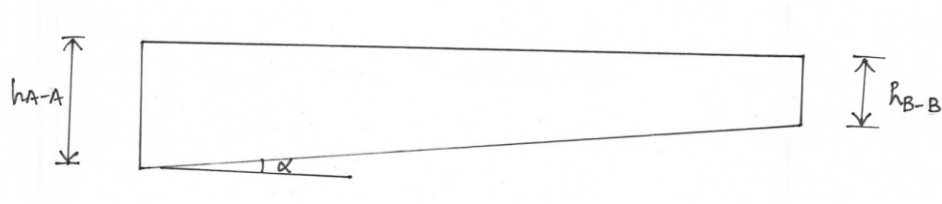


Figure E.8: Cross-section forces at ULS

$$V_{Ed} = 1.5(V_{A-A} - N_{cu} \sin \alpha) \quad (E.15)$$

$$\alpha = \tan^{-1} \left(\frac{h_{A-A} - h_{B-B}}{\frac{L}{2} - \frac{w_{pier}}{2}} \right)$$

Assumed $w_{pier} = 2m$

$$v_{Ed} = \frac{V_{Ed}}{bd} = 4.54 MPa \quad (E.16)$$

where

$$b = 2d_4 - 0.5 \sum 2\phi_{duct}$$

Shear Resistance of Concrete without any Stirrups

$$v_{Rdc} \geq v_{min} + k_1 \sigma_{cp} \quad (E.17)$$

where

$$k_1 = 1 + \sqrt{\frac{200}{d}}$$

σ_{cp} compressive stress in the concrete due to prestressing.

$$\Rightarrow v_{Rdc} \geq 1.76 MPa$$

$$\Rightarrow v_{Ed} \geq v_{Rdc} \quad (E.18)$$

\Rightarrow check $V_{Rd,max}$

$$v_{Rd,max} = \sigma_{cd} * \sin \theta \cos \theta = \alpha_{cw} v_1 f_{cd} \sin \theta \cos \theta \quad (E.19)$$

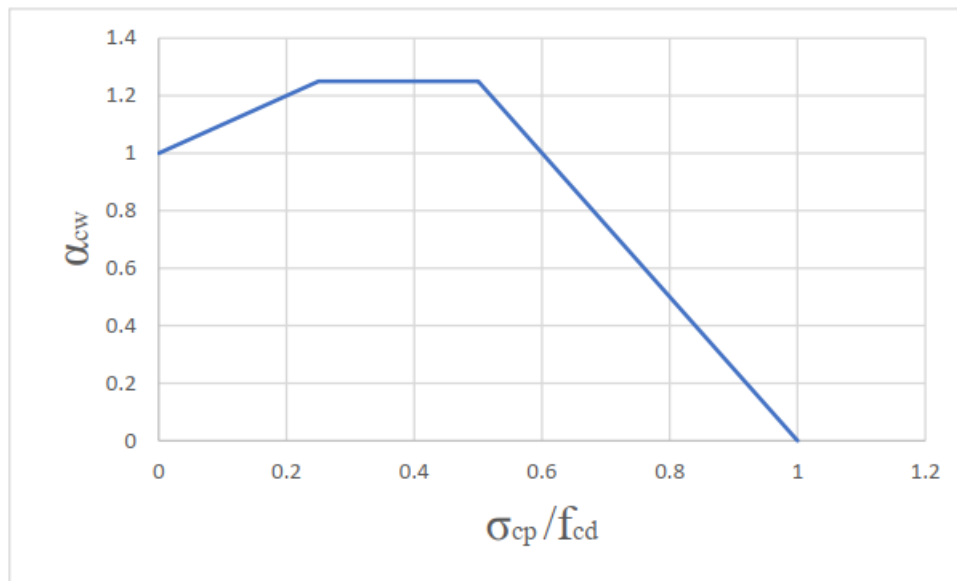


Figure E.9: Modification factor for the transverse tension in the compression strut

Figure E.9 shows the modification factor for the effect of transverse tension between in the compression strut. where

According to EC2,

$$21.8^\circ \leq \theta \leq 45^\circ \quad (\text{E.20})$$

$$\Rightarrow v_{Rd,max} = 12.9 \text{ MPa}$$

Now,

$$v_{Rd,max} > v_{Ed}$$

\Rightarrow design the shear stirrups

Design of Shear Stirrups

According to iStructE,

$$\theta = 0.5 \sin \left[\frac{5.56 V_{Ed}}{b d f_{ck} \left(1 - \frac{f_{ck}}{250}\right)} \right] = 19.58^\circ \quad (\text{E.21})$$

But, According to EC2,

$$21.8^\circ \leq \theta \leq 45^\circ$$

$$\theta(\text{adopted}) = 21.8^\circ$$

Now, according to EC2 the concrete contribution to the shear resistance of a shear reinforced beam is equal to zero.

$$V_{Rd,s} = V_{Ed}$$

$$V_{Rd,s} = V_{Ed} = V_{Ed} = \frac{A_{sw} f_{yd} z c o t \theta}{s} \quad (E.22)$$

⇒ spacing (provided) = 200 mm.

Mean shear crack width calculation using proposed Model-IV for mean shear crack width

Now, for stirrup spacing of 200 mm c/c

$$w_{avg} = 2.14 \text{ mm} \quad (E.23)$$

Now, ACI- 318 [34] recommends that crack width be limited to 0.41mm in a reinforced concrete structural element under service loading conditions. Therefore, the stirrup spacing has to be reduced. The mean shear crack width can be reduced to 0.41mm with 50 mm stirrup spacing. Now, this may pose execution challenges. In that case, shear reinforcement with higher bar diameter should be deployed.

The mean shear crack width with the original design method was found to be 2.146 mm and the stirrup spacing provided was 200 mm. However, ACI 318 [34] specifies the mean acceptable crack width equal to 0.41 mm under service loads. It is found that to bring the mean shear crack width value to the acceptable limit, the stirrup spacing should be reduced to 50mm. It may be noted that in the design of the cantilever balanced bridge, several assumptions are made which may be more conservative than the practical design scenarios in practice. However, the goal is to underscore the fact that a design which is shear safe at ULS according to the accepted design norms may not be shear-sufficient at SLS from the perspective mean shear crack width control. The same issue is seen in case of Alvik and Grondal bridges in Sweden where extensive shear cracking is observed under service loads within a few days of putting the bridges into service. This highlights the impact that the proposed mean shear crack width and shear deflection models can have on mitigating the problem of large shear crack widths in service condition.

E.3. Proposed Models and Quality Management

Quality in a project delivery means "Supply the customers with what they want to standards and specifications they want and at the price that suit their needs" [58].

Quality = Stakeholder satisfaction.

According to Maylor,

Satisfaction = perception-expectation

where

perception quality of the output

expectation desired level of quality of output

Now, in case of a bridge design, client expectations cannot be lowered to enhance the satisfaction. A client expects that the bridge should not undergo severe shear cracking under service loads application. Therefore, to increase client satisfaction, perception should be

increased. The proposed design methodology ensures that the designed bridge is not vulnerable to severe shear cracking under the application of service loads. Therefore, perception is increased which in turn increases the quality of the finished product which is the design of the bridge girder in this case.

Cost of Quality

There are two types of cost of quality.

1. Cost of achieving good quality

- (a) Prevention: These are costs incurred to raise the quality of the product to meet customer satisfaction.
- (b) Appraisal: These are the costs incurred to evaluate the process and their outputs with the goal of establishing compliance with the quality.

2. Cost of poor quality

- (a) Internal failure costs: These correction costs are incurred when the product is still inside the company office and compound and not yet received by the customer for example repair and re-evaluation.
- (b) External failure costs: These correction costs are incurred when the product/ service has already been delivered to the customer and fault/ flaw is detected after the receipt by the customer for example penalty and recall costs.

In the context of this MSc thesis work, it is clear that the cost of poor quality of current design method is the external failure cost since the failure can only be brought to notice after it has occurred in the structure (the failure/ fault has already stepped out of the design office and can no more be controlled internally). The proposed design methodology reduces/ prevents this external cost, however, another cost is incurred with it. The proposed design method comes with the cost of prevention. The cost of prevention comes in the form of additional design effort cost and additional material and placement labor cost in case shear reinforcement enhancement is found necessary (using the proposed models) for controlling shear crack width and shear deflection under allowable limits. Usually the cost of external failure is higher than the cost of prevention. Thus, the proposed design methodology can bring about huge savings in maintenance cost throughout the life span of the structure.

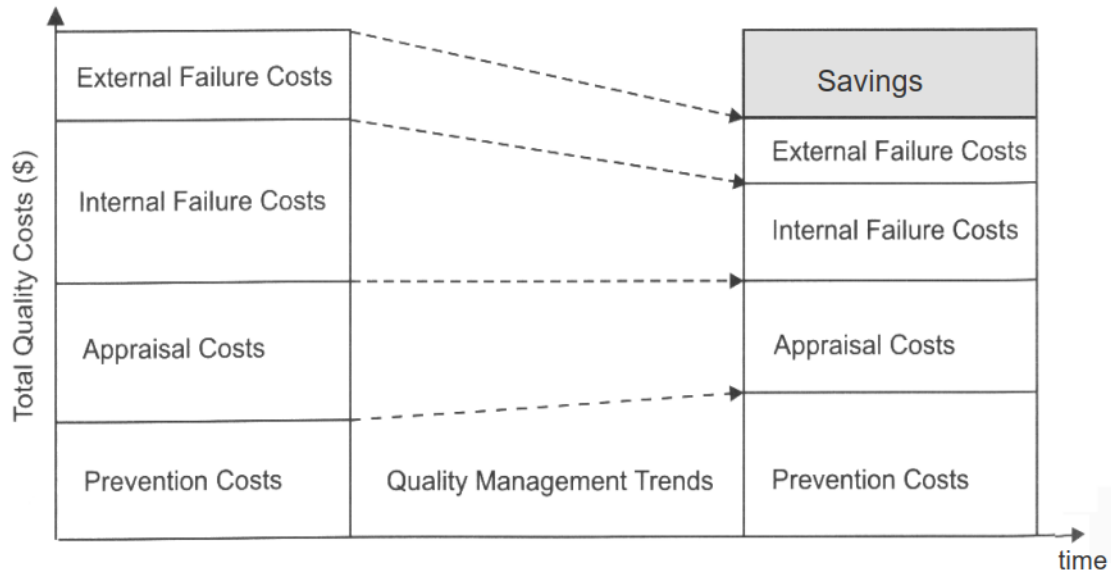


Figure E.10: Original and New position of the perceived risk of extensive shear cracking in a bridge girder under service loads [58]

E.4. Proposed Models and Time to Maintenance

Maintenance refers to the set of activities that is needed to keep the required function(s) available at the agreed level of service. The area under the probability density function is constant. However, the proposed design method leads to better performance not only in SLS but the enhanced shear reinforcement (if found in analysis) will increase the shear capacity in ULS as well. This leads to the shifting of the mean maintenance time to a higher value. Similarly, other values are shifted towards right and therefore, entire gamma probability density function plot shifts rightward. If it is assumed that the maintenance occurring beyond the mean time to maintenance is significantly aimed at improving the load carrying capacity of the bridge at the ULS (and maintenance before mean time to maintenance is generally for serviceability related issues) then there is a possibility of the gamma PDF curve becoming right skewed. This is because the current design methodology already provides sufficient ULS resistance. The enhanced design methodology will further increase the resistance at ULS and depending on the magnitude of the enhancement right skewness may get introduced in the probability density function. Figure E.11 shows the original and the shifted probability density function (PDF). Figure E.12 shows the shifted and skewed (and shifted) probability density function of the maintenance for the proposed design method (which proposes application of engineering models for the calculation of mean shear crack width and shear deflection in addition to the currently used design checks for bending moment resistance, shear resistance check and check for flexural crack widths).

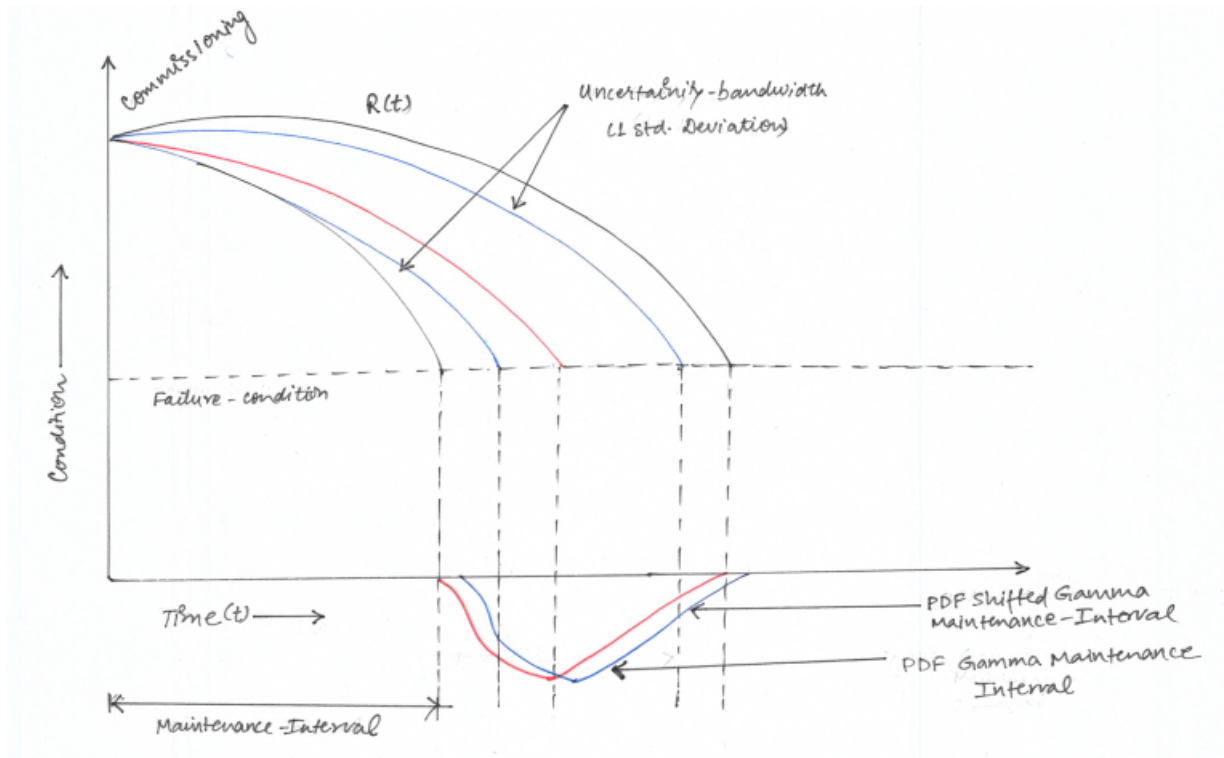


Figure E.11: Original and New position of the perceived risk of extensive shear cracking in a bridge girder under service loads

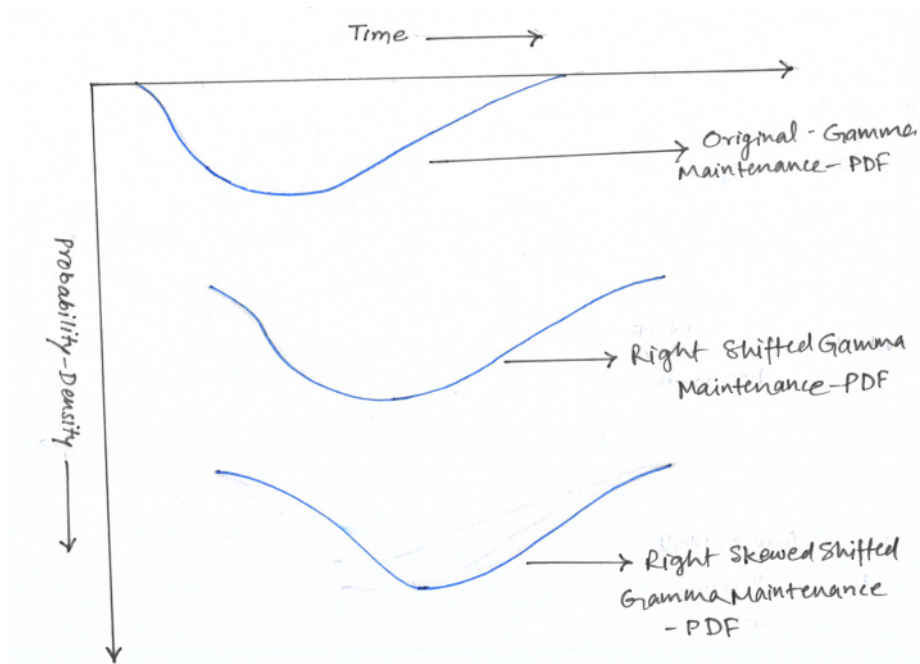


Figure E.12: Original and New position of the perceived risk of extensive shear cracking in a bridge girder under service loads

E.5. Proposed Models and Cost Range Estimates

Typically, the price of a project comprises cost of direct materials and direct labor, project overheads, general overheads and profit of the contractor(s). The design of the structure may be contracted to an engineering office by the client, or the contractor may have their own in-house engineering design team. The proposed mean shear crack width and shear deflection models introduce an additional design step in the shear design of slender reinforced concrete beams. This has implications on the design cost as well as the construction cost should a shear enhancement is made based on the analysis of mean shear crack width and shear deflection under service loads. Thus, the baseline cost (or prime cost) of the project is also likely to increase. This will cause the changes in the estimated costs by contractors during the tendering phase. In most cases, the estimated total cost of a project is not a fixed number but usually it is defined as a range between the pessimistic and optimistic estimate of the cost. Such an estimate is called the range cost estimate and it is necessary to know the spread of the probable finished total cost of the project. The range estimate is typically characterized by different values like P10, P50 and P90 with a likelihood of not being exceeded by the actual total cost of the project by 10%, 50% and 90% respectively.

where

P_{10}	Optimistic estimate (10% chance of being better)
m	most likely estimate (mode of the distribution)
P_{50}	median estimate (the 50%- 50% outcome)
P_{90}	Pessimistic estimate (10% chance of being worse)

Figure E.13 shows the various cost range estimates of a project.

Based on the interviews with a few practicing bridge engineers (who prefer to stay anonymous), it is revealed that the material costs can vary anywhere between 20%-40% of the total cost of the project. The reinforcement (design and material) cost is a fraction of the total cost of the project. The proposed design method may increase the proposed shear reinforcement volume to up to 4 times (say) in extreme cases as also see in the example of the cantilever balanced bridge presented earlier. Assuming that the reinforcement cost accounts for 40 % (conservative estimate) of the total material and design cost of the project. It is also assumed that the material and design cost accounts for 40% of the total project cost (including cost of land acquisition, labour cost, documentation and legal cost, material and design cost). This implies that reinforcement cost can be as high as 16% of the total project cost in extreme cases.

Assuming the two extreme situations where the application of the proposed mean shear crack width and shear deflection models do not increase the provided shear reinforcement and the case in which four times the original calculated shear reinforcement amount is provided, the mean scenario is assumed where the proposed models recommend the application of 200% more of the original amount of stirrups. Thus, this increment leads to an increase in the total cost of the project by 24.24% (assuming the reinforcement cost is 16% of the total cost of the project). Figure E.14 shows the qualitative change in the probability density function of the cost range estimate due to the adoption of the proposed design method.

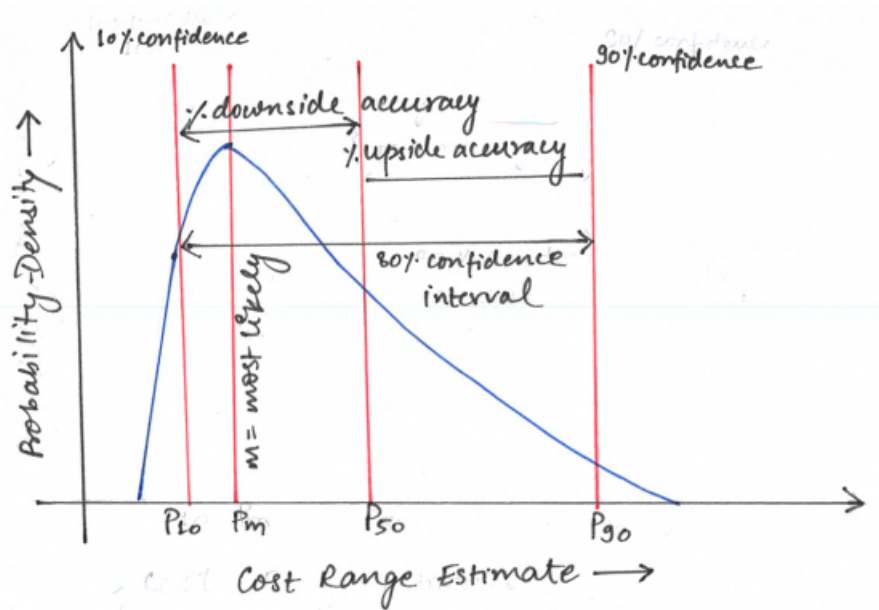


Figure E.13: Original and New position of the perceived risk of extensive shear cracking in a bridge girder under service loads

Maturing of a Cost Range Estimate

There are two key drivers of the cost range estimates.

1. **Variability:** This comprises variation in scope, materials and time required to finish a project. This variation is directly reflected in the total finished cost of the project.
2. **Risk:** A risk is an uncertain, future event, that, if it occurs has a negative or positive impact on project promises [39]. The risk event tend to directly affect the CAPEX (Capital Expenditure) of the project.

The two inferences can be drawn regarding the influence of the proposed design method on the cost range estimate.

- (a) The current design method performs better in terms of accuracy of the estimates of the total project cost (including the maintenance cost) as compared to the conventional design method.
- (b) The proposed method brings down the probability of the severe consequences of the critical service life maintenance issues and thus, their influence on the CAPEX.

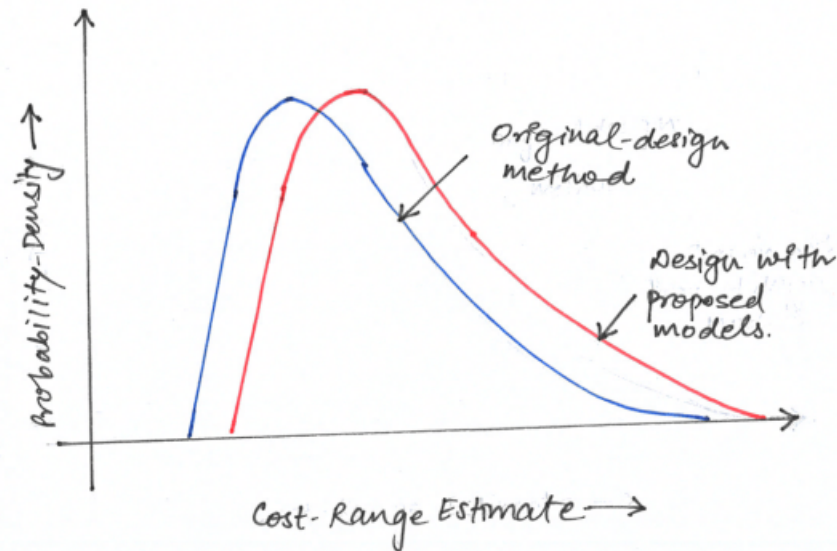


Figure E.14: Original and New position of the perceived risk of extensive shear cracking in a bridge girder under service loads

The range estimates are reduced by the reducing variability and responding to risk events. The proposed method certainly addresses the risk of potential shear cracking occurring under service loads and at the same time leads to more accurate estimations off the total finished cost of the project (including the maintenance cost). Therefore, the proposed method plays a role in maturing the cost range estimate of the project.

Sample case for quantifying the effect of proposed design method using Delphi-Beta Method

The Table E.1 and Table E.2 show the calculation for finding the resultant distribution of the total cost of a project based on the conventional design method and the proposed design method respectively. The cost of land acquisition and cost of civil works is assumed to have a Beta- distribution spread as shown in Figure E.15.

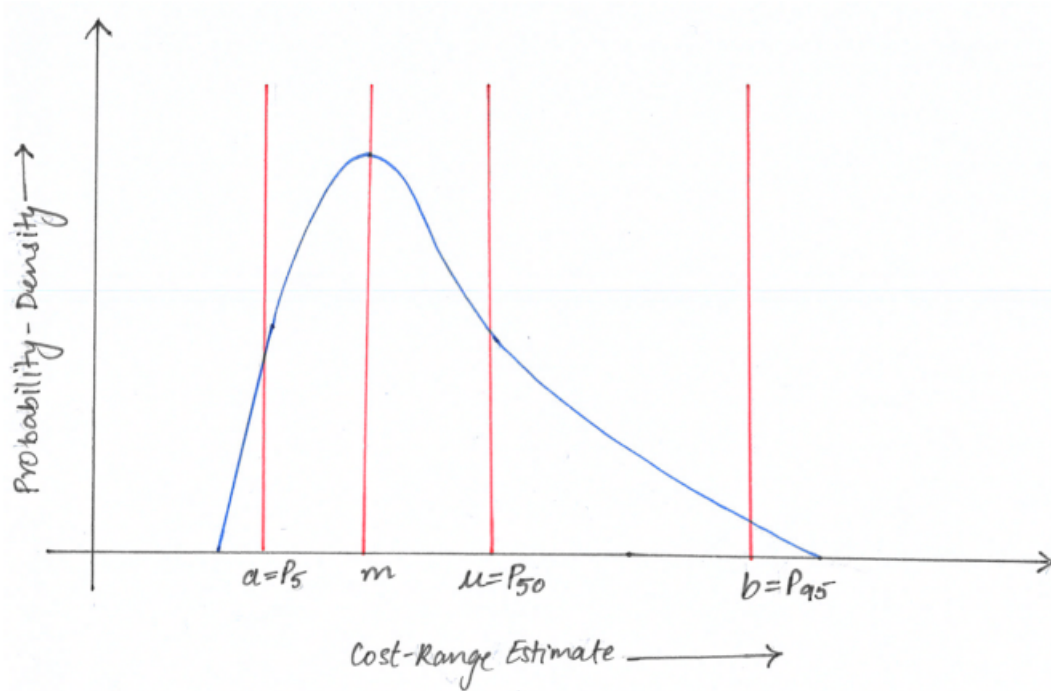


Figure E.15: Original and New position of the perceived risk of extensive shear cracking in a bridge girder under service loads

where

a	Optimistic estimate (5% chance of being better)
m	most likely estimate (mode of the distribution)
b	Pessimistic estimate (5% chance of being worse)

In the discussion in the beginning of section E.5, it is estimated that the material cost accounts for about 16% of the total project cost in extreme situations. It is mentioned that a 200% increment in the stirrups amount increases the total project cost by 24.24%. Now, let us assume that the design cost is roughly equal to 4% of the total cost of civil works in the project. Assuming that the equal design effort is required for design for Bending Moment as well as Shear Force, based on the calculations done in this MSc thesis, it is found that design time (assumed cost increases in same proportion as time) for shear is increased by 30% due to additional checks. This implies that increased design cost of the project due to the adoption of proposed design method = $4\% \times 50\% \times 30\%$ of the cost of civil works. This amounts to 0.6% increase in the cost of civil works. Let us conservatively assume that cost of civil works is increased by 1%. Therefore, the total increase in the cost of the civil works (material + design) due to the application of the proposed design method over conventional design method leads to a total increment of $(24.24 + 1)\%$ in the cost of civil works. Let us assume a total increment of 26% occurs as a conservative approximation. The estimated mean values of the cost of land acquisition and cost of civil works are taken in a proportion based on the real costs from an internal report of a design company outside of The Netherlands. The optimistic and pessimistic estimates are chosen randomly. Moreover, the estimates for the conventional and the proposed design methods stay the same for the cost of land acquisition. The cost of civil works (for the proposed design method) is obtained by increasing the estimates by 26% of the original values used in the conventional design method.

Table E.1: Cost range estimate for the original design method using Delphi-Beta method

Parameter	Formula	Value
Estimate of Mean cost of land acquisition	Estimated value	8 million Euros
Estimate of Mean cost of civil works	Estimated value	2.8 million Euros
Estimate of Optimistic cost of land acquisition	Estimated value	5.5 million Euros
Estimate of Optimistic cost of civil works	Estimated value	1.9 million Euros
Estimate of Pessimistic cost of land acquisition	Estimated value	12 million Euros
Estimate of Pessimistic cost of civil works	Estimated value	4 million Euros
Mean of the distribution of land acquisition cost	$\mu_1 = \frac{a + 4m + b}{6}$	8.25 million Euros
Standard Deviation of the distribution of land acquisition cost	$\sigma_1 = \frac{b - a}{6}$	1.08 million Euros
Mean of the distribution of cost of civil works	$\mu_2 = \frac{a + 4m + b}{6}$	2.85 million Euros

Standard Deviation of the distribution of cost of civil works	$\sigma_2 = \frac{b - a}{6}$	0.35 million Euros
Mean of the Normal distribution of total	$\mu = \mu_1 + \mu_2$	11.1 million Euros
Standard Deviation of the Normal distribution of total cost	$\sigma = \sqrt{\sigma_1^2 + \sigma_2^2}$	1.138 million Euros

Based on the comparison of the mean values of normal distribution of the total project cost from the conventional and proposed design methods, it is clear that the proposed design method increases the total project commissioning cost by 9.37% in this example. Now, this value of increment in the cost is applicable only for this example and for this particular proportion of the costs of land acquisition and cost of civil works. A more detailed study is needed to establish the general range of increment by the adoption of the new design method.

Table E.2: Cost range estimate for the proposed design method using Delphi-Beta method

Parameter	Formula	Value
Estimate of Mean cost of land acquisition	Estimated value	8 million Euros
Estimate of Mean cost of civil works	Estimated value	3.52 million Euros
Estimate of Optimistic cost of land acquisition	Estimated value	5.5 million Euros
Estimate of Optimistic cost of civil works	Estimated value	2.39 million Euros
Estimate of Pessimistic cost of land acquisition	Estimated value	12 million Euros
Estimate of Pessimistic cost of civil works	Estimated value	5.04 million Euros
Mean of the distribution of land acquisition cost	$\mu_1 = \frac{a + 4m + b}{6}$	8.25 million Euros
Standard Deviation of the distribution of land acquisition cost	$\sigma_1 = \frac{b - a}{6}$	1.08 million Euros
Mean of the distribution of cost of civil works	$\mu_2 = \frac{a + 4m + b}{6}$	3.59 million Euros

Standard Deviation of the distribution of cost of civil works	$\sigma_2 = \frac{b - a}{6}$	0.44 million Euros
Mean of the Normal distribution of total	$\mu = \mu_1 + \mu_2$	11.84 million Euros
Standard Deviation of the Normal distribution of total cost	$\sigma = \sqrt{\sigma_1^2 + \sigma_2^2}$	1.17 million Euros

E.6. Shear Cracking Risk Assessment

A risk is an uncertain, future event, that, if occurs has a negative impact or positive impact on project promises [39]. In this MSc thesis, the discussion is focused on the risk involved with current design method in practice which does not involve calculation of mean shear crack width and shear deflection due to the lack of availability of the practical models. Risk is usually expressed as the product of probability of its occurrence times the potential impact it can have on the objectives. Based on the probability and potential impact of the risk, different strategies are used to deal with these risks within the constraints of time, money etc. Figure E.17 shows the four extreme categories of risk depending on the values of probability and potential impact. There are only a few cases reported in the literature with the problem of severe shear cracking under service loads (example Alvik and Grondal bridges in Sweden). Therefore, risk due to shear deficient design (for shear crack width and shear deflection control) seems to be a risk with low probability but high consequences. Therefore, such a risk can be categorized as a medium risk according to Hastings [27]. Now, the proposed method helps reduce the probability of occurrence of this risk. Moreover, the increased shear reinforcement also reduces the potential impact since the ductility of the structure is most likely increased due to additional amount of stirrups (if required by the analysis with the proposed models). The shear deficient design of the reinforced concrete beams can lead to various types of risks. Table E.3 shows the identified primary technical, socio-political and business categories risks in the form of a risk-register. It is important to assess the effectiveness of the risk-response post implementation of the measure. In the present case, the improved design method with proposed models for mean shear crack width and shear deflection is taken as the risk response posed by the applica-

tion of current design methods without assessment of mean shear crack width and shear deflection.

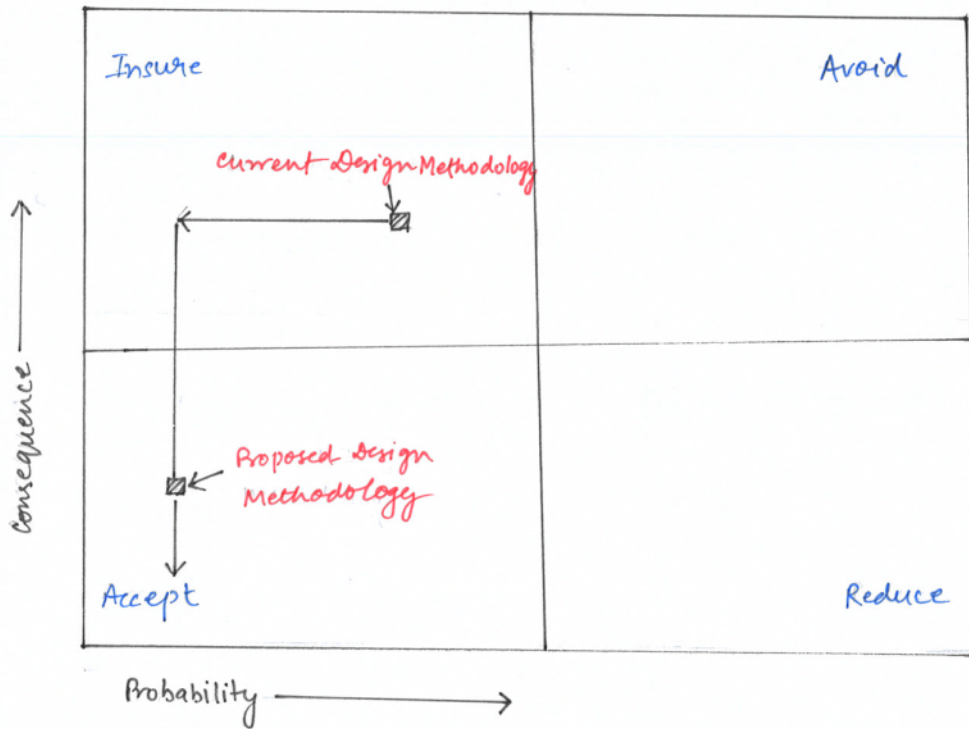


Figure E.16: Original and New position of the perceived risk of extensive shear cracking in a bridge girder under service loads

Likelihood	Consequence				
	Insignificant	Minor	Moderate	Major	Severe
Almost certain	Medium	Medium	High	High	Extreme
Likely	Medium	Medium	Medium	High	Extreme
Moderate	Low	Medium	Medium	High	High
Unlikely	Low	Low	Medium	Medium	High
Rare	Low	Low	Low	Medium	Medium

Figure E.17: Different Levels of risk depending on the likelihood and consequences as defined by Hastings [27]

Table E.3: Semi-quantitative Risk register for a shear deficient bridge design for mean shear crack width control under service loads

Nr.	Category	Risk Description			Pre-response Assessment		Risk-Response	Post-response-Assessment			
		Cause	Risk Event	Consequence	Probability	Impact		Probability	Impact	Post-risk action	Secondary risk
(I)	Technical	Bridge girder is shear deficient in SLS	may show large crack widths under service loads	Maintenance cost of the project becomes too high and exceeds budget	60%	High maintenance costs	Improved design in office for SLS	25%	reduced maintenance cost within budget	data storage for design and corresponding crack width monitoring	extended construction time because of extra placement of stirrups
(II)	Socio-political	Bridge girder is shear deficient in SLS	may show large crack widths under service loads	Perception of risk and eminent structural failure	60%	complaints and loss of public trust	Improved design in office for SLS	25%	co-operation by people during maintenance	interview people for reaction to the maintenance operations, plan and speed	increased project budget; less funds for other projects
(III)	Business	Bridge girder is shear deficient in SLS	may show large crack widths under service loads	Lost client trust and brand reputation	60%	penalty; lack of timely payments; poor future business associations	Improved design in office for SLS	25%	higher client satisfaction	quality and customer satisfaction surveys with clients	increased design time

E.7. Conclusion

In this Appendix, several aspects of an infrastructure project (a cantilever balanced bridge in this case) are discussed. These aspects are quality, risk-management and maintenance. The proposed models help attain high quality standards by facilitating the design of a structure (bridge) that meets the serviceability requirements of the structure. The proposed models help prevent excessive shear crack widths which can jeopardize the functionality of the structure and pose durability problems. The cracking also affects the aesthetics of the infrastructure. Moreover, extensive shear cracking also poses different types of risks. While it deteriorates the structure and causes technical risks on one hand, it also causes socio-political risk of criticism and loss of public trust as well as business risk of bad reputation and discontinued business relationship with the clients.

It is seen that the proposed design method delays the mean time to critical maintenance. The robust design comes with a cost of extra design and material (shear reinforcement) but prevents excessive maintenance costs in the later phases. Therefore, it is cost-effective from life cycle cost point of view. Overall the proposed methods facilitate improved quality, reduced risk and reduced maintenance cost but requires an investment in the form of high initial design effort and material cost (in case the structure is found shear deficient in SLS).

E.8. Reflection

My MSc journey was a little different from other peers in the Department because I chose to pursue IDM annotation along with my MSc in Structural Engineering. I have to be honest to admit that initially it was a bit challenging and uncomfortable for me to think about design from management point of view. As a Structural Engineer, we are trained in a particular way of thinking about structures especially the load carrying capacity of the structures. However, it was only in the course "Infrastructure Management" that I realized the other crucial factors that have equal or even more influence on the structure like risk management and financial planning etc. Learning about Risk registers and NPV as a tool to compare the alternatives are some of my personal key takeaways from the course.

The course on "Integral Systems Design" was a unique course for me. It challenged me heavily and eventually shifted my perspective about looking at structures and infrastructural projects from systems point of view. A structure has a lot of entities and components which interact with each other through various interfaces.

I admit that I was not very fond of working in teams and preferred to do tasks myself more than relying on help from others until I followed the course "Collaborative Design and Engineering". It was a daunting task to position myself to contribute in a big team of 30 students from different disciplines with different perspectives and collaborate together to produce a coherent report with small contribution from each team member. I learnt the importance of communication with other team members and how crucial it is to seek feedback from the peers. This is especially important when you are a part of the project where your work has huge implications on the quality and usability of the project deliverable. The course on "Financial Engineering" sparked my enthusiasm to learn more about investment tools and stock markets, inflation etc. I realized that it is quite empowering to be able to predict the financial parameters that can help make informed choices in different scenarios. In my opinion, you are not a complete engineer without some knowledge of basic financial terms like interest, discount rate, inflation and the means to calculate these and use these

to compare the financial viability of different projects.

The course "Information Systems in Construction Industry" gave me the confidence that any software tool can be learnt if there is a focused practice and tolerance for large number of hit and trials in the beginning to know the most used commands. I was always fascinated by the Softwares like Revit and heard about Relatics. The course gave me the necessary foundation and sparked my interest to learn more about these these softwares. I learnt that learning any new software tool is messy in the beginning but a stage comes when it becomes enjoyable and easy. The point is you have to be willing to stick through that initial phase of mastering the basic most used commands of the software. Last but not the least, the IDM part of my thesis challenged me to find the wider implications of my research work in practice. It helped me in assessing the potential scale of impact of my thesis work on various aspects of the project like project cost, quality, maintenance and risk-management. The "IDM Annotation" focus of my work established coherence between the technical engineering aspects and the engineering management aspects of the infrastructure projects like bridge- design, construction and maintenance. I realized that this coherence is the key towards useful and successful projects in the construction industry. It took me a while to figure out the elegant way to document the potential consequences of my work but the time spent was fully worth it. I can take a small pride in acknowledging that although I do not have an in depth knowledge about construction management, yet I feel comfortable in having discussions with my Construction Management Master colleagues and I definitely am in a better position to do that thanks to the "IDM Annotation". I would highly recommend this annotation to the students willing to challenge themselves to come out of their comfort zone to become a τ Engineer. You should definitely follow the annotation to know what that really means.

Appendix F

F.1. Dowel Action

THIS Appendix describes a proposed methodology to predict the dowel action contribution to the shear resistance of a reinforced concrete beam. The dowel action of the longitudinal reinforcement can be evaluated based on the mechanical analogy of Beam on Elastic Foundation and Extended to Beam on Inelastic Foundation [43]. The reinforcement and the surrounding concrete are modelled as beam and elastic foundation (comprising of springs) in this model. The following are the equations given by Hetenyi [30] based on the assumption that beam and the elastic foundation behaves elastically.

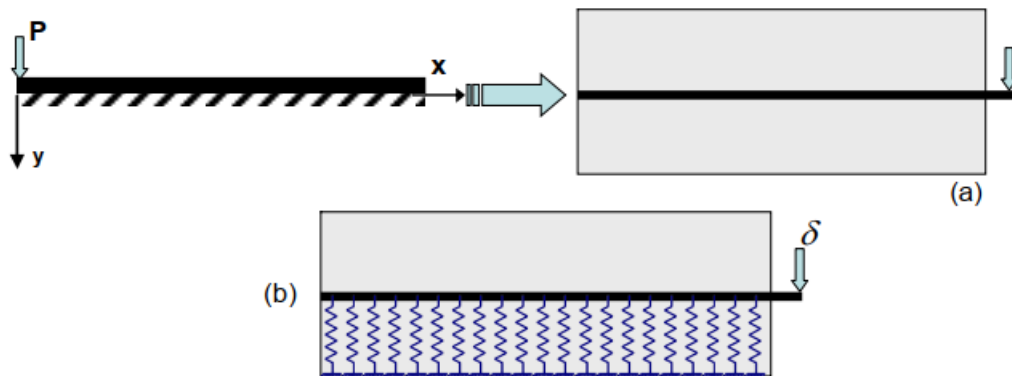


Figure F1: Schematic representation of RC beam as beam on elastic foundation[43]

$$y(x) = \frac{2P\lambda}{k_s} D_{\lambda x} \quad (E1)$$

$$\Theta(x) = \frac{-2P\lambda^2}{k_s} A_{\lambda x} \quad (E2)$$

$$M(x) = \frac{-P}{\lambda} B_{\lambda x} \quad (\text{E3})$$

$$V(x) = -P \cdot C_{\lambda x} \quad (\text{E4})$$

$$L_{c0} = \frac{3\Pi}{4} \sqrt[4]{\frac{4E_s I_b}{k_{fc} d_b}} \quad (\text{E5})$$

where

$k(s)$ spring stiffness simulating reinforcement bar and the surrounding concrete

$y(x)$ deflection profile of the beam

$\theta(x)$ rotation profile of the beam

$M(x)$ moment profile of the beam

$V(x)$ shear profile of the beam

$E(s)$ Modulus of Elasticity of steel

$I(b)$ Moment of Inertia of the bar

$E(s)$ Modulus of Elasticity of steel

$$k_{fc} = \frac{150f_c^{0.85}}{d_b} \quad (\text{E6})$$

$$A_{\lambda x} = e^{-\lambda x} (\cos \lambda x + \sin \lambda x) \quad (\text{E7})$$

$$B_{\lambda x} = e^{-\lambda x} (\sin \lambda x) \quad (\text{E8})$$

$$C_{\lambda x} = e^{-\lambda x} (\cos \lambda x - \sin \lambda x) \quad (\text{E9})$$

$$D_{\lambda x} = e^{-\lambda x} (\cos \lambda x) \quad (\text{E10})$$

$$\lambda = \sqrt[4]{\frac{k_s}{4E_s I_b}} \quad (\text{E11})$$

To account for the non-linearity due to crushing and fracture damages in the vicinity of the shear plane, the concept of curvature influencing length, L_c which is initially used by Maekawa and Qureshi (1996)[42] is used. This curvature influencing zone influences the stiffness of the subgrade given by the following equations.

$$k_s = \begin{cases} 220f_c^{0.85}, & \text{if } DI \leq 0.02 \\ \frac{220f_c^{0.85}}{(1 + 3(DI - 0.02)^{0.8})^4}, & \text{if } DI \geq 0.02 \end{cases} \quad (\text{E12})$$

where DI is the damage index and it is a dimensionless parameter.

$$DI = \frac{\delta}{d_b} \quad (\text{E13})$$

A better expression for the DI accounts for the deterioration of the bond due to damage by crushing and fracture. This expression considers the effect of the bar slip.

$$DI = \left(1 + \frac{150S}{d_b}\right) \frac{\delta}{d_b} \quad (\text{E14})$$

where S is slip and can be obtained based on the harmonization of the equations of [52] Shima et al. by [53]. Figure E.2 shows the local slip and bond stress around a reinforcement bar embedded in concrete.

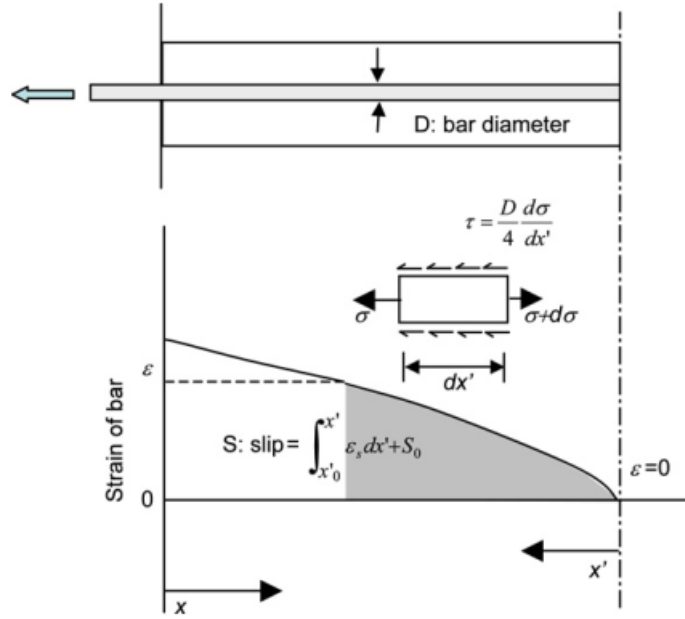


Figure F2: Bond stress and local slip around a reinforcement bar [53].

$$a = 2\left(1 + \left(\frac{2x}{L_d}\right)^{1.2}\right) \geq 2, x \geq L_d/2 \tag{F.15}$$

$$s = \epsilon_s(a + 3500\epsilon_s) \tag{F.16}$$

$$s = \epsilon_y(a + 3500\epsilon_y), \epsilon_y \leq \epsilon_s < \epsilon_{sh} \tag{F.17}$$

where

$\epsilon(sh)$ strain at the strain hardening

$\epsilon(y)$ strain at the yielding

$\epsilon(s)$ free strain in the bar

$L(d)$ bond deterioration length

is the normalized slip.

Here, s

$$S = \frac{d_b}{K_{fc}} s \tag{F.18}$$

$$K_{fc} = \frac{f_c^{2/3}}{20} \tag{F.19}$$

In our case $x = d$ where d is the effective depth. Qureshi and Maekawa found that the length of the bond deterioration zone is about 5 times the diameter of the reinforcement bar in case of pure axial pullout and greater in case of combined slipping and axial pullout. In this case, we have assumed $L_d = 5d_b$.

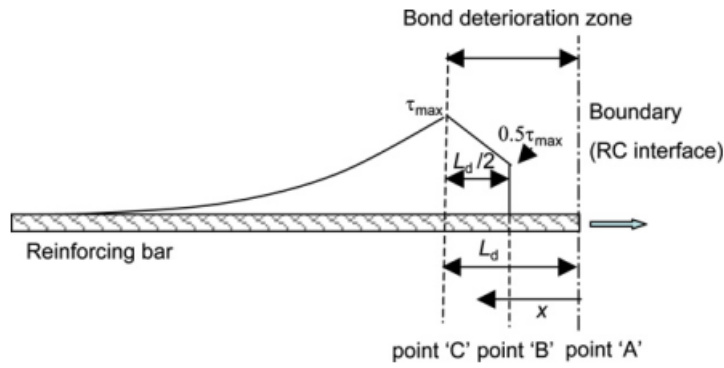


Figure F3: Bond deterioration zone around the RC interface [53].

Figure F.3 shows the bond deterioration zone near RC interface. Also, we have assumed that the longitudinal bars will not yield under service load. The dowel force is significantly influenced by the concrete side cover and concrete bottom cover. The amount of dowel force mobilized is dependent on the relative magnitude of these cover values respectively. Now,

$$w(x) = \frac{d}{dx} V(x) = 2P\lambda e^{-\lambda x} \cos(\lambda x) \tag{E.20}$$

$$w(x) = 0 \rightarrow L_i = \frac{\pi}{2\lambda} \tag{E.21}$$

$$V_d = \int_0^{\frac{\pi}{2\lambda}} w dx = 1.21P \tag{E.22}$$

where

$$P = \frac{k_s \delta}{2\lambda} \tag{E.23}$$

In case $c_b < c_s$

$$V_d = 1.21 \left(\frac{c_b}{c_s} \right) P \tag{E.24}$$

The iterative procedure to calculate the dowel force proposebelow is based on the determination of the right value of the damage index.

1. Assume a value for the damage index DI .

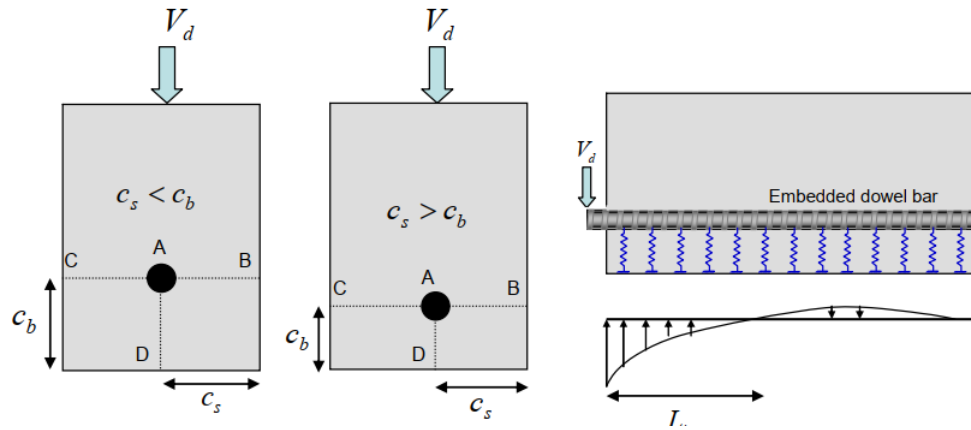


Figure E.4: The two cases for beam cover splitting [Moradi et al]

2. Calculate k_s and δ based on this value of DI .
3. Evaluate the ϵ_s and S
4. Now calculate the value of DI_{calc} given in (Equation F.14)
5. if $DI=DI_{calc}$, the process stops. Otherwise, make a new estimate of DI and repeat Steps 1-5.
6. Calculate P from(Equation F.23) and then calculate V_d from (Equation F.24).

Bibliography

- [1] Standard specifications for concrete structures. *Tokyo, Japan*, 2002.
- [2] ACI Committee 318. Building code requirements for structural concrete (aci 318-08) and commentary. *American Concrete Institute, Farmington Hills, MI*, 2008.
- [3] ASCE-ACI Committee 426. The shear strength of reinforced concrete members. *JStruct Div*, 99(6):1091–1187, 1973.
- [4] Joint ACI-ASCE Committee 445. Recent approaches to shear design of structural concrete (aci 445r-99). *Farmington Hills, MI*, 1999.
- [5] CSA Committee A23.3. Design of concrete structures (csa a23.3-04). *Canadian Standards Association, Rexdale, ON, Canada*, 2004.
- [6] S. Ahmad and P. Bhargava. Shear strength models for reinforced concrete slender beams: a comparative study. *Structures*, 16:119–128, 2018.
- [7] Vecchio F.J. Bentz, E.C. and M.P. Collins. Simplified modified compression field theory for calculating shear strength of reinforced concrete elements. *ACI Materials Journal*, 103(4):614–624, 2006.
- [8] Comité Euro International Du Béton. Cep-fip model code 1990. *Thomas Telford Service Ltd., London*, () , 1990.
- [9] S. Betongföreningen. Svenska betongföreningens handbok till eurokod 2. *Tech. rep., Svenska Betongföreningen*, volym i.), 2010.
- [10] S.B. Bhide. Reinforced concrete elements in shear and tension. *Univ. of Toronto, Dept. of Civil Engng.*, 87-02, 1987.
- [11] S.B. Bhide and M.P. Collins. Influence of axial tension on the shear capacity of reinforced concrete members. *Structural Journal*, 86(5):570–581, 1989.
- [12] R.C. Braam. Concrete structures 2 -cie 3150 reader. *CiTG, TU Delft*,).
- [13] Chi K.N. Chiu, C.K. and F.C. Lin. Experimental investigation on the shear crack development of shear-critical high-strength reinforced concrete beams. *Journal of Advanced Concrete Technology*, 12(7):223–238, 2014.
- [14] A. Cladera and A.R. Mari. Shear design procedure for reinforced normal and high-strength concrete beams using artificial neural networks. part ii: beams with stirrups. *Engineering structures*, 26(7):927–936, 2004.
- [15] Marí A. Bairán J.M. Ribas C. Oller E. Cladera, A. and N. Duarte. The compression chord capacity model for the shear design and assessment of reinforced and prestressed concrete beams. *Structural concrete*, 17(6):1017–1032, 2016.

- [16] M.P. Collins. Towards a rational theory for rc members in shear. *Journal of the Structural Division*, 104(4), 1978.
- [17] M.P. Collins and D. Mitchell. Prestressed concrete structures (vol.9). *Englewood Cliffs, NJ: Prentice Hall.*,), 1991.
- [18] Paris. Comite Euro-International du Beton/Federation Internationale de la Precontrainte. Ceb-fip model code for concrete structures, 3rd edition. *Comite Euro International Du Beton*, 1978.
- [19] C.E. De Normalisation. Eurocode 2: Design of concrete structures, part 1-1: General rules and rules for buildings. *Comite European De Normalisation (CEN), Lausanne, Switzerland*, 2004.
- [20] P. G. Debernardi and M. Taliano. Shear deformation in reinforced concrete beams with thin webs. *Mag. Concr. Res.*, 58(3):157–171, 2006.
- [21] B. L. Meyers Deflections of concrete structures, G. M. Sabnis and eds. F. Roll. Dilger, w., and abele, g. (1974). "initial and time-dependent shear deflection of reinforced concrete t-beams. *American Concrete Institute, Farmington Hills, MI*.
- [22] Lee S.C. Deluce, J.R. and E.J. Vecchio. Crack model for steel fiber-reinforced concrete members containing conventional reinforcement. *ACI Structural Journal*, 111(1):93–102, 2014.
- [23] fib (International Federation for Structural Concrete). Ceb-fip model code 2010.first complete draft, vol 2, chaps.(7–10). *fib Bulletin*, 562010, 2013.
- [24] James G. Long term monitoring of the alvik and gröndal bridges. *Byggkonstruktion, TRITABKN Rapport 76*):48, 2004. doi: www.byv.kth.se.
- [25] Pimanmas A. Maekawa K. Hansapinyo, C. and T. CHAISOMPHOB. Proposed model of shear deformation of reinforced concrete beam after diagonal cracking. *Doboku Gakkai Ronbunshu*, 725:305–319, 2003.
- [26] Mantawy A. Soliman J. Sherif A. Hassan, T.K. and S.H. Rizkalla. Bond characteristics and shear behavior of concrete beams reinforced with high-strength steel reinforcement. *Advances in Structural Engineering*, 15(2):303–318, 2012.
- [27] N.A.J. Hastings. Physical asset management: With an introduction to iso55000. *Springer*,), 2015.
- [28] Liu Z. He, Z.Q. and Z.J. Ma. Shear deformations of rc beams under service loads. *Journal of Structural Engineering*, 143(1), 2016.
- [29] A. Hejll. Structural health of bridges: monitor, assess and retrofit. *Doctoral dissertation, Luleå tekniska universitet*,), 2004.
- [30] M. I. Hetenyi. Beams on elastic foundation: Theory with applications in the fields of civil and mechanical engineering. *Ann Arbor, The University of Michigan Press*.

- [31] B. Hu and Y.F. Wu. Minimum shear reinforcement in normal, medium, and high-strength concrete beams. *Journal of Structural Engineering*, 147:666–678, 2017.
- [32] B. Hu and Y.F. Wu. Effect of shear span-to-depth ratio on shear strength components of rc beams. *Engineering Structures*, 168:770–783, 2018.
- [33] ACI (American Concrete Institute). Building code requirements for structural concrete (aci 318-11) and commentary. , *Farmington Hills, MI*, 2011.
- [34] ACI (American Concrete Institute). Building code requirements for structural concrete and commentary. *ACI 318–14, Farmington Hills, MI*, 2014.
- [35] H. B. Kupfer and K. H. Gerstle. Behavior of concrete under biaxial stresses. *J Eng Mech Div*, 99:853–866, 1973.
- [36] Choi I.J. Lee, J.Y. and S.W. Kim. Behavior of concrete beams reinforced with astm a 1035 grade 100 stirrups under shear. *ACI Structural Journal*, 108(5), 2011.
- [37] Choi S.H. Lee, J.Y. and D.H. Lee. Structural behaviour of reinforced concrete beams with high yield strength stirrups. *Magazine of Concrete Research*, 68(23):1187–1199, 2016.
- [38] Lee D.H. Lee J.E. Lee, J.Y. and S.H. Choi. Shear behavior and diagonal crack width for reinforced concrete beams with high-strength shear reinforcement. *ACI Structural Journal*, 112(3), 2015.
- [39] M. Leijten. Project management-epa1412-spm4416-spm8000. *Lecture Slides, CiTG, TU Delft*,).
- [40] F. Leonhardt and R. Walther. The stuttgart shear tests, 1961. *Cement and Concrete Association, London*.
- [41] B. Li and C.T.N. Tran. Determination of inclination of strut and shear strength using variable angle truss model for shear-critical rc beams. *Structural Engineering and Mechanics*, 41(4):459–477, 2012.
- [42] K. Maekawa and J. Qureshi. Computational model for reinforcing bar embedded in concrete under combined axial pullout and transverse displacement. *Proceeding of JSCE*, 31 (538):227–239, 1996.
- [43] Soltani M. Moradi, A.R. and A.A. Tasnimi. A simplified constitutive model for dowel action across rc cracks. *Journal of advanced concrete technology*, 10(8):264–277, 2012.
- [44] Hosny A. Rizkalla S. Munikrishna, A. and P. Zia. Behavior of concrete beams reinforced with astm a 1035 grade 100 stirrups under shear. *ACI Structural Journal*, 108(1):34–41, 2011.
- [45] J. Nie and C. S. Cai. Deflection of cracked rc beams under sustained loading. *J. Struct. Eng.*, 6(708):708–716, 2000. doi: 10.1061/(ASCE)0733-9445(2000)126.

- [46] Yamada K. Yokozawa K. Niwa, J. and H. Okamura. Revaluation of the equation for shear strength of reinforced concrete beams without web reinforcement. *Doboku Gakkai Ronbunshu*, 372:167–176, 1986.
- [47] AASHTO (American Association of State Highway and Transportation Officials). Aashto-lrfd bridge design guide specifications for gfrp-reinforced concrete bridge decks and traffic railings, washington, dc. 2009.
- [48] O.B. Olalusi. Present state of eurocode 2 variable strut inclination method for shear design and possible improvement. *Structures*, 19:48–57, 2012.
- [49] Li B. Pan, Z. and Z. Lu. Effective shear stiffness of diagonally cracked reinforced concrete beam. *Journal of Structural Engineering*, 59:95–103, 2014.
- [50] Park R. Phillips M. Paulay, T. Horizontal construction joints in cast in place reinforced concrete. *ACI Special Publications*, 42(51):599–616, 1974.
- [51] UEDA T. SATO, Y. and Y. KAKUTA. Shear strength of prestressed concrete beams with frp tendon. *Concrete library international*, 27):189–208, 1996.
- [52] Chou L. Shima, H. and Okamura H. Micro and macro models for bond in reinforced concrete. *Journal of Faculty of Engineering, The University of Tokyo*, 39(2):133–194, 1987.
- [53] M. Soltani and K. Maekawa. Path-dependent mechanical model for deformed reinforcing bars at rc interface under coupled cyclic shear and pullout tension. *Engineering Structures*, 30 (4):1079–1091, 2008.
- [54] A.K. Tureyen and R.J. Frosch. Concrete shear strength: Another perspective. *Structural Journal*, 100(5):609–615, 2003.
- [55] Hejll A. Täljsten, B. and G. James. Carbon fiber-reinforced polymer strengthening and monitoring of the gröndals bridge in sweden. *Journal of Composites for Construction*, 11(2):227–235, 2007.
- [56] SATO Y. ITO T. UEDA, T. and K. NISHIZONO. Shear deformation of reinforced concrete beam. *Doboku Gakkai Ronbunshu*, (711):205–215, 2002.
- [57] E.J. Vecchio and M.P. Collins. The modified compression-field theory for reinforced concrete elements subjected to shear. *ACI J.*, 83(2):219–231, 1986.
- [58] A. Verbraeck. Project management-epa1412-spm4416-spm8000. *Lecture Slides, CiTG, TU Delft*,).
- [59] J.Y.L. Voo and S.J. Foster. Variable engagement model for fibre reinforced concrete in tension ,uniciv report no. r-420. *School of Civil and Environmental Engineering, The University of New South Wales, Australia*, 2003.
- [60] Dai J.G. Wang, T. and J.J. Zheng. Multi-angle truss model for predicting the shear deformation of rc beams with low span-effective depth ratios. *Engineering Structures*, 91:85–95, 2015.

- [61] van der Veen C. de Boer A. Yang, Y. and D.A. Hordijk. Investigation of v_{min} based on experimental research. *fib Symposium, Cape Town*, 2016.
- [62] Walraven J. Yang, Y. and J.D. Uijl. Shear behavior of reinforced concrete beams without transverse reinforcement based on critical shear displacement. *Journal of Structural Engineering*, 143(1):04016146–1–04016146–13, 2017.
- [63] Y. Yang. Shear behaviour of reinforced concrete members without shear reinforcement, a new look to at an old problem. *TU Delft Research Repository, Ph.D. Thesis*, 2014.
- [64] Y. Yang. Lecture slides cie-5127, concrete bridges. *CiTG, TU Delft*,), 2019.
- [65] Ueda T. Zakaria, M. and Z. Wu. Evaluating and proposing prediction models of shear crack width in concrete beams. *Journal of Japan Society of Civil Engineers, Ser. E2 (Materials and Concrete Structures)*, 67(2):245–263, 2011.
- [66] Ueda T. Wu Z. Zakaria, M. and L. Meng. Experimental investigation on shear cracking behavior in reinforced concrete beams with shear reinforcement. *Journal of Advanced Concrete Technology*, 7(1):79–96, 2009.
- [67] P. D. Zararis. Shear strength and minimum shear reinforcement of reinforced concrete slender beams. *Structural Journal*, Structural Journal:203–214, 2003.
- [68] P. D. Zararis and G.C. Papadakis. Diagonal shear failure and size effect in rc beams without web reinforcement. *Journal of structural engineering*, 127–7:733–742, 2001. doi: [https://doi.org/10.1061/\(ASCE\)0733-9445\(2001\)127:7\(733\)](https://doi.org/10.1061/(ASCE)0733-9445(2001)127:7(733)).
- [69] T.C. Zsutty. Beam shear strength prediction by analysis of existing data. *Journal Proceedings*, 65(11):943–951, 1968.